CANADIAN THESES ON MICROFICHE

I.S.B.N.

THESES CANADIENNES SUR MICROFICHE

National Library of Canada
Collections Development Branch

Canadian Theses on
Microfiche Service

Ottawa, Canada
K1A 0N4

Bibliothèque nationale du Canada
Direction du développement des collections

Service des thèses canadiennes
sur microfiche

NOTICE

The quality of this microfiche is heavily dependent upon the quality of the original thesis submitted for microfilming. Every effort has been made to ensure the highest quality of reproduction possible.

If pages are missing, contact the university which granted the degree.

Some pages may have indistinct print especially if the original pages were typed with a poor typewriter ribbon or if the university sent us a poor photocopy.

Previously copyrighted materials (journal articles, published tests, etc.) are not filmed.

Reproduction in full or in part of this film is governed by the Canadian Copyright Act, R.S.C. 1970, c. C-30. Please read the authorization forms which accompany this thesis.

AVIS

La qualité de cette microfiche dépend grandement de la qualité de la thèse soumise au microfilmage. Nous avons tout fait pour assurer une qualité supérieure de reproduction.

S'il manque des pages, veuillez communiquer avec l'université qui a conféré le grade.

La qualité d'impression de certaines pages peut laisser à désirer, surtout si les pages originales ont été dactylographiées à l'aide d'un ruban usé ou si l'université nous a fait parvenir une photocopie de mauvaise qualité.

Les documents qui font déjà l'objet d'un droit d'auteur (articles de revue, examens publiés, etc.) ne sont pas microfilmés.

La reproduction, même partielle, de ce microfilm est soumise à la Loi canadienne sur le droit d'auteur, SRC 1970, c. C-30. Veuillez prendre connaissance des formules d'autorisation qui accompagnent cette thèse.

THIS DISSERTATION
HAS BEEN MICROFILMED
EXACTLY AS RECEIVED

LA THÈSE A ÉTÉ
MICROFILMÉE TELLE QUE
NOUS L'AVONS REÇUE

NL-339 (r. 82/08)

Canada

0-315-19354-9

National Library of Canada | Bibliothèque nationale du Canada

Canadian Theses Division | Division des thèses canadiennes

Ottawa, Canada
K1A 0N4

67262

PERMISSION TO MICROFILM — AUTORISATION DE MICROFILMER

• Please print or type — Écrire en lettres moulées ou dactylographier

Full Name of Author — Nom complet de l'auteur

SANTANU KUMAR DAS

Date of Birth — Date de naissance	Country of Birth — Lieu de naissance
12 JANUARY 1956	INDIA

Permanent Address — Résidence fixe

SAPTARSHEE
BHUBANESWAR-751002
INDIA

Title of Thesis — Titre de la thèse

MODAL NOISE AND DISTORTION
IN OPTICAL FIBER TELECOMMUNICATIONS

University — Université

UNIVERSITY OF ALBERTA

Degree for which thesis was presented — Grade pour lequel cette thèse fut présentée

Ph. D

Year this degree conferred — Année d'obtention de ce grade	Name of Supervisors — Nom du directeur de thèse
Spring 1984	Dr. C.G. ENGLEFIELD Dr. P.A. GOUD

Permission is hereby granted to the NATIONAL LIBRARY OF CANADA to microfilm this thesis and to lend or sell copies of the film.

The author reserves other publication rights, and neither the thesis nor extensive extracts from it may be printed or otherwise reproduced without the author's written permission.

L'autorisation est, par la présente, accordée à la BIBLIOTHÈQUE NATIONALE DU CANADA de microfilmer cette thèse et de prêter ou de vendre des exemplaires du film.

L'auteur se réserve les autres droits de publication; ni la thèse ni de longs extraits de celle-ci ne doivent être imprimés ou autrement reproduits sans l'autorisation écrite de l'auteur.

Date	Signature
17 April 1984	Santanu das

NL-91 (4/77)

THE UNIVERSITY OF ALBERTA

MODAL NOISE AND DISTORTION IN OPTICAL FIBER TELECOMMUNICATIONS

by

SANTANU DAS

©

A THESIS

SUBMITTED TO THE FACULTY OF GRADUATE STUDIES AND RESEARCH

IN PARTIAL FULFILMENT OF THE REQUIREMENTS FOR THE DEGREE

OF DOCTOR OF PHILOSOPHY

DEPARTMENT OF ELECTRICAL ENGINEERING

EDMONTON, ALBERTA

SPRING 1984

THE UNIVERSITY OF ALBERTA

RELEASE FORM

NAME OF AUTHOR Santanu Das

TITLE OF THESIS Modal Noise and Distortion in Optical Fiber Telecommunications

DEGREE FOR WHICH THESIS WAS PRESENTED Doctor of Philosophy

YEAR THIS DEGREE GRANTED Spring 1984

Permission is hereby granted to THE UNIVERSITY OF ALBERTA LIBRARY to reproduce single copies of this thesis and to lend or sell such copies for private, scholarly or scientific research purposes only.

The author reserves other publication rights, and neither the thesis nor extensive extracts from it may be printed or otherwise reproduced without the author's written permission.

(SIGNED) Santanu das

PERMANENT ADDRESS:

Saptarshee

Bhubaneswar - 751002

INDIA

DATED 6th Feb. 1984

THE UNIVERSITY OF ALBERTA

FACULTY OF GRADUATE STUDIES AND RESEARCH

The undersigned certify that they have read, and recommend to the Faculty of Graduate Studies and Research, for acceptance, a thesis entitled Modal Noise and Distortion in Optical Fiber Telecommunications submitted by Santanu Das in partial fulfilment of the requirements for the degree of Doctor of Philosophy.

Paul A. Gford C. G. Englefield

Supervisors

External Examiner

Date 6th Feb '84

ABSTRACT

The transmission characteristics of optical fiber splices/connectors and microbends are analyzed in detail in order to elucidate the modal noise and distortion behavior due to temporal fluctuations in the power loss. The theory uses an electromagnetic analysis and is based on approximating the parabolic-index fiber modes by Laguerre-Gaussian functions. Closed form solutions for the coupling coefficients between the guided modes of two fibers that are either separated in the longitudinal direction, or are tilted or offset with respect to each other at the splice, are used to evaluate the loss and its fluctuation amplitude by a transmission matrix formalism. The sensitivity of the resulting modal noise and distortion with respect to a wavelength shift of the laser diode source and to random thermal and mechanical stresses on the fiber are determined for coherent and partially coherent illumination. Experimental results of the power loss and modal distortion are presented and are shown to be in close agreement with the theory. Using this theory, the dependence of the modal noise and of the splice loss on wavelength, numerical aperture and index matching are examined for a uniform as well as a steady state power distribution in the transmitting fiber. It is shown that splice-induced modal noise can be reduced substantially by increasing the operating wavelength and by using a partially coherent laser diode that emits in many longitudinal modes. A microbending loss theory, based on a perturbation approximation to the power diffusion between modes, is described. New measurements on the average power loss are shown to verify this theory. Also, an estimate made of the excess transient loss due to mode coupling is found to be in good agreement with previously published data. The microbending loss dependence on the wavelength, numerical aperture, fiber winding pitch and jacket relaxation time are investigated. The effect of such jacket relaxation on the phase stability of ultra-stable frequency distribution systems is discussed. Mode-mode interference is shown to be the cause of microbending loss fluctuations from which the magnitude of the modal noise and distortion are determined on a statistical basis. Based on this, the observed phenomenon of excess harmonic distortion in long multimode fibers is explained. It is predicted that modal noise varies as the square of the loss per microbend and linearly as the number of microbends, indicating that uniformly distributed losses due to small amplitude microbends are much less critical than large localized losses along the fiber transmission line. Concluding remarks summarize the findings of this thesis and indicate how modal noise and distortion can be minimized in optical fiber systems.

ACKNOWLEDGEMENTS

I wish to thank Dr. P.A. Goud and Dr. C.G. Englefield for their constant help, advice and encouragement throughout the work. Thanks are also extended to the members of the examining committee for reviewing this work. My appreciation to Mr. Bert Telder for his skilful technical assistance at various stages of the project, and to my colleagues R. Razdan, S. Mysore and other members of the Optical Communications Group for many helpful discussions.

Appreciation is also extended to the following:

— Mr. L. Zalzalah (Edmonton Telephones) for supplying the OTDR and the fusion splicer.

— Mr. D.J. Eccleston (Corning Glass Works) for furnishing the values of the fiber and jacket parameters.

— Mr. R.E. Epworth (Standard Telecommunication Labs), Dr. A. Dandridge (Naval Research Labs) and Dr. K. Stubkjaer (Technical University of Denmark) for supplying much needed data regarding laser diode characteristics.

— Dr. D. Marcuse (Bell Labs) and Mr. J. Blackburn (Harry Diamond Labs) for helpful discussions over the phone.

— Dr. G. Lutes (JPL) and Dr. L. Maleki (JPL) for discussions regarding microbending related phase fluctuations in NASA's DSN.

— Dr. A. Javed (Bell Northern Research) for his advice and stimulating discussions.

— Alberta Government Telephones for providing me with a fellowship.

I would also like to express my sincere thanks to my parents, teachers and friends who have contributed in one way or another towards the completion of the work reported in this thesis.

Table of Contents

Chapter		Page
1.	INTRODUCTION	1
	1.1 Components of Fiber-optic Systems	1
	1.2 Noise and Nonlinear Distortions due to the Transmission Channel	2
	1.3 Historical Review	4
	1.4 Research Objectives	9
	1.5 Thesis Organization	10
2.	REVIEW OF BASIC PROPERTIES OF OPTICAL FIBERS AND CONNECTORS	12
	2.1 Optical Fiber Characteristics	12
	2.1.1 Field Solutions for Modes in a Parabolic-Index Profile Fiber	13
	2.1.2 Dispersion	19
	2.1.3 Guided Mode Attenuation	21
	2.1.4 Numerical Aperture	23
	2.2 Operating Wavelength	23
	2.3 Fiber Connectors and Splices	25
	2.4 Modal Noise and Distortion	25
	2.4.1 Source Coherence	25
	2.4.2 Speckle Patterns	27
	2.4.3 Modal Noise	27
	2.4.4 Exploration of Possible Speckle Conditions	28
	2.4.5 Modal Distortion	29
3.	TRANSMISSION CHARACTERISTICS OF A FIBER CONNECTOR : THEORY	30
	3.1 Derivation of the Instantaneous Power Coupling Efficiency	30
	3.1.1 Steady State Modal Power Distribution	34
	3.2 Illumination with Coherent Light	36
	3.3 Illumination with Partially Coherent Light	37
	3.4 Power Loss	39
	3.5 dc Signal-to-Modal Noise Ratio	39
	3.6 Modal Distortion	40

3.7 Conclusions 41

4. EVALUATION OF LOSS, MODAL NOISE AND DISTORTION DUE TO AXIAL OFFSET 42

4.1 Evaluation of Modal Amplitude Coupling Coefficients 42

4.2 Experimental Set Up 45

4.3 Results and Discussion 48

4.3.1 Power Loss 48

4.3.2 Modal Noise 49

4.3.3 Modal Distortion 50

4.4 Conclusions 51

5. EVALUATION OF LOSS, MODAL NOISE AND DISTORTION DUE TO LONGITUDINAL OFFSET 63

5.1 Propagation of a Gaussian Beam 63

5.2 Evaluation of Modal Amplitude Coupling Coefficients 65

5.3 Results 66

5.3.1 Power Loss 66

5.3.2 Modal Noise 67

5.3.3 Modal Distortion 69

5.4 Conclusions 70

6. EVALUATION OF LOSS, MODAL NOISE AND DISTORTION DUE TO TILT OFFSET 83

6.1 Calculation of the Modal Amplitude Coupling Coefficients 83

6.2 Results and Discussion 87

6.2.1 Splice Loss 88

6.2.2 Modal Noise 89

6.2.3 Modal Distortion 90

6.3 Conclusions 91

7. MODAL ANALYSIS OF LOSS, NOISE, AND DISTORTION DUE TO FIBER IMPERFECTIONS 99

7.1 Fiber Imperfections and Mode coupling 99

7.2 Derivation of the Instantaneous Power Loss 103

7.3 Excitation With Coherent Source 118

7.4 Excitation With Partially Coherent Sources 121

7.5 Numerical Evaluation of and Experiment on Microbending Loss 124

7.6 Modal Noise and Distortion 129

7.7 Conclusions 133

8. SUMMARY AND CONCLUSIONS 151

REFERENCES 161

APPENDIX A1
Computer Program (Axial Offset) 180

APPENDIX A2
Computer Program (Longitudinal Offset) 185

APPENDIX A3
Computer Program (Tilt Offset) 188

APPENDIX A4
Mode Coupling Coefficients for Fiber Imperfections 191

APPENDIX A5
Computer Program (Fiber Imperfections) 193

List of Tables

Table		Page
5.1	Loss reduction expressed as a percentage of the air gap loss, when index-matching is used instead of an air gap ($4<d/a<20$). The figures in the bracket denote the air gap loss in dB. NA=0.2, a=25 μm, λ=0.82 μm (V=39) or λ=1.55 μm (V=21).	68
7.1	Normalized power loss coefficient $\gamma/d\cdot\emptyset(\Delta\beta_0)$ in mm^{-3}. The power spectrum exponent p is defined in Ref. [106].	125
7.2	Numerical values of parameters used to calculate the power spectrum $\emptyset(\Delta\beta_0)$ of the refractive index fluctuation.	128
7.3	Values of the fiber and source parameters studied in Ref. [140] (Fig. 7.16) and in our experiment (Fig. 7.17).	147
8.1	Power loss trend with increasing wavelength. The figures within the bracket denote the maximum deviation of the power loss, expressed as a percentage of the highest loss value at a given offset. 0.82 μm$<\lambda<$1.55 μm.	155

List of Figures

Figure		Page
1.1	Noise sources in a fiber-optic communication system.	3
1.2	Transmission loss mechanisms in an optical fiber. Modal noise occurs due to the mode-selective losses shown in the figure.	5
2.1	Field distribution Ψ (r) as a function of the radial coordinate r. Fiber radius a = 25 μm and beam radius w_o = 5.6 μm.	16
2.2	(a) Guided core modes of equal transverse orders l = p = 1 with different orientation and polarization of their electric (solid arrow) and magnetic (broken arrow) fields. (b) Field distribution of the HE_{11} mode. (c) and (d) Transverse electric field and intensity distribution of two LP_{11}- modes and their composition from exact modes of the parabolic-index fiber.	18
2.3	Mode-space diagram for graded-index fiber. The dots represent the guided modes.	20
2.4	The maximum acceptance angle of a step-index fiber.	24
2.5	Schematic of two butt-coupled fibers with different types of geometrical misalignments.	26
3.1	Schematic configuration of a fiber followed by a fiber connector.	31
4.1	Geometry of two coupled fibers 1 and 2 axially offset by Δa.	43
4.2	Experimental set up to study power loss and modal distortion due to axial offset.	46
4.3	Photographs of the fiber endfaces at the splice (fiber cleave 1).	47
4.4	Loss vs. axial offset for uniform and steady state modal power distribution. Geometric optics (uniform power) results are shown in dotted line. a = 25 μm.	49
4.5	Experimental data and theoretical loss values for a steady state modal power distribution. a = 25 μm, NA = 0.2, and λ = 0.82 μm for the experimental results.	51
4.6	Coupling efficiency $<\eta>$ and its standard deviation $\delta(\eta)$, as a function of normalized offset for a coherent source. Both uniform (U) and steady state (SS) modal power distributions are considered. a = 25 μm and V = 21.	52
4.7	dc-SNR for a coherent source as a function of the coupling loss. The dashed curves are obtained from speckle theory. a = 25 μm.	53
4.8	dc-SNR for partially coherent sources with coherence time τ_c. Splice loss = 1 dB, α = 2.2 and a = 25 μm.	54
4.9	Normalised rms value of the derivative of the coupling efficiency with respect to emission frequency for a coherent source. α = 2.2 and a = 25 μm.	56
4.10	Normalized rms value of the derivative of the coupling efficiency with respect to emission frequency for a partially coherent source. Splice loss = 1 dB, a = 25 μm and α = 2.2.	57

4.11 Modal distortion $R_{2f/f}$ as a function of normalized offset for a partially coherent source. NA=0.2, a=25 μm, V=39, f=55 MHz, m=0.25, τ_c=35 ps, τ_{rms}=0.15 ns, and $\Omega_m/2\pi$=2 GHz. 58

4.12 Photographs of the endfaces of the transmitting and the receiving fiber for cleave no. 2. 60

4.13 Modal distortion for different cleaves. Experimental parameters same as in Fig. 4.11. 61

4.14 Modal distortion for different modulation frequencies f_m with fiber cleave 1. Experimental parameters same as in Fig. 4.11. 62

5.1 Two fibers separated by a longitudinal gap 'd'. At z=d, the free space LG beam radius is w_d 64

5.2 Power loss due to normalized spacing d/a for uniform (U) and steady state (SS) modal power distributions. Both air gap (AG) and index-matching (IM) are considered. a=25 μm, λ =1.55 μm, NA=0.2. 67

5.3 Power loss vs. normalized spacing d/a as a function of NA for steady state modal power distribution with an air gap. a=25 μm, λ =0.82 μm. 69

5.4 Power loss vs. normalized spacing d/a as a function of wavelength for an air gap. a=25 μm, NA=0.2. 70

5.5 Theoretical (TH) and experimental (EXPT) power loss values vs. normalized spacing (d/a) for an air gap. a=25 μm, V=39. 72

5.6 Variation of coupling efficiency $\langle\eta\rangle$ and its standard deviation $\delta(\eta)$ with normalized gap width d/a, for an air gap (AG) and an index-matched gap (IM). NA=0.2, a=25 μm and V=21. 73

5.7 dc-SNR as a function of coupling loss, for a coherent source. NA=0.2 and a=25 μm. 75

5.8 dc-SNR behavior as a function of gap loss, as predicted by : 1) modal analysis assuming a uniform power distribution and coherent illumination, and 2) speckle theory. NA=0.2 and a=25 μm. 76

5.9 dc-SNR for partially coherent sources with coherence time Coupling loss = 1 dB, a=25 μm, NA=0.2, and τ_{rms} =0.15 ns. 77

5.10 Variation of the normalized rms value of the derivative of the coupling efficiency with coupling loss, for coherent illumination. NA=0.2, a=25 μm, and τ_{rms} =0.15 ns. 79

5.11 Normalized rms value of the derivative of the coupling efficiency for partially coherent sources with coherence time τ_c . Coupling loss = 1 dB, a=25 μm, NA=0.2, and τ_{rms} =0.15 ns. 80

5.12 Modal distortion $R_{2f/f}$, as a function of normalized gap width for a partially coherent source. NA=0.2, a=25 um, V=39, f=55 MHz, m=0.25, τ_c =35 ps, τ_{rms} =0.15 ns, and $\Omega_m/2\pi$=2 GHz. 81

6.1 Cross-section of butt-jointed fibers with tilt offset. The angle between the axes of the two joining fibers is θ 84

6.2 Loss vs. normalized tilt offset Θ_N at butt-jointed fibers. Theoretical results are for a tilt at a fusion splice, whereas the data corresponds to a tilt at a connector. Results for equivalent axial offset according to Eq. (6.7) are shown by dotted lines for a uniform power distribution. $\Delta=0.0092$. 89

6.3 Coupling efficiency $<\eta>$ and its standard deviation $\delta(\eta)$ as a function of normalized tilt for a coherent source. $V=21$ and $\Delta=0.0092$. 91

6.4 dc-SNR for a coherent source as a function of splice loss incurred by tilt. Results for an equivalent axial offset according to Eq. (5.7) are shown by dotted lines 92

6.5 dc-SNR for partially coherent sources with coherence time τ_c. Both tilt and axial offsets are considered. Splice loss = 1 dB and $\alpha=2.2$. 94

6.6 Normalised rms value of the derivative of the coupling efficiency with respect to emission frequency for a coherent source. $\alpha=2.2$. 95

6.7 Normalised rms value of the derivative of the coupling efficiency with respect to emission frequency for a partially coherent source. Tilt loss = 1 dB and $\alpha=2.2$. 96

6.8 Modal distortion as a function of normalized tilt Θ_N for a partially coherent source. All experimental parameters except the modulation index 'm', are the same as in Fig. 4.11. m= 50 % and $\Omega_m/2\pi=4$ GHz. Theoretical results are for a tilt at a fusion splice, whereas the data corresponds to a tilt at a connector. 97

7.1 Spectral β range of guided and radiation modes of parabolic-index fibers. 105

7.2 (a) Schematic cross section of a cable consisting of optical fibers stranded about a central member and surrounded by an encapsulating material.
(b) Schematic lengthwise view of the cable with arrows indicating the force exerted by the encapsulating material as a fiber passes over a bump. From Ref. [105]. 114

7.3 Fiber with core-cladding interface distortions connected on both sides to two pieces of ideal fiber each L_0 long. A single bump is assumed to lie between $z=Z$ and $z=Z+d$. 116

7.4 Theoretical microbending loss vs. linear pressure for parabolic-index fibers. NA=0.2, a=25 μm. 129

7.5 Theoretical values of the microbending loss vs. linear pressure at λ =0.82 μm for parabolic-index fibers with different NA values. 130

7.6 Experimental set up for microbending loss studies. CMS designates the Cladding Mode Stripper. 132

7.7 Representative sandpaper roughness function. RA denotes the standard deviation of the surface roughness. 133

7.8 Experimental microbending loss values as a function of the linear pressure f_0 for load-unload cycles of 10 s and 100 s time intervals. Theoretical values are shown for a=25 μm, NA=0.2, and V=39. 134

7.9 Length- and winding pitch-dependent attenuation measurements as a function of the linear pressure. Theoretical values for a uniform and a steady state power distribution are shown for a=25 μm, NA=0.2, and V=39. 136

7.10 Microbending loss as a function of the linear pressure f_0 for V=39. Experimental results of Eccleston [187] are compared with theoretical predictions of Eq. (7.49). 138

7.11 dc-SNR vs. microbending loss for coherent illumination. L=1 km, and the number of imperfections=1000. 140

7.12 dc-SNR vs. microbending loss for different lengths of fiber (coherent source). a=25 μm, NA=0.2, V=21 and the number of imperfections= 1 per meter. 141

7.13 dc-SNR for partially coherent sources with coherence time . Microbending loss =1 dB/km, number of imperfections=1 per meter and τ_{rms}=1 ns/km. 142

7.14 Normalized loss fluctuations as a function of the microbending loss for coherent illumination. L=1 km, number of imperfections=1000 and τ_{rms}=1 ns/km. 144

7.15 Modal distortion $R_{2t/t}$ for a partially coherent source. Microbending loss= 1 dB/km, τ_{rms}=1 ns/km, Ω_m =10' rad/sec, and the number of imperfections= 1 per meter. 145

7.16 Theoretical modal distortion results as a function of microbending loss for the experimental parameters taken from Refs. [140],[189]. N_b denotes the number of fiber imperfections. 148

7.17 Experimental data on $R_{2t/t}$ as a function of the microbending loss. Theoretical curves have been drawn for the values of the parameters listed in Table 7.3. N_b denotes the number of fiber imperfections. 149

LIST OF SYMBOLS

a	fiber core radius
a_μ	rapidly oscillating amplitude of mode μ
A	magnitude of the refractive index fluctuation
A_μ	slowly varying amplitude of mode μ
$b(z)$	core-cladding interface distortion
$B(\theta)$	power spectrum of $b(z)$
c	velocity of light in vacuum
$C_{\mu\nu}$	coupling coefficient between modes μ and ν
$[C]$	mode coupling matrix with coefficients $C_{\mu\nu}$
d	spacing between fiber ends; average length of fiber imperfections
D	correlation length of the random bends
$\vec{D}$	displacement density
$\vec{E}$	electric field vector
E_j	elastic modulus
$E_{\mu t}$	transverse electric field distribution of mode μ
f	optical frequency
f_m	modulation (rf) frequency
$f_\bullet$	linear pressure
$f(z)$	distribution function of the refractive index fluctuations
$f(\omega)$	spectral component of wave form
$F_{\mu\times}$	interference coefficient between modes μ and $\times$
$[F]$	transmission matrix with coefficients $F_{\mu\times}$
$F_s(\theta)$	Fourier sine transform of $f(z)$
$G(\Delta\omega)$	autocorrelation function of the source

H	Hermitian
H_e	effective stiffness of the fiber and the jackets
$\vec{H}$	magnetic field vector
$H_m(x)$	Hermite polynomial
$H(a,b;c,z)$	Hypergeometric series
i	integer value, increment
$I(r)$	near-field intensity distribution
I_{th}	threshold current
j	imaginary unit ($=\sqrt{-1}$)
$J_n(x)$	Bessel function of order n
k	wave number in free space
k_m	wave number in region m ($=n_m k$)
$K_{\mu\nu}$	mode coupling coefficient for the transverse index distortion
l	integer value, circumferential mode number
L	fiber length; propagation length
L_o	length of ideal fiber in between sections of imperfect fiber
L_c	coherence length
$L_q^{(l)}$	generalized Laguerre polynomial
m	compound mode number; modulation index
M	highest compound mode number
M_l	number of longitudinal modes of emission
n	refractive index
n_1	refractive index on the axix of the fiber (at $r=0$)
n_2	cladding refractive index
N	total number of guided modes

N_b	total number of fiber imperfections
p	integer value, radial mode number
P	total power in all fiber modes
P_μ	power of mode μ
P(t)	modulated power leaving the source
q	integer value . (one less than the radial mode number)
r	radial coordinate
R	autocorrelation function of the fiber imperfection
$R_{2f/f}$	relative second harmonic distortion
$R_{3f/f}$	relative third harmonic distortion
t	time
T	transpose
$\vec{u}$	unit vector
V	normalized frequency parameter
V_g	group velocity
w_o	beam or mode radius
W	modal power weights
x	Cartesian coordinate
y	Cartesian coordinate
z	Cartesian coordinate; cylindrical axial coordinate
Z	distance of an imperfection from the source

α	exponent of power-law profile
β	phase constant
γ	attenuation constant
γ_t	total fiber attenuation
$\Gamma(\ )$	power spectrum of the source auto-correlation function $G(\Delta\omega)$
δ	Dirac's delta function
$\delta(\eta)$	standard deviation of the efficiency
Δ	relative index difference
Δa	transverse offset between axes
$\Delta\beta$	difference between phase constants
$\Delta\tau$	delay difference over fiber length L
$\Delta\nu$	spectral bandwidth
η	efficiency
ε	permittivity
ε_1	Neumann number
ε_r	relative permittivity
θ	angle between fiber axes (tilt angle); phase angle
Θ	spatial frequency, mechanical frequency of fiber deformation
Θ_{max}	maximum acceptance angle
Θ_N	normalized tilt
λ	wavelength
μ	permeability
σ	standard deviation of f(z)
$\sigma(\eta)$	variance of the efficiency
τ	group delay per unit fiber length
τ_c	source coherence time
τ_{rms}	root mean square intermodal delay over fiber length L
$\tau_{\mu\nu}$	modal delay difference between modes μ and ν
τ_g	group delay
ϕ, Φ	phase angle; cylinder coordinate,
$\Phi(\ ), \Phi(\ )$	power spectrum of f(z)

ψ	phase angle
$\psi(r)$	wave function
ω_c	center frequency (angular) of emission
$\Omega(t)$	modulated optical frequency (angular)
Ω_m	maximum frequency (angular) deviation of the laser diode from the center frequency of emission
$< >$	average value
∇^2	Laplacian

LIST OF ABBREVIATIONS

AG	air gap
APD	avalanche photodiode
CPC	composite protective coating
DSN	Deep Space Network
e.m.	electromagnetic
EXPT.	experiment
IM	index-matched gap
LD	laser diode
LED	light emitting diode
LG	Laguerre-Gauss
LP	linearly polarized
NA	numerical aperture
OTDR	optical time domain reflectometer
POM	polyoxymethylene
PVC	polyvinyl chloride
SS	steady state (modal power distribution)
TEM	transverse electro-magnetic
TH.	theory
U	uniform (modal power distribution)

CHAPTER I

INTRODUCTION

The serious pursuit of guided wave optical communications dates back to 1966, when Kao and Hockham [1] of Standard Telecommunications Laboratories in England speculated that glass fiber losses as low as 20 dB/km should be achievable. Because of the immense bandwidth potential of optical fibers, many leading laboratories then mounted a broadly based research effort in optical transmission materials and devices [2]. Optical fiber telecommunications became technologically possible in 1970 when workers at Corning Glass Works [3] produced the first communication-grade fiber with loss under 20 dB/km. In 1977, prototype fiber-optic links were put to work for the first time carrying live telephone traffic for the Bell System and General Telephone [4]. Today, telephone companies around the world are routinely installing fiber-optic links along vital routes [5],[6].

1.1 Components of Fiber-optic Systems

Like any communication system, a fiber-optic link includes a transmitter, a transmission medium, and a receiver. Fiber-optic links are designed to accept input signals and produce output signals in standard electrical formats but, inside the transmission medium, the signal propagates in the form of light.

The transmitter consists of a light source and its modulator. At present, Light Emitting Diodes (LED) and semiconductor laser diodes (LD) are the most suitable light sources for optical fiber telecommunications. The LED emits incoherent light and has a quite linear relation between current and light output. The linearity can be within a few per cent. The fundamental type of LED for optical communication is the surface-emitting type. The three main limitations of this device with respect to wide-band networks are low power coupled into the fiber, limited modulation bandwidth and significant spectral width [7]. The prime advantages of a LD are its capability for direct modulation into the GHz range, its ability to launch in the order of 1 mW into a standard graded-index fiber and its small spectral width of 2 nm or less. An inherent complication of the LD is its temperature-dependent threshold current. This can, however, be compensated for with fairly simple control circuitry [7].

The principal component of the fiber-optic transmission channel is the fiber; for an operational system it is, however, also necessary to consider the loss and noise characteristics of

the optical connectors, splices, and other passive components such as isolators, couplers, power splitters, etc. The fiber is basically a light-guidance system (dielectric waveguide), and is generally cylindrical in shape. It consists either of a core of transparent dielectric material of refractive index n_1, whose walls are in contact with a second dielectric material of a lower refractive index n_2 (step-index fiber), or else a core whose refractive index becomes progressively lower away from the center (graded-index fiber). The fiber confines and guides light along its axial length with minimal loss by total internal reflection inside its core. Optical fibers are incorporated into a cable assembly, which provides tensile strength, external protection, and handling properties comparable to those of equivalent-diameter coaxial cables. Splicing is required to permanently join two fibers, whereas connectors are employed for frequent demounting and reconnection. These connectors are essential elements of a repeater station and are the terminals of rearrangeable optical patch-cords or of plug-in electronics boards containing LDs or optical detectors [2].

At the receiving end of a fiber-optic system, a photodetector converts optical power input to an electric current output; this can either be a PIN diode or an avalanche photodiode (APD). The principal figure of merit for a receiving system is the minimum input optical power needed to achieve a given performance level at a given information rate. This receiver sensitivity is a function not only of the optical detector, but also depends critically on the characteristics of the preamplifier.

1.2 Noise and Nonlinear Distortions due to the Transmission Channel

The noise performance of a fiber-optic system is usually determined by a combination of several types of shot noise [8], thermal noise [8], excess noise in multiplication [8], and source noise [7]. However, when laser diodes are used as the source, noise and nonlinear distortion can occur due to three additional effects: longitudinal mode partitioning, reflections back into the LD, and mode selective loss mechanisms (see Fig. 1.1) along the transmission channel [9].

Partition noise occurs because of fluctuations in the partitioning of different lasing modes in the total laser light output. These fluctuations are not observed when the lasing spectrum is detected uniformly, but they cause considerable distortion at the receiving end of a fiber exhibiting material dispersion. Different lasing modes then suffer different delays

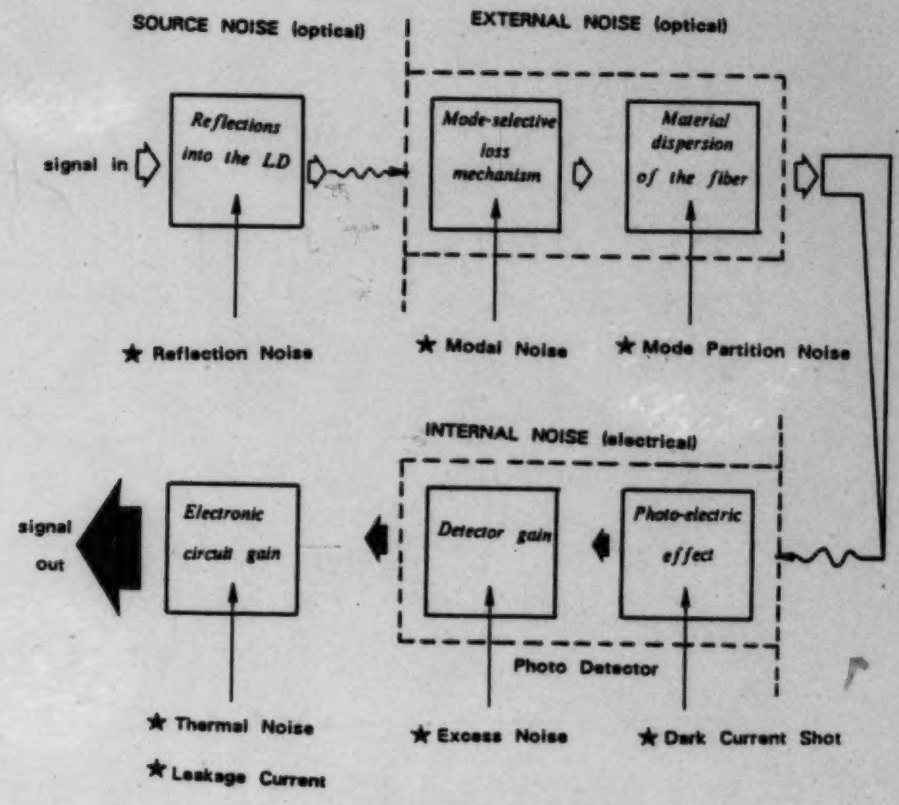

Figure 1.1 Noise sources in a fiber-optic communication system.

through the fiber, and hence the fluctuations of different lasing modes are separated in time and no longer compensate [10]-[12].

When a part of the LD output power launched into the fiber is fed back due to reflection at coupling lenses, the fiber endface, or connectors, the LD light begins to fluctuate at frequencies that are multiples of the reciprocal round-trip time (i.e., external cavity between the LD and the discontinuity where reflections occur) [13],[14]. This disturbs the dc power [15], the linearity of the laser [16], the noise distribution [17]-[21], the frequency response [22],[23], and may cause bit-errors [24]. To reduce the optical feedback to a tolerable level, an optical isolator may have to be inserted between the laser and the fiber, with the drawback of additional cost and insertion loss [25].

Modal noise is an undesired amplitude modulation generated at points along the transmission channel where mode-selective losses occur [26] (see Fig. 1.2). Such mode-selective loss can occur in splices and connectors, most types of couplers [27], poor fiber-to-detector coupling [28], and even due to microbending of the fiber axis [29],[30]. Modal noise is directly related to the coherence properties of the source and the propagation properties of the employed fibers [26], and has been shown to degrade the bit error rate (BER) of digital systems [31] and the signal-to-noise ratio (SNR) in analog systems [32]. Nonlinear distortions (modal distortions) also arise in analog systems because current modulation of a laser diode yields not only modulation of the optical power but also of the emission frequency [33]. This latter effect modulates the mode selective loss, yielding nonlinear transmission behavior [34]. The investigation in this thesis is restricted to the twin problems of modal noise and distortion, since they exert a significant influence on system performance [35].

1.3 Historical Review

The problem of modal noise has received much attention since it was first identified by Epworth in 1978 [26]. It has been analysed using modal theory as well as speckle theory. Using modal analysis, Petermann [34],[36]-[38] has theoretically modeled the wavelength-dependent transmission at connectors. Experimental and theoretical investigation of modal distortion has been performed by Olesen *et al.* [28],[39],[40], and Jintong and Peida [41]. Using wave theory and Fourier optics, Pask [42] studied the modal noise due to the connector proposed by Culshaw [43]. Heckmann [44],[45] has analysed the polarization modal

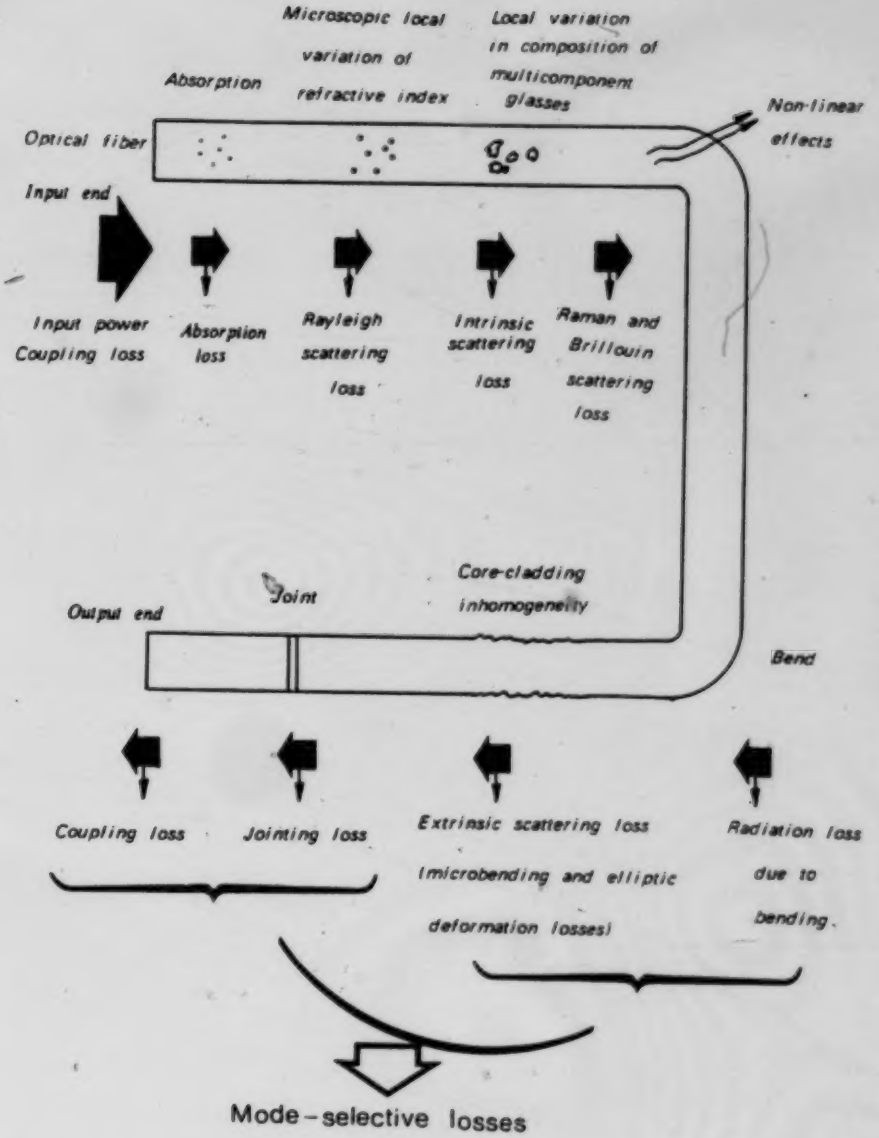

Figure 1.2 Transmission loss mechanisms in an optical fiber. Modal noise occurs due to the mode-selective losses shown in the figure.

noise due to splices in single mode fibers operated either below or above cut-off. Based on speckle theory, modal noise has been studied by Daino *et al.* [46],[47], Hjelme and Mickelson [48], Hill *et al.* [49],[50], Kanada and Aoyama [51], Rawson *et al.* [30],[52]-[54], and Weierholt *et al.* [55]. Some of the techniques that have been suggested to reduce modal noise and distortion include 'superimposed pulse modulation' (Sato and Asatani [56]), 'frequency dithering' (Vanderwall and Blackburn [57],[58]), 'coherence length reduction' (Khoe *et al.* [59]) and 'focused beam spot excitation' (Saijonmaa and Halme [60]); each of the techniques mentioned has its own limitations [57],[60].

The power loss analysis for coupling between fibers has been attempted by ray theory and also by modal theory. Using ray theory, coupling losses were quantified by Young [61], Di Vita and Vanucci [62], Gloge [63], Miller [64] and Mettler [65],[66], Thiel and Hawk [67], Neumann and Weidhass [68], and Opielka and Rittich [69]. The application of modal theory to the connector loss analysis is not new. As far back as 1964, Kogelnik [70] had formulated the transformation laws of Laguerre-Gaussian beams in order to study mismatch problems in optical resonators and periodic sequences of lenses. This approach was extended by Marcuse [71] to study the excitation of parabolic-index fibers by incoherent sources as well as to determine single mode fiber splice losses [72]. Coupling between single mode fibers has also been investigated by Cardama and Kornhauser [73], Guttman and Krumpholz [74], Gambling *et al.* [75], Hosain *et al.* [76], Wagner and Tomlinson [77], Cook *et al.* [78], Murakami *et al.* [79], and Bisbee [80]. Recently, Tokiwa *et al.* [81] have examined the joint characteristics between polarization maintaining single mode fibers.

Cherin and Rich [82] were the first to show how the measured transmission loss of a splice in a fiber optic system can be significantly affected by the type of source used, the source's location relative to the splice, and the characteristics of the fibers on either side of the splice [83]. The mode mixing effects giving rise to a 'long-length' splice loss [84] were investigated by Kummer [85],[86] and by White and Mettler [87]; the latter used Laguerre-Gauss mode matching to calculate the loss due to parameter mismatch and axial offset between multimode parabolic-index fibers. With a different approach, mode conversion effects at graded-index fiber splices were further examined by Kitayama *et al.* [88] using a mode transfer matrix, and by Meron and Marom [89] using a geometric analysis. Joint loss dependence on mismatch parameters in graded-index fiber splices has been investigated by

Coppa *et al.* [90].

A modal analysis of the offset and tilt losses for fiber splices was carried out by Sakai and Kimura [91] using a staircase function to approximate the refractive index profile; loss evaluations were, however, restricted to the case of a dual mode fiber, since numerical integrations were involved. Again, using a modal approach, Rizzoli and Someda [92], and Kashima [93],[94] approximated the fiber modes by Hermite-Gaussian functions to theoretically investigate the transmission loss and mode mixing effects at parabolic-index fiber splices. In Ref. [94], the modal power distribution in the transmitting fiber is described by a trial function, and that used by Daido *et al.* [95] and Shigesawa *et al.* [96] is based on near-field pattern measurements. In addition to these theoretical investigations of the splice loss, several experimental results have been reported (see [97] for complete lists), which are not, however, comparable due to different experimental conditions, such as different lengths of optical fiber, different sources, use of mode strippers, etc. [84].

So far, the existing literature on power loss, modal noise and distortion due to fiber-fiber connections have been discussed. To study mode coupling (both weak and strong) and microbending in single and multimode fibers, modal theory has been employed, quite successfully and rather extensively. Differential equations for the average power in randomly perturbed waveguides were first derived by Young [98] and solved for the propagation of optical waves in hollow dielectric and metallic tubes by Bergeest and Unger [99]. A coupled mode theory describing mode coupling due to random bends has been developed by Marcuse [100] and has been applied to the study of a step index fiber [101], a parabolic index fiber [102], and fibers having a more general class of index profiles [103]. This theory also gives a first estimate of the power fluctuations (in an ensemble sense) that occur when the power in a subset of fiber modes is considered [104].

The distortion losses caused by microbending in a fiber cable were analysed by Olshansky [105],[106]; he also studied the excess loss produced by random perturbations whose longitudinal spatial frequencies were below the range required for mode coupling in optical fibers [107],[108]. Curvature coupling and power spectra of random bends in single mode fibers and cables have been investigated by Gambling and Matsamura [109], Petermann [110]-[113], Furuya and Suematsu [114], Blow *et al.* [115] and Danielsen [116]. Bend behavior of polarising optical fibers has been examined by Varnham *et al.* [117]. Experimental and

theoretical investigation of strong mode coupling has been performed by Jeunhomme and Pocholle [118]-[120] for a dual mode step-index fiber. Many authors have also used the ray theory to carry out leaky ray analysis in optical fibers and thereby predict bending losses. They include Gloge [121], Rousseau and Arnaud [122], Love and Pask [123], Snyder [124], and Winkler *et al.* [125].

Cherin and Murphy [126] used a quasi-ray analysis to quantify crosstalk between multimode optical fibers, and also to determine the effects of lossy coatings on the transmission energy in a multimode step-index fiber [127]. The plastic deformation of such fiber coatings under lateral force was investigated by Hannay [128] and more recently by Katsuyama *et al.* [129]; nylon buffering effects have been examined by Tatekura *et al.* using a variational method [130]. The effect of fiber packaging on transmission loss was studied theoretically by Gloge [131], and verified experimentally by Gardener [132]. The transmission properties of optical fiber before and after cable manufacture have been investigated experimentally by Buckler *et al.* [133], and Yamamoto *et al.* [134], and that due to cable laying and burying by Kojima *et al.* [135]. Yoshizawa *et al.* [136] have investigated the optical-loss change due to excess shrinkage of nylon-jacketed optical fibers after heating.

Tanifuji and Tokuda [137] have predicted that interference of nonorthogonal field vectors for different modes at the receiving face of the detector, in association with oscillation frequency fluctuations of the laser diode, can give rise to amplitude fluctuations in long multimode fibers. Piazzolla *et al.* [138] have reported on low frequency signal fluctuations in an optical cable laid underground, probably caused by vibrations and thermal and mechanical stresses. Zeidler and Schicketanz [139] have shown that statistical mode mixing along the fiber line can smooth out the fluctuations of the input field distribution of laser diodes with filamentary emission patterns. Stubkjaer [140] has observed harmonic distortion of light signals transmitted via long multimode graded-index fibers, the origin of which is still unknown, because Meslener's [141] dispersion-induced distortion theory has been unable to explain it. In this thesis, a theoretical explanation is presented for Stubkjaer's experimental results.

1.4 Research Objectives

The main aim of this thesis is to give a systematic description of the mode selective loss mechanisms in fiber-optic communication systems, and then to study the modal noise and distortion characteristics in detail. In view of this, the following research objectives are identified:

1. To analyse the loss, modal noise and distortion caused by axial, angular and longitudinal misalignments between two near-parabolic multimode fibers; to examine the dependence of these quantities on the wavelength, numerical aperture, index-matching and source coherence, and to compare the results for a uniform modal power distribution with those obtained using a steady state power distribution.
2. To experimentally verify (i) the loss and modal distortion predictions in (1) and (ii) the dependence of modal distortion on, (a) the modulation frequency of the source, and (b) the quality of the cleave of the coupled fiber endfaces.
3. To compute and verify the power loss due to microbending by a power diffusion approximation (assuming the highest order guided modes to be leaky).
4. To investigate and verify the length dependent attenuation and the dynamic loss characteristic of jacketed fibers.
5. To theoretically model the modal noise and distortion characteristics for microbending in the presence of mode-mode interference in parabolic-index multimode fibers, and thereby explain Stubkjaer's [140] measurements.

There are two reasons for restricting the analysis primarily to parabolic-index multimode fibers. Firstly, they have a high information carrying capacity and are in widespread use. Secondly, compared with step-index multimode fibers, they support fewer modes and have far less intermodal dispersion, two properties which enhance modal noise [42] and make it readily measurable. This enhancement of modal noise is also achieved by using a single-longitudinal mode laser which is more coherent than its multimode counterpart [33]; the other advantage is that mode partion noise is avoided [11].

The theoretical study presented in this thesis uses modal analysis, because of the accuracy and versatality of such an approach. Ray theory can only predict the loss; it is unable to quantify modal noise and distortion in fiber systems. Besides, the ray approximation becomes inaccurate [142] when the number of modes guided by the fiber is small. Speckle

theory, as applied to fiber connectors, has not yet matured to the stage where it can predict either of the three items, namely: loss, modal noise and distortion for partially coherent illumination as well as a steady state power distribution [46]-[55]. So far, speckle theory has only successfully predicted the dc-modal noise values for coherent excitation and a uniform power distribution [49].

Perhaps the only drawback of modal analysis is that it is necessary to calculate a large number of mode coupling terms (the number of terms increases as the square of the number of guided modes in the fiber). This could take considerable computation time (although many of the coupling terms vanish), depending on the type of mode selective loss mechanism. However, this requirement should not be a serious limitation when a closed form solution to the mode coupling (or the overlap) integral exists, as in the case of a parabolic-index fiber with an unlimited profile (also called the infinite square law medium). In this thesis therefore, the modes of the truncated parabolic profile will be approximated by the Laguerre-Gaussian modes of the infinite square-law medium [71],[143]. The grounds on which this assumption is made will be discussed in detail in Chapter 2.

1.5 Thesis Organization

Chapter 2 provides a review of the fundamentals of wave propagation in fibers and other basic properties, namely, attenuation, numerical aperture (NA), and dispersion. Sources of loss for connectors and splices are identified. An in-depth qualitative treatment of the phenomenon of modal noise and distortion is also presented.

An electromagnetic modal theory is presented in Chapter 3 to analyse the power loss, modal noise and distortion due to connector offsets (axial, longitudinal and tilt). An analytical expression is derived for the steady state power distribution across the transmitting fiber's cross-section just before the connector.

In Chapter 4, Hermite-Gauss mode matching is used to calculate the modal amplitude coupling coefficients for the case of an axial offset at a splice/connector. These coefficients are similar to the ones derived by Petermann [34], but are slightly different from those found by Kashima [94]. The theory in the previous chapter is employed to calculate the power loss, modal noise and distortion for this case. Experimental results are presented and compared with the theory. The effect of the modulation frequency and fiber cleave quality on the modal

distortion is also discussed.

In Chapter 5, the case of a longitudinal gap between two multimode fibers has been considered. The diffracted Laguerre-Gaussian (LG) beams of the transmitting fiber are matched to the receiving fiber LG modes to yield the modal amplitude coupling coefficients for a gap [70],[175]. The power loss, modal noise and distortion are then evaluated numerically using the general theory developed in Chapter 3, both for an index matched gap and for an air gap (for the case of a uniform as well as a steady state power distribution), and verified experimentally. The modal noise and distortion values at a given loss are compared for the axial and the longitudinal misalignments.

Chapter 6 deals with a tilt offset between two multimode fibers; the mode coupling coefficients are evaluated by LG mode matching using the overlap integral formulated by Sakai and Kimura [91]. The power loss and modal distortion results (calculated using the theory of Chapter 3) are shown to be in good agreement with experimental measurements made with a long, spliced input fiber. For a given loss and source coherence specification, the modal noise and distortion results for all the three geometrical misalignments (from the results of Chapters 4 and 5) are then compared.

In Chapter 7, a modal analysis of the loss, noise and distortion due to fiber imperfections is performed. The theory is based on a power diffusion approximation and on the assumption that the highest order guided modes are leaky. Experimental results on the power loss are shown to be in close agreement with the theory. Further, the modal distortion predictions of the theory are verified by Stubkjaer's [140] measurements. Theoretical and experimental results are also presented for the length-dependent attenuation and dynamic loss characteristics of jacketed fibers.

The concluding Chapter 8, summarizes the findings of this study, and presents suggestions for further work. The noise and distortion characteristics of different mode selective loss mechanisms are compared for different source and fiber parameters. The implications of time-dependent microbending statistics on the phase stability are discussed. Suggestions are made regarding optimization of certain system parameters (e.g., wavelength of transmission, source coherence, modal power distribution etc.) in order to minimize modal noise and distortion in fiber-optic communication systems.

CHAPTER II

REVIEW OF BASIC PROPERTIES OF OPTICAL FIBERS AND CONNECTORS

The theory of optical fibers is well understood and has been described in several books [144]-[153] and tutorial papers [154]-[156]. This chapter however, attempts to give a simplified description of those characteristics which are directly relevant to the work in this thesis, namely, the modal properties, guided mode attenuation, dispersion and numerical aperture. The proper design of a communication system using optical fibers as the transmission medium requires a knowledge of the transmission characteristics of the connectors and splices used to join lengths of fiber. Thus, intrinsic and extrinsic connector loss parameters are also discussed in this chapter, followed by a qualitative description of the phenomenon of modal noise and distortion.

2.1 Optical Fiber Characteristics

Optical fibers may be classified into two categories on the basis of their modal properties, namely, singlemode and multimode fibers. A mode is an allowable field configuration that satisfies Maxwell's equations and all of the boundary conditions of the problem. Multimode fibers usually have many hundreds of modes at the wavelength of operation; they may have step- or graded refractive index profiles. Step index, single- or multi mode fibers are the simplest fibers structurally. They consist of a lower index cladding region surrounding a higher index core region, with abrupt boundaries between the core and the cladding. The cladding refractive index greatly affects the light-guiding properties of the fiber. The cladding also adds mechanical strength to the fiber and reduces scattering loss due to dielectric discontinuities. To protect the guiding region from absorbing surface contaminants with which the fiber may come in contact, a coating is added while the fiber is being drawn.

The core/cladding index discontinuity factor (also called the relative index difference)

$$\Delta = \frac{n_1 - n_2}{n_1} \tag{2.1}$$

where n_1 is the refractive index at the center of the core and n_2 denotes the refractive index of the cladding, is usually made only a fraction of a percent ($\Delta << 1$). Using a small Δ permits a core radius to be used that is large compared to a wavelength, which is more convenient and

furthermore, for multimode fibers tends to reduce the optical path length difference of the different modes (i.e., reduces the delay dispersion), thus increasing the usable bandwidth. Fibers with a small Δ are called 'weakly guiding fibers', because the modes are only weakly bound to the fiber i.e., the modal evanescent fields extend further out into the cladding than for a large index step at the core-cladding boundary.

In the case of graded index fibers, the index of refraction follows a power law in the radial direction

$$n^2(r) = n_1^2 \left[1 - 2\Delta\left(\frac{r}{a}\right)^{\alpha}\right] \quad , \quad 0 \leq r \leq a \tag{2.2}$$

where a is the core radius of the fiber, r is the radial distance from the fiber axis and α denotes the exponent of the refractive index profile. Graded index fibers act as a continuous focussing medium that continually refocuses the beam as it travels along the fiber. This refocusing tends to reduce the delay dispersion, resulting in a higher bandwidth when compared with multimode step index fibers. In this thesis, both the theory and experiments involve near-parabolic-index fibers (α close to 2). Field solutions for the modes in such fibers are derived in the next section.

2.1.1 Field Solutions for Modes in a Parabolic-Index Profile Fiber

In cylindrical coordinates (r,ϕ,z), the following system of second-order partial differential equations (derived from Maxwell's equations [84]) holds for the components of the time-harmonic electric field vector $\vec{E}$ [157]:

$$\nabla^2 \vec{E} + n^2(r)\, k^2 \vec{E} = -\nabla \{ \vec{E}\, \nabla_r [\log_e n^2(r)] \} \tag{2.3}$$

where

$k = \omega(\mu_0 \varepsilon_0)^{\frac{1}{2}}$ = free space wave number

$\omega = 2\pi f$ = angular frequency

μ_0 = magnetic permeability of free space

ε_0 = dielectric permittivity of free space

$\nabla_r (n^2) = \vec{u}_r \frac{\partial n^2}{\partial r}$ = gradient in radial direction

$\vec{u}_r$ = unit vector in the radial direction

If the refractive index changes only gradually in the radial direction, the term on the right-hand side of (2.3) remains small and can be neglected. The vector equation (2.3) may then be separated into three scalar wave equations, one for each Cartesian component of $\vec{E}$. For its x-component, E_x

$$(\nabla^2 + n^2(r)k^2)\ E_x = 0 \tag{2.4}$$

This scalar wave equation is solved for guided modes of the graded-index fiber by letting

$$E_x = \Psi(r) \begin{Bmatrix} \cos & \ell\phi \\ \sin & \ell\phi \end{Bmatrix} e^{-j\beta z} \tag{2.5}$$

The z-dependence according to $\exp(-j\beta z)$ in this product postulates a wave that propagates with a phase constant β radians/meter along the fiber when harmonic time dependence is assumed. The periodic ø-dependence according to cos lø or sin lø with integer values of l defines the circumferential order l. Introducing the trial solution (2.5) into the wave equation (2.4) and separating the variables results in the following ordinary differential equation for the function $\Psi(r)$

$$\frac{d^2\Psi}{dr^2} + \frac{1}{r}\frac{d\Psi}{dr} + k_r^2\Psi = 0 \tag{2.6}$$

The separation constant k_r is given by

$$k_r = \left[n^2(r)\ k^2 - \beta^2 - \frac{\ell^2}{r^2} \right]^{\frac{1}{2}} \tag{2.7}$$

The equations derived so far hold for any axially symmetric index profile that has a gradual index change in the radial direction, but no index change in the longitudinal direction. As discussed earlier, we restrict the analysis to parabolic-index fibers. We now also let the parabolic distribution with $\alpha=2$ in (2.2), extend in the radial direction without limit, instead of being truncated at r=a. This approach saves extensive numerical work [71],[157], without seriously affecting the accuracy of the solution. In such an unlimited parabolic profile (also called an infinite square law medium) the refractive index vanishes at

$$r = a/\sqrt{2\Delta} \tag{2.8}$$

and turns imaginary for larger radii. We are, however, not concerned with this region, since the fields of those solutions which are of practical interest do not extend out as far as this radius. With the radial wave number k_r of the unlimited parabolic profile given by

$$k_r = \left[n_1^2 k^2 \left(1 - 2\Delta \left(r/a\right)^2\right) - \beta^2 - \frac{\ell^2}{r^2} \right]^{1/2} \tag{2.9}$$

the differential equation (2.6) assumes a form that corresponds to the equation of a parabolic cylinder [157]. Solutions of this equation are of the form

$$\Psi(r) = \left(\frac{\sqrt{2}r}{w_0}\right)^{\ell} \quad L_q^{(\ell)} \left(\frac{2r^2}{w_0^2}\right) \quad e^{\frac{-r^2}{w_0^2}} \tag{2.10}$$

where $L_q^{(l)}(\ )$ represents the generalized Laguerre polynomial of order l and degree q; l as well as q assume only integer values, with l as the number of zeros in the azimuthal direction ø and q in the radial direction r. $L_q^{(l)}(u)$ is given by the polynomial

$$L_q^{(\ell)}(u) = \sum_{n=0}^{q} \frac{(-u)^n}{n!} \frac{(q+\ell)!}{(2\ell)!\ (q-\ell)!} \tag{2.11}$$

The beam radius w_0 is defined by [157]

$$w_0 = \left(\frac{a}{n_1 k}\sqrt{\frac{2}{\Delta}}\right)^{1/2} \tag{2.12}$$

and determines how far the fields extend in the radial direction. Fig. 2.1 shows the field distribution $\Psi(r)$ as a function of r for typical fiber parameters ($a=25\ \mu m$, $n_1=1.47$, $\lambda=0.82\ \mu m$, $\Delta=0.01$ and $w_0=5.6\ \mu m$) for l=q=0, l=1 and q=0, l=0 and q=1, and l=q=1. Beyond $r=w_0$, (2.10) decays quite rapidly to extremely small values at radii which are only little larger than w_0. The beam radius w_0 is related to the normalized frequency V of the parabolic-index fiber by [157]

$$V = 2\left(\frac{a^2}{w_0^2}\right) = kan_1\sqrt{2\Delta} \tag{2.13}$$

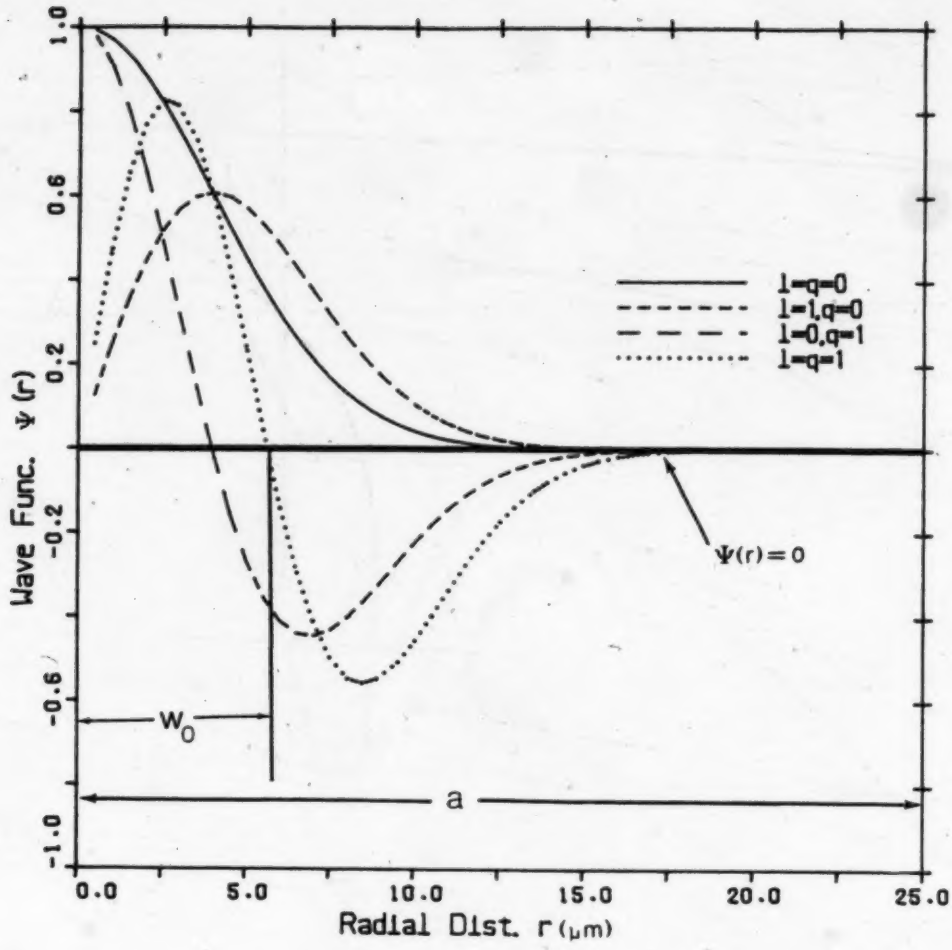

Figure 2.1 Field distribution ψ (r) as a function of the radial coordinate r. Fiber radius $a = 25\ \mu m$ and beam radius $w_0 = 5.6\ \mu m$.

For weakly guiding fibers, the longitudinal field is small compared to the transverse field. The total field under these conditions is nearly entirely transverse electromagnetic and, locally, it has the characteristics of a uniform plane wave. The polarization of this field is nearly linear and uniform over any fiber cross-section. Hence these guided modes are designated as linearly polarized (LP_{lp}) modes [158]. The index values l and p represent the circumferential and radial order of the mode, respectively. The radial order p is related to the degree q of the Laguerre polynomial of the radial field distribution by $p=q+1$. There are four LP_{lp} modes for each set of integers l and p ($l \neq 0$). Two of these modes are polarized in the x-direction and the other two in the y-direction. Each of these pairs has two different circumferential orientations of the field distribution, depending on whether cos lø or sin lø is used in (2.5).

Fig. 2.2 (a) illustrates these four different versions of transverse field polarization and distribution for the simple example of the LP_{11}- mode. The solid arrows (in the fiber core cross-section) with their direction and length indicate the polarization and strength, respectively, of the transverse electric field. The LP_{11}- mode of this particular example is a combination of the HE_{21}- mode (the field distribution is shown in Fig. 2.2 (b)) with either the axially symmetric E_{01}- mode or the H_{01}- mode. Fig. 2.2 (c) and (d) illustrate these combinations of HE_{21} and E_{01} as well as of HE_{21} rotated by $\pi/4$ in its transverse field distribution and combined with H_{01} [157]. In Fig. 2.2 (d), the electric field is also polarized in the x-direction but the orientation is changed due to the replacement of cos lø by sin lø and vice versa.

The phase constant β with which a given LP_{lp} mode propagates along the fiber is obtained by substituting (2.10) in (2.6), namely

$$\beta = n_1 k \left[1 - \frac{2\sqrt{2\Delta}}{n_1 ka} (2q + \ell + 1) \right]^{\frac{1}{2}} \qquad (2.14)$$

The modal fields (2.5) approximate the modes of the parabolic-index fiber at radius $r<a$ for small values of q and l. For large values of q and l, the fields extend strongly beyond $r=a$ so that (2.10) is no longer a good approximation to the fiber modes. However, modes reaching strongly into the cladding are no longer guided by the fiber core. For this reason, (2.10) is regarded as an approximation for all '**guided**' fiber modes, with the relation

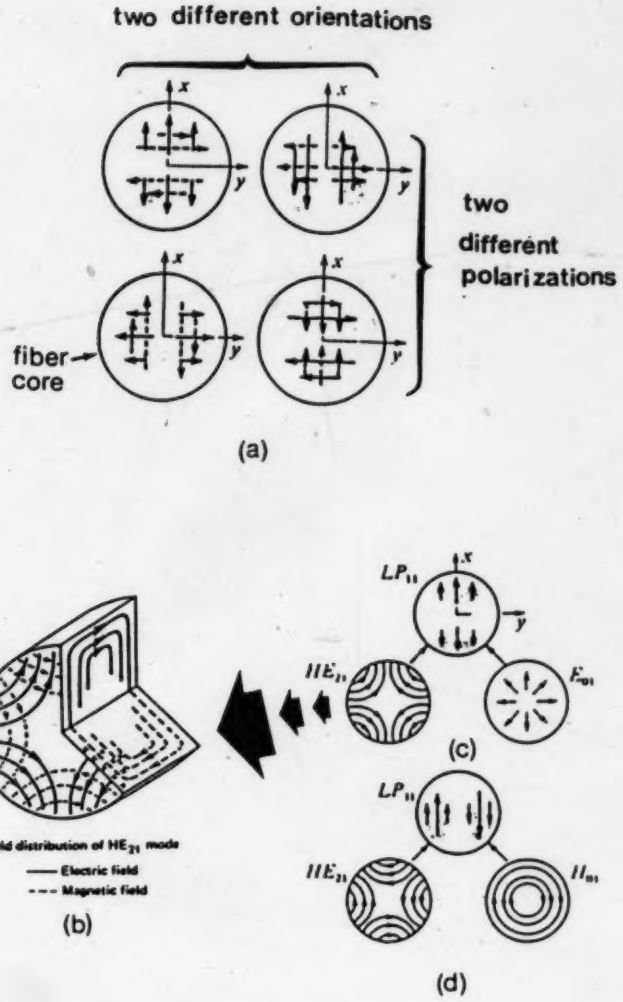

Figure 2.2 (a) Guided core modes of equal transverse orders l=p=1 with different orientation and polarization of their electric (solid arrow) and magnetic (broken arrow) fields. (b) Field distribution of the HE_{21} mode. (c) and (d) Transverse electric field and intensity distribution of two LP_{11}- modes and their composition from exact modes of the parabolic-index fiber.

$$\beta = n_2 k = n_1 (1 - \Delta)\ k \tag{2.15}$$

taken as a cutoff condition for the guided modes [71]. The total number of guided modes is obtained from (2.14) and (2.15). These two equations yield the following equation for the guided mode boundary in mode number space [71]

$$(2q + \ell + 1)_{max} = n_1 ka\sqrt{\frac{\Delta}{2}} = \left(\frac{a}{w_0}\right)^2 = M \tag{2.16}$$

where M is called the highest compound mode number. Fig. 2.3 shows the mode-number space defined by the two variables q and l. The diagonal line (the hypotenuse of the triangle) is defined by (2.16) and the guided modes lie inside the triangle shown in the figure. Eq. (2.14) shows that modes with equal values of the compound mode number,

$$m = 2q + \ell + 1 \tag{2.17}$$

have equal propagation constants. These modes lie on straight lines parallel to the diagonal line in mode-number space shown in Fig. 2.3. The total number of modes is approximately equal to four times the area of this triangle, since there are four LP_{lp} modes for each set of values q and l ($l \neq 0$). Thus, the total number of modes in a parabolic-index fiber is

$$N = (n_1 ka)^2\ \frac{\Delta}{2} = V^2/4 \tag{2.18}$$

2.1.2 Dispersion

When a narrow pulse of optical energy is injected into a fiber it will generally spread out in time as it propagates along the fiber. This behaviour is due to dispersion, and it causes the usable bandwidth of a fiber to be length dependent. There are three main causes of dispersion in a fiber; waveguide effects, material dispersion, and modal dispersion. Waveguide dispersion [84] arises principally because of the wavelength dependence of the modal 'V' number. This waveguide dispersion for waveguide modes in a multimode fiber is negligibly small for all modes not close to cutoff. Since those modes near cutoff usually carry only a small fraction of the total power and usually suffer a higher loss, the dispersion contribution from this source is generally not significant and can be disregarded [84].

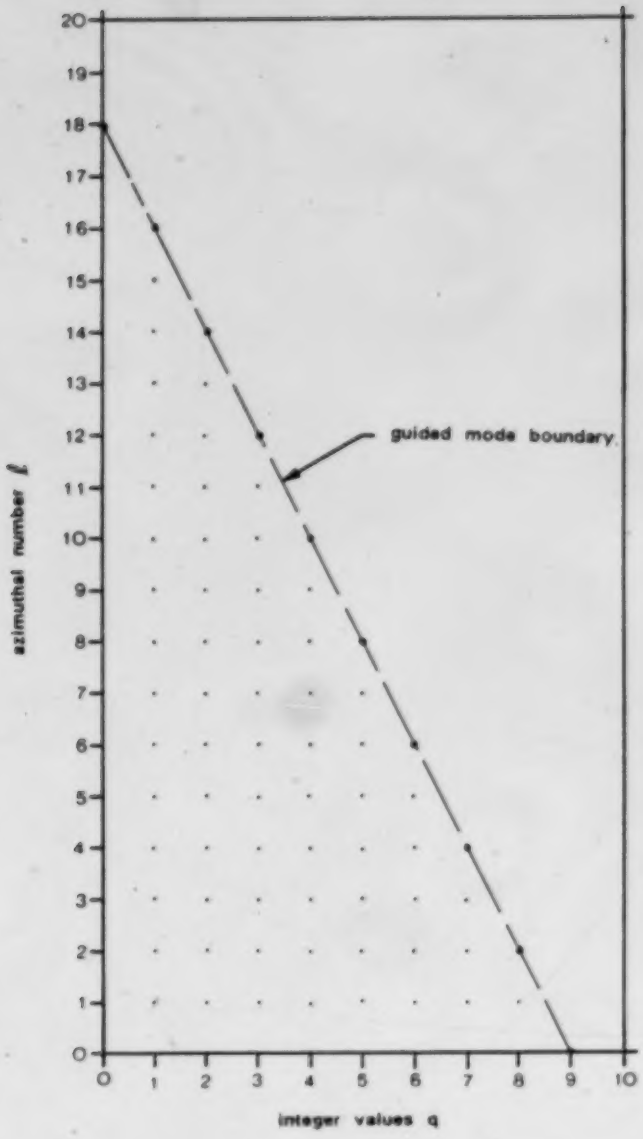

Figure 2.3 Mode-space diagram for graded-index fiber. The dots represent the guided modes.

Material dispersion may be termed intramodal dispersion and is particularly significant for single mode fibers. This source of dispersion occurs because the group velocity V_g of a mode is a function of wavelength. The pulse spreading over a fiber of length L can be shown to be given approximately by [84]

$$\Delta\tau_m = \frac{L}{c}\left(\frac{\Delta\lambda}{\lambda_0}\right)\lambda_0^2\,\frac{d^2 n_1}{d\lambda^2} \tag{2.19}$$

where $\Delta\lambda = \lambda_2 - \lambda_1$ = spread of wavelength about a center wavelength λ_0

$\Delta\lambda/\lambda_0$ = relative spectral width of the source

$\lambda_0^2\left(d^2 n_1/d\lambda^2\right)$ = dispersion of glass.

For singlemode injection lasers with narrow linewidths and operating at 1.3 μm or 1.55 μm wavelengths, material dispersion can be as low as 1 ps/km [7].

Modal or intermode dispersion is caused by the different group delays of the modes; it typically determines the bandwidth capabilities of multimode fibers. The group delay for each mode through a fiber of length L is given by

$$\Delta\tau_g = L\,\frac{d\beta}{d\omega} = \frac{L}{c}\,\frac{d\beta}{dk} \tag{2.20}$$

Neglecting the varying dispersion properties between the core and the cladding, the intermode delay spread $\Delta\tau_g$ for a graded-index fiber has been shown to be [159]

$$\Delta\tau_g = \frac{L}{c}\,n_1\left[1 + \Delta\left(\frac{\alpha-2}{\alpha+2}\right)\left(\frac{m}{M}\right)^{\frac{2\alpha}{\alpha+2}} + \Delta^2\left(\frac{3\alpha-2}{3\alpha+4}\right)\left(\frac{m}{M}\right)^{\frac{4\alpha}{\alpha+2}}\right] \tag{2.21}$$

2.1.3 Guided Mode Attenuation

Attenuation in optical fibers is due to the bulk material as well as due to waveguide imperfections. The bulk attenuation comprises: the intrinsic absorption of the basic material ; that caused by impurities in the glass; atomic defect absorption, also scattered radiated light [149].

Intrinsic scattering due to microscopic local variations of the refractive index causes a fourth-power dependence of loss on wavelength. This is the law of Rayleigh scattering and occurs when the scattering objects have dimensions small compared to the wavelength of the incident light. If the glass consists not of one but of several material components, the index of refraction varies not only due to density fluctuations frozen in at the softening point, but also to statistically random distributions of the polarizable components. This local variation in composition of multicomponent glasses causes additional scattering and loss. In addition to these two intrinsic scattering loss mechanisms, one can induce scattering through non-linear effects such as stimulated Raman and Brillouin scattering. High power levels (e.g., 500 watts for Raman scattering) are required for these effects to have a significant effect on fiber attenuation [149].

Imperfections in the waveguide structure may result in a scattering loss at the waveguide inhomogeneities (core-cladding interface not being smooth) and losses at waveguide bends. The fiber core cross-section will not be quite round nor be perfectly uniform in the axial direction; it shows some ellipticity or higher-order deviation from roundness, and its roundness will change along the fiber. In addition, a fiber will never be perfectly straight. Pulling a fiber from a preform or out of a melt results in a fairly straight structure, but further processing such as coating and cabling introduce deviation of the fiber axis from a straight line. This is called microbending. These deviations of the fiber from the perfect geometry and perfect index distribution lead to coupling among modes. They no longer propagate independently from each other, but exchange power [149].

If the fiber guides only its fundamental mode, fiber imperfections couple it to leaky modes and the radiation field. The fundamental mode loses power due to radiation and thus suffers additional attenuation. If the fiber guides many modes, some or all modes exchange power and, in addition, lose power to leaky modes and the radiation field. The interaction between guided modes changes the overall dispersion characteristics of the multimode fiber, while the radiation of power adds to its transmission loss. A detailed discussion of this latter effect is presented in Chapter 7.

2.1.4 Numerical Aperture

The numerical aperture (NA) is an important parameter, as it affects properties such as the light gathering efficiency, pulse distortion, microbending loss and curvature loss of the fiber [156]. Moreover, it enters into the determination of the normalized frequency V. The NA of a step-index fiber is defined as the sine of its maximum acceptance angle (see Fig. 2.4); i.e.,

$$NA = \sin \theta_{max} = (n_1^2 - n_2^2)^{\frac{1}{2}} \simeq n_1 \sqrt{2\Delta} \tag{2.22}$$

In (2.22), the effect of skew rays has been ignored [160]. When measurements of NA are made on short fiber lengths, higher order guided modes and leaky modes may be present, the effect of which is to increase the measured NA. These modes suffer a higher rate of attenuation, so the effective NA decreases with increasing distance [156].

For graded index fibers, the light incident on the core at a radial distance r from the fiber axis will propagate as a guided mode only if it is within the local numerical aperture NA(r) at that point. This is given as [160]

$$NA(r) \simeq n_1 \sqrt{2\Delta} \left[1 - \left(\frac{r}{a} \right)^{\alpha} \right]^{\frac{1}{2}} \qquad 0 \leq r \leq a \tag{2.23}$$

The graded index fiber NA thus decreases as one moves away from the fiber axis.

2.2 Operating Wavelength

In practice, optical fibers are designed for use at certain wavelengths, since the attenuation and the dispersion characteristics of the fiber are different at different wavelengths. The optical wavelengths used most widely so far are in the 0.8-0.9 μm range, due to the ready availability of suitable components. The next ones available are in the 1.3 μm and 1.5-1.6 μm range. Efforts are also underway to develop practical mid-infrared fluoride glass optical fibers, which would transmit at wavelengths as long as 6-8 μm, much longer than the 1.6 μm cutoff of silica glass fibers [4]. In this thesis, theoretical results have been derived for different wavelength regions of interest. Since V is wavelength dependent, the theory uses V as an independent parameter rather than the wavelength wherever possible.

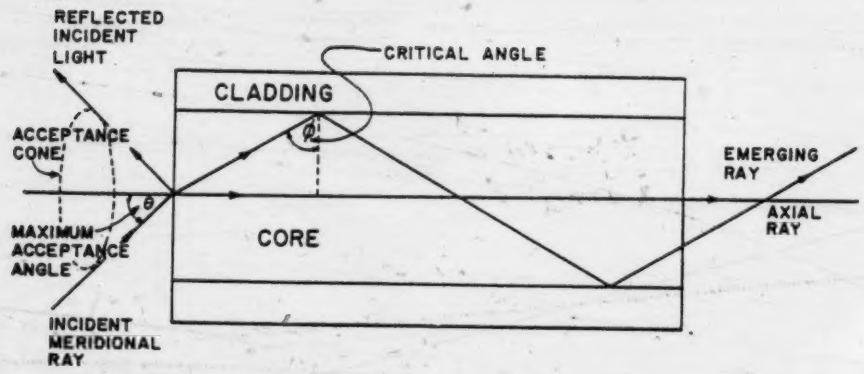

Figure 2.4 The maximum acceptance angle of a step-index fiber.

2.3 Fiber Connectors and Splices

Depending on the application, two jointing techniques are used for optical fibers. A permanent splice is usually employed whenever two fibers are joined to form a link. A connector is usually employed whenever the fiber joint has to be readily demountable. This situation typically arises at the interface of an optical cable with a receiver or a transmitter, and in laboratory experiments. The primary objective in making a connection is to join two optical fibers with minimum possible insertion loss. This loss is divided into two groups: (1) intrinsic losses, and (2) extrinsic losses.

Intrinsic losses are due to differing characteristics of the optical fibers at the jointing point, while the extrinsic losses originate from inaccuracies in the execution of a joint. The significant parameters that contribute to the intrinsic losses are:

1. difference between core diameters,
2. difference between the maximum value of the refractive index,
3. difference between the refractive index profiles of the two jointing fibers.

Extrinsic losses are those arising from

1. imperfections of the quality of the two end surfaces with reference to smoothness, flatness, orthogonality to their longitudinal axes (face tilt),
2. longitudinal gaps, axial and angular misalignments between the fibers (see Fig. 2.5).

In Chapter 3, the theory of the transmission characteristics of a fiber connector is discussed in detail. In Chapters 4,5, and 6, we evaluate the amplitude coupling coefficients between discrete modes when axial, longitudinal and/or tilt offset is present at the connector in order to compute the power loss, modal noise and distortion. Our experimental conditions simulate field situations as far as possible and are well accounted for by the theory.

2.4 Modal Noise and Distortion

2.4.1 Source Coherence

The laser diodes used in optical fiber systems frequently have a high temporal and spatial coherence when oscillating in the single longitudinal and the single transverse mode, respectively. They exhibit multilongitudinal mode behavior under high speed modulation without d.c. bias. Under d.c. bias, the spectrum tends to be narrowed. It is also found that

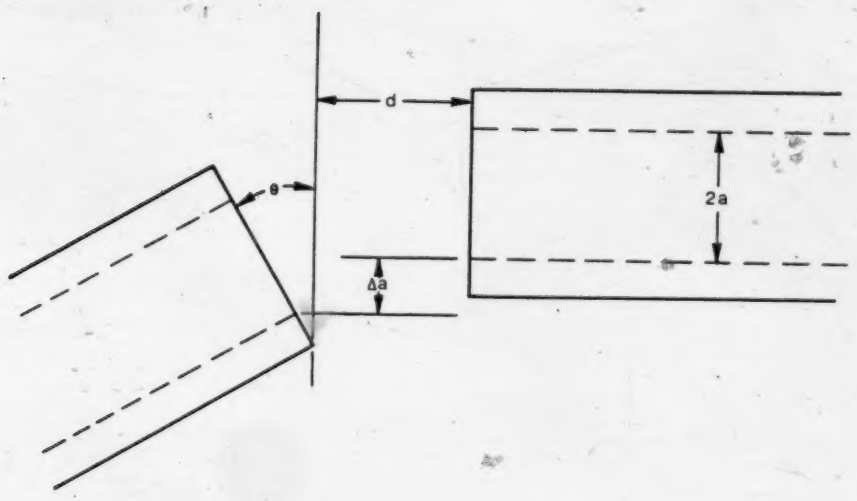

Δa – axial offset
d – longitudinal offset
θ – tilt offset

Figure 2.5 Schematic of two butt-coupled fibers with different types of geometrical misalignments.

the d.c. bias required for single mode operation is such that the instantaneous current always stays $\geq 1.2\, I_{th}$[161], where I_{th} is the threshold current. Furthermore, the intensity of the nonlasing modes (or amplified spontaneous emission modes) is found to decrease as the excitation current is increased.

A source coherence time τ_c, or spectral bandwidth $\Delta\nu$, can be defined as the time by which the light may be delayed and yet correlate or interfere with the undelayed light. For a single longitudinal mode laser, the spectral width is equal to the line width of the mode, which is in the MHz range [7]. For a multimode laser, the spectral width depends on the number of modes and the spacing between adjacent modes [33]. The coherence length L_c is the coherence time multiplied by the propagation velocity but, since the velocity is a function of the refractive index, the medium must be specified.

2.4.2 Speckle Patterns

When the light from a coherent or partially coherent laser is launched into a multimode fiber, a speckle pattern appears at the far end of the fiber due to mode-mode interference [162]. Two modes do not interfere at the output plane of the transmitting fiber when the distance traveled is such that their intermodal delay exceeds the coherence time of the source [163]. The speckle pattern is very sensitive with respect to movement of the fiber, temperature, as well as source frequency. The number of speckles is proportional to the number of propagating modes and there will be $\pi[2a(NA)/\lambda]^2$ in the cross section of a step-index fiber, each $\lambda(NA)/2$ in diameter (finest resolution) [27]. For the case of a graded-index fiber, all the speckles are not of the same size, owing to space variant speckle statistics across the fiber core [52]. The speckles will be coarser if the fiber is underfilled, i.e., fewer modes are excited than the fiber can support. The smearing out of the speckle patterns is related to the spectral bandwidth of the source and to the propagation length [163]. After this distance, the total pattern is smoothed due to the sum of the intensities of the different modes [27].

2.4.3 Modal Noise

The presence of speckle in a lossy region can lead to uncertainty in the loss value in a fiber-optic system. In an axial, angular or longitudinally misaligned fiber-to-fiber joint (splice or demountable connector), the loss will be determined by spatial filtering, i.e., by the amount

of offset, as well as the fraction of near or far field speckles intercepted by the core of the second fiber. Time variation of spatial filtering caused by dynamic changes in speckle patterns gives rise to a loss fluctuation, which in turn amplitude modulates the transmitted signal. This has been referred to as modal noise.

The dynamic changes in speckle patterns are caused by changes in phase between different modes, which are due either to fluctuations in the delays between modes when the fiber is mechanically distorted (causing local changes in refractive index), or to a source frequency deviation, or both. The conditions necessary for the generation of modal noise can be summarised as [26]:

1. narrow spectral width (long coherence time),
2. modal or spatial filtering, and
3. time variation of modal or spatial filtering.

Apart from a connector, modal or spatial filtering can also be caused by dirty fiber ends [29], mode selective couplers, switches, power splitters and modulators, and even microbending [27],[29],[30]. Transmission of the optical signal through a polarization-sensitive element is also an effective alternative to spatial filtration in meeting the conditions for modal noise [164].

2.4.4 Exploration of Possible Speckle Conditions

Several papers [46]-[50] show a close agreement between the theoretical and measured modal noise caused by flexing or heating a fiber, which randomly perturbs the intermode delays (phases) and give rise to randomly changing speckle patterns downstream. This form of modal noise is insignificant in most transmission systems as the changes are slow and only gives rise to noise below the system frequency band. In a real optical fiber transmission system, frequency fluctuations of the laser cause much faster speckle movement and this is the cause of practical modal noise. These spectral fluctuations can be longitudinal mode partition noise, chirping or FM (frequency modulation) noise. The change of speckle pattern at a given location is proportional to the frequency deviation and the preceding mode dispersion. For 0.8-0.9 μm LDs, the dominant FM mechanism for modulation frequencies below 1 MHz is heating; the laser cavity becomes longer as the current (power) is increased. The resulting slow drift in the center frequency has been referred to as chirping. At higher modulation frequencies the thermal effect falls off, leaving a residual FM, probably caused by changes in carrier density

which result in changes in refractive index [165].

2.4.5 Modal Distortion

Since the modulation of a laser diode yields both a modulation of the optical power and of the emission wavelength, the transmission loss at a connector is modulated, yielding a nonlinear transmission behaviour [34],[36]-[39]. This has been referred to as modal distortion. Modal distortion resulting from interference between a single pair of modes appears as a sinusoidal ripple of frequency [27]

$$f_r = \Delta\tau_g \frac{df}{dt} \qquad (2.24)$$

where $\Delta\tau_g$ is the intermode delay and (df/dt) denotes the rate of change of optical frequency of the source. From (2.24), one would expect a low modal distortion frequency at short distances from the source, since the very small transit time $\Delta\tau_g$ will result in very small frequency differences among the modes of the fiber. At greater distances from the source, the larger modal transit time differences produce much higher beat frequencies among the modes [166]. However, the analysis is not so straightforward for a multimode fiber guiding hundreds of modes, and for a partially coherent source. In Chapter 3, a detailed mathematical analysis is carried out for such cases.

CHAPTER III

TRANSMISSION CHARACTERISTICS OF A FIBER CONNECTOR : THEORY

A detailed theory of the modal noise and distortion due to fiber connectors has been given in Ref. [34], which is modified here for the case of a steady state power distribution in the transmitting fiber. In this chapter, the transmission characteristics of an optical fiber connector are analyzed, considering the configuration as shown in Fig. 3.1, in which the laser light is launched into fiber 1 (transmitting fiber) of length L. Fiber 1 is coupled to fiber 2 (receiving fiber) by means of a fiber connector which exhibits one or more geometrical misalignments (e.g., axial, longitudinal and/or tilt). Fiber 1 is assumed to be perfectly straight, exhibiting no mode coupling. Reflections at the fiber connector are ignored in this theory. Therefore, the following results also apply if a semiconductor laser together with an optical isolator are used.

3.1 Derivation of the Instantaneous Power Coupling Efficiency

The electric field of fiber 1 at the fiber connector is expressed as

$$E_1 = \sum_{\nu=1}^{N_1} A_\nu \exp\left[j(\phi_\nu - \tau_\nu(\omega-\omega_0))\right] \exp(j\omega t)\, \vec{E}_{\nu_1} \qquad (3.1)$$

where

$\omega = \frac{2\pi c}{\lambda}$ = angular emission frequency of the laser source

c = speed of light in vacuum

λ = wavelength of emission

ω_0 = arbitrary center frequency

τ_ν = delay of the νth mode in fiber 1

N_1 = total number of modes guided by fiber 1

A_ν = real amplitude of mode ν

ϕ_ν = phase at $\omega=\omega_0$

$\vec{E}_{\nu_1}$ = electric field of the νth mode of fiber 1

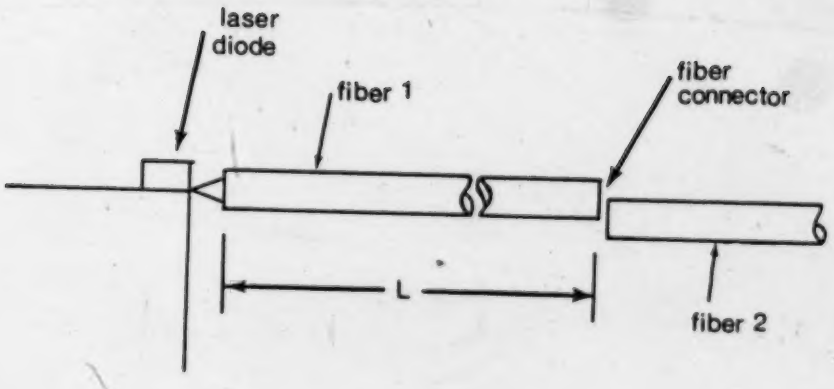

Figure 3.1 Schematic configuration of a fiber followed by a fiber connector.

$\vec{E}_{\nu 1}$ is normalized as

$$\int (\vec{E}_{\nu_1} \times \vec{H}^*_{\mu_1}) \, \vec{u}_z \, dA = \begin{cases} 0 \text{ for } \nu \neq \mu \\ 1 \text{ for } \nu = \mu \end{cases} \tag{3.2}$$

where $\vec{H}_{\mu 1}$ = magnetic field of the μth mode of fiber 1

$\vec{u}_z$ = unit vector in axial direction

The integration in (3.2) extends over the whole fiber cross section. The power, carried by mode ν in fiber 1, will be denoted as $P_{\nu 1}$ and is given as

$$P_{\nu_1} = A_\nu^2 \tag{3.3}$$

The electric field of fiber 1 has to be matched to the electric field of fiber 2

$$\vec{E}_2 = \sum_{\mu=1}^{N_2} B_\mu \exp(j\omega t) \, \vec{E}_{\mu 2} \tag{3.4}$$

where B_μ = complex amplitude of the μth mode of fiber 2

N_2 = total number of modes guided by fiber 2

The modal field $\vec{E}_{\mu 2}$ is also normalized as in (3.2). The transverse components of $\vec{E}_2$ and $\vec{E}_1$ have to be matched at the fiber connector, yielding

$$B_\mu = \sum_{\nu=1}^{N_1} A_\nu \exp\left[j(\phi_\nu - \tau_\nu(\omega - \omega_0)) \right] C_{\nu\mu} \tag{3.5}$$

with the mode coupling coefficient

$$C_{\nu\mu} = \int (\vec{E}_{\nu_1} \times \vec{H}^*_{\mu_2}) \, \vec{u}_z \, dA \tag{3.6}$$

The instantaneous power coupling efficiency η at the fiber connector is given as

$$\eta = \frac{\text{power (fiber 2)}}{\text{power (fiber 1)}} = \sum_{\mu=1}^{N_2} |B_\mu|^2 \Big/ \sum_{\nu=1}^{N_2} |A_\nu|^2 \tag{3.7}$$

Since

$$\sum_{\nu=1}^{N_1} A_\nu^2 = \sum_{\nu=1}^{N_1} P_{\nu_1} = P_1 \tag{3.8}$$

denotes the total power guided by fiber 1, (3.7) with (3.5) yields

$$\eta = \frac{1}{P_1} \sum_{\mu=1}^{N_2} \sum_{\nu=1}^{N_1} \sum_{x=1}^{N_1} \sqrt{P_{\nu_1} P_{x_1}} \exp\left[j(\phi_{\nu x} - \tau_{\nu x}(\omega-\omega_0))\right] C_{\nu\mu} C^*_{x\mu} \tag{3.9}$$

where

$$\phi_{\nu x} = \phi_\nu - \phi_x$$

$$\text{and} \quad \tau_{\nu x} = \tau_\nu - \tau_x$$

We define sets of normalized mode power weights W_ν according to

$$W_\nu = P_{\nu_1}/P_{1f} \tag{3.10}$$

where P_{1_f} is the power in the fundamental mode of fiber 1. Let us assume that the total number of modes guided by both the fibers 1 and 2 are equal to N, i.e., $N_1=N_2=N$; substituting (3.10) into (3.9) and reordering the sum in (3.9) yields

$$\eta = \frac{\sum_{\nu}^{N} \sum_{x}^{N} \sqrt{W_\nu W_x} \cos\left(\phi_{\nu x} - \tau_{\nu x}(\omega-\omega_0)\right) F_{\nu x}}{\sum_{\nu x}^{N} \sqrt{W_\nu W_x}} \tag{3.11}$$

with

$$F_{\nu\varkappa} = \sum_{\mu=1}^{N} C_{\nu\mu}\, C^{*}_{\varkappa\mu} \qquad (3.12)$$

The coefficient $F_{\nu\varkappa}$ determines the transmission characteristics of a connector. $F_{\nu\nu}$ gives the efficiency with which the power of mode ν of fiber 1 is coupled to fiber 2 whereas $F_{\nu\varkappa}$ with $\nu \neq \varkappa$ is an interference coefficient [34], giving the amplitude with which the coupling efficiency fluctuates due to interference between modes ν and $\varkappa$ of fiber 1. In matrix notation we can write

$$[F] = [C]\,[\bar{C}]^{T} \qquad (3.13)$$

where [F] is called the transmission matrix and $[\bar{C}]^{T}$ denotes the conjugate transpose of the mode coupling matrix [C]. In Chapters 4,5 and 6, the transmission matrix is evaluated from the mode coupling coefficients which are specific to the particular geometrical misalignment present in the fiber connector.

The modal power distribution in fiber 1 affects the coupling efficiency (3.11). A uniform power distribution is consistent with assuming equal mode excitation, equal mode attenuation and no mode coupling; for this case $W_{\nu} = 1$ for all ν values. In the next section we calculate values for W_{ν} for the steady state case.

3.1.1 Steady State Modal Power Distribution

Depending on the optical source type and on the fiber length, random low frequency physical perturbations along the fiber can produce significant differential mode attenuation. Eventually a steady state power distribution is reached, which is independent of the distance z along the fiber. With parallel beam injection (as is the case with a fiber coupled to a singlemode laser), the normalised near-field power distribution I(r) for the steady state case varies as [167]

$$\underset{z\to\infty}{I(r)} = \frac{\sqrt{1 - \left(\frac{r}{a}\right)^{2}}}{\left(\frac{r}{a}\right)} \qquad 0 < r \leq a \qquad (3.14)$$

Assuming that the guided modes in a degenerate mode group (i.e., guided modes that have the same propagation constant, but different angular number 'l') carry the same amount of

power, the modal power distribution P_ν (m) for a fiber with a parabolic-profile is related to I(r) through [168]

$$P_\nu(m) = \frac{-K}{r} \left[\frac{dI(r)}{dr} \right]_{r = aR(m)} \tag{3.15}$$

where K is a constant and the mode coordinate R(m) is defined as [168]

$$R(m) = \left[\frac{1}{2\Delta} \left(1 - \frac{\beta^2(m)}{n_1^2 k^2} \right) \right]^{1/2} \tag{3.16}$$

The mode group number dependence of (3.16) and hence of (3.15), is implicit in the propagation constant β given by (2.14). Substituting (2.14) into (3.16) yields

$$R(m) \simeq \left(\frac{m}{M}\right)^{1/2} \tag{3.17}$$

where the highest mode group number M is defined as in (2.16). Differentiation of (3.14) with respect to r and substitution in (3.15) then yields

$$P_\nu(m) = \frac{K'}{\left(\frac{m}{M}\right)^{3/2} \sqrt{1-\frac{m}{M}}} \qquad \text{for } 1 \leq m < M \tag{3.18}$$

where K' is a constant. The modal power weights W_ν defined according to (3.10) are obtained as

$$W_\nu = \frac{P_{\nu 1}}{P_{1_f}} = \frac{P_\nu(m)}{P_\nu(1)} = m^{-3/2} \left[\frac{M-1}{M-m} \right]^{1/2} \qquad 1 \leq m < M \tag{3.19}$$

for a steady state power distribution. In (3.19), mode ν belongs to the mode group m.

Apart from its modal power distribution dependence, the coupling efficiency (3.11) also depends on ω and on the phase difference $\phi_{\nu\times}$. These $\phi_{\nu\times}$ determine the speckle pattern at the endface of fiber 1 and are unpredictable because they depend on stresses subjected to the fiber, temperature and other environmental effects. Hence, the coupling efficiency is examined on a statistical basis in the following section.

3.2 Illumination with Coherent Light

We first assume that the fiber is excited by a coherent source emitting at $\omega=\omega_0$. The average over $\phi_{\nu x}$ will be denoted by the angle brackets $< >$, where it is understood that $\phi_{\nu\nu}=0$ and that

$$\phi_{\nu x} = -\phi_{x\nu} \quad ; \quad \phi_{\nu x} + \phi_{x\mu} = \phi_{\nu\mu} \tag{3.20}$$

The direct average of η is obtained from (3.11) as

$$<\eta> = \sum_{\nu=1}^{N} W_\nu F_{\nu\nu} \Big/ \sum_{\nu=1}^{N} W_\nu \tag{3.21}$$

The standard deviation of the coupling efficiency is

$$\delta(\eta) = \sqrt{<\eta^2> - <\eta>^2} \tag{3.22}$$

since it gives the mean amplitude with which η fluctuates around $<\eta>$. We first determine

$$(\eta-<\eta>)^2 = \frac{1}{\sum_{\nu x} W_\nu W_x} \sum_{\substack{\nu=1 \\ \nu\neq x}}^{N} \sum_{x=1}^{N} \sum_{\substack{\mu=1 \\ \mu\neq m}}^{N} \sum_{m=1}^{N} \cos(\phi_{\nu x}) \cos(\phi_{\mu m}) \times \sqrt{W_\nu W_x W_\mu W_m}\, F_{\nu x} F_{\mu m} \tag{3.23}$$

When averaging over $\phi_{\nu x}$, $\phi_{\mu m}$, all terms vanish except those for which $\nu=\mu$ and $x=m$ or $\nu=m$ and $x=\mu$, yielding

$$\delta^2(\eta) = <\eta^2> - <\eta>^2 = <(\eta-<\eta>)^2> = \frac{1}{\sum_{\nu x} W_\nu W_x} \sum_{\substack{\nu=1 \\ \nu\neq x}}^{N} \sum_{x=1}^{N} W_\nu W_x (F_{\nu x})^2 \tag{3.24}$$

For estimating noise and nonlinear distortions, one is interested in the derivative of η with respect to ω which is obtained as the derivative of (3.11)

$$\frac{d\eta}{d\omega} = \frac{1}{\sum_{\nu=1}^{N} W_\nu} \sum_{\nu=1}^{N} \sum_{x=1} \tau_{\nu x}' \sqrt{W_\nu W_x} \sin(\phi_{\nu x} - \tau_{\nu x}(\omega-\omega_0)) F_{\nu x} \tag{3.25}$$

The mean square value of $d\eta/d\omega$ is derived in a similar manner to (3.24) yielding

$$\langle \left(\frac{d\eta}{d\omega}\right)^2 \rangle = \frac{1}{\left(\sum_\nu W_\nu\right)^2} \sum_{\nu x} \tau^2_{\nu x} W_\nu W_x (F_{\nu x})^2 \tag{3.26}$$

3.3 Illumination with Partially Coherent Light

We now consider illumination with a partially coherent source with an emission line spectral component $f(\omega)$, normalized according to

$$\int_0^\infty f(\omega)\, d\omega = 1 \tag{3.27}$$

The coupling efficiency between the fibers for this partially coherent source is

$$\eta_s = \int_0^\infty f(\omega)\, \eta(\omega)\, d\omega \tag{3.28}$$

The direct average of (3.28) is obtained as

$$\langle \eta_s \rangle = \langle \int_0^\infty f(\omega)\, \eta(\omega)\, d\omega \rangle = \int_0^\infty f(\omega) \langle \eta \rangle\, d\omega = \langle \eta \rangle \tag{3.29}$$

and the mean square value

$$\langle \eta_s^2 \rangle = \langle \left(\int_0^\infty f(\omega)\eta(\omega)\, d\omega \right)^2 \rangle = \langle \int_0^\infty \int_0^\infty f(\omega) f(\Omega) \eta(\omega) \eta(\Omega)\, d\omega d\Omega \rangle$$

$$= \int_0^\infty \int_0^\infty f(\omega) f(\Omega) \langle \eta(\omega) \eta(\Omega) \rangle d\omega\, d\Omega \tag{3.30}$$

where the correlation function $\langle \eta(\omega)\ \eta(\Omega) \rangle$ is obtained by setting $\Omega = \omega + \Delta\omega$, as

$$R(\Delta\omega) = \langle \eta(\omega)\eta(\omega+\Delta\omega)\rangle = \langle\eta\rangle^2 + \frac{1}{\sum_\nu W_\nu^2} \sum_{\nu\times} \cos(\tau_{\nu\times}\Delta\omega)$$

$$\times \quad (F_{\nu\times})^2 \quad W_\nu W_\times \tag{3.31}$$

Similar to R($\Delta\omega$), we introduce the autocorrelation function of the source

$$G(\Delta\omega) = \int f(\omega)\ f(\omega+\Delta\omega)\ d\omega \tag{3.32}$$

so that (3.30) yields

$$\langle \eta_s^2 \rangle = \int_{-\infty}^{\infty} G(\Delta\omega)\ R(\Delta\omega)\ d(\Delta\omega) \tag{3.33}$$

The variance of η_s is

$$\delta^2(\eta_s) = \langle \eta_s^2 \rangle - \langle \eta_s \rangle^2$$

$$= \sum_{\substack{\nu=1 \\ \nu\neq\times}} \sum_{\times=1} \frac{\Gamma\ (\tau_{\nu\times})\ W_\nu W_\times (F_{\nu\times})^2}{\sum_\nu W_\nu^2} \tag{3.34}$$

with

$$\Gamma\ (\tau) = \int_{-\infty}^{\infty} G(\Delta\omega)\ \cos(\tau\Delta\omega)\ d\ (\Delta\omega) \tag{3.35}$$

Let us assume a Lorentzian line shape centered at $\omega=\omega_c$

$$f(\omega) = \frac{2\tau_c/\pi}{1 + \left[(\omega-\omega_c)^2\ (2\tau_c)^2\right]} \tag{3.36}$$

with the coherence time τ_c. Equation (3.35) then yields

$$\Gamma\ (\tau) = \exp\ (-\ |\tau|/\tau_c) \tag{3.37}$$

From (3.37) it is seen that, for a coherent source ($\tau_c \to \infty$), (3.34) reduces to (3.24), while for decreasing τ_c, the fluctuations of η_s also decrease. Any modulation of the

center frequency ω_c also changes the coupling efficiency η_s. The result for the mean square value of $d\eta_s/d\omega_c$ is

$$\left\langle \left(\frac{d\eta_s}{d\omega_c}\right)^2 \right\rangle = \frac{\sum_{\nu x} \Gamma(\tau_{\nu x})\ \tau_{\nu x}^2\ W_\nu W_x (F_{\nu x})^2}{\left(\sum_\nu W_\nu\right)^2} \tag{3.38}$$

The derivation of (3.38) is very similar to the derivation of (3.34).

3.4 Power Loss

As expected, the average coupling efficiency for a coherent source is the same as that for a partially coherent source. In fact, the expression for the power coupling efficiency could have been derived simply from a random phase argument between the modes of the transmitting fiber [87]. The power loss in decibels is

$$\text{Loss} = -10 \log (\langle \eta \rangle) \tag{3.39}$$

The loss value predicted by (3.39) is valid only if the length of the receiving fiber is short enough (a few meters) so that the change in the receiving fiber's loss (as a result of differential mode attenuation) due to mode mixing at the connector, is negligible [83].

3.5 dc Signal-to-Modal Noise Ratio

If the fluctuations of the coupling efficiency —as introduced by external fluctuations (e.g., pressure, temperature) or by wavelength fluctuations— have spectral components which are fully within the modulation band, one simply obtains for the dc-signal/noise ratio (dc-SNR) [169]

$$\text{dc - SNR} = \left[\frac{\langle \eta \rangle}{\delta(\eta)}\right]^2 \tag{3.40}$$

This signal/noise ratio estimate is certainly a worst case estimate [169].

The calculation of $\delta(\eta)$ according to (3.24) or (3.34) involves the summation of a very large number of terms. For instance, if fiber 1 carries 190 modes of each polarization

(V=39), the summation involves 36,100 terms. Since this calculation takes considerable computation time, it has been proposed in Ref. [49] that, for a coherent source, one can approximate the form of (3.24) using speckle theory to arrive at a simpler expression

$$\delta(\eta) \simeq \langle\eta\rangle \left[\frac{1 - \langle\eta\rangle}{N \langle\eta\rangle}\right]^{\frac{1}{2}} \tag{3.41}$$

In Chapters 4 and 5, the values of the dc-SNR according to (3.40) will be presented using the exact $\delta(\eta)$ from (3.24), as well as that from the speckle theory using (3.41).

3.6 Modal Distortion

Nonlinear distortion of a transmitted signal can occur because the direct modulation of a semiconductor laser diode yields not only a modulation of the optical power, but also yields a modulation of the emission wavelength or frequency [37],[165]. The modulation of the emission frequency of a LD may be expressed as

$$\omega_c(t) = \omega_{co} + \Omega_m \cos(\omega_m t) \tag{3.42}$$

where ω_m is the angular modulation frequency (rf signal) and Ω_m is the maximum deviation from the center frequency of emission. We may restrict the discussion to the special case where

$$\omega_m << \Omega_m$$
$$\text{and } \omega_m << 1/\tau_{rms} \tag{3.43}$$

In this case, the power in fiber 2, $P_2(t)$, is related to the power in fiber 1, $P_1(t)$, as

$$P_2(t) = P_1(t) \cdot \eta_s(\omega_c(t)) \tag{3.44}$$

which is a nonlinear relationship. The higher order harmonic distortions can be obtained from (3.44) with (3.11). They depend on the phase difference $\phi_{\nu\times}$ and therefore vary if the speckle pattern varies. When the averaging is done with respect to all possible speckle patterns, the relative second harmonic distortion $R_{2f/f}$ (also referred to as modal distortion) for a

single longitudinal mode emission has been shown to be [34]

$$R_{2f/f} \quad [dB] \quad \Big|_{av} \simeq 20 \log \left[\frac{\left(\left\langle \left(\frac{d\eta}{d\omega_c} \right)^2 \right\rangle \right)^{\frac{1}{2}} \Omega_m}{2 \langle \eta \rangle} \right] \qquad (3.45)$$

Equation (3.45) holds as long as ω may be considered as linear within the frequency range $\omega \pm \Omega_m$.

3.7 Conclusions

In this chapter, the theory for the transmission characteristics of a fiber connector has been presented and formulae for the power loss, modal noise and distortion have been given. The theory has accounted for coherent as well as partially coherent illumination; the mode power weights corresponding to a uniform and a steady state power distribution have been derived. Numerical values for the loss, noise and distortion are obtained in Chapters 4, 5 and 6, with the help of the modal amplitude coupling coefficients which are derived separately for the axial, longitudinal and tilt misalignment.

CHAPTER IV

EVALUATION OF LOSS, MODAL NOISE AND DISTORTION DUE TO AXIAL OFFSET

In this chapter, the derivation of the modal amplitude coupling coefficients similar to the ones found by Petermann [34] is shown for axial offsets. These coefficients differ slightly from those derived by Kashima [94]. They yield a power loss which converges to the geometrical optics limit for fibers with high V, assuming a uniform power distribution. The theoretical formalism of Chapter 3 is used to evaluate the steady state power loss, modal noise and distortion. Modal noise results obtained from speckle theory are compared with those derived from modal analysis. Experimental results are presented and are shown to be in close agreement with the theory. Using this theory, the dependence of loss, noise and distortion on wavelength, numerical aperture and source coherence are also examined.

4.1 Evaluation of Modal Amplitude Coupling Coefficients

For given orders l, q, four linearly polarized (LP) modes exist: two polarizations E_x and E_y and two orientations sin lø and cos lø. Coupling occurs only between modes of the same polarization and orientation [34]. The coupling coefficients between E_x-E_x modes and E_y-E_y modes are equal. Therefore, only E_x- modes will be considered in the following.

The geometry of two coupled fibers 1 and 2 is shown in Fig. 4.1 where $\phi \rightarrow \phi_1$ and $r \rightarrow r_1$ for fiber 1 and $\phi \rightarrow \phi_2$ and $r \rightarrow r_2$ for fiber 2 (the subscripts 1 and 2 refer to fibers 1 and 2 respectively). For LP modes, we may use a normalization different from (3.2) according to

$$\frac{2}{w_0^2} \int E_{x\nu} E_{x\mu} \, dA = \delta_{\nu\mu} \tag{4.1}$$

yielding the modal amplitude coupling coefficient

$$C_{\nu\mu} = \frac{2}{w_0^2} \int E_{x\nu_1} E_{x\mu_2} \, dA \tag{4.2}$$

The Laguerre-Gauss function according to (2.5) may be expanded in terms of Hermite-Gauss functions ($x = r\cos\phi$, $y = r\sin\phi$), yielding for the x- component of the electric field [102]

$$E_x(i,j) = A'_{ij} H_i\left(\frac{\sqrt{2}}{w_0} x\right) H_j\left(\frac{\sqrt{2}}{w_0} y\right) \exp\left(\frac{-(x^2+y^2)}{w_0^2}\right) \tag{4.3}$$

with $\times \; e^{-j\beta z}$

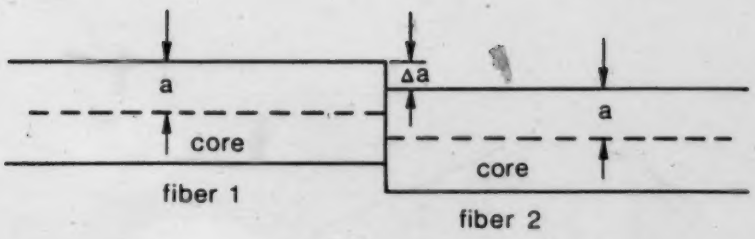

(a) lateral view

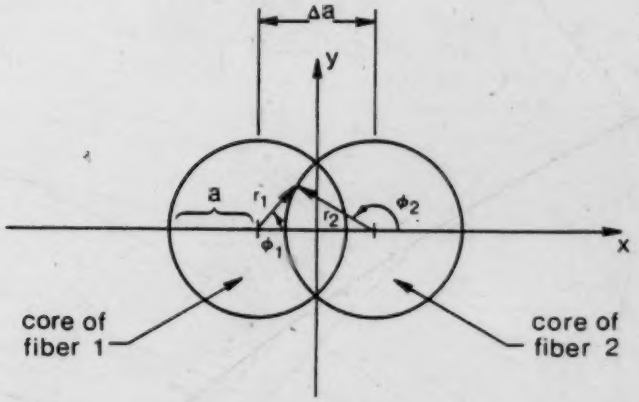

(b) transverse view

Figure 4.1 Geometry of two coupled fibers 1 and 2 axially offset by Δa.

$$A'_{ij} = 1/\left[\pi\ 2^{i+j}\ i!j!\ \right]^{\frac{1}{2}} \tag{4.4}$$

The mode function (4.3) is already properly normalized. There is also an electric field component along the longitudinal direction (giving rise to hybrid modal fields), but, for small refractive index changes, it is negligible, so that the modes can be approximated by TEM waves. The functions H_i and H_j are Hermite polynomials of order i and j (note that $i+j=2q+1$) [34]. Thus, the coupling coefficient (4.2) can be denoted as

$$C_{\nu\mu} = C(i,j,I,J,) \tag{4.5}$$

with integers i,j denoting the mode ν of fiber 1 and I,J denoting the mode μ of fiber 2. With the coordinates of Fig. 4.1, (4.2) reduces to

$$\begin{aligned} C_{\nu\mu} = \int_{-\infty}^{\infty}\int_{-\infty}^{\infty} & A'_{ij}\ A'_{IJ}\ H_i\left(\frac{\left[x+\frac{\Delta a}{2}\right]\sqrt{2}}{w_0}\right) H_j\left(\frac{\sqrt{2}\ y}{w_0}\right) \\ & \times\ \exp\left\{-\left(\frac{\left[x+\frac{\Delta a}{2}\right]^2+y^2}{w_0^{\,2}}\right)\right\} \\ & \times\ H_I\left(\left[x-\frac{\Delta a}{2}\right]\frac{\sqrt{2}}{w_0}\right)\ H_J\left(\frac{\sqrt{2}}{w_0}\ y\right) \\ & \times\ \exp\left\{-\left(\frac{\left[x-\frac{\Delta a}{2}\right]^2+y^2}{w_0^{\,2}}\right)\right\} \\ & \times\ d\left(\frac{x\sqrt{2}}{w_0}\right)\ d\left(\frac{y\sqrt{2}}{w_0}\right) \end{aligned} \tag{4.6}$$

which, after integration can be written as [170]

$$C_{\nu\mu}(i,I) = \left(\frac{i!}{I!}\right)^{\frac{1}{2}} 2^{\left(\frac{I-i}{2}\right)} \left(\frac{\Delta a}{\sqrt{2}w_0}\right)^{I-i} L_i^{I-i}\left(\frac{\Delta a^2}{w_0^2}\right) \exp\left(-\frac{\Delta a^2}{2w_0^2}\right)$$

$$\text{for} \quad i \leq I \qquad (4.7)$$

$$\text{and} \quad j = J$$

and

$$C_{\nu\mu}(I,i) = C_{\nu\mu}(i,I)\,(-1)^{i-I} \qquad (4.8)$$

$L_i(\,)$ is the Laguerre function defined in (2.11). For $J \neq j$, $C_{\nu\mu} = 0$. Eq. (4.6) has been solved by use of the integral 7.377 in Ref. [170].

4.2 Experimental Set Up

The power loss and modal distortion measurements were made as a function of the axial offset Δa between two near parabolic-index multimode fibers for different modulation frequencies f_m. The experimental set up is shown in Fig. 4.2. A single longitudinal mode laser diode (GO-DIP) with $\tau_c = 35$ pS [171], was used to excite the 170 m long source fiber. The second harmonic distortion of the RF generator was less than -60 dB. At the output of the 170 m transmitting fiber, $R_{2f/f} \simeq$-52 dB and $R_{3f/f} \simeq$-55 dB for a modulation frequency f_m of 55 MHz and a modulation depth m of 25 percent [171]. For these modulation conditions, $\Omega_m/2\pi \cong 2$ GHz [172]. The problem of harmonic distortion due to the Fabry-Perot cavity at the gap [173] and degradation of the source linearity by optical feedback [16] should not be significant in this experiment, because the former is noticeable only at high values of $\Omega_m/2\pi$ ($\simeq$80 GHz), and the latter occurs only with substantial coupling of a coherent reflected wave back into the laser. These conditions have been avoided by using a low Ω_m and a long source fiber [174].

Since a splice with substantial loss can change the modal properties of the receiving fiber [84], a short (3 m) receiving fiber was used. The fiber endfaces were of good quality, with no visible mist or hackle. Photographs of the two coupled endfaces are shown in Fig. 4.3 (fiber cleave 1). The splice was not index matched and the distance was carefully controlled by a x-y-z micro-positioner. Mode strippers were placed both before and after the

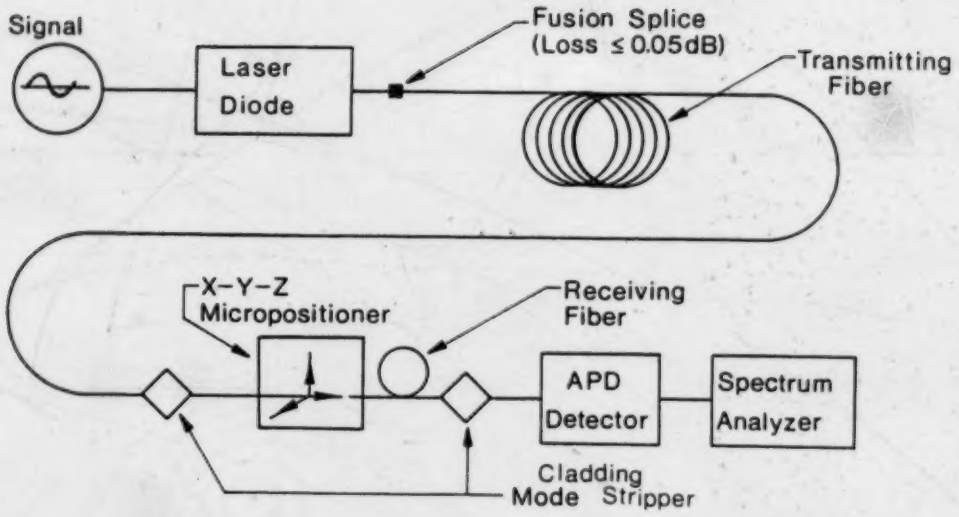

Figure 4.2 Experimental set up to study power loss and modal distortion due to axial offset.

(a)

(b)

Figure 4.3 Photographs of the fiber endfaces at the splice (fiber cleave 1). (a) Transmitting end and (b) receiving end. The receiving fiber is excited with a He-Ne laser.

micro-positioner to eliminate any spurious cladding modes.

An optical multimeter recorded the power loss. For the distortion measurements, the output intensity from the receiving fiber was detected by a large area APD detector so that there was no mode selective loss or distortion due to the fiber-detector coupling. The harmonic distortion was measured using a spectrum analyzer.

4.3 Results and Discussion

Results of numerical evaluations of equations (3.39), (3.40) and (3.45), pertaining to the power loss, modal noise and distortion respectively, are presented in this section; the relevant computer program is listed in Appendix A1. Experimental results are also discussed and shown to be in close agreement with the theory.

4.3.1 Power Loss

Splice loss predictions for axial offset with a uniform as well as steady state modal power distribution for several values of V are shown in Fig. 4.4 using (4.7) alongwith (3.39). A typical multimode fiber has been considered with $2a = 50$ μm and $NA = 0.2$. For this fiber, $V = 21$, $V = 29$ or $V = 39$ for $\lambda = 1.55$ μm, $\lambda = 1.1$ μm and $\lambda = 0.82$ μm, respectively. If a uniform modal power distribution is assumed, it is well known that as V increases, the electromagnetic field analysis should asymptotically approach the geometrical optics predictions [87]. In Fig. 4.4, the maximum deviation of modal analysis results ($V = 39$) from that predicted by geometric optics is $\simeq 0.04$ dB, this being probably caused by the coupling of power to the bound modes of the receiving fiber through the evanescent cladding fields [87]. This effect cannot be predicted using geometrical optics. It is also observed that for offsets $\leqslant 0.4\,a$, a uniform power distribution exaggerates splice loss values when long fiber lengths are used on the transmitting side. However, for offsets in excess of $0.4\,a$, the predictions of both the power distributions match closely.

Fig. 4.4 also shows that the splice loss is smaller at a longer wavelength for a uniform power distribution because of a wider electromagnetic field spread for longer wavelengths according to (2.12). In the case of a steady state power distribution, the added effect of the implicit wavelength dependence due to the allowed spectrum of bound modes according to (2.16) and (3.19) predominates. This reverses the V dependence of the splice loss for

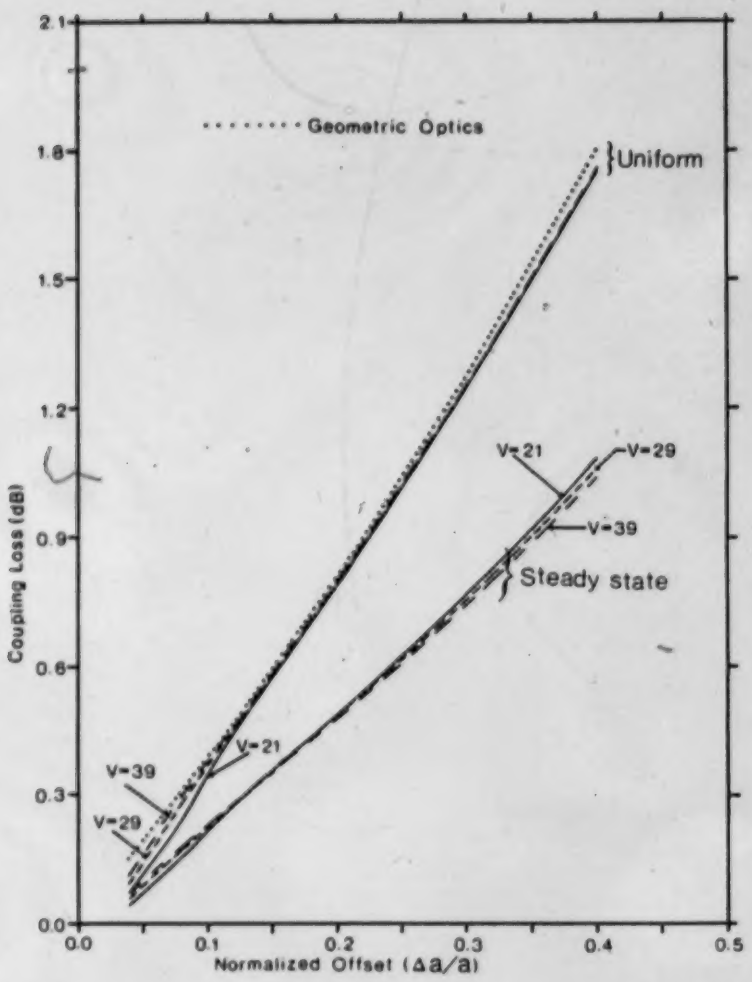

Figure 4.4 Loss vs. axial offset for uniform and steady state modal power distribution. Geometric optics (uniform power) results are shown in dotted line. a=25 μm.

$\Delta a/a > 0.12$, i.e., the splice loss is greater at a longer wavelength. To our knowledge, such an effect has not been reported before.

Fig. 4.5 shows the steady state splice loss in the offset range $0 \leq \Delta a/a \leq 1$. For small offsets ($< 10\ \mu m$), the experimental data shown in the figure are probably in error due to the poor resolution ($\approx 10\ \mu m$) of the x-y-z micropositioner. Otherwise, fairly good agreement is obtained between the theory and the data.

4.3.2 Modal Noise

Using (4.7), the values for $<\eta>$ and $\delta(\eta)$ are calculated according to (3.21) and (3.24) respectively, for V=21 and coherent illumination . The numerical evaluations are shown in Fig. 4.6 for a uniform as well as a steady state power distribution. It is seen that a uniform power distribution not only underestimates the magnitude of the coupling efficiency but can also overestimate the magnitude of the standard deviation of the coupling efficiency.

The dc-SNR for different V, calculated using (3.40) for a coherent source are shown as a function of the splice loss in Fig. 4.7. Varying the core radius, wavelength or NA (or a combination of all three) can vary V; however the value of the core radius was fixed at 25 μm in all numerical evaluations. Thus, different V in Fig. 4.7 can signify different wavelengths and/or different NA values. Results of modal analysis as well as speckle theory have been presented. The results show that the speckle theory predictions of (3.41) hold as long as the number of modes N guided by the fiber is very large and for coupling losses in excess of about 1 dB [169], and only for a uniform power distribution.

Fig. 4.8 shows the improvement in the dc-SNR as a function of τ_{rms}/τ_c for a partially coherent source and a splice loss of 1 dB. For V=21, the dc-SNR is seen to improve by at least an order of magnitude when a partially coherent source with $\frac{\tau_{rms}}{\tau_c}=10$ is used instead of a coherent source. Some error is introduced due to the use of LP-modes, since the delay differences of the true modes within one LP-mode group are small but do not vanish as (2.21) would suggest [34]. This leads to a pessimistic estimation of dc-SNR values.

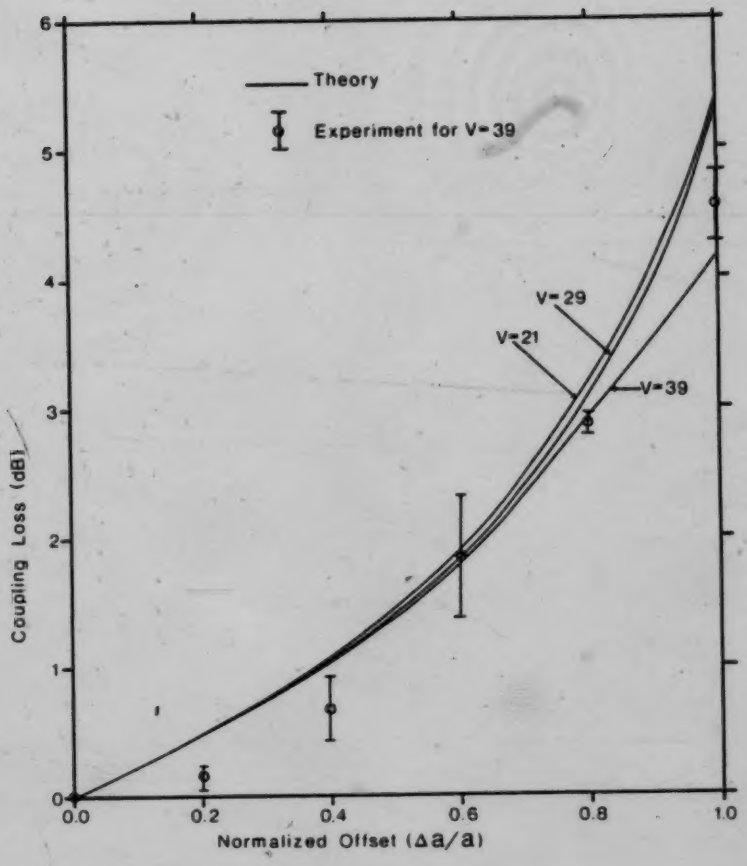

Figure 4.5 Experimental data and theoretical loss values for a steady state modal power distribution. a=25 μm, NA=0.2, and λ =0.82 μm for the experimental results.

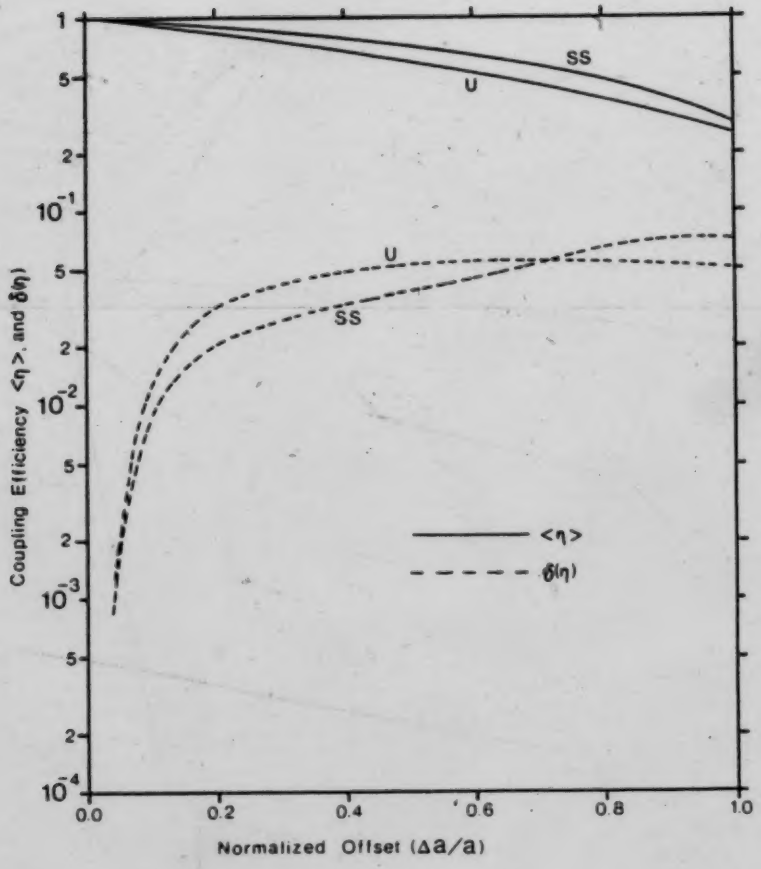

Figure 4.6 Coupling efficiency $<\eta>$ and its standard deviation $\delta(\eta)$ as a function of normalized offset for a coherent source. Both uniform (U) and steady state (SS) modal power distributions are considered. $a = 25\ \mu m$ and $V = 21$.

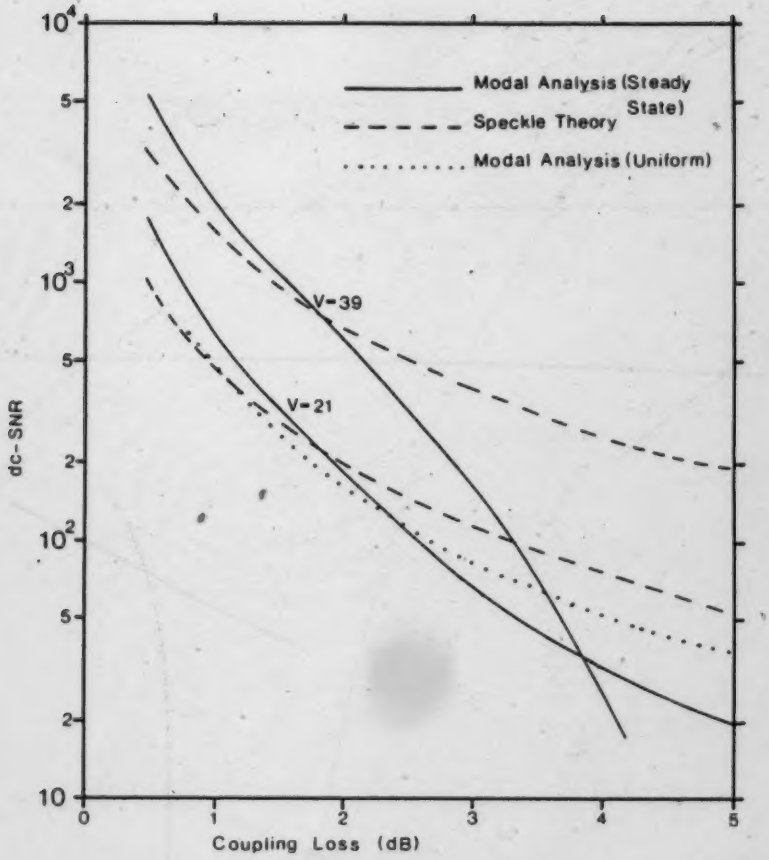

Figure 4.7 dc-SNR for a coherent source as a function of the coupling loss. The dashed curves are obtained from speckle theory. a = 25 μm.

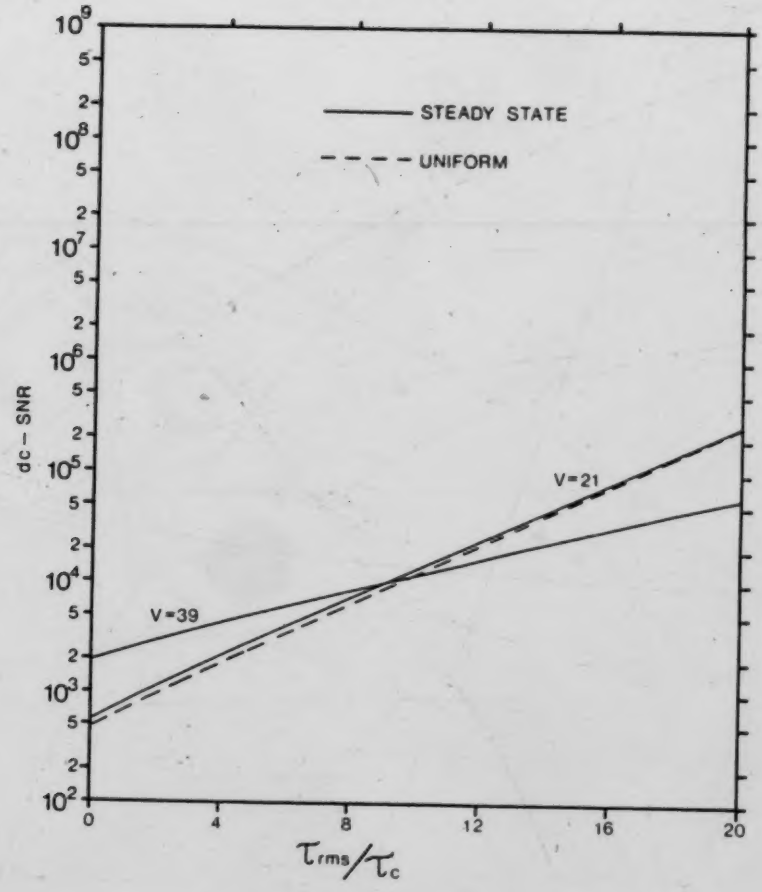

Figure 4.8 dc-SNR for partially coherent sources with coherence time τ_c. Splice loss = 1 dB, $\alpha = 2.2$ and $a = 25\ \mu m$.

4.3.3 Modal Distortion

In order to determine the sensitivity of the coupling efficiency with respect to a shift of the emission frequency, the rms value of $\frac{d\eta}{d\omega}$ for a coherent source (calculated according to (3.26)) is shown in Fig. 4.9, normalised with respect to $<\eta>\tau_{rms}$. It is seen that, for transmission losses exceeding 3 dB, a fiber with V=39 is unsuitable for low-distortion optical communication systems because the accompanying random level fluctuations will be very large. For V=39 and with large axial offsets, the rapid increase of the normalized fluctuations occurs only with the steady state power distribution assumption; the corresponding values for V=21 are decreased according to (3.26) and (3.19) because of a smaller M. We have checked that, with a uniform power distribution assumption, the fluctuation curve for V=39 does not increase as sharply and that it stays below the V=21 curve for all splice loss values.

Fig. 4.10 shows the dependence of the rms value of $\frac{d\eta_s}{d\omega_c}$ (calculated according to (3.38)) on the source coherence time τ_c for a transmission loss of 1 dB. With decreasing τ_c (increasing $\frac{\tau_{rms}}{\tau}$), the fluctuations decrease, but the decrease is faster for V=21 than for V=39. Fig. 4.10 is accurate because the contribution of the interference between modes with small $\tau_{\mu\nu}$ yields only a small contribution in (3.38).

Experimental results for $R_{2f/f}$ are plotted in Fig. 4.11 for λ =0.82 μm, NA=0.2, a=25 μm, α=2.2, τ_c=35 pS, f_m=55 MHz, m=0.25, τ_{rms}=0.15 nS and $\Omega_m/2\pi$ =2 GHz (fiber cleave 1 of Fig. 4.3 was used). Theoretical $R_{2f/f}$ values according to (3.45) for these parameters are also shown assuming a uniform as well as a steady state modal power distribution. It is well known that a uniform power distribution cannot prevail in this experimental fiber (transmitting) because the source is not incoherent [167], and because the modes are differentially attenuated [167]. It is also true that the experimental fiber is not long enough to attain the steady state. Hence, the actual modal power distribution will lie somewhere between these two extremes. However, Fig. 4.11 shows that the distortion data are in better agreement with the uniform power distribution assumption, than with the steady state assumption. This is probably due to the fact that the micrometer readings corresponding to intermediate axial offset values are in error because of the poor resolution of the x-y-z micro-positioner (10 μm). Also, (3.45) yields a $R_{2f/f}$ value that is averaged over all possible speckle patterns; for certain speckle patterns, wide variation in $R_{2f/f}$ can occur [34].

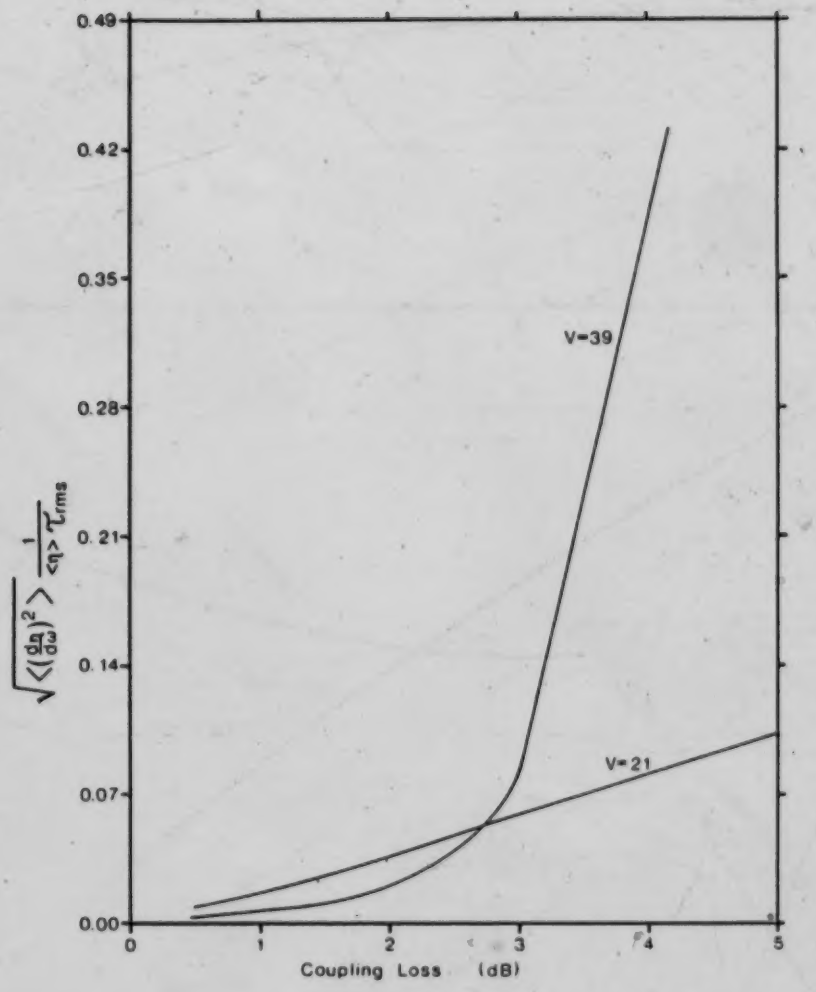

Figure 4.9 Normalised rms value of the derivative of the coupling efficiency with respect to emission frequency for a coherent source. $\alpha = 2.2$ and $a = 25\ \mu m$.

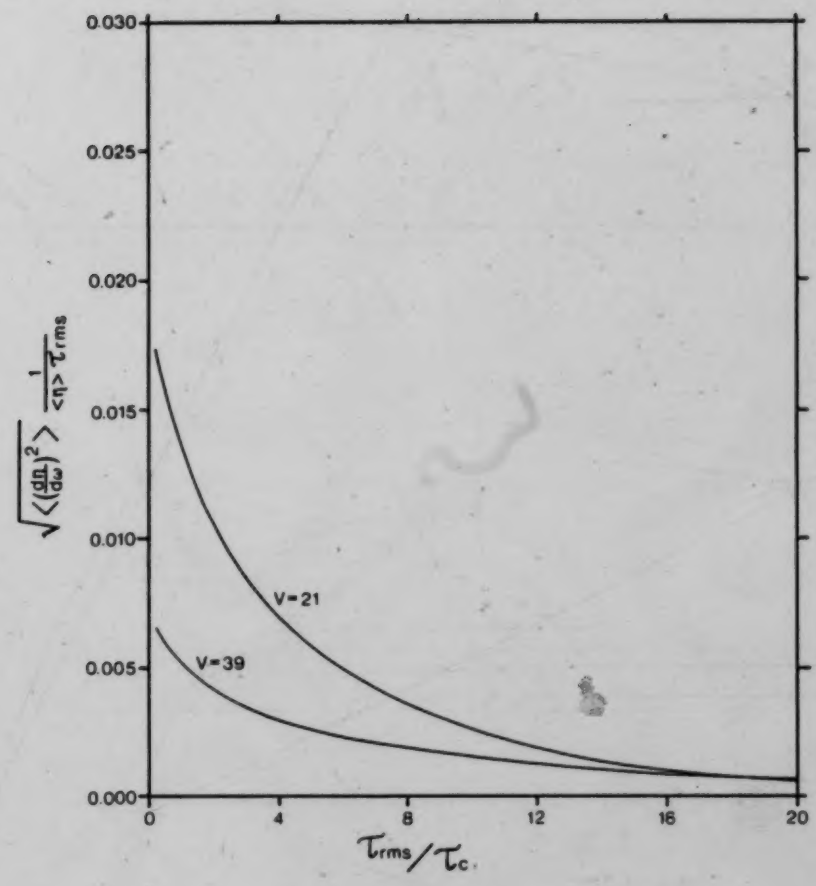

Figure 4.10 Normalized rms value of the derivative of the coupling efficiency with respect to emission frequency for a partially coherent source. Splice loss = 1 dB, a=25 μm and α=2.2.

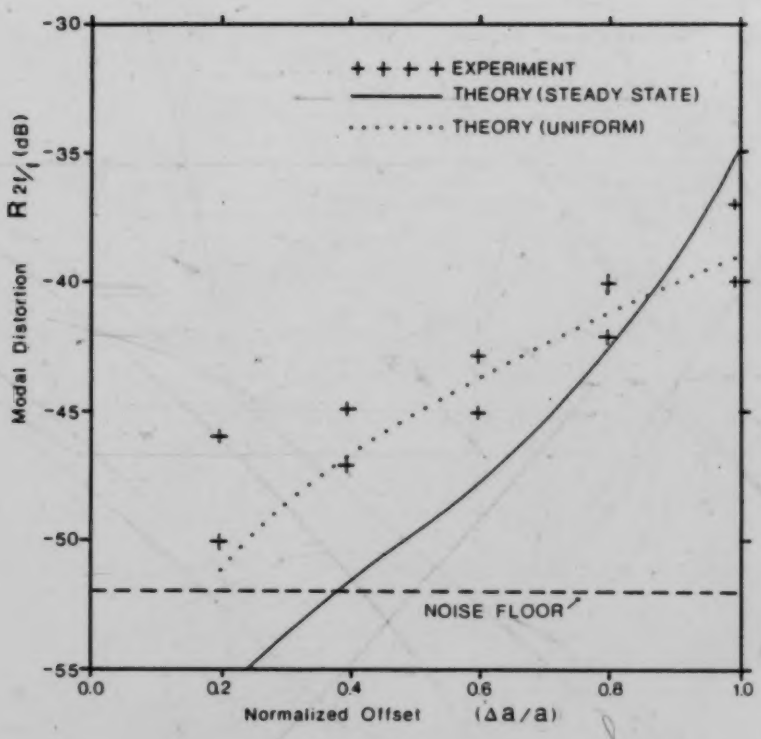

Figure 4.11 Modal distortion $R_{2f/f}$, as a function of normalized offset for a partially coherent source. NA=0.2, a=25 μm, V=39, f_m=55 MHz, m=0.25, τ_c =35 ps, τ_{rms} =0.15 ns, and $\Omega_m/2\pi$=2 GHz.

The effect of the cleave surface quality on the modal distortion (Fig. 4.12 shows the photographs of the fiber endfaces for cleave 2) is shown in Fig. 4.13. The cleave with less mist, hackle and surface contaminants (i.e., fiber cleave 1 shown in Fig. 4.3) exhibits better results. Experimental modal distortion values for different modulating frequencies f_m (100 KHz, 10 MHz and 55 MHz) with fiber cleave 1 are shown in Fig. 4.14. Experiments at lower f_m yielded higher $R_{2f/f}$ values, in agreement with the relationship between f_m and Ω_m [27].

4.4 Conclusions

Numerical evaluations of the power loss, modal noise and distortion due to axial offset at a fiber-fiber connection have been carried out. The measured data on the loss and modal distortion were found to lie close to the theoretical curves. For small offsets ($\leq 0.12\ a$), the loss was seen to decrease with increasing wavelength. At larger offsets (i.e., $> 0.12\ a$), the loss increased with wavelength. Modal noise results obtained from speckle theory were shown to be in close agreement with those of electromagnetic analysis for losses in excess of 1 dB, and only when a uniform power distribution and coherent illumination are assumed. Large random level fluctuations (5-7 %) in the power coupled to the receiving fiber, were seen to occur for coupling losses in excess of 3 dB for a singlemode source. Also, such fluctuations were found to drop off rapidly with decreasing source coherence, and particularly for fibers with a low mode volume.

Figure 4.12 Photograph of the endface of the receiving fiber for cleave no. 2. The transmitting fiber is the same as in Fig. 4.3(a).

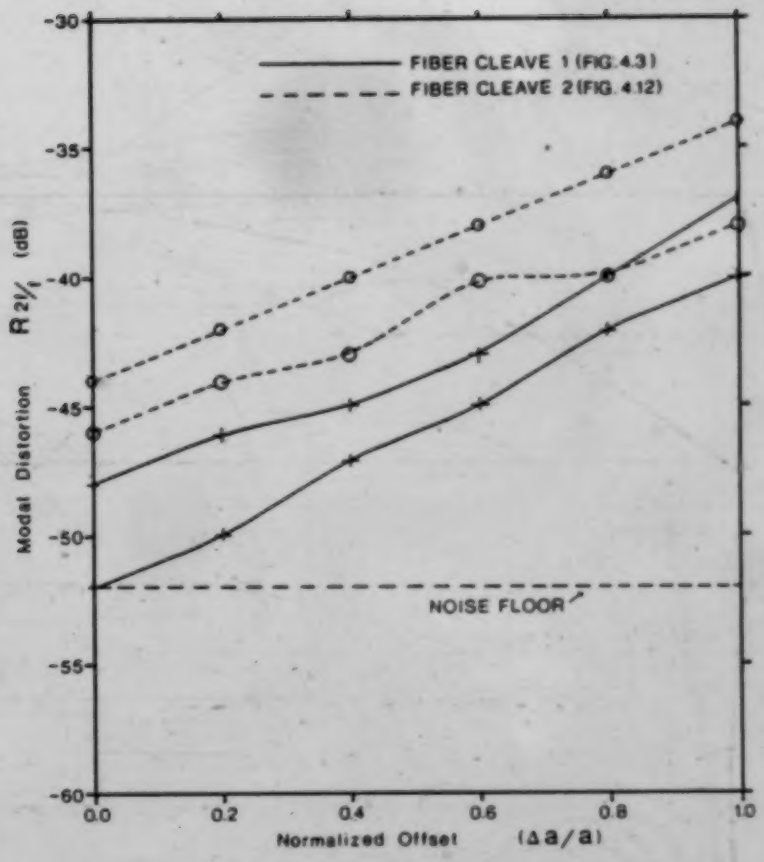

Figure 4.13 Modal distortion for different cleaves. Experimental parameters same as in Fig. 4.11.

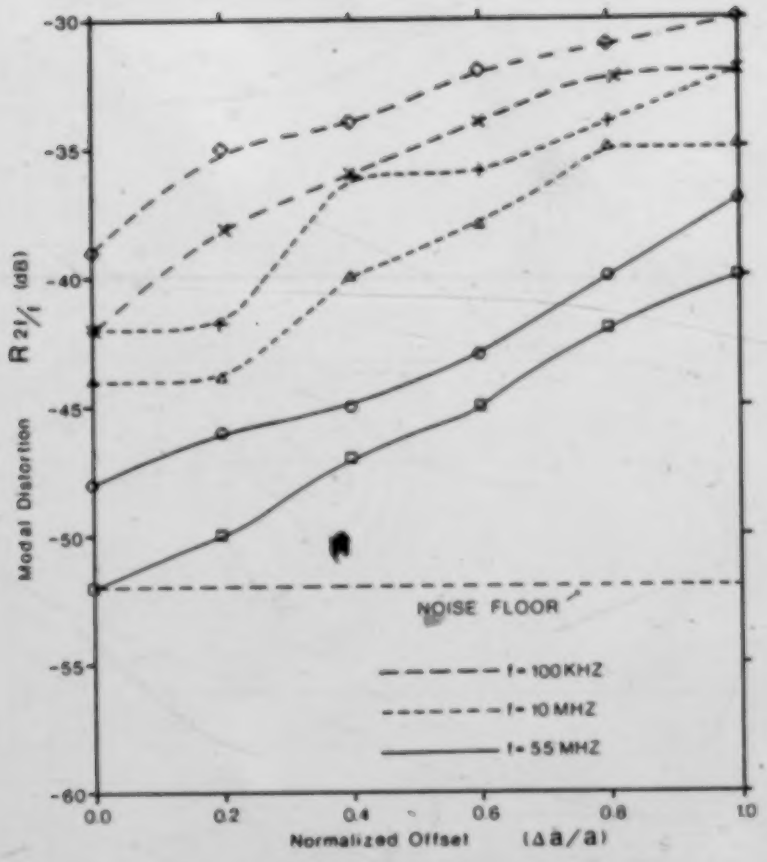

Figure 4.14 Modal distortion for different modulation frequencies f_m with fiber cleave 1. Experimental parameters same as in Fig. 4.11.

CHAPTER V

EVALUATION OF LOSS, MODAL NOISE AND DISTORTION DUE TO LONGITUDINAL OFFSET

The power loss, modal noise and distortion caused by a longitudinal gap between two multimode parabolic-index fibers is evaluated by using the modal amplitude coupling coefficients (derived in this chapter) along with the theoretical formalism of Chapter 3. These coupling coefficients are obtained by the method of Laguerre-Gauss mode matching, i.e., the fiber LG modes are matched to the diffracted free space modes at the gap. Such gaps, index-matched or dry, constitute one of the mode selective loss mechanisms in fiber components such as connectors, couplers and power splitters.

The effect of a steady state and of a uniform modal power distribution in the transmitting fiber on the power loss and noise are discussed. Also, the dependence of the loss, modal noise and distortion on the wavelength, source coherence, fiber numerical aperture and index matching is examined. It is found that, for coherent illumination and a given loss, the modal noise and distortion due to a gap are generally as severe as or worse than those due to an axial offset between two fibers. It is also shown that, when a partially coherent source is used, the transmission characteristics of a gap can be improved by increasing the operating wavelength. Experimental results have been obtained for the power loss and modal distortion; they are shown to be in close agreement with the theory.

5.1 Propagation of a Gaussian Beam

Consider a longitudinal gap of distance d between two identical parabolic-index multimode fibers (see Fig. 5.1), each with a beam radius w_0 defined in (2.12). At the plane $z=0$, the transmitting fiber LG modes join smoothly with the free space LG modes of radius w_0. Here, the beam modes have a planar phase front. However, due to diffraction, the free space unguided LG modes in the gap diverge, and the beam radius w_d at the plane $z=d$ is [153]

$$w_d = w_0\left[1+\left(\frac{2d}{k_m w_0^2}\right)^2\right]^{\frac{1}{2}} \tag{5.1}$$

where $k_m = n_m k$ designates the wave number of the matching medium between both

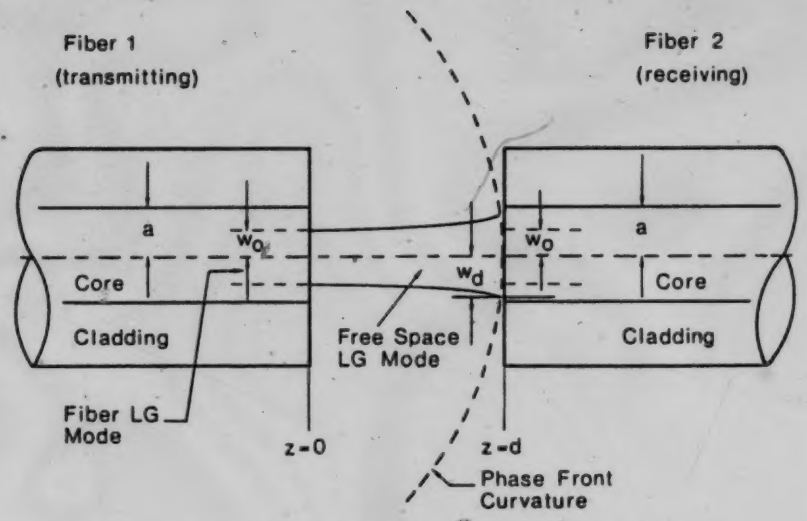

Figure 5.1 Two fibers separated by a longitudinal gap 'd'. At z=d, the free space LG beam radius is w_d.

fibers and n_m is the refractive index of this medium. The free space LG modes with beam radius w are now matched to the receiving fiber LG modes with beam radius w_0. To simplify the analysis, phase front curvature at the plane z=d is not included in this theory.

5.2 Evaluation of Modal Amplitude Coupling Coefficients

Assume a wave $\Psi_{q_1 l_1}$ (as described by (2.10), with the subscript 1 of q and l refering to fiber 1) of unit power being transmitted from fiber 1 in Fig. 5.1. Its beam radius at the reference plane is w_d. This will excite in fiber 2 a set of $\Psi_{q_2 l_2}$ (the subscript 2 of q and l refers to fiber 2) modes with field $C_{q_1 l_1, q_2 l_2} \Psi_{q_2 l_2}$, where the $C_{q_1 l_1 q_2 l_2}$ are the modal amplitude coupling coefficients. Because azimuthal symmetry is preserved at the longitudinal gap, only modes with the same azimuthal number couple. Thus,

$$C_{q_1 \ell_1 q_2 \ell_2} = C_{q_1 q_2 \ell} \quad \text{for } \ell_1 = \ell_2 = \ell \tag{5.2}$$

such that

$$C_{q_1 \ell_1 q_2 \ell_2} = 0 \quad \text{for } \ell_1 \neq \ell_2 \tag{5.3}$$

With the help of the orthogonality relations [70] for the modes of (2.8), the coupling coefficient between mode ν and mode μ of fibers 1 and 2 respectively is

$$C_{\nu\mu} = C_{q_1 q_2 \ell} = \left(\frac{2}{w_0 w_d}\right)^{\ell+1} \left[\frac{q_1!\, q_2!}{(q_1+\ell)!\,(q_2+\ell)!}\right]^{\frac{1}{2}} \int_0^\infty r^{2\ell} \times L_{q_1}^{\ell}\left(\frac{2r^2}{w_d^2}\right) L_{q_2}^{\ell}\left(\frac{2r^2}{w_0^2}\right) \exp\left(\frac{-r^2}{w_0^2 + w_d^2}\right) dr^2 \tag{5.4}$$

A closed form solution exists for (5.4) and is given by [70]

$$C_{\nu\mu} = \left(\frac{2w_0 w_d}{w_0^2 + w_d^2}\right)^{\ell+1} \left[\frac{(q_1+q_2+\ell)!}{q_1!\, q_2!\, (q_1+\ell)!\,(q_2+\ell)!}\right]^{\frac{1}{2}} \left(1 - \frac{2w_0^2}{w_0^2 + w_d^2}\right)^{q_1} \left(1 - \frac{2w_d}{w_0 w_d}\right)^{q_2} \times H\left[-q_1, -q_2, -q_1 - q_2 - \ell, \left(\frac{w_0^2 + w_d^2}{w_d^2 - w_0^2}\right)^2\right] \tag{5.5}$$

where H is a hypergeometric series, defined by

$$H\ (a,b,c,z) = 1 + \frac{a.b}{c}\ z + \frac{a(a+1)\ b(b+1)}{c(c+1)\ 2!}\ z^2 + \ldots . \qquad (5.6)$$

5.3 Results

In this section we show the results of the numerical evaluation of (3.39), (3.40) and (3.45) for the loss, modal noise and distortion for a longitudinal gap between two identical fibers without any axial or tilt offset [175],[176]; the relevant computer program is listed in Appendix A2. We also discuss the experimental results and show that they are in good agreement with the predicted steady state loss and modal distortion values.

5.3.1 Power Loss

We begin by comparing the splice loss values (evaluated according to (5.5) and (3.39)) for a uniform modal power distribution with those for the steady state distribution, for typical fiber parameters. The loss is plotted as a function of the normalized spacing d/a in Fig. 5.2. It is observed that the power loss corresponding to the uniform distribution is approximately 1.75 to 2 times higher than as that for the steady state case. It is also seen that index-matching, as opposed to an air gap, increases the coupling efficiency considerably by decreasing the beam divergence in the gap. The loss of an index-matched gap is 44 % (V=39, steady state) less than the loss due to an an air gap, when d/a=4. The amount of loss reduction is dependent on the Gaussian beam divergence in the gap, and hence it varies with the modal power distribution, the V number and d/a. These results are shown in Table 5.1.

Fig. 5.3 shows the steady state loss values (again calculated via (5.5) and (3.39)) for three different NA values; 0.1, 0.15 and 0.2 for $\lambda = 0.82\ \mu m$ and $a = 25\ \mu m$. The corresponding V numbers are 21, 29 and 39. There is a significant improvement in the loss values as the NA decreases, because of the larger relative beam radius (i.e., electromagnetic field spread) and consequently smaller beam divergence.

Using (5.5) and (3.39), numerical results for the wavelength dependence of the gap loss are shown in Fig. 5.4 for a steady state as well as a uniform power distribution. Two factors interplay here:

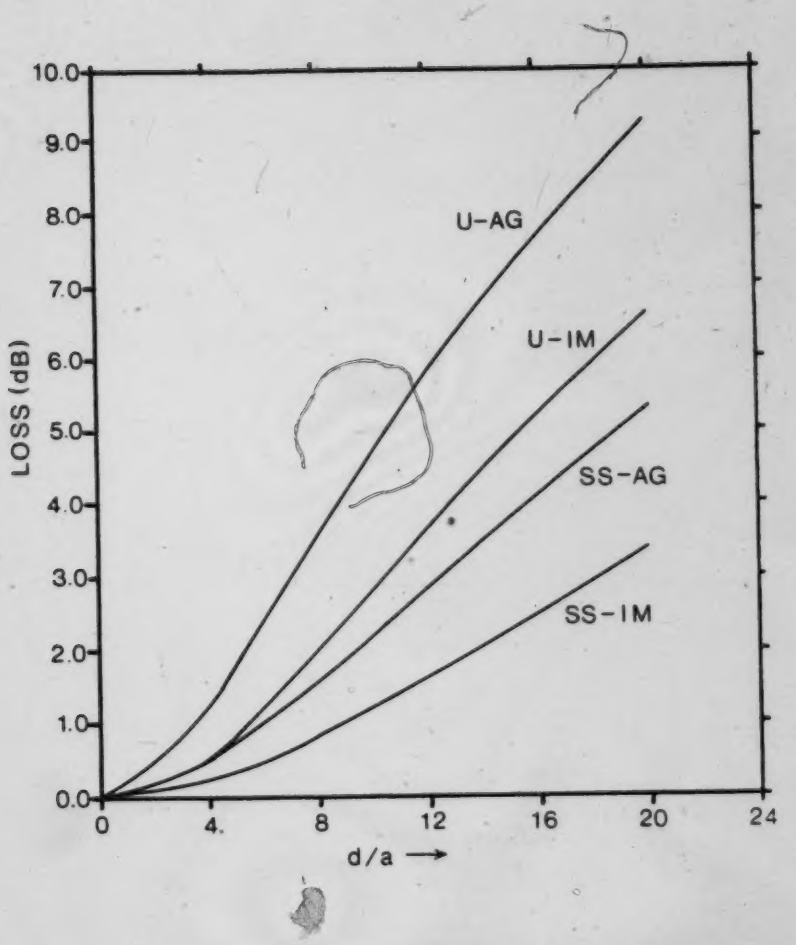

Figure 5.2 Power loss due to normalized spacing d/a for uniform (U) and steady state (SS) modal power distributions. Both air gap (AG) and index-matching (IM) are considered. a=25 μm, λ=1.55 μm, NA=0.2.

Table 5.1 Loss reduction expressed as a percentage of the air gap loss, when index-matching is used instead of an air gap ($4<d/a<20$). The figures in the bracket denote the air gap loss in dB. NA=0.2, a=25 μm, λ=0.82 μm (V=39) or λ =1.55 μm (V=21).

$\frac{d}{a}$		4	8	12	16	20
Steady State	V=39	44% (0.71)	41% (1.93)	37% (3.15)	34% (4.27)	32% (5.3)
	V=21	59% (0.67)	45% (1.95)	40% (3.33)	37% (4.63)	34% (5.86)
Uniform	V=39	50% (1.16)	44% (3.48)	37% (5.70)	33% (7.59)	29% (9.18)
	V=21	61% (1.22)	44% (3.58)	37% (4.82)	32% (7.63)	28% (9.21)

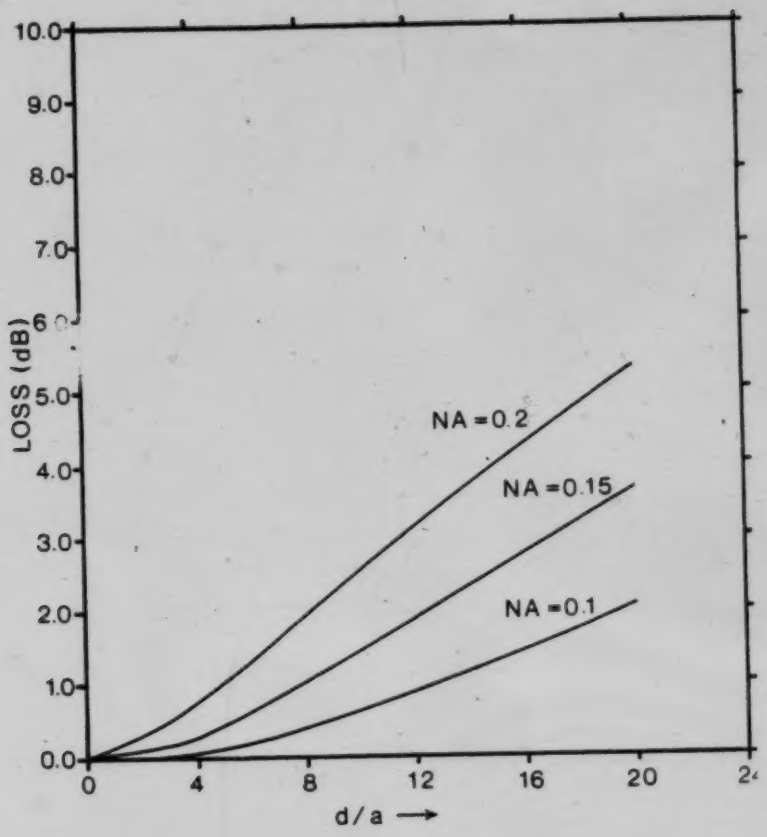

Figure 5.3 Power loss vs. normalized spacing d/a as a function of NA for steady state modal power distribution with an air gap. a = 25 μm, λ = 0.82 μm.

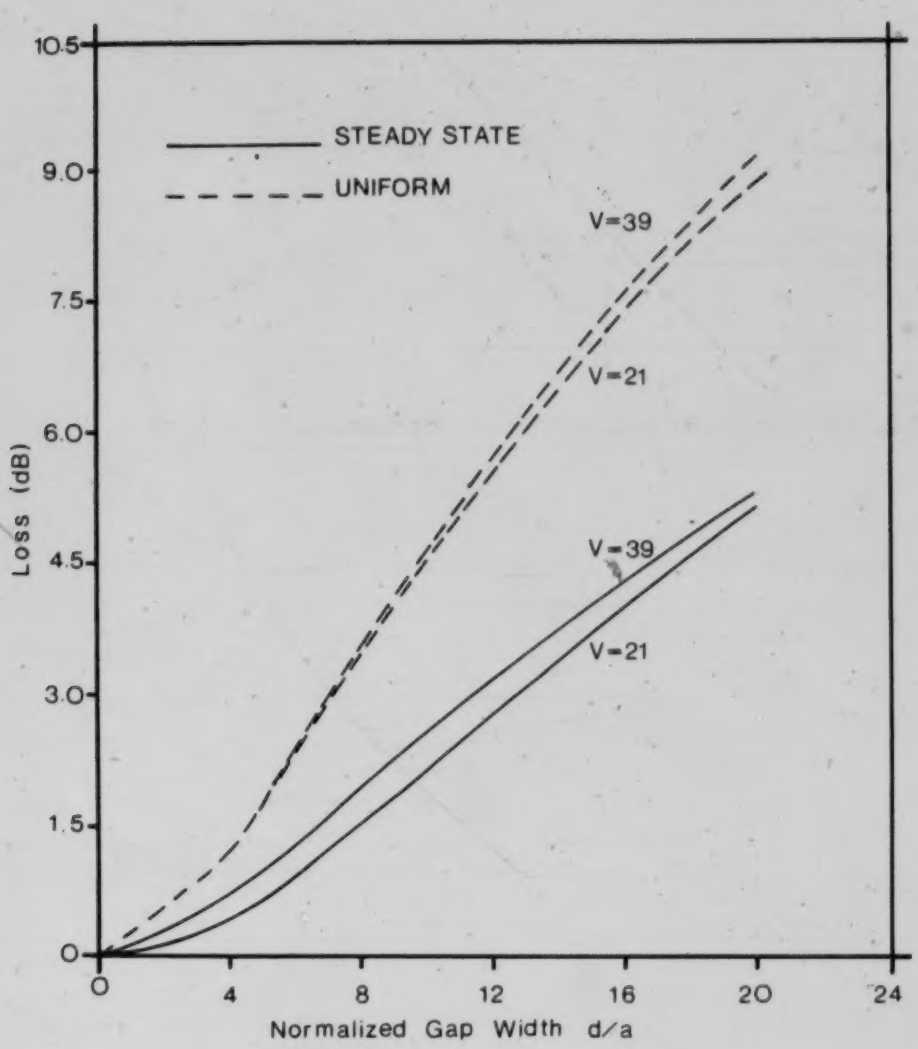

Figure 5.4 Power loss vs. normalized spacing d/a as a function of wavelength for an air gap. a=25 μm, NA=0.2.

1. The explicit wavelength dependence of the beam divergence according to (5.1), leading to greater mode mismatch at longer wavelengths.
2. The implicit wavelength dependence through (2.12), which yields a larger relative beam radius at longer wavelengths, and hence lower divergence via (5.1) and lower loss.

The combined contribution from these two opposing factors is seen to yield quite wavelength-independent gap loss.

The gap loss values were experimentally determined using the set up shown in Fig. 4.2. The cleaved endfaces of the fibers are the ones shown in Fig. 4.3. The spacing was not index matched and the distance d was carefully controlled by the x-y-z micropositioner. The data are plotted in Fig. 5.5 for $\lambda = 0.82$ μm, $a = 25$ μm and $NA = 0.2$, corresponding to $V = 39$. Theoretical values of the loss for these parameters are also shown. The graph shows that the experimental results are in good agreement with the steady state power distribution assumption, rather than with the uniform model. Some discrepancy at larger spacing values is possibly due to the fact that the modal power distribution had not quite attained the steady state in the fiber used in the experiment. Under the steady state assumption, the higher order modes carry much less power than the lower order ones. At high d/a values, the higher order modes are coupled the least. Thus, the weighting factors in (3.19) underestimate their contribution to the overall loss, if steady state has not actually been reached.

5.3.2 Modal Noise

The coupling efficiency and its standard deviation have been evaluated using (5.5), (3.21) and (3.24) for an air gap and for an index-matched gap, assuming typical fiber parameters. The results are shown in Fig. 5.6; a coherent source ($\tau_c \to \infty$) and a steady state power distribution have been assumed. It is seen that index-matching can improve the dc-SNR, both by increasing the coupling efficiency $\langle \eta \rangle$ and by decreasing the standard deviation of the coupling efficiency $\delta(\eta)$, with the former being important at large gap separation d. Fig. 5.6 also shows that, for high coupling efficiency ($\langle \eta \rangle > 0.9$), $\delta(\eta)$ is very small, corresponding to the LG mode-matched condition; however, $\delta(\eta)$ increases rapidly with increasing gap width to a limiting value of about 5 % for $\langle \eta \rangle < 0.9$. Hence, to first order, $\langle \eta \rangle$ is the only parameter that determines the dc-SNR values for gaps whose loss exceeds 0.5 dB ($\langle \eta \rangle \cong 0.9$).

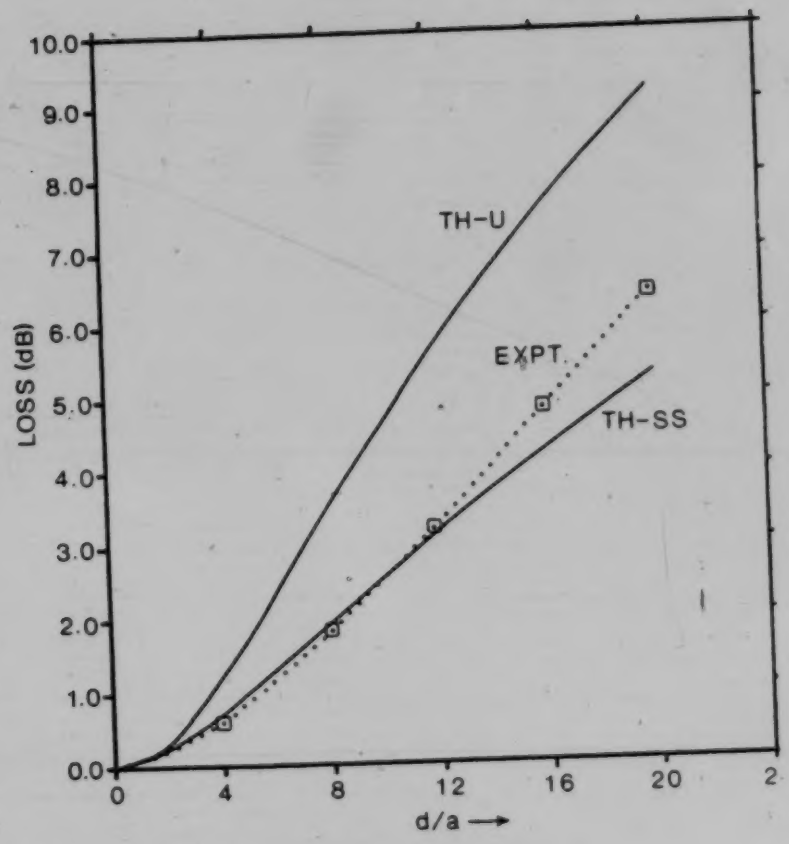

Figure 5.5 Theoretical (TH) and experimental (EXPT) power loss values vs. normalized spacing (d/a) for an air gap. a=25 μm, V=39.

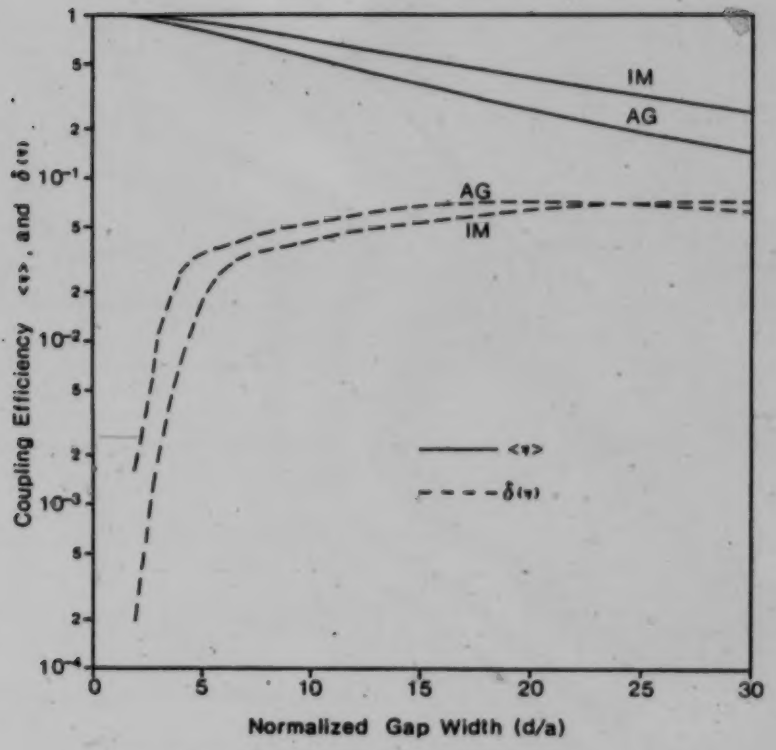

Figure 5.6 Variation of coupling efficiency $<\eta>$ and its standard deviation $\delta(\eta)$ with normalized gap width d/a, for an air gap (AG) and an index-matched gap (IM). NA=0.2, a=25 μm and V=21.

If the dc-SNR is plotted as a function of gap loss rather than of gap width, the curves for an air gap and for an index-matched gap almost merge, as shown in Fig. 5.7 (for coherent illumination). Also shown in this figure are the dc-SNR results for an axial offset from Chapter 4, assuming a steady state power distribution. Although the nature of the coupling and the magnitude of the modal amplitude coupling coefficients are different at a gap from that at an axial offset, the resulting dc-SNR is seen to depend only on the magnitude of the mode selective loss.

Calculation of the dc-SNR using modal analysis involves the summation of a large number of terms (e.g., 10,000 terms when V=39, for coupling between modes of the same polarization and the same orientation). Many of these terms vanish due to azimuthal symmetry; still, the calculation takes considerable computation time. To avoid this, the simpler expression (3.41) derived from speckle theory, can be used to make a rapid estimate of modal noise. Eq. (3.41) has been shown to be valid for parabolic-index fibers [55], although its application is restricted to the case of a closed speckle regime [50] (i.e., no coupling to cladding modes) and primarily axial misalignments [50]. In spite of these restrictions, we may compare the dc-SNR predictions according to (3.41) with the exact results from modal analysis for a gap, assuming a uniform power distribution and coherent illumination. For coupling losses exceeding 1 dB, Fig. 5.8 shows that the dc-SNR predicted by (3.41) is reasonably close to the numerically evaluated results of modal analysis. This is because the dc-SNR according to (3.40) is almost only dependent on $\langle\eta\rangle$ once $\delta(\eta)$ has reached its limiting value (see Fig. 5.6). However, for low gap losses, and when the number N of modes guided by fiber 1 is small, speckle theory yields a larger fluctuation of the coupling efficiency than modal analysis. Hence, the use of (3.41) becomes questionable for gap losses smaller than 1 dB.

Fig. 5.9 shows the improvement in the dc-SNR for a partially coherent source (increasing $\frac{\tau_{rms}}{\tau_c}$) over that for coherent illumination for a transmission loss of 1 dB ($\langle\eta\rangle = 0.8$). Both longitudinal gap and axial offset have been considered. The intermodal delay τ_{ux} has been calculated according to (2.21). It is seen from Fig. 5.9 that, for partially coherent excitation and fixed loss, axial offsets generate more modal noise than longitudinal ones. This is because, with partially coherent sources the far field interference pattern (corresponding to the gap case) becomes much finer compared to the near field one (which corresponds to the axial offset case). This behavior cannot be predicted using the

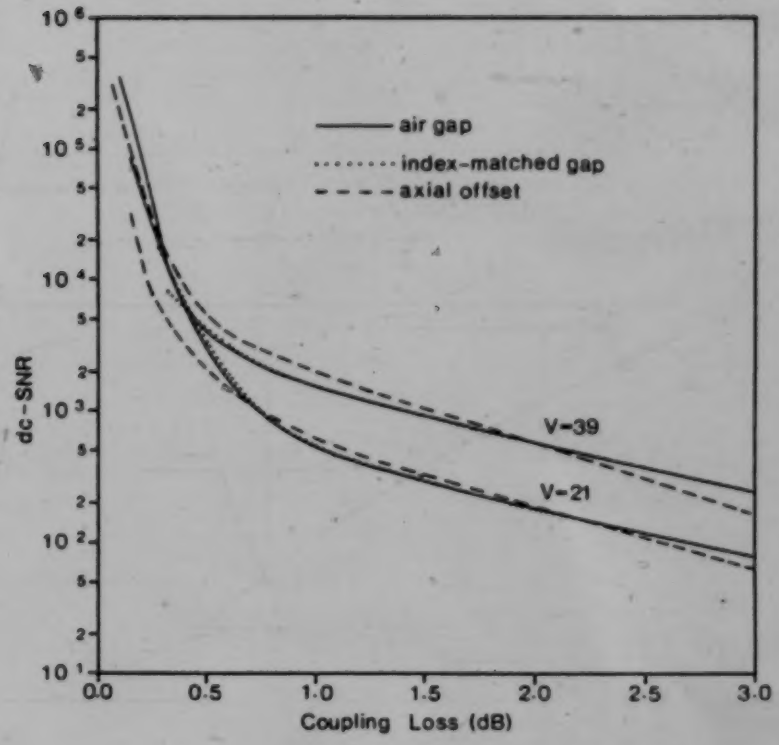

Figure 5.7 dc-SNR as a function of coupling loss, for a coherent source. NA = 0.2 and a = 25 μm.

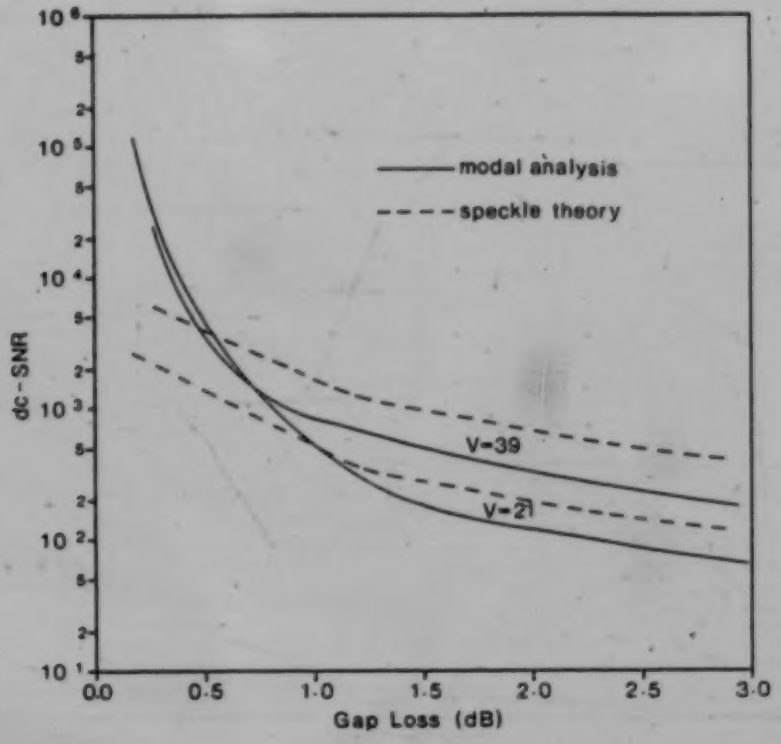

Figure 5.8 dc-SNR behavior as a function of gap loss, as predicted by : 1) modal analysis assuming a uniform power distribution and coherent illumination, and 2) speckle theory. NA=0.2 and a=25 μm.

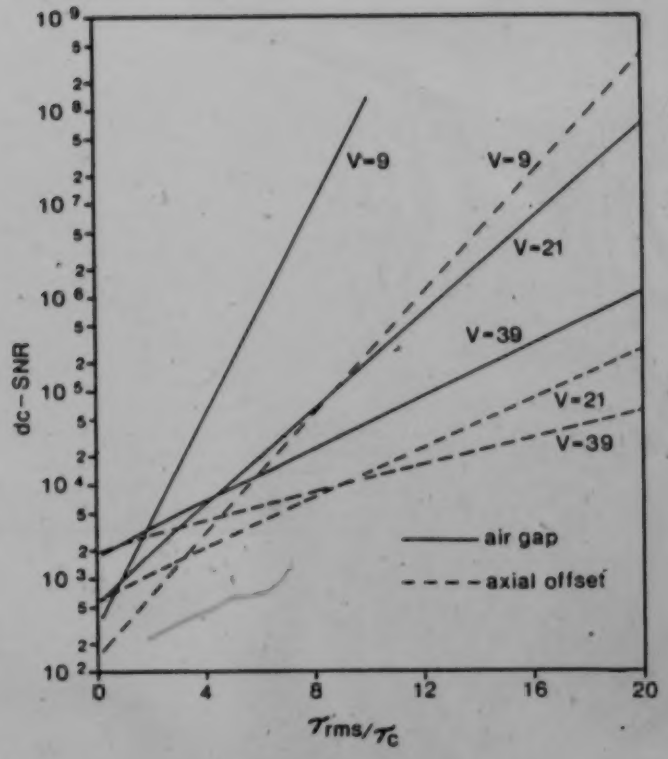

Figure 5.9 dc-SNR for partially coherent sources with coherence time τ_c. Coupling loss = 1 dB, a=25 μm, NA=0.2, and τ_{rms}=0.15 ns.

speckle theory expression (3.41), since the effect of speckle contrast at the endface of fiber 1 has not been included.

In view of the current development in fiber technology of glasses that operate optimally at longer wavelengths, the behavior of modal noise with increasing wavelength is also of interest. It is found that the dc-SNR for a partially coherent source improves substantially with increasing wavelength (decreasing V). In fact, when $\frac{\tau_{rms}}{\tau_c} = 20$, the dc-SNR for V=9 is better by seven orders of magnitude compared to V=39. This is because the delays (between adjacent modes in the β-space) for a low V fiber may exceed the source coherence time, thus leading to a smoother speckle pattern.

5.3.3 Modal Distortion

Eq. (3.26) is normalized with respect to $<\eta>\tau_{rms}$; the resulting expression denotes the sensitivity of the coupling efficiency with respect to a shift of the emission frequency. These values are plotted for coherent illumination in Fig. 5.10. The error in using LP-modes is avoided here because a small $\tau_{\nu\times}$ makes only a small contribution to (3.26). For a coherent source, and for identical power loss, it is observed that the magnitude of the fluctuation due to a gap for V=21 is higher than that due to an axial offset (V=21 or V=39). This is most easily understood if we consider separating two fiber ends until only one speckle of the far field pattern falls on the core of the second fiber. Clearly a large change in the interference pattern due to a small source wavelength shift can now cause a dark region to be coincident with the fiber core, resulting in 100 % amplitude modulation of the signal.

As the temporal coherence decreases (increasing $\frac{\tau_{rms}}{\tau_c}$), the rms fluctuations $\sqrt{<(\frac{d\eta}{d\omega_c})^2>}\,\frac{1}{\tau_{rms}<\eta>}$ also decrease, but the decrease is faster for a gap than for an axial offset. This property, valid for partial coherence, is shown graphically in Fig. 5.11. For V=21 and a gap loss of 1 dB, the rms fluctuation amplitude is only 0.3 percent at $\tau_{rms}/\tau_c = 10$ compared to 3 percent when the source is coherent. With increasing wavelength, the fluctuations also decrease. When $\frac{\tau_{rms}}{\tau_c} = 20$, the fluctuation for a gap is three orders of magnitude smaller at V=9 compared to V=39.

Experimental results for modal distortion $R_{2f/f}$ are plotted in Fig. 5.12 and show good agreement with the theoretical predictions from (3.45). The theoretical curves have been plotted for an air- and for an index-matched gap. It is worthwhile to note that both optical

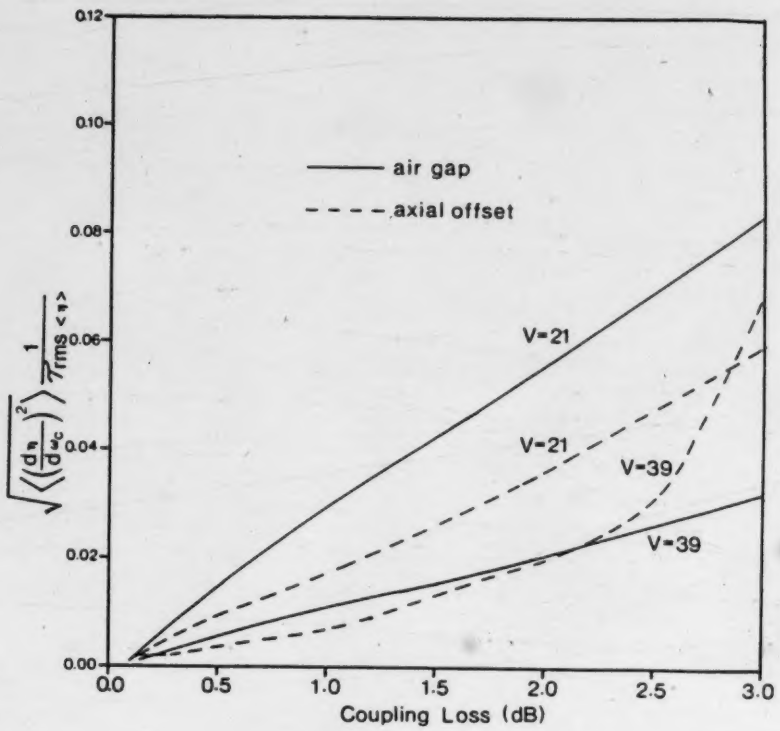

Figure 5.10 Variation of the normalized rms value of the derivative of the coupling efficiency with coupling loss, for coherent illumination. NA = 0.2, a = 25 μm, and τ_{rms} = 0.15 ns.

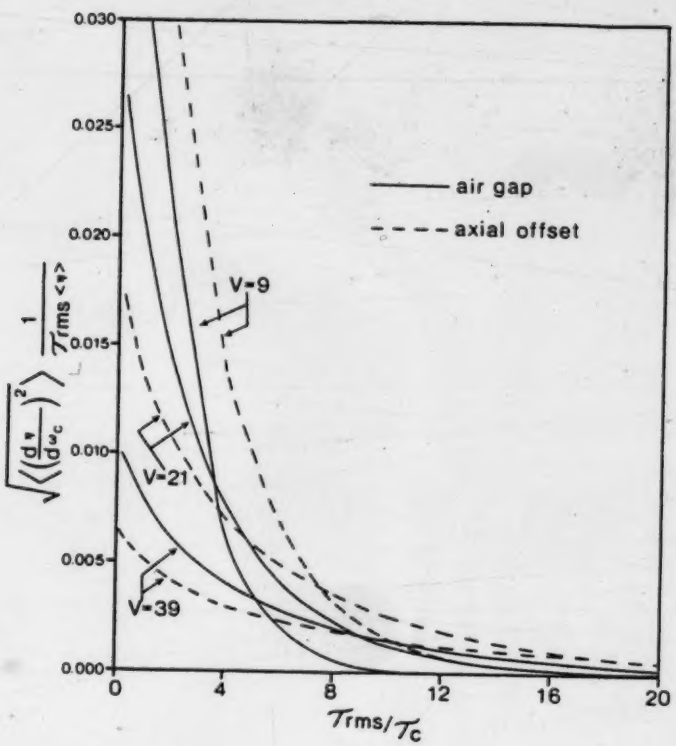

Figure 5.11 Normalized rms value of the derivative of the coupling efficiency for partially coherent sources with coherence time τ_c. Coupling loss = 1 dB, a=25 μm, NA=0.2, and τ_{rms} =0.15 ns.

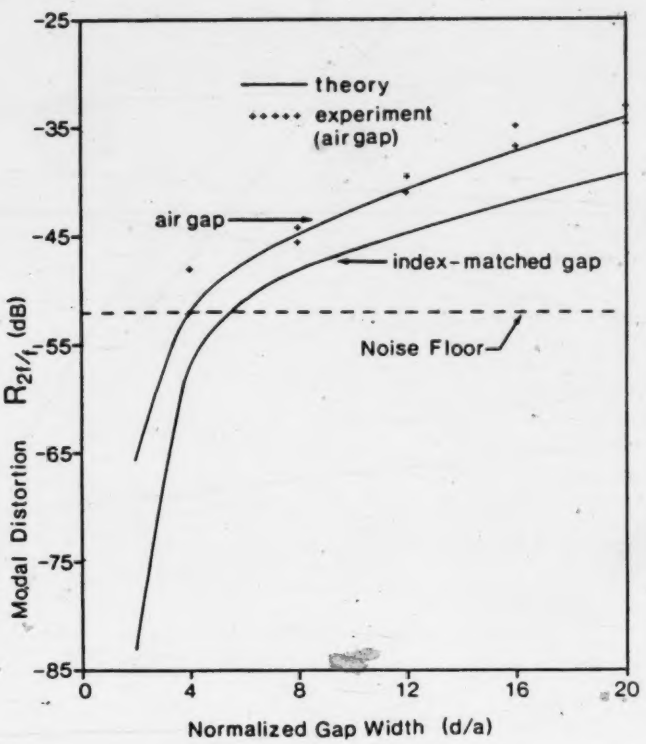

Figure 5.12 Modal distortion $R_{2f/f}$, as a function of normalized gap width for a partially coherent source. NA=0.2, a=25 um, V=39, f=55 MHz, m=0.25, τ_c =35 ps, τ_{rms} =0.15 ns, and $\Omega_m/2\pi$=2 GHz.

feedback and the Fabry-Perot cavity effect at a gap can be totally eliminated by index-matching, but not modal distortion. For a power loss of only 1 dB in an index-matched gap, the modal distortion $R_{2f/f}$ can be as high as -40 dB (V=39 and coherent source) which may be unacceptable for analog transmission. A loss of this magnitude can be produced by a gap whose width is 4 times the core diameter for an index-matched case, and only 3 times the core diameter for an air gap.

5.4 Conclusions

The transmission characteristics of a longitudinal gap between two near parabolic-index fibers have been discussed; the power loss, modal noise and distortion generated due to this gap have been quantified using modal analysis and verified experimentally. The power loss is almost wavelength-independent and decreases significantly for fibers with a lower numerical aperture. If index-matching is used as opposed to an air-gap, the loss reduces by $\tilde{=}$ 0.3 dB at a normalized spacing of 4, and by $\tilde{=}$ 2 dB when the normalized spacing is 20.

For a given gap width, index matching is seen to improve the noise and distortion figures considerably over its air gap counterpart. However, for a given loss, the magnitude of the noise and distortion for an index-matched gap are the same as for an air gap. It was also found that, with coherent illumination and for a given loss, the modal noise and distortion due to a gap are generally as severe as or worse than those caused by an axial offset. Hence, if a coherent source is used, good quality analog transmission will not be possible, even with modest values of gap loss present, because the modal distortion will be unacceptably high. However, our results show that, as the temporal coherence decreases, the power fluctuations at a gap decrease much more than those at an axial offset; the decrease is also greater when the number of guided modes is small (longer wavelength). These results suggest that, to obtain low-noise and low-distortion optical fiber communications, a partially coherent source should be used, operating in the longer wavelength region.

CHAPTER VI

EVALUATION OF LOSS, MODAL NOISE AND DISTORTION DUE TO TILT OFFSET

In this chapter, a tilt offset between two near parabolic-index multimode fibers is characterized. Since a geometrical optics analysis provides only a limited description of the effect of tilt on the transmission characteristics (e.g., loss for a uniform power distribution and high mode volume fiber) at a splice, we use an electromagnetic theory for a complete treatment of the steady state conditions and noise characteristics. In order to avoid numerical integration, the modal amplitude coupling coefficients are determined in closed form using the overlap integral formulated by Sakai and Kimura [91].

The theoretical loss predictions agree with previously published theoretical results for tilt offsets for a dual mode fiber, and also with those predicted by geometrical optics using a uniform power distribution. Furthermore, the loss and modal distortion results agree with new experimental measurements made with a long, spliced input fiber. Using a uniform distribution, this analysis corroborates a previously reported geometric optics result that fiber axis tilt at the splice is equivalent to an axial offset. It is also shown that this equivalence applies to the prediction of loss values only, and the approximation gets worse as the fiber mode volume decreases. For partially coherent illumination and a given loss, the modal noise results for tilt offset are shown to be higher than those due to axial or longitudinal offsets. However, for coherent excitation, numerical results of modal noise for all three geometrical misalignments are found to be very similar.

6.1 Calculation of the Modal Amplitude Coupling Coefficients

The modal amplitude coupling coefficient $C(q_1l_1; q_2l_2)$, for mode q_1l_1 of the transmitting fiber and mode q_2l_2 of the receiving fiber is obtained directly from the theory of excitation of weakly guiding fibers as given in (4.2). Fig. 6.1 illustrates a fiber splice cross-section with tilt of angle θ. Cylindrical coordinate systems (r_1, ϕ_1, z_1) and (r_2, ϕ_2, z_2) are employed for the sending (fiber 1) and receiving (fiber 2) fibers respectively. The fields in the plane $z_2=0$ are given by multiplying the fields at the $z_1=0$ plane in the sending fiber by the phase factor $\exp(-j\beta z_1)$. For small θ, integration of (4.2) over $0<\phi_1=\phi_2<2\pi$ leads to [91]

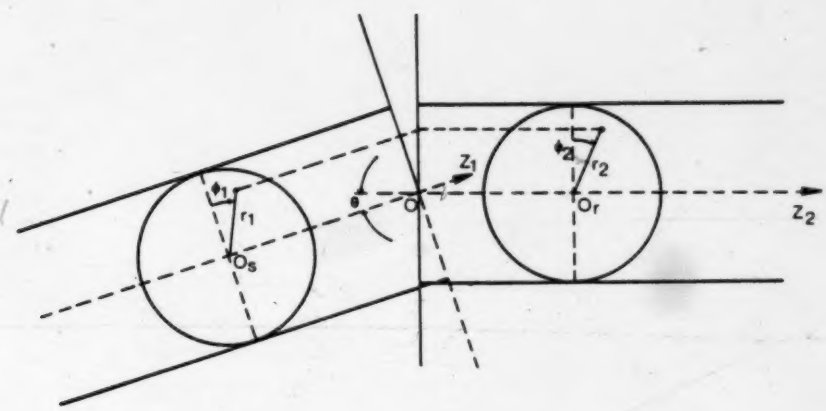

Figure 6.1 Cross-section of butt-jointed fibers with tilt offset. The angle between the axes of the two joining fibers is θ .

$$C_{\nu\mu} = \frac{2}{w_0^2} C'_{\ell_1 q_1} \; C'_{\ell_2 q_2} \; \pi a^2 \int_0^\infty f\left(\frac{r}{a}\right) g\left(\frac{r}{a}\right) \Big\{ j^{\ell_1+\ell_2} J_{\ell_1+\ell_2}(\beta_g \theta r) + j^{\ell_1-\ell_2} J_{\ell_1-\ell_2}(\beta_g \theta r) \Big\} \left(\frac{r}{a}\right) d\left(\frac{r}{a}\right) \tag{6.1}$$

where $r_1 \simeq r_2 = r$

$$C'_{\ell q} = \sqrt{\frac{e_\ell}{\pi} \frac{q!}{(\ell+q)!}}$$

$$e_\ell = \begin{cases} 1 & \text{for } \ell=0 \\ 2 & \text{for } \ell\neq 0 \end{cases}$$

$f\left(\frac{r}{a}\right)$ = radial variable of the transverse electric field of sending fiber.

$g\left(\frac{r}{a}\right)$ = radial variable of the transverse electric field of the receiving fiber.

$J_n(z)$ = Bessel function of order n

with the help of the integration formula

$$\int_0^\pi (\cos n\phi) \exp(jz\cos\phi)\, d\phi = \pi (j)^n J_n(z) \tag{6.2}$$

It is found that $C_{\nu\mu}$ becomes imaginary when the difference between l_1 and l_2 is odd. The appearance of an imaginary value is due to the phase shift between modes at the splice. For weak guidance, the propagation constant β_g is rewritten as $(V/a\sqrt{2\Delta})$, so that $C_{\nu\mu}$ is obtained as a function of the normalized tilt offset $\theta_N = \theta/\sqrt{2\Delta}$ and V. When the modal fields as given by (2.8) are used, closed form solution to (6.1) exists in terms of Laguerre polynomials [170]

$$C_{\nu\mu} = \frac{1}{2}\,(e_{\ell_1} e_{\ell_2})^{\frac{1}{2}} \left[\frac{q_1!\; q_2!}{(q_1+\ell_1)!\,(q_2+\ell_2)!}\right]^{\frac{1}{2}} (-1)^{q_1+q_2} \exp(-y)$$

$$\Bigg\{ j^{\ell_1+\ell_2}\; V^{\frac{\ell_1+\ell_2}{2}}\; 2^{-(\ell_1+\ell_2)}\; \Theta_N^{\ell_1+\ell_2}\; L_{q_1}^{\ell_2-\Delta q}(y)\; L_{q_2}^{\ell_1+\Delta q}(y)$$

$$+\, j^{|\Delta\ell|}\; V^{\frac{|\Delta\ell|}{2}}\; 2^{-|\Delta\ell|}\; \Theta_N^{|\Delta\ell|}\; \frac{(q_k+\ell_k)!}{q_k!}\; \times$$

$$L_{qi}^{q_k-q_i}(y)\; L_{q_k+\ell_k}^{|\Delta\ell|+q_i-q_k}(y) \Bigg\} \qquad (6.3)$$

Where: $y = \Theta_N^2\, \frac{V}{4}$

$\Delta\ell = \ell_1 - \ell_2$

$\Delta q = q_1 - q_2$

$$i = \begin{cases} 1 & \text{for } \ell_1 > \ell_2 \\ 2 & \text{for } \ell_1 \leqslant \ell_2 \end{cases}$$

$$k = \begin{cases} 1 & \text{for } \ell_1 \leqslant \ell_2 \\ 2 & \text{for } \ell_1 > \ell_2 \end{cases}$$

To arrive at (6.3), the well documented integral

$$\int_0^\infty s^{p+1}\; e^{-\alpha s^2}\; L_m^{p-\sigma}(\alpha s^2)\; L_n^{\sigma}(\alpha s^2)\; J_p(xs)\, ds$$

$$= (-1)^{m+n}\; (2\alpha)^{-(p+1)}\; x^p\; e^{-x^2/4\alpha}\; L_m^{\sigma-m+n}\left(x^2/4\alpha\right)$$

$$L_n^{p-\sigma+m-n}\left(x^2/4\alpha\right) \qquad (6.4)$$

Re $p > -1$

was used, alongwith the relationship

$$L_n^{-\delta}(x) = (-1)^{\delta} \; x^{\delta} \; \frac{(n-\delta)!}{n!} \; L_{n-\delta}^{\delta}(x) \tag{6.5}$$

The mode coupling matrix [C] is complex; when multiplied with its conjugate transpose (also called Hermitian transpose), the resulting interference matrix [F] is Hermitian

$$[F] = [C]\overline{[C]}^{T} = [C][C]^{H} \tag{6.6}$$

with all real diagonals. From here on, we proceed in the same manner to evaluate the power loss, modal noise and distortion as was done for axial and longitudinal offsets.

6.2 Results and Discussion

Equation (6.3), alongwith (3.39), (3.40) and (3.45) can be used to calculate the splice loss, modal noise and distortion for tilt offsets, respectively. The relevant computer program is listed in Appendix A3. To validate our analysis, comparison will be made with existing theories wherever possible. Most existing results on tilt offset are geometrical optics evaluations of splice loss, and the modal power distribution equivalent to any assumed ray distribution is difficult to evaluate in general. However, the ray distribution equivalent to the uniform modal power distribution is well documented [87], and comparison of splice loss predictions for this case demonstrates this analysis is probably accurate. Calculated results and experimental measurements on tilt loss, modal noise and distortion are shown in the sections that follow. Although the theoretical values have been evaluated for the case of a tilt between fusion spliced fiber (see Fig. 6.1), the experimental data correspond to a tilt between two butt-coupled fibers in a demountable connector (see Fig. 2.3). The modal analysis for the latter case is difficult because the phase change can no longer be denoted simply by $\exp[j\theta r \cos \phi]$. By a translation of the z-coordinate to the $r=a$ plane, the appropriate phase factor will be given, either by $\exp[j\theta(a - r\cos\phi)]$ or by $\exp[j\theta(a + r\cos\phi)]$, thus no closed form solution can be found to the integration (6.1).

6.2.1 Splice Loss

This section presents the results for splice loss associated with tilt of the fiber axis for identical fibers. The numerical evaluation assumes that there is no end separation and thus no diffraction. For small tilt offsets ($< 10°$), diffraction effects can be ignored because in Chapter 5 it is demonstrated that end separation as wide as a core diameter sustains very little loss (< 0.4 dB for $V=39$, steady state distribution and not index-matched).

Using (6.3) and (3.39), the predictions for a uniform as well as a steady state power distribution are shown in Fig. 6.2 as a function of the normalized tilt offset Θ_N ($V=21$ and $V=39$). In our calculations, a tilt offset of 1° corresponds to $\Theta_N=0.13$, the evaluated loss values are 0.267 dB for the steady state assumption and 0.485 dB for the uniform case ($V=39$). For experimental measurements, the set-up of Fig. 4.2 was used, with the x-y-z micropositioner replaced by a rotation stage (Ardel Kinamatic). The rotation stage did not have high resolution ($\tilde{=}$ 1°), further it exhibited backlash ($=5°$). Hence, the angle markings on the rotation stage were recalibrated accordingly. Consequently, some error in data was unavoidable. Although the tilt loss data applies to the case of a connector and the theoretical values to a fusion splice, we still compare both results. The tilt data areseen to lie between the steady state curve and the uniform distribution curve suggesting that the power distribution has not quite achieved the 'steady state'. Apart from the discrepancy that can be attributed to the different geometries considered (i.e., fusion splice for the theory and demountable connector for the experiment), some theoretical error could also be due to the fact that in the evaluation of the mode coupling coefficients in (6.1), all guided mode propagation constants were approximated by the $r=0$ plane wave propagation constant. This approximation could underestimate the actual tilt loss.

In Ref. [63], geometrical optics was used to show that fiber axis tilt at a splice is equivalent to an axial offset via the relationship

$$\frac{\theta}{\sqrt{2\Delta}} = \frac{\Delta a}{a} \qquad (6.7)$$

It is of interest to check if this equivalence is valid from the modal analysis for a pure tilt or axial offset. Therefore, loss values for axial offset according to (6.7) for a uniform power distribution are also shown in Fig. 6.2, and the good correspondence demonstrated for fibers

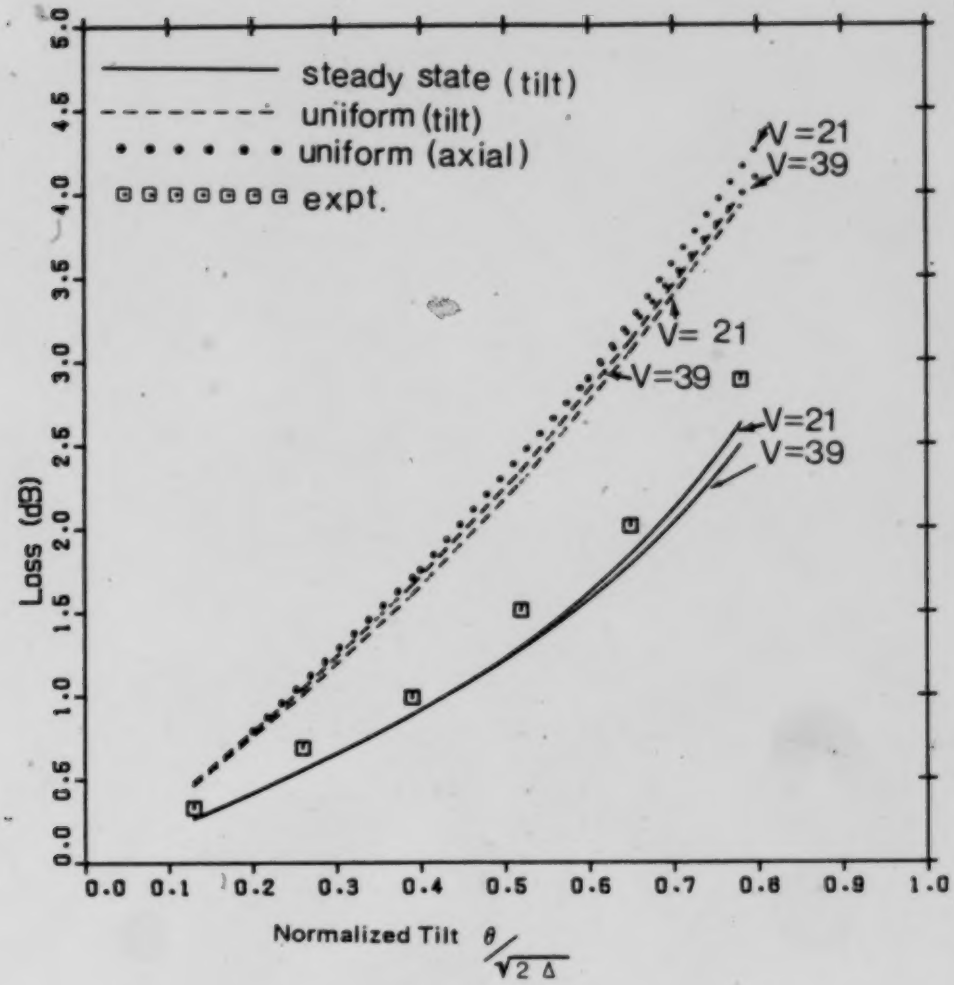

Figure 6.2 Loss vs. normalized tilt offset Θ_N at butt-jointed fibers. Theoretical results are for a tilt at a fusion splice, whereas the data corresponds to a tilt at a connector. Results for equivalent axial offset according to Eq. (6.7) are shown by dotted lines for a uniform power distribution. $\Delta = 0.0092$.

with a high mode volume (i.e., a high V). This corroborates the well known fact that modal analysis results agree well with geometric optics findings under certain conditions (i.e., a high V and a uniform power distribution). It remains to be seen (in the next section) if, for a given source coherence and loss, one can expect equal amounts of modal noise and distortion for tilt and axial offset.

We will also compare tilt loss results based on the LG-modes of the infinite square-law medium with those obtained using a staircase approximation for the index profile [91]. The analysis in Ref. [91] was restricted to a dual-mode parabolic-index with V=3.518. The core region was divided into twenty layers (or staircases) and a tilt loss of 0.2 dB was obtained for the LP_{01} mode when $\theta_N=0.152$. Our analysis using (6.3) yields a loss of 0.18 dB. We have checked the LP_{01} mode loss for other values of θ_N ; the maximum discrepancy between the results of the two approximations (i.e., infinite square-law and the staircase) is found to be less than ±15 %.

6.2.2 Modal Noise

The mechanism that gives rise to modal noise at axial offsets and gaps is also responsible for yielding a SNR deterioration at a tilt. The modal amplitude coupling coefficients for an axial offset are all real, but those for a gap are complex if the phase front curvature effects are included; however, the coefficients for a tilt offset are either real or imaginary. Fig. 6.3 shows the coupling efficiency $\langle\eta\rangle$ and its standard deviation $\delta(\eta)$ with tilt for V=21 and coherent illumination. When compared with Fig. 4.6 (axial offset), it is found that $\delta(\eta)$ for a tilt is usually higher than that for an axial offset for all values of $\langle\eta\rangle$, both for a uniform and for a steady state power distribution. Also, when comparison is made on the basis of (6.7), for tilt is found to be usually higher than that for an axial offset. For example, at $\theta/\sqrt{2\Delta}=\Delta a/a=0.5$, $\delta(\eta$ for an axial offset is 5 %, whereas that for a tilt is 8 % (uniform distribution, V=21).

In Fig. 6.4, the dc-SNR according to (3.40) has been plotted as a function of the splice loss for a coherent source. The dc-SNR for a tilt is always found to be lower than its axial offset counterpart, irrespective of the V number, and regardless of the power distribution (see Fig. 6.4 and Fig. 5.7). Thus, the foregoing rigorous theoretical treatment shows that a tilt offset indeed behaves differently from an axial offset as far as modal noise is concerned.

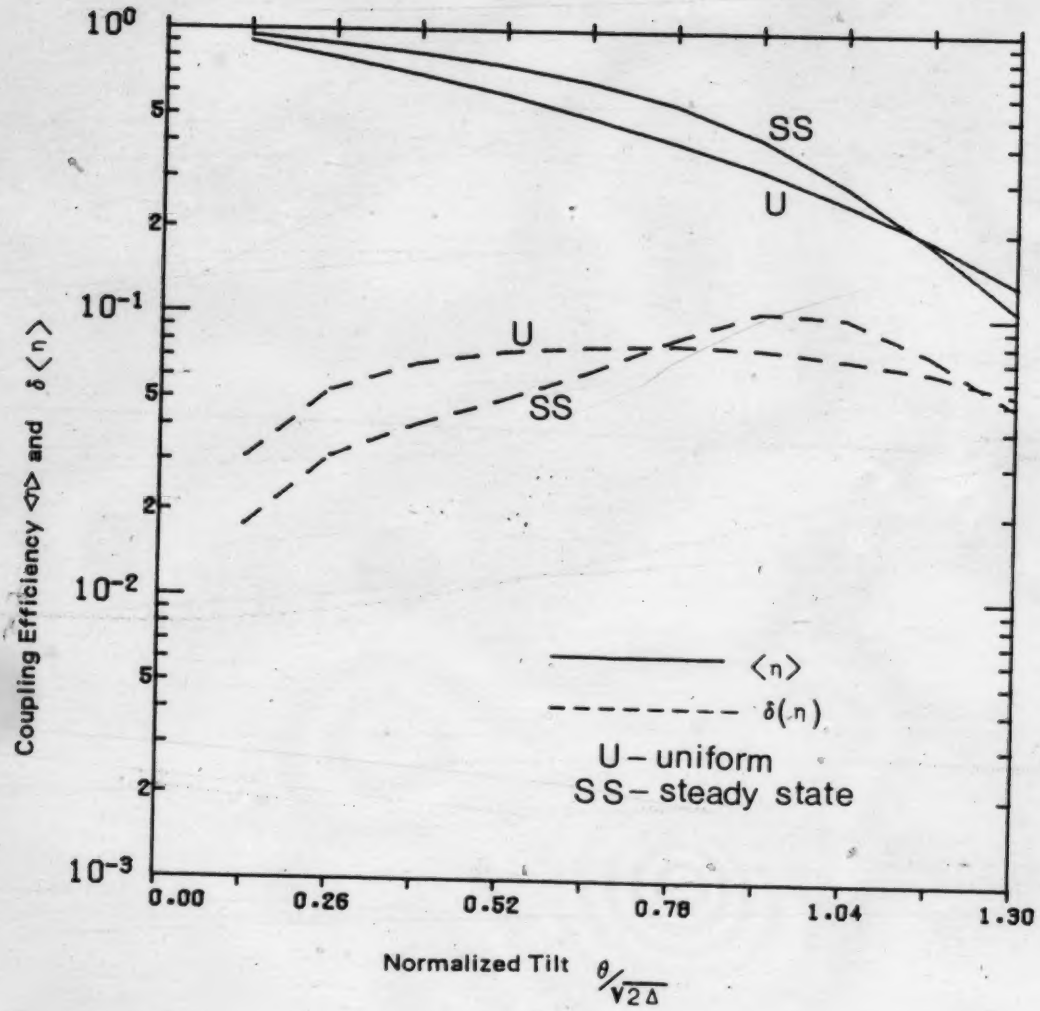

Figure 6.3 Coupling efficiency $<\eta>$ and its standard deviation $\delta(\eta)$ as a function of normalized tilt for a coherent source. V=21 and Δ=0.0092.

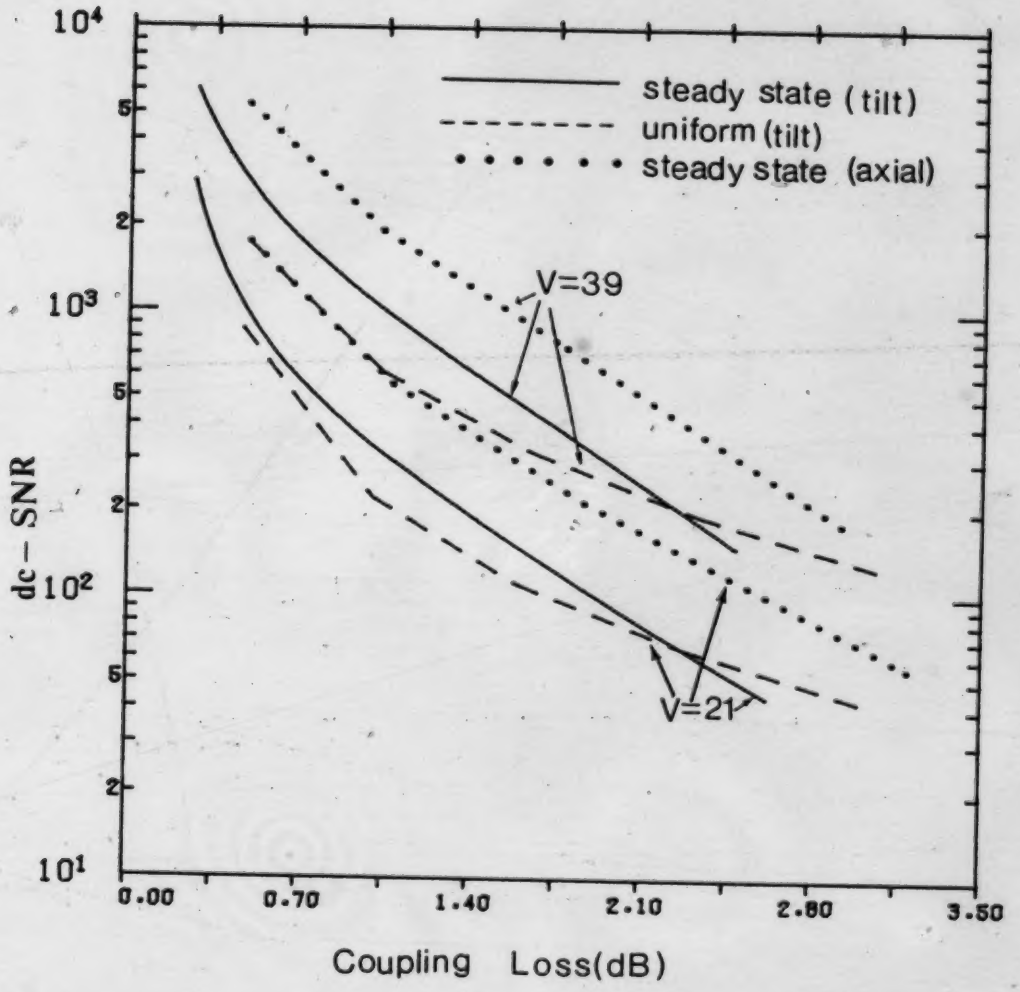

Figure 6.4 dc-SNR for a coherent source as a function of splice loss incurred by tilt. Results for an equivalent axial offset according to Eq. (5.7) are shown by dotted lines.

However, the dc-SNR differences for all three types of misalignments are within an order of magnitude for coherent excitation. We may then, for all practical purposes, conclude that the magnitude of modal noise is only dependent on the amount of mode selective loss. This is a very interesting and useful result, since it suggests that the connector loss alone can be used to predict the modal noise values without any a priori knowledge about the type of geometrical misalignment present at that connector. For partially coherent sources however, this prediction is not quite valid.

As Fig. 6.5 shows, the improvement in the dc-SNR for a tilt is minimal as τ_{rms} / τ_c increases. Furthermore, with decreasing coherence, the V=21 and V=39 curves do not cross over as they did for gaps or axial offsets. As compared to coherent excitation, the dc-SNR at $\frac{\tau_{rms}}{\tau_c} = 20$ improves by a factor of 10^5 for an air gap, by 500 for an axial offset, and by a meager 30 for a tilt offset (V=21, splice loss = 1 dB).

6.2.3 Modal Distortion

The derivative of the coupling efficiency with respect to the emission frequency (3.26) is normalized and plotted as a function of the tilt loss in Fig. 6.6 for a coherent source. Comparison with Fig. 5.10 shows that $\sqrt{\langle (\frac{d\eta}{d\omega_c})^2 \rangle} \frac{1}{\tau_{rms} \langle \eta \rangle}$ for a tilt is almost of the same order of magnitude as that due to a gap or an axial offset. As a function of partial coherence τ_{rms} / τ_c, the decrease in the normalized fluctuation $\sqrt{\langle (\frac{d\eta}{d\omega_c})^2 \rangle} \frac{1}{\tau_{rms} \langle \eta \rangle}$ for a tilt is again found to be slow compared to either an axial offset or a gap, as can be seen from Fig. 6.7 and Fig. 5.11. Thus, the high frequency modal noise (due to source wavelength shifts) and distortion characteristics show a striking resemblance to that of the dc-modal noise (due to fiber flexing, temp. changes etc.) discussed in the earlier section.

Experiments were carried out to measure the modal distortion $R_{2f/f}$ as a function of the tilt offset and the results are shown in Fig. 6.8. All experimental conditions except the modulation index, were the same as those for an axial offset or a gap. The modulation index had to be increased to 50 % in order to keep the fundamental signal frequency significantly above the noise floor of the spectrum analyzer. Because of a doubling of 'm' (as compared to the axial offset or a gap case), the maximum frequency shift $\Omega_m / 2\pi$ doubled [177]. Its new value i.e., 4 GHz, was used in the theoretical calculations according to (3.45).

The lower limit of the data lies midway between the uniform and the steady state distribution

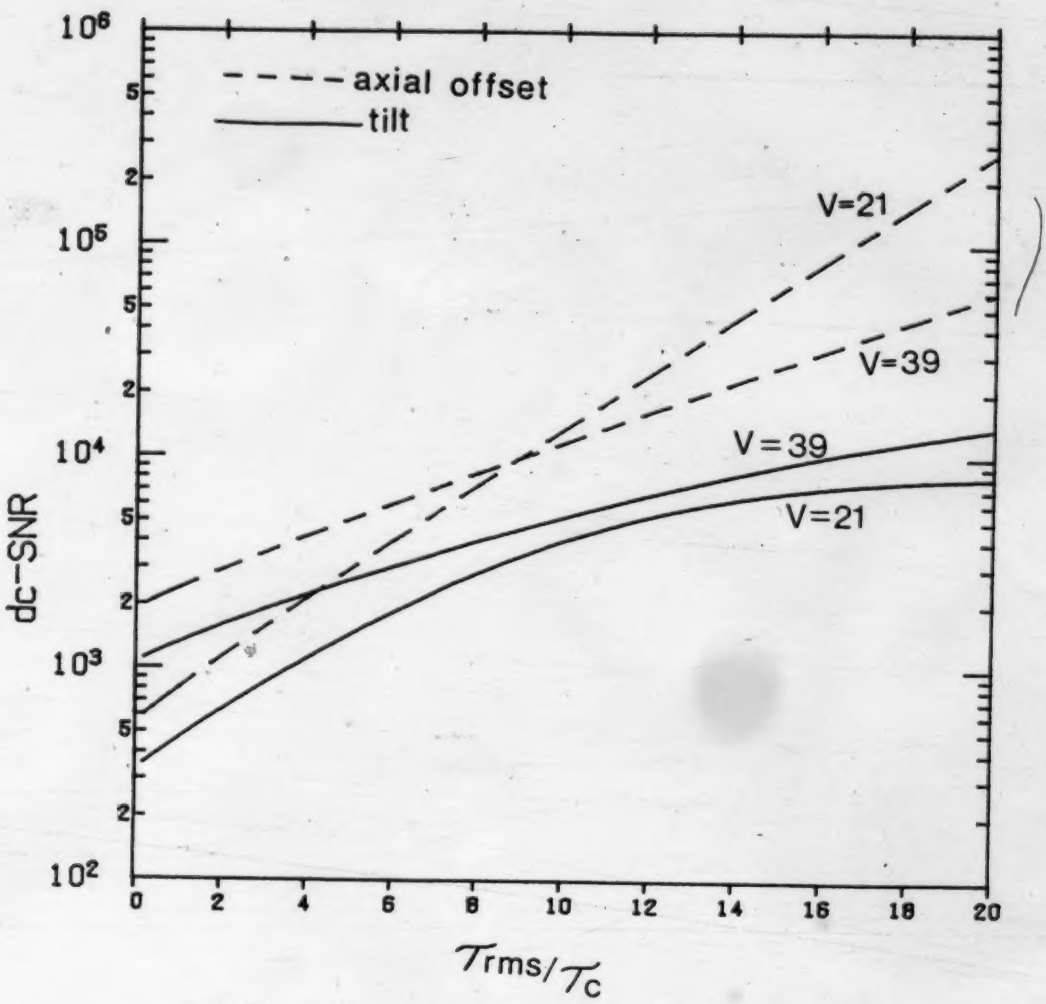

Figure 6.5 dc-SNR for partially coherent sources with coherence time τ_c. Both tilt and axial offsets are considered. Splice loss = 1 dB and $\alpha = 2.2$.

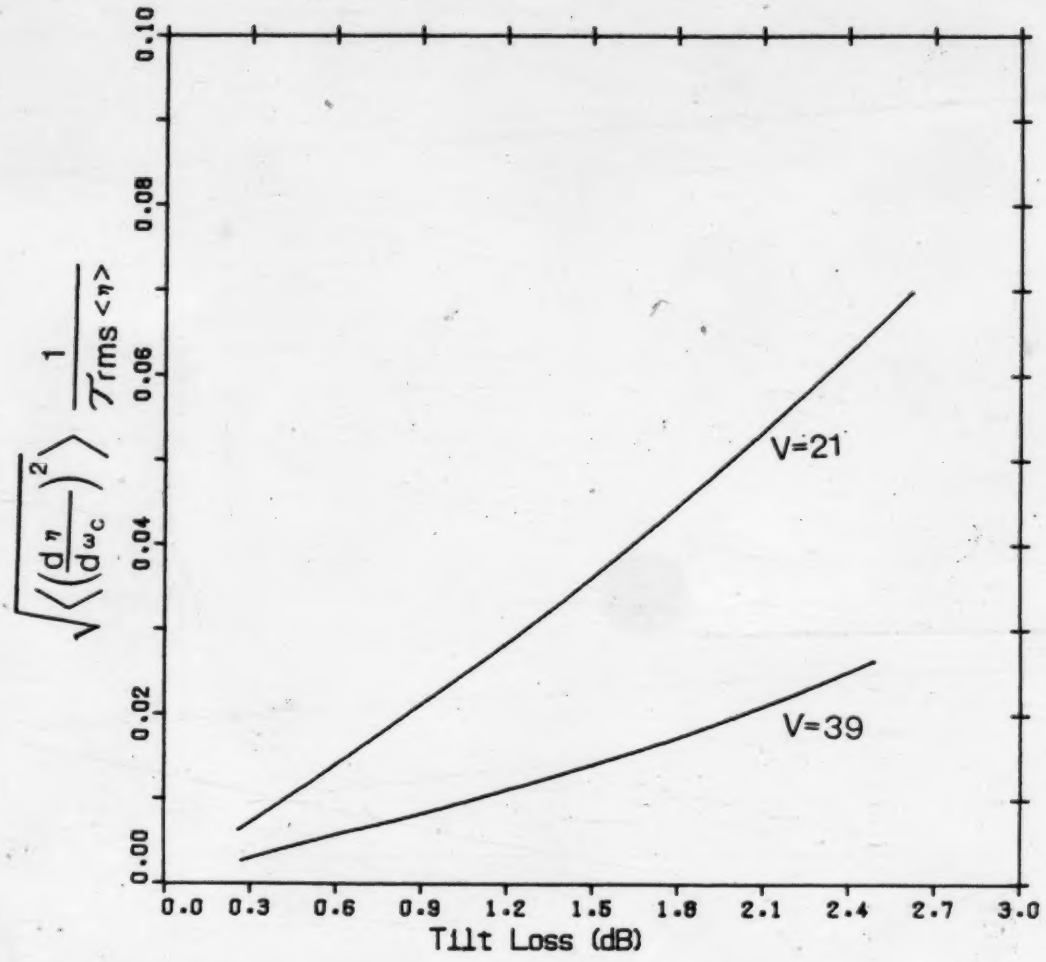

Figure 6.6 Normalised rms value of the derivative of the coupling efficiency with respect to emission frequency for a coherent source. $\alpha = 2.2$.

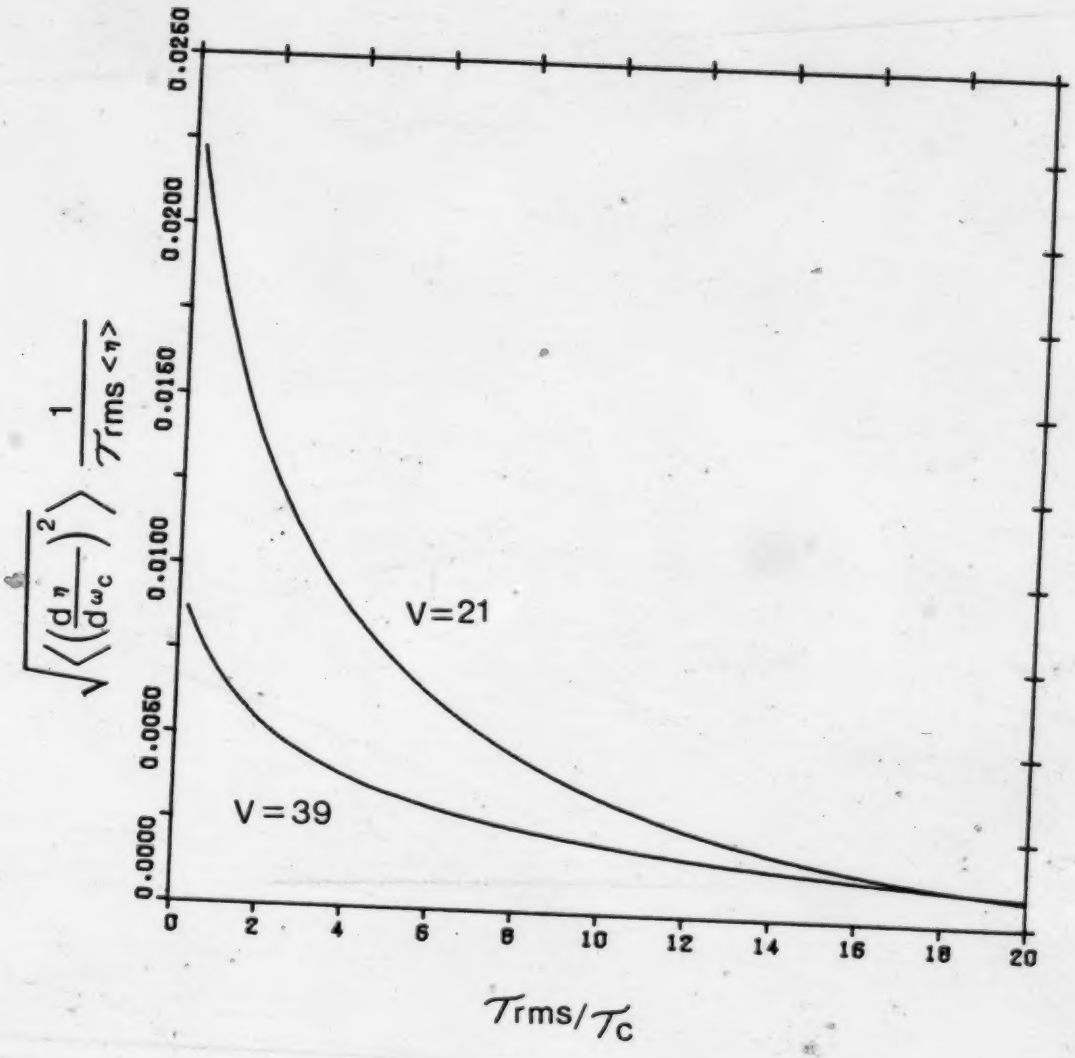

Figure 6.7 Normalised rms value of the derivative of the coupling efficiency with respect to emission frequency for a partially coherent source. Tilt loss = 1 dB and α=2.2.

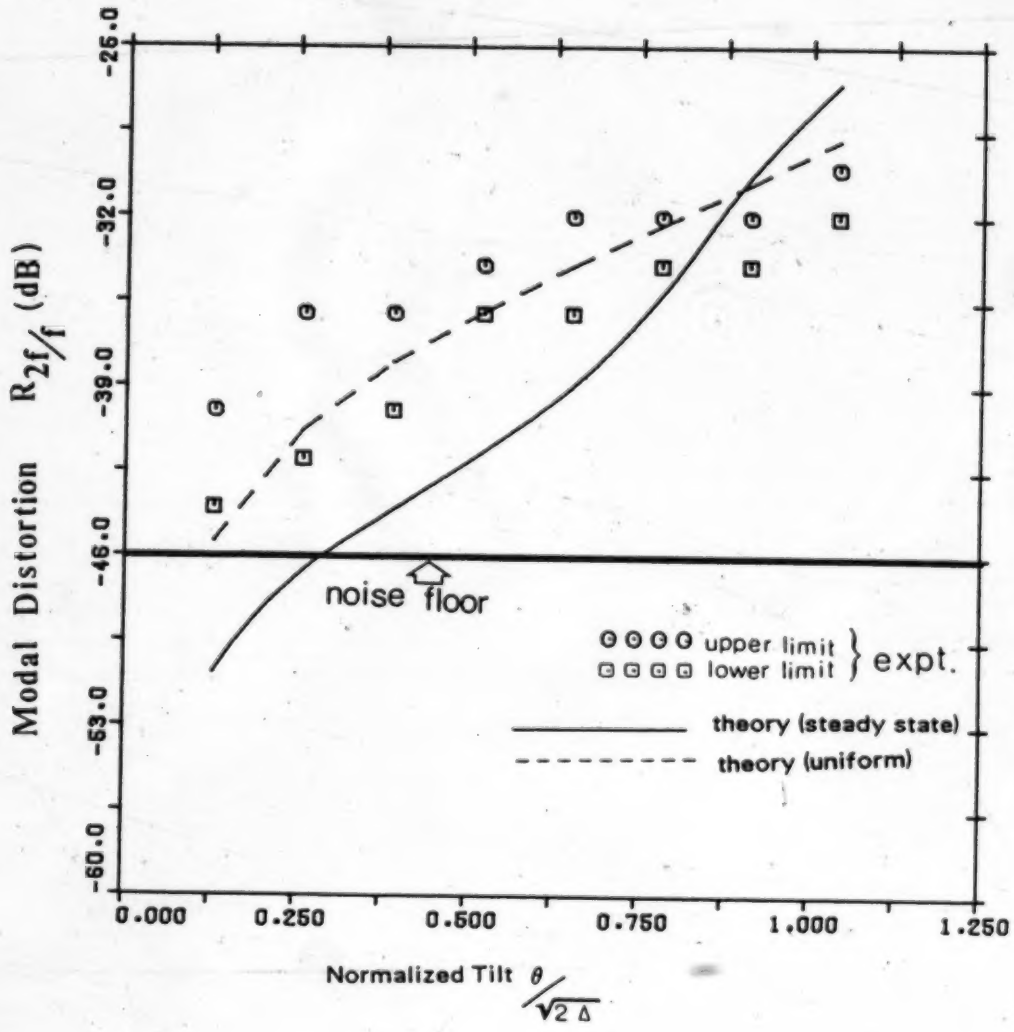

Figure 6.8 Modal distortion as a function of normalized tilt θ_N for a partially coherent source. All experimental parameters except the modulation index 'm', are the same as in Fig. 4.11. m= 50 % and $\Omega_m/2\pi$=4 GHz. Theoretical results are for a tilt at a fusion splice, whereas the data corresponds to a tilt at a connector.

curves; the upper limit of $R_{2f/f}$ is quite unsteady, probably due to temperature effects [140].

6.3 Conclusions

A performance comparison of the three geometrical misalignments show that to an order of magnitude, the modal noise values (for coherent illumination) are only dependent on the amount of mode selective loss. For partially coherent sources and a given loss, modal noise decreases the most for longitudinal gaps, followed by axial offset and then by tilt. Hence, maximum care must be taken to avoid tilt offsets in fiber-fiber couplings. Our analysis predicts that without tilts, a partially coherent source with a low mode volume fiber will yield quite satisfactory SNR performance.

CHAPTER VII

MODAL ANALYSIS OF LOSS, NOISE, AND DISTORTION DUE TO FIBER IMPERFECTIONS

In this chapter, theoretical and experimental investigations are described for determining the transmission characteristics of a fiber for coherent and for partially coherent illumination. The measured values of the average power loss are shown to be in close agreement with the theory. Using this theory, the dependence of microbending loss on the wavelength, NA, and modal energy distribution are examined. A theoretical estimate is made for the excess transient losses, which is in agreement with Olshansky's measurements [178]. A model is proposed to predict the modal noise and distortion values generated by fluctuations in the power loss due to fiber imperfections. Based on this model, good agreement is obtained with the experimental results of Stubkjaer [140]. It is predicted that, for a given total loss, a few large amplitude imperfections are more critical than a number of smaller imperfections. Also, very modest values of microbending loss ($\leqslant$0.5 dB/km) could seriously affect noise performance in long-distance ($\geqslant$10 km) multimode fiber communications.

7.1 Fiber Imperfections and Mode coupling

In the previous chapters, the parabolic-index fibers were assumed to be of perfectly straight and circularly symmetric geometry, with their refractive index changing smoothly radially, but not in the circumferential or axial direction along the fibers. In this ideal case, all guided modes propagate independently from each other and suffer only the attenuation due to bulk loss from absorption and Rayleigh scattering. Similarly, the leaky modes of such perfect fibers propagate independently from each other and are attenuated because they are not totally internally reflected [149].

Actual fibers are, however, never quite perfect in this sense. Apart from the microscopic fluctuations (correlation distances short compared to the wavelength of light) due to the random molecular structure of the material, the refractive index also deviates macroscopically ('profile deformation') from its circularly symmetric distribution. The refractive index will then depend not only on the radial coordinate of the fiber but also will change in the circumferential as well as in the longitudinal direction. In addition, core-cladding interface deformations are unintentionally introduced during the fiber pulling process. When

the preform is reduced to fiber form in an oxyhydrogen flame-pulling apparatus, the instability of the flame as a heat source or slight movements of the fiber because of air currents and back-flame effects, or combinations of these, probably contribute to this type of imperfection. The core of such a fiber has an elliptical cross section, and the observed variations consist of changes in the ellipticity. The modes in an elliptical fiber are complicated and are difficult to apply to a mode-mixing analysis. For this reason, it is assumed [179] that the fiber core nominally has a circular cross section that deforms itself randomly into an ellipse; hence, this kind of deformation is called 'elliptic deformation' or 'squeezing'. It was predicted in Ref. [179] that this 'elliptic deformation' model is capable of yielding order-of-magnitude estimates of the performance of an actual fiber. A third kind of irregularity is that a fiber will never be perfectly straight. Processing of the bare fiber such as coating and cabling, and also cable laying and burying introduce minute deviations of the fiber axis from a straight line. This type of deformation is called 'microbending'. Lastly, nonuniform pulling speeds and varying preform geometry introduce low frequency diameter variations.

All these 'perturbations' of the fiber from a perfect geometry and a perfect index distribution are roughly divisible into two classes: those perturbations that have longitudinal spatial frequencies sufficiently high to produce mode coupling, and those that do not. Microbending and elliptic deformation fall into the first category whereas profile deformation and diameter variations belong to the second category. When mode coupling is present, the modes no longer propagate independently from each other, but exchange power with other guided modes, and lose power to the radiation modes. Power transfer to other guided modes results in a reduction in pulse dispersion. Each guided mode travels at its own characteristic group velocity. Some power traveling in a fast mode is eventually transferred to a slow mode, while power starting out in a slow mode finds itself at least partially in a fast mode; so that the extremes of the group velocity spread are partly equalized. Transfer of power to the radiation modes results in excess waveguide losses since the power is carried away from the core region into the (infinite) cladding. If the illumination is coherent or partially coherent, the transmitted signal can also be degraded by modal noise and distortion [27],[48].

Mode coupling is typically dominated by transitions between modes differing by 1 or 2 in their azimuthal mode number l [146]. Thus, $|\Delta l| = 1$ transitions arise from microbending effects which induce coupling between neighboring mode groups, while $|\Delta l| = 2$ transitions

between modes within a mode group or between alternate mode groups are generated by variations of the fiber ellipticity along its axis. While the perturbations present in an actual optical fiber are stochastic in nature, the mode coupling is still dominated by the phase-matched longitudinal perturbation components if the fiber length is sufficiently long. Consequently, in an optical fiber with a nearly parabolic profile, microbending effects that induce $\Delta l = \pm 1$ transitions between mode groups will be dominated by scales of the order of a millimeter, while the $\Delta l = \pm 2$ transitions within a group are governed by scales of from centimeters to meters, depending on the degree of degeneracy of the mode group [180].

The power loss due to the low frequency profile and diameter variations are caused by a decrease in the mode volume so that the core modes adiabatically acquire the characteristics of leaky or refracted modes [107]. In contrast to this, analysis of the coupling between modes due to microbending and due to elliptic deformation is an ideal application for a diffusion theory of the power coupling process. Since only the nearest or the alternate neighbors couple directly to each other, power redistributes itself by jumping from mode to mode in the same way as particles diffuse through real space. Finally, only the highest or the next highest order modes couple and lose power to the continuous spectrum of radiation modes. Such coupling (i.e., intergroup) can be classified as weak or strong.

Weak coupling means that departure of the fiber from perfect geometry is either slight or at least slow, so that changes of the slowly varying field amplitudes caused by the imperfections are very long compared to the wavelength of light or, in the statistical case, compared to the correlation length of the imperfections. Hence, changes in the modal power distribution take place over distances that are very long compared to the wavelength of light (1000 wavelengths). The analysis in this chapter will be restricted to weak coupling, since undesired random mode coupling in slightly distorted multimode fibers is always weak, [146] and is thus amenable to the perturbation approximation of the coupled wave equations [146].

The system of coupled wave equations include an infinite set of coupled integro-differential equations which are hard to solve for the case of a randomly deformed multimode fiber. The complexity of the coupled wave equations is caused by the fact that they contain too much information; i.e., a detailed description of the phase and amplitude of all the modes at any point z along the fiber. For incoherent illumination, one is seldom interested in the phases of individual modes and very rarely in the exact amplitude of each mode. For this

case, the coupled power equations in Ref. [100] were derived from the coupled wave equations using a perturbational analysis, assuming the phases of the complex field amplitudes to be sufficiently random. The coupled power equations only deal with the average power; they show how the total power carried by the fiber is distributed among the modes and how this distribution evolves as a result of coupling and loss processes. These equations hold only for relatively weak coupling, since the second- and higher order terms are neglected.

Using weak mode coupling theory, we may analyse the power loss for the case of coherent or partially coherent illumination at the fiber input. An important assumption in this analysis is that the modes of a degenerate mode group carry equal amounts of power [101]. Arnaud [181] strongly objects to this postulate on the ground that there are no plausible deformation mechanisms that could satisfy the tight-coupling approximation requiring the curvature power spectrum at zero spatial frequency to be infinite, or at least very large. However, it has been shown [179] that the modes with the same principal mode number are coupled very strongly by large amplitudes at low spatial frequencies. This fact has been observed whenever power spectra of fiber distortions have been measured [179]. Further, Kawakami and Tanji [182] have demonstrated that the intragroup coupling strength of the elliptic deformation type is at least an order of magnitude stronger than the intergroup coupling due to microbending. Hence, it can be safely assumed that deformations other than bending cause tight coupling among the degenerate modes so that they carry approximately equal amounts of power.

A further assumption in our analysis requires that the isothermal power diffusion process be very dominant over the adiabatic tunneling of power from the core modes to the leaky and the refracted modes. This assumption is valid since most practical low-loss optical cables have microbending loss as the major loss component. In any case, the extra loss term can always be inserted phenomenologically. For the same reason, the nearly flat Fourier spectrum that causes Rayleigh scattering from a given guided mode to all guided and radiation modes in the forward as well as the backward direction can be ignored. As in previous chapters, the delays between the degenerate modes within one LP mode group have been assumed to vanish, since for fibers with a parabolic-profile, modes that have the same principal mode number have approximately the same propagation constants [149].

7.2 Derivation of the Instantaneous Power Loss

The aim of this section is to derive the instantaneous power loss due to a single fiber imperfection. Our starting point is the set of coupled wave equations for the slowly varying amplitude (envelopes) A_μ defined by [100]

$$a_\mu = A_\mu e^{j(\omega t - \beta_\mu z)} \tag{7.1}$$

and

$$\beta_\mu(\omega) \simeq \beta_\mu(\omega_0) + \left.\frac{d\beta_\mu}{d\omega}\right|_{(\omega-\omega_0)} (\omega-\omega_0) = \beta_\mu^0 + \tau_\mu' (\omega-\omega_0) \tag{7.2}$$

$\omega = \frac{2\pi c}{\lambda}$ = angular emission frequency of the laser source

ω_0 = arbitrary center frequency under dc-bias

β_μ = propagation constant of mode μ

$\left.\frac{d\beta_\mu}{d\omega}\right|_{\omega-\omega_0} = \tau_\mu'$ = modal delay per unit length

with a_μ being the rapidly oscillating mode amplitude travelling in the positive z-direction with harmonic time dependence. In (7.2), second and higher order terms of the Taylor expansion for β_μ around the center frequency ω_0 have not been included since the source is assumed to have a small spectral width and/or frequency deviation. The coupled wave equations can be expressed in the form [146]

$$\frac{dA_\mu}{dz} = \sum_{\substack{\nu=1 \\ \nu\neq\mu}}^{N} C_{\mu\nu} A_\nu e^{-j(\beta_\mu - \beta_\nu)z} \tag{7.3}$$

$C_{\mu\nu} = K_{\mu\nu} f(z)$ = mode coupling coefficient

$f(z)$ = distortion function for the refractive index

$K_{\mu\nu}$ = constant term independent of z

N = total number of guided modes

It is seen that $C_{\mu\nu}$ is a measure of the degree to which the distortion $f(z)$ causes an overlap of

the fields of the modes μ and ν. We use the function $f(z)$ to describe the axial dependence of the deviation of the refractive index distribution as well as a related function $b(z)$ to describe the core radius deviation from its nominal value. The Fourier transforms $F(\theta)$ of $f(z)$, and $B(\theta)$ of $b(z)$, are defined as

$$\left.\begin{aligned} F(\theta) &= \lim_{L \to \infty} \left(\frac{1}{\sqrt{L}} \int_0^L f(z)\, e^{j\theta z}\, dz \right) \\ \text{and} \\ B(\theta) &= \lim_{L \to \infty} \left(\frac{1}{\sqrt{L}} \int_0^L b(z)\, e^{j\theta z}\, dz \right) \end{aligned}\right\} \tag{7.4}$$

From (7.3) and (7.4) it is seen that coupling between two modes labeled μ and ν is caused by the particular Fourier component of $f(z)$ (or of $b(z)$) according to the law

$$\beta_\mu - \beta_\nu = \theta \tag{7.5}$$

It is well known [153] that optical fibers possess a discrete spectrum of guided modes and a continuous spectrum of radiation modes. The range of possible eigenvalues (propagation constants β_g) of the guided modes is given by

$$n_2 k_0 < |\beta_g| < n_1 k \tag{7.6}$$

($n_2 k_0$ is the plane wave propagation constant of the cladding and $n_1 k$ is the propagation constant at the center of the core $r=0$), and that of propagating radiation modes for real values of β_r,

$$0 \leq |\beta_r| < n_2 k_0 \tag{7.7}$$

The ranges of (7.6) and (7.7) are mutually exclusive, but they meet at $n_2 k_0$ as shown in Fig. 7.1. There is, however, another possible range of values of β_r

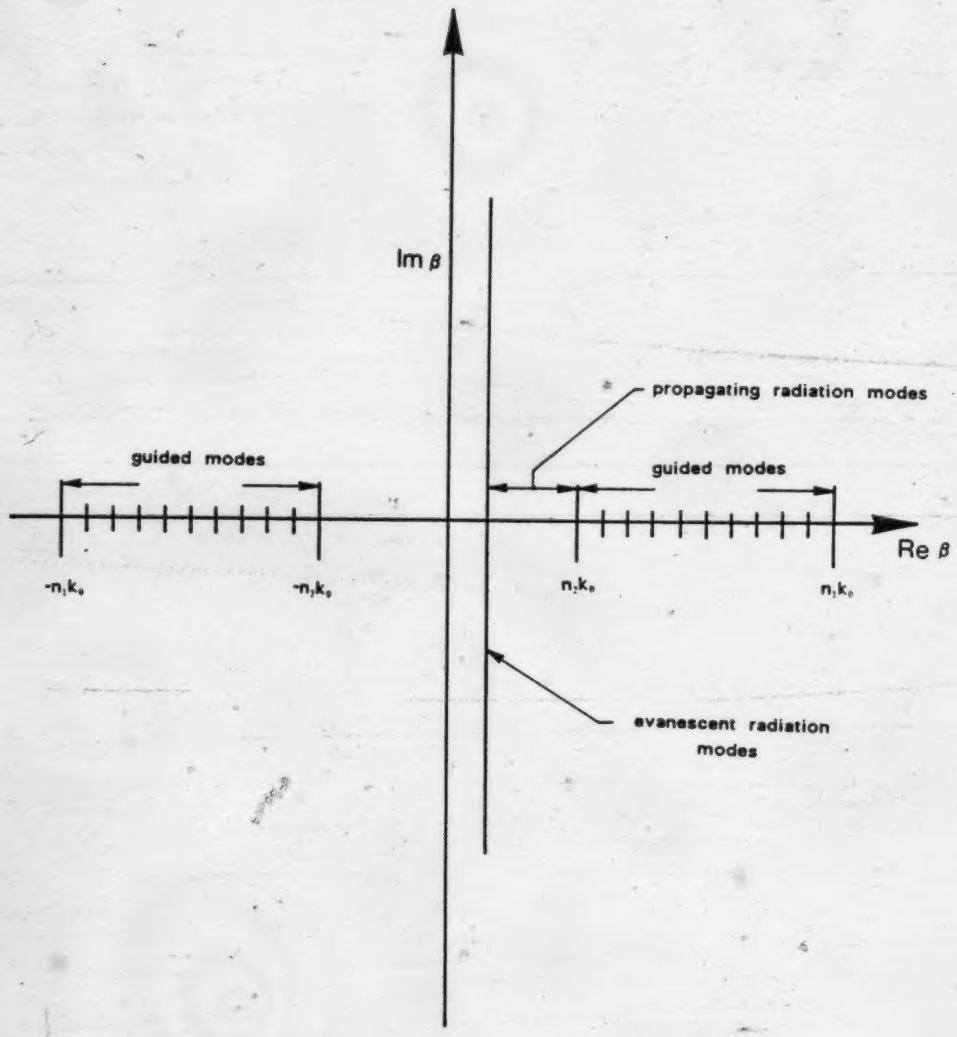

Figure 7.1 Spectral β range of guided and radiation modes of parabolic-index fibers.

$$\beta_r = -j\ |\beta| \tag{7.8}$$

with

$$0 < |\beta| < \infty \tag{7.9}$$

corresponding to evanescent modes of the continuous spectrum of modes. These modes are necessary to express the fine details of the field shape close to the surface of the fiber. However, they do not carry any power away from the guide, and are thus not very important for the study of radiation losses of the guided modes.

With an appropriate selection rule [183], coupling among guided modes of the step-index fiber has the property that the differences (7.5) increase with increasing mode number [183]. Cutting the Fourier spectrum (7.4) off at a maximum spatial frequency Θ_{max} then stops mode coupling at a given mode number, so that coupling between guided modes of lower order and modes with the highest mode numbers is prevented. Since only the highest order modes are near (in mode number space) to the radiation modes, coupling between guided and radiation modes is thus avoided. Because of the almost constant differences between propagation constants of neighboring modes, mode coupling in parabolic-index fibers requires only a narrow spectrum of spatial frequencies Θ. This feature of the modes of the parabolic-index fiber causes a problem, since it makes it harder to discriminate between coupling among guided modes and coupling from guided to radiation modes.

Theoretically, a guided mode with propagation constant β_g should couple directly to the radiation modes using the entire spatial frequency spectrum in the range [146]

$$\beta_g - n_2 k_0 < \Theta < \beta_g + n_2 k_0 \tag{7.10}$$

However, most practical, randomly bent fibers have spatial Fourier spectra that drop off very rapidly with increasing spatial frequency so that only a narrow region of the spatial frequency spectrum, near

$$\Theta = \beta_g - n_2 k_0 \tag{7.11}$$

is actually responsible for radiation losses. Measurements made in Ref. [184] and other corroborating evidence have shown that restriction (7.11) is indeed true.

We assume that the longitudinal refractive index perturbation $f(z)$, as a stochastic distribution, is ergodic and stationary; this means its statistical properties are independent of the location along the fiber. The statistics of such a random process can be expressed in terms of an autocorrelation function

$$R(u) = R(-u) = \langle f(z)\ f(z \pm u) \rangle \tag{7.12}$$

that has appreciable values only over a limited range of its argument [146]. The symbol $\langle\ \rangle$ indicates an ensemble average over statistically similar waveguides. The distance $u=D$ at which the function $R(u)$ has decreased to a fraction of its maximum value — usually to $1/e$ — is called the correlation length, since it is a measure of the distance over which the displacement of the core boundary correlates with itself. At $u=0$, $R(u)$ has a maximum, since at this point it consists of the average value of the square of the function. As the value of u is increased, $R(u)$ decreases because for some members of the ensemble, $f(x)$ assumes different signs at $x=z$ and $x=z+u$. Hence two parameters that characterize the statistical process are the correlation length D, and

$$R(0) = \sigma^2 \tag{7.13}$$

(called the variance of $f(z)$), since it is always assumed that the average of $f(z)$ vanishes

$$\langle f(z) \rangle = 0 \tag{7.14}$$

by choosing an appropriate reference fiber. If we define the coupling coefficient (for the transverse distortion, see Equation (7.3))

$$K_{\mu\mu} = 0 \tag{7.15}$$

we can drop the restriction $\nu \neq \mu$ in (7.3). Conservation of power leads to the relationship [146]

$$K_{\mu\nu} = -K^*_{\nu\mu} \tag{7.16}$$

where the asterisk indicates complex conjugation. The average power of mode μ is

$$P_\mu = < |a_\mu|^2 > = < |A_\mu|^2 > \tag{7.17}$$

Taking the z-derivative of this average power:

$$\frac{dP_\mu}{dz} = < \frac{dA_\mu}{dz} \quad A_\mu^* > + < A_\mu \frac{dA_\mu^*}{dz} > = < \frac{dA_\mu}{dz} \quad A_\mu^* > + \text{cc} \tag{7.18}$$

The notation 'cc' indicates that the complex conjugates of the terms already appearing in the equation are to be added. Substituting (7.3) into (7.18) we obtain

$$\frac{dP_\mu}{dz} = \sum_{\nu=1}^{N} K_{\mu\nu} <A_\nu A_\mu^* f(z)> \exp\left[j(\beta_\mu - \beta_\nu) z\right] + \text{cc} \tag{7.19}$$

The field amplitudes $A_\mu(z')$ and $f(z)$ are uncorrelated if

$$z - z' > D \tag{7.20}$$

and due to this lack of correlation

$$<A_\nu(z') \quad A_\mu^* \quad (z') \quad f(z)> = <A_\nu(z') A_\mu^*(z')> <f(z)> \tag{7.21}$$

Hence, the field amplitude at point z must be expressed in terms of the field amplitudes at point z'. If we can assume that the field amplitudes change only slightly over distances that are large compared to D, one can consider A_μ as nearly constant and obtain the following perturbation solution of (7.3) [146]

$$A_\mu(z) = A_\mu(z') + \sum_{\nu=1}^{N} K_{\mu\nu} A_\nu \int_{z'}^{z} f(x) \exp\left[j(\beta_\mu - \beta_\nu) x\right] dx \tag{7.22}$$

Using the weak coupling assumption and ideas of perturbation theory [146], (7.22) is substituted in (7.19) to yield

$$\frac{dP_\mu}{dz} = \sum_{\nu\times}\Big\{K_{\mu\nu}K_{\nu\times}\ \langle A_\times(z')A^*_\mu(z')\rangle\ \exp\ \left[j(\beta_\mu-\beta_\nu)z\right]$$

$$\int_{z'}^{z} \langle f(z)\,f(x)\rangle\ \exp\left[j(\beta_\nu-\beta_\times)x\right]\,dx$$

$$+\ K_{\mu\nu}K^*_{\mu\times}\ \langle A_\nu(z')\ A^*_\times(z')\rangle\ \exp\ \left[j(\beta_\mu-\beta_\nu)\ z\right]$$

$$\int_{z'}^{z} \langle f(z)\,f(x)\rangle\ \exp\left[-j(\beta_\mu-\beta_\times)x\right]\,dx\Big\} + \text{cc} \qquad (7.23)$$

In addition to using (7.14) and (7.21), second order terms have been neglected in the spirit of the weak coupling assumption and the perturbation theory. Only cross products of the first and second terms in (7.22) are included in (7.23). Since R(u) contributes only over a range on the order of the correlation length D, the lower integration limit in (7.23) can be changed from z' to $-\infty$,

$$\exp\left[j(\beta_\mu-\beta_\nu)z\right]\int_{z'}^{z} \langle f(z)\,f(x)\rangle\ \exp\left[j(\beta_\nu-\beta_\times)x\right]\,dx$$

$$= \exp\left[j(\beta_\mu-\beta_\times)z\right]\int_0^\infty R(u)\ \exp\left[-j(\beta_\nu-\beta_\times)u\right]\,du \qquad (7.24)$$

and

$$\exp\left[j(\beta_\mu-\beta_\times)z\right]\int_{z'}^{z} \langle f(z)\,f(x)\rangle\ \exp\left[-j(\beta_\mu-\beta_\times)x\right]\,dx$$

$$= \exp\left[j(\beta_\times-\beta_\nu)z\right]\int_0^\infty R(u)\ \exp\left[j(\beta_\mu-\beta_\times)u\right]du \qquad (7.25)$$

The complex conjugate terms in (7.23) contribute the complex conjugate of the integrals already stated in (7.24) and (7.25). Thus summation of (7.24) and its cc yields

$$\exp\left[j(\beta_\mu-\beta_\times)z\right]\int_0^\infty R(u)\ \exp\left[-j(\beta_\nu-\beta_\times)u\right]\,du\ +\ \text{cc}$$

$$=\cos\left[(\beta_\mu-\beta_\times)z\right]\Phi\ (\beta_\nu-\beta_\times)\ +\ 2\ \sin\left[(\beta_\mu-\beta_\times)z\right]\ F_s\ (\beta_\nu-\beta_\times) \qquad (7.26)$$

and for (7.25) and its cc, we obtain

$$\exp\left[j(\beta_x-\beta_\nu)z\right]\int_0^\infty R(u)\quad\exp\left[j(\beta_\mu-\beta_x)u\right]du + cc$$

$$= \cos\left[(\beta_x-\beta_\nu)z\right]\Phi\ (\beta_\mu-\beta_x) + 2\sin\left[(\beta_x-\beta_\nu)z\right]F_s\ (\beta_\mu-\beta_x) \quad (7.27)$$

where the complex Fourier transform $\Phi(\beta_\nu-\beta_x)$ of the autocorrelation function $R(u)$ constitutes the power spectrum of the distribution

$$\Phi\ (\Theta) = \sqrt{\frac{1}{2\pi}}\int_0^\infty R(u)\ \exp\left(-j\Theta u\right)du \quad (7.28)$$

and $F_s(\beta_\nu-\beta_x)$ denotes the Fourier sine transform of $R(u)$

$$F_s(\theta) = \sqrt{\frac{2}{\pi}}\int_0^\infty R(u)\ \sin\left(\Theta u\right)\ du \quad (7.29)$$

Eq. 7.27 is properly normalized to take care of the constant terms $1/(2\pi)$ and $2/\pi$ in front of the integral signs of (7.28) and (7.29) respectively; the independent variable Θ in this spectral distribution represents the angular spatial frequency of the respective spectral component. Substituting of (7.26) and (7.27) in (7.23), and summing over all modes μ yields

$$\sum_\mu \frac{dP_\mu}{dz} = \sum_{\mu\nu x} K_{\mu\nu}K_{\nu x}\sqrt{P_\mu P_x}\ \Big\{\cos\left[(\beta_\mu-\beta_x)z\right]\ \Phi\ (\beta_\nu-\beta_x) + 2\sin\left[(\beta_\mu-\beta_x)z\right]\ F_s\ (\beta_\nu-\beta_x)\Big\}$$
$$+ \sum_{\mu\nu x} K_{\mu\nu}K_{\mu x}\sqrt{P_\nu P_x}\ \Big\{\cos\left[(\beta_x-\beta_\nu)z\right]\Phi\ (\beta_\mu-\beta_x) + 2\sin\left[(\beta_x-\beta_\nu)z\right]F_s\ (\beta_\mu-\beta_x)\Big\} \quad (7.30)$$

where

$$\sqrt{P_\mu} = A_\mu$$

$$\sqrt{P_x} = A_x$$

$$\sqrt{P_\nu} = A_\nu$$

Eq. (7.30) relates the change of power (with respect to distance) of guided mode μ to the mode coupling coefficients (for the transverse distortion) and the power spectrum of the distortion. Only when the mode μ is coupled to a leaky or a radiation mode does its power get lost. However, since we assume that the amplitude of the spatial power spectrum of the coupling function decreases rapidly with increasing spatial frequencies, it is sufficient to consider only coupling to the leaky guided modes and ignore the radiation mode spectrum [185]. In doing so, one avoids the use of the more complicated radiation loss integral [153] to which useful approximations covering the whole range of correlation lengths have not yet been found [153].

The power in the leaky modes is radiated at a much higher rate than it diffuses at cut-off from guided into leaky modes, so that no power can ever accumulate in these leaky modes. We can assume that the highest order modes labeled ν are these leaky modes [185] and that they carry zero power. Thus the radiation loss can be calculated by computing the coupling coefficients $K_{\mu\nu}$ and $K_{\nu\times}$ of the lower order modes μ and $\times$ to the highest order mode ν. With $P_\nu = 0$, (7.30) can be simplified to

$$\sum_{\mu} \frac{dP_\mu}{dz} = \sum_{\mu\nu\times} K_{\mu\nu} K_{\nu\times} \sqrt{P_\mu P_\times} \left\{ \cos \left[(\beta_\mu - \beta_\times) z \right] \Phi \quad (\beta_\nu - \beta_\times) \right.$$

$$\left. + 2 \sin \left[(\beta_\mu - \beta_\times) z \right] F_s \ (\beta_\nu - \beta_\times) \right\} \tag{7.31}$$

Next, the phase relationships in (7.31) are examined by finding out which deformation mechanisms can give rise to nonvanishing $K_{\mu\nu}$ and $K_{\nu\times}$.

The fiber is assumed to be weakly guiding and has slight core boundary imperfections determined by the function [146]

$$r\ (x,y,z) = a + b(z) \cos\ (n\phi + \psi) \tag{7.32}$$

a = core radius of the fiber

n = an integer

ϕ = azimuthal angle

ψ = random phase function

$b(z)$ = actual displacement of the fiber axis from perfect straightness

For the particular cases of microbending and elliptic deformation, n=1 and n=2 respectively, whereas for random diameter variations, n=0 [146]. The equivalent index distribution of the imperfect fiber is given as [149]

$$n_i^2 = n_0^2(r) + n_p^2 (r,\phi,z) \tag{7.33}$$

with $n_0(r)$ as the circularly symmetric and longitudinally homogeneous index distribution of the perfect fiber and $n_p^2 (r,\phi,z)$ a perturbation of the nominal index distribution. This term n_p^2 can be expanded into a Fourier series with respect to ϕ

$$n_p^2 (r,\phi,z) = \sum_n f_n(z)\ g_n(r)\ \cos\ (n\phi+\Psi) \tag{7.34}$$

where $f_n(z)$ contains all the longitudinal dependence of the refractive-index fluctuations and $g_n(r)\cdot\cos(n\phi + \Psi)$ contains the transverse dependence. The quantity $C_{\mu\nu}$, defined in (7.3), is given by [149]

$$C_{\mu\nu} = \frac{k_0^2}{2\beta_\mu} \iint E_{\mu t}\ E_{\nu t}^*\ n_p^2\ r\ dr\ d\phi \tag{7.35}$$

where

$E_{\mu t}$ = normalized transverse electric field vector of mode μ

The longitudinal electric field components E_z have been omitted from the scalar product appearing under the integral sign in (7.35) since to order of magnitude [146]

$$\frac{E_z}{E_t} \simeq \frac{(n_e^2-n_2^2)^{\frac{1}{2}}}{n_e} << 1 \tag{7.36}$$

with the effective refractive index n_e defined by $\beta = n_e k$, that must satisfy the relation

$$n_2 < n_e < n_1 \tag{7.37}$$

Since the difference n_1-n_2 is assumed to be very small, the inequality on the right-hand side of (7.36) is justified. Thus, for coupling between guided modes, the contribution of the E_z components to the scalar product of the electric field vectors can safely be neglected. This is

also valid for coupling between a weakly guided and a forward directed radiation mode. However, (7.35) is not applicable to radiation problems in which the radiation, which is excited by a guided mode, escapes at a 90° angle with respect to the waveguide axis.

In (7.35), by stripping the longitudinal index distortion f(z) from $C_{\mu\nu}$, one obtains $K_{\mu\nu}$ which depends only on the transverse index distortion and has the form

$$K_{\mu\nu} = \frac{k}{2\beta_\mu} \iint E_{\mu t} E^*_{\nu t} g_n(r) \cos(n\phi+\Psi) r \, dr \, d\phi \tag{7.38}$$

These coefficients are derived in Appendix A4 for an infinite parabolic-profile. The ø integration in (7.38) restricts coupling to modes whose ø symmetries are related by

$$l_\mu \pm l_\nu = \pm n \tag{7.39}$$

l_μ = azimuthal number of mode μ

According to (7.31), power loss occurs when the mode labeled $\times$ (belonging to the mode group $m_\times$) is immediately adjacent to the leaky and radiation modes labeled ν in the β-space. Mode μ can belong to any mode group m_μ, but its contribution to the summation in (7.31) is significant, only if

$$m_\mu = m_\times$$

$$\text{or } m_\mu = m_\times - 1 \tag{7.40}$$

corresponding to the cases of microbending and elliptic deformation respectively. Based on the results of cabling experiments [105], it is hypothesized that bumps in either the fiber or the central member of the cable (see Fig. 7.2) are responsible for causing the lateral displacement b(z) of the fiber axis, or equivalently the refractive index fluctuation f(z) of the core. The exact form of the correlation function that should be attributed to either f(z) or b(z) is unknown. The following autocorrelation function is sometimes used as a convenient model [146]

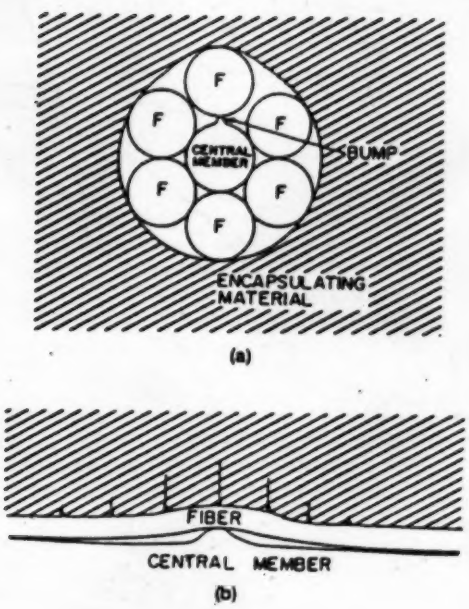

Figure 7.2 (a) Schematic cross section of a cable consisting of optical fibers stranded about a central member and surrounded by an encapsulating material.
(b) Schematic lengthwise view of the cable with arrows indicating the force exerted by the encapsulating material as a fiber passes over a bump. From Ref. [105].

$$R(u) = \sigma^2 \exp\left(\frac{-|u|}{D}\right) \tag{7.41}$$

where

$\sigma^2 = A^2$ for f(z)

$\sigma^2 = \frac{A^2 a^2}{16 n_1^4} \Delta^2$ for b(z)

A = amplitude of the refractive index fluctuation

The Fourier transform of an exponential function is a Lorentzian function. Thus, from (7.28) we obtain the power spectrum of f(z)

$$\Phi(\theta) = \frac{2\sigma^2}{D\left[\theta^2 + (1/D)^2\right]} \tag{7.42}$$

and of b(z)

$$B(\theta) = \Phi(\theta) \frac{a^2}{16\, n_1^4 \Delta^2} \tag{7.43}$$

Simillarly, from (7.29) we obtain

$$F_s(\theta) = \frac{2\sigma^2 \theta}{\left[\theta^2 + (1/D)^2\right]} \tag{7.44}$$

Thus, $\Phi(\theta)$ and $F_s(\theta)$ are related by

$$F_s(\theta) = Q.\Phi(\theta) \tag{7.45}$$

where

$Q = D.\theta$

In a typical application we may assume that two sections of perfect fiber are connected to each other with a piece of imperfect fiber as shown in Fig. 7.3. Without any loss of generalization, it may also be assumed that this imperfect fiber of length 'd' contains only a

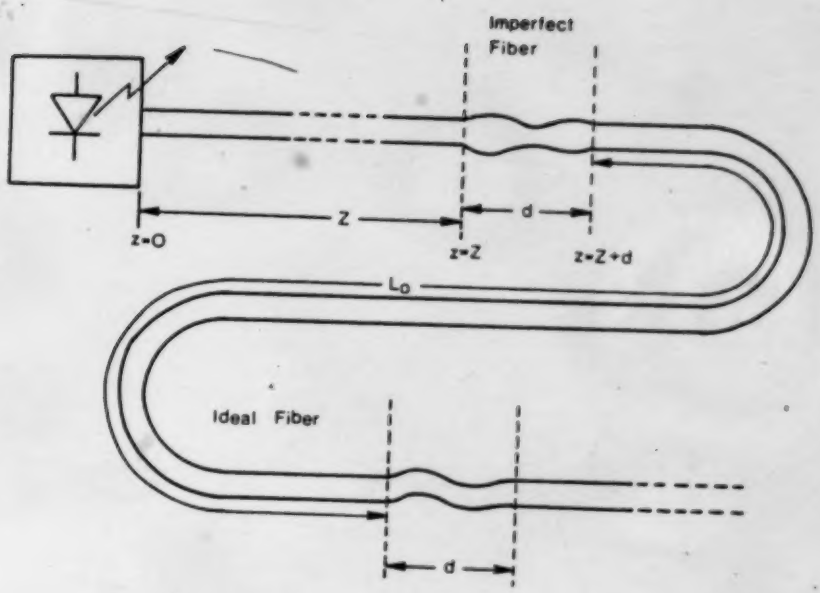

Figure 7.3 Fiber with core-cladding interface distortions connected on both sides to two pieces of ideal fiber each L_o long. A single bump is assumed to lie between $z=Z$ and $z=Z+d$.

single bump. The average separation L_o between two imperfect fiber pieces (hence, between two bumps) is large compared to the correlation length D of the distortion. There are N_b such sections, implying that there are in total N_b bumps over a fiber of length L. The instantaneous power loss due to a single bump at a distance Z from the source (see Fig. 7.3), is found by substituting (7.45) in (7.31) and integrating the latter from Z to Z+d

$$\Delta P(z) = \sum_{\mu\mu} F_{\mu\mu} P_{\mu} \Phi(\Delta\beta_0)\, d + \sum_{\substack{\mu\times \\ \mu\neq\times}} F_{\mu\times} \sqrt{P_{\mu} P_{\times}}\, \frac{\Phi(\Delta\beta_0)}{\Delta\beta_0} \times$$

$$\left\{ \sin\left[\phi_{\mu\times} + \tau'_{\mu\times}(\omega-\omega_0)(Z+d)\right] - \sin\left[\Psi_{\mu\times} + \tau'_{\mu\times}(\omega-\omega_0) Z\right] \right.$$

$$\left. - Q\cos\left[\phi_{\mu\times} + \tau'_{\mu\times}(\omega-\omega_0)(Z+d)\right] + Q\cos\left[\Psi_{\mu\times} + \tau'_{\mu\times}(\omega-\omega_0)Z\right] \right\} \quad (7.46)$$

with

$$F_{\mu\times} = \sum_{\nu} K_{\mu\nu} K_{\nu\times} = \text{interference coefficient}$$

$$\Delta\beta_0 = |\beta^0_{\nu} - \beta^0_{\times}| = |\beta^0_{\mu} - \beta^0_{\times}| = \sqrt{2\Delta}/a$$

$$\phi_{\mu\times} = (\beta^0_{\mu} - \beta^0_{\times})(Z+d) + \theta_{\mu\times}$$

$$\Psi_{\mu\times} = (\beta^0_{\mu} - \beta^0_{\times})\, Z + \theta'_{\mu\times}$$

$\theta_{\mu\times}$ and $\theta'_{\mu\times}$ = random phase fluctuations due to temperature changes and other environmental effects.

We have approximated $\Delta\beta$ by $\Delta\beta_0$ in the expression for the power spectrum since $\Delta\beta_0$ is at least three to four orders of magnitude greater than $\{\tau'_{\mu\times}(\omega-\omega_0)\}$ [146]. From (7.46) it is interesting to note that it is only one spatial frequency $\Delta\beta_0$ (corresponding to the spatial frequency of microbending) of the power spectrum $\Phi(\Delta\beta_0)$, that is actually responsible for the power loss. The coefficient $F_{\mu\times}$ determines the transmission characteristics of the imperfect fiber. $F_{\mu\mu}$ gives the average power loss in agreement with the coupled power theory [100], while $F_{\mu\times}$ with $\mu \neq \times$, may be considered as an interference coefficient, giving the amplitude with which the power loss fluctuates due to interference between modes μ and $\times$ of the fiber. The $\Psi_{\mu\times}$ and $\phi_{\mu\times}$ determine the modal phase relationships at Z and

Z+d respectively; they are practically unpredictable due to the presence of the random variables $\theta'_{\mu\times}$ and $\theta_{\mu\times}$ in them. Hence, some statistical properties of the power retention efficiency for a single bump, given by

$$\eta(z) = 1 - \frac{\Delta P(z)}{P} \tag{7.47}$$

is presented in the following section. P denotes the total power in the fiber and $\Delta P(z)/P$ is a measure of the relative power loss due to a single bump.

7.3 Excitation With Coherent Source

Assume that the fiber is illuminated by a coherent source, emitting at $\omega=\omega_0$. The average over $\Psi_{\mu\times}$ and $\phi_{\mu\times}$ will be denoted by the angle brackets $\langle\ \rangle$; it is understood that $\Psi_{\mu\mu}=\phi_{\mu\mu}=0$. The direct average of $\eta(z)$ for a single bump is obtained from (7.46) and (7.47) as

$$\langle\eta(z)\rangle\big|_d = 1-\gamma \tag{7.48}$$

where

$$\gamma = \frac{1}{P}\sum_{\mu}\sum_{\mu} P_\mu F_{\mu\mu} \Phi(\Delta\beta_0)\, d \tag{7.49}$$

is the power loss in nepers. In (7.48) the incident mode has not changed except for the fact that its amplitude is slightly reduced. Applying (7.48) repeatedly, each time with the reduced value of the incident mode power, allows us to obtain the power at the end of a fiber of length L with a total of N_b bumps as

$$P = P_0\, e^{-\gamma N_b} \tag{7.50}$$

where P_0 is the total power in the fiber at z=0. It is seen that (7.50) is equivalent to Eq. (9.3-22) of Ref. [153] which was derived for a slab waveguide with sinusoidal wall perturbations; it holds for small values of $\gamma\cdot\lambda/d$ and improves in accuracy as the angle

increases at which the radiation leaves the waveguide (λ = wavelength) [153].

The standard deviation of the power retention efficiency for a single bump can be written as

$$\delta(\eta) = \sqrt{\langle \eta^2 \rangle - \langle \eta \rangle^2} \tag{7.51}$$

since it gives the mean amplitude with which η fluctuates around $\langle \eta \rangle$. We first determine

$$(\eta - \langle \eta \rangle)^2 \Big|_d = \frac{1}{P^2} \sum_{\mu} \sum_{\varkappa} \sum_{\nu} \sum_{k} \sqrt{P_\mu P_\varkappa P_\nu P_k}\, F_{\mu\varkappa} F_{\nu k} \frac{\Phi^2(\Delta\beta_0)}{\Delta\beta_0^2}$$

$$(1+Q^2) \left\{ \sin(\phi_{\mu\varkappa}) - \sin(\Psi_{\mu\varkappa}) - Q\cos(\phi_{\mu\varkappa}) + Q\cos(\Psi_{\mu\varkappa}) \right\}$$

$$\times \left\{ \sin(\phi_{\nu k}) - \sin(\Psi_{\nu k}) - Q\cos(\phi_{\nu k}) + Q\cos(\Psi_{\nu k}) \right\} \tag{7.52}$$

When averaging over $\phi_{\mu\varkappa}$, $\phi_{\nu k}$ as well as $\Psi_{\mu\varkappa}$, $\Psi_{\nu k}$, all terms vanish besides those for which $\mu=\nu$ and $\varkappa=k$ or $\mu=k$ and $\varkappa=\nu$, yielding

$$\delta^2(\eta)\Big|_d = \langle \eta^2 \rangle - \langle \eta \rangle^2 = \langle (\eta - \langle \eta \rangle)^2 \rangle$$

$$= \frac{\sum_{\mu\varkappa} P_\mu P_\varkappa F_{\mu\varkappa}^2}{\xi^2} \frac{\gamma^2}{d^2 \Delta\beta_0^2} (1 + Q^2)$$

$$= \sum_{\mu\varkappa} P_\mu P_\varkappa F_{\mu\varkappa}^2 \; \gamma^2/\xi^2 \tag{7.53}$$

where $\xi^2 = \sum_{\mu} P_\mu^2 F_{\mu\mu}^2$

$1/d^2\Delta\beta_0^2 \simeq 0$ since $d\Delta\beta_0 >> 1$

In deriving (7.53), we have also assumed for sake of simplicity that the average length of the imperfection d is approximately equal to the correlation length D. This assumption will yield the worst case modal noise values. Since the N_b bumps are all uncorrelated (because $L_0 > D$), the variance at the end of the fiber is given as

$$\delta^2(\eta)\big|_L = N_b \quad \delta^2(\eta)\big|_d$$

$$= \sum_{\substack{\mu\times \\ \mu\neq\times}} P_\mu P_\times F_{\mu\times}^2 \cdot \gamma_t^2 / (\xi^2 . N_b) \tag{7.54}$$

where $\gamma_t = \gamma . N_b$ = total loss in the fiber

So far, we have ignored absorption and scattering losses. If all modes suffer identical losses, we only need to multiply (7.53) by the total loss a signal suffers in travelling through the fiber. However, since our objective is to derive an expression for the dc signal-to-noise ratio, the absorption term drops out in the end because signal and noise suffer identical losses. The dc-SNR at the fiber end is, therefore

$$dc - SNR = \left[\frac{\langle \eta \rangle\big|_L}{\delta(\eta)\big|_L} \right]^2 = \frac{e^{-2\gamma t}}{\delta^2(\eta)\big|_L} \tag{7.55}$$

For estimating the nonlinear distortion one is interested in the derivative of $\eta(z)$ with respect to ω

$$\frac{d\eta}{d\omega} = \frac{1}{P} \sum_{\mu\times} \sqrt{P_\mu P_\times}\, F_{\mu\times} \frac{\Phi(\Delta\beta_\ell)}{\Delta\beta_0} \Big\{ \tau'_{\mu\times} (Z + d) \cos(\phi_{\mu\times}) - \tau'_{\mu\times} Z \cos(\Psi_{\mu\times}) + Q . \tau'_{\mu\times} (Z + d) \sin(\phi_{\mu\times}) - Q . \tau'_{\mu\times} . Z . \sin(\Psi_{\mu\times}) \Big\} \tag{7.56}$$

For a given bump far from the source ($Z >> d$), the mean square value of $d\eta/d\omega$ is obtained from (7.56)

$$\left\langle \left(\frac{d\eta}{d\omega} \right)^2 \right\rangle = \frac{\sum P_\mu P_\times F_{\mu\times}^2 \tau'^2_{\mu\times} Z^2 \gamma^2}{\xi^2} \tag{7.57}$$

Since it would be impossible to evaluate (7.57) for the N_b bumps, without a knowledge about the distance Z of the bump from the source, we assume that all the bumps are uniformly distributed over the whole fiber and that they are equispaced with

$$Z = \frac{L}{N_b} . x \tag{7.58}$$

where $x = 0,1,2 \cdots N_b$ is an integer. At the end of the fiber of length L, (7.57) simplifies to

$$\left\langle \left(\frac{dn}{d\omega}\right)^2 \right\rangle \Big|_L = \frac{\sum P_\mu P_x F_{\mu x}{}^2 \tau_{\mu x}^2 \gamma_t^2}{3 \cdot \xi^2 \cdot N_b} \tag{7.59}$$

where

$$\tau_{\mu x} = \tau'_{\mu x} L$$

7.4 Excitation With Partially Coherent Sources

The derivation of the variance of the coupling efficiency η_s for a single bump for the case of partially coherent illumination is very similar to the derivation of (7.53), and when (3.30) to (3.33) are used

$$\delta^2(\eta_s) = \langle \eta_s{}^2 \rangle - \langle \eta_s \rangle^2$$

$$= \frac{1}{P^2} \sum_{\substack{\mu x \\ \mu \neq x}} \Gamma(\tau'_{\mu x}) P_\mu P_x F_{\mu x}{}^2 \frac{\Phi^2(\Delta\beta_0)}{\Delta\beta_0{}^2} (1 + Q^2) \tag{7.60}$$

with $\Gamma(\tau)$ defined in (3.37) for a Lorentzian spectrum. For a coherent source, (7.60) reduces to (7.53); for decreasing τ_c the fluctuations of η_s also decrease. When summed up over the whole fiber length (7.60) yields

$$\delta^2(\eta_s)\Big|_L = \frac{1}{P^2} \sum_{\substack{\mu x \\ \mu \neq x}} \left\{ \int_0^{N_b} e^{-\frac{|\tau_{\mu x}| x}{\tau_c \cdot N_b}} dx \right\} \times \{ \cdots\cdots \}$$

$$= \sum_{\substack{\mu x \\ \mu \neq x}} \frac{P_\mu P_x (F_{\mu x}{}^2/\tau_{\mu x}) (1 - e^{-|\tau_{\mu x}|/\tau_c}) \tau_c \gamma_t^2}{\xi^2 \cdot N_b} \tag{7.61}$$

The dc-SNR for a partially coherent source is then obtained in the same manner as (7.55) was derived. Any modulation or fluctuation of the center frequency ω_c also changes the coupling efficiency η_s. The result for the mean square value of $d\eta_s/d\omega_c$ is

$$\left\langle \left(\frac{d\eta_s}{d\omega_c}\right)^2 \right\rangle\Big|_d = \frac{1}{P^2}\sum_{\mu x} \Gamma(\tau_{\mu x})\ \tau_{\mu x}^{2'}\ Z^2 P_\mu P_x F_{\mu x}^2\ \frac{\Phi^2(\Delta\beta_0)}{\Delta\beta_0^2}$$

$$\times\ (1+Q^2) \qquad (7.62)$$

The derivation of (7.62) is straightforward and is very similar to the derivation of (7.60). Over the fiber length L, (7.62) reduces to

$$\left\langle \left(\frac{d\eta_s}{d\omega_c}\right)^2 \right\rangle = \frac{1}{\xi^2 N_b} \sum_{\substack{\mu x \\ \mu \neq x}} P_\mu P_x F_{\mu x}^2\ \tau_{\mu x}^2 \left\{\frac{2}{\alpha^3} - e^{-\alpha}\left(\frac{1}{\alpha} + \frac{2}{\alpha^2} + \frac{2}{\alpha^3}\right)\right\} \gamma_t^2 \qquad (7.63)$$

where $\alpha = \tau_{\mu x}/\tau_c$

We proceed to evaluate the modal distortion $R_{2f/f}$ as outlined in Ref. [34] (also see Eq. (3.45)), keeping in mind that the theoretical formalism is the same for the bump as it is for the connector once the wavelength dependent transmission characteristics in (7.63) have been established. The result is

$$R_{2f/f}\ [\text{dB}] \simeq 10 \log\left[\frac{\gamma_t^2\ \Omega_m^{-2}}{4\xi^2 N_b \cdot M_\ell} \sum_{\substack{\mu x \\ \mu \neq x}} P_\mu P_x F_{\mu x}^2\ \tau_{\mu x}^2 \times \left(-\frac{2}{\varepsilon^3} + e^{\varepsilon}\left[\frac{1}{\varepsilon} - \frac{2}{\varepsilon^2} + \frac{2}{\varepsilon^3}\right]\right)\right] \qquad (7.64)$$

where $\varepsilon = 2\gamma_t - |\tau_{\mu x}|/\tau_c$

M_ℓ = total number of longitudinal modes

This expression is in the desired form and can be simplified even further for partially coherent sources whose $\tau_c << \tau_{rms}$, and if the loss term γ_t is small. With this approximation

$$-\frac{2}{\varepsilon^3} \; >> \; e^{\varepsilon}\left(\frac{1}{\varepsilon} - \frac{2}{\varepsilon^2} + \frac{2}{\varepsilon^3}\right) \tag{7.65}$$

so that (7.64) simplifies to

$$R_{2f/f} \simeq 10 \log\left[\sum_{\substack{\mu\times \\ \mu\neq\times}} \frac{P_\mu P_\times \left(F^2_{\mu\times}/\tau_{\mu\times}\right) - \tau_c^3 \; \gamma_t^2 \; \Omega^2 m}{2 \; \xi^2 \cdot N_b \cdot M_\ell}\right] \tag{7.66}$$

Eq. (7.66) shows the dependence of the modal distortion on various source and fiber parameters; however, because of the restriction (7.65), its range of applicability is rather limited. Consequently, in this chapter, all modal distortion calculations are carried out according to (7.64).

The modal noise and distortion due to fiber imperfections are seen to be high when a given loss is produced by a small number of bumps. Keeping the loss constant, if one increases the number of bumps so that the mean loss per bump decreases, then the associated noise and distortion also decrease. Since an isolated bump of small amplitude produces a small loss, from a modal noise point of view, a large number of tiny bumps are preferable to a few large ones. However, N_b cannot be made to exceed L/d, because then the bumps will be overlapping and this analysis does not apply. In the limit of vanishing N_b and/or bump height, the loss also vanishes so that there is no modal noise and distortion. The worst case occurs when there is only one bump generating all the mode selective loss. In this situation, the bump behaves like a splice.

Before numerical values of the modal noise and distortions can be obtained, it is necessary to have a rough estimate of the total number of bumps in the fiber transmission line. Although this is a difficult task, recent work of Rourke [186] suggests that it is possible to measure the insertion loss of a single microbend using an OTDR. In fact, for a 10 μm amplitude microbend, he measured a 0.026 dB loss. Hence, in a 1 km long fiber, only 39 bumps (all 10 μm in amplitude) are required to produce a loss of 1 dB. Such high amplitude deformations may not occur in practice; however, Ref. [186] gives important information about the relationship between the bump height and the microbending loss from which rough

estimates of N_b can be made.

7.5 Numerical Evaluation of and Experiment on Microbending Loss

In this section we want to evaluate the microbending loss according to (7.49) based on the power diffusion approximation and assuming that the highest order mode group is leaky. We compare these results with those obtained previously by Marcuse [102], Gloge [131], Olshansky [106], and Gardener [132] and obtain good agreement. Experimental loss values have been obtained for microbending; these as well as Eccleston's [187] data supports the theory using the power spectrum of the form given in Ref. [131] for fibers that are pressed against an elastic rough surface.

According to its definition (7.42), the power spectrum of the refractive index fluctuation $\emptyset(\Delta\beta_0)$ has the dimension of millimeters. If we divide γ/d (power loss per unit length) by $\emptyset(\Delta\beta_0)$, the resulting expression is called the normalized power loss coefficient and has the dimension mm^{-2}. In Table 7.1, $\gamma/d\cdot\emptyset(\Delta\beta_0)$ has been evaluated from (7.49) using the mode coupling coefficients derived in Appendix A4. All the modes belonging to mode group M-1 are assumed coupled via microbending to the highest order leaky modes of the mode group M, since their fields reach into the vicinity of the waveguide wall and consequently suffer very high losses. Previously published steady state normalized power loss coefficients approached asymptotically by long fibers are also shown in Table 7.1 [102],[106] ,[131]. The values of the parameters are, core radius $a=25\ \mu m$, $n_1=1.47$, and $\Delta=0.0092$. It is found that the coefficients $\gamma/d\cdot\emptyset(\Delta\beta_0)$ calculated according to (7.49) are slightly higher than the corresponding steady state values of Ref. [102] and Ref. [131] because of our assumption that the highest order guided modes are leaky. In Ref. [102] and Ref. [131], the guided modes were coupled to the continuous spectrum of radiation modes. From Table 7.1 it is seen that (7.49) can yield the magnitude of the transient losses when a uniform power distribution is used; these are seen to be about 1.75 times higher than the corresponding steady state loss values ($V=21$ and $V=39$). Furthermore, the wavelength dependence of the microbending loss is cleary exhibited in (7.49) through $F_{\mu\mu}$. At longer wavelengths (low V number) the power loss coefficient is lower because the mode coupling strength follows $\lambda^{-\frac{1}{2}}$. However, dispersion in the fiber's relative index difference Δ will increase $\emptyset(\Delta\beta_0)$ at longer wavelengths, so that in practice the loss is found to increase with wavelength. This dependence has been observed by

Table 7.1 Normalized power loss coefficient $\gamma/d\text{-}\emptyset(\Delta\beta_o)$ in mm^{-2}. The power spectrum exponent p is defined in Ref. [106].

Results of Eq.(7.49)				Marcuse [102]	Gloge [131]	Olshansky [106] $_{p=2}$
Uniform		Steady State				
V=21	V=39	V=21	V=39	Steady State	Steady State	Steady State
3.76×10^{4}	7.8×10^{4}	2.16×10^{4}	4.45×10^{4}	1.33×10^{4}	1.33×10^{4}	4.0×10^{3}

Blow *et al.* [115] and Yoshizawa *et al.* [136] for single mode fibers, by Gardener [131] for the step-profile multimode fibers, and by Murakami *et al.* [188] for P_2O_5-doped graded-index fibers.

Before γ can be computed, it is necessary to calculate $\emptyset(\Delta\beta_0)$. The calculation of $\emptyset(\Delta\beta_0)$ from the power spectrum $B(\Delta\beta_0)$ of the fiber's lateral displacement b(z) entails a knowledge of the magnitude of the rms deviation σ , as well as that of the correlation distance D of the core boundary deformation. The parameter σ can only be determined from a backscattered light analysis [179]; the experimental technique for this is rather elaborate and cumbersome. Hence, we may use the simple theory of Ref. [131] to calculate the power spectrum $B(\Delta\beta_0)$ when a jacketed (or bare) fiber is pressed against an elastic rough surface. Based on this model, $B(\Delta\beta_0)$ has been shown to be [131]

$$B(\Delta\beta_0) = \frac{1.7}{\left[1+\frac{He}{De}\Delta\beta_0^4\right]^2} \frac{\sigma^2 D}{(D.\Delta\beta_0)^6} \left[1+\frac{64}{225}\frac{\sigma^4 H_e^{5/4}}{f_0^4}\frac{D_e^{3/2}}{D^{10}}\right]^{-1/4} \tag{7.67}$$

where

σ = standard deviation of surface roughness

D = correlation distance

$\Delta\beta_0 = \sqrt{2\Delta}/a$

f_0 = linear pressure

$H_e = H_f + H_{j1} + H_{j2}$ = combined stiffness of fiber and jackets

$H_f = \pi/4\ E_f \cdot a_1^4$

E_f = modulus of silica

a_1 = fiber cladding radius

$H_{j1} = \pi/4\ E_{j1}\ (a_2^4 - a_1^4)$

E_{j1} = modulus of inner (soft) jacket

a_2 = outer radius of inner jacket

$H_{j2} = \pi/4\ E_{j2}\ (a_3^4 - a_2^4)$

E_{j2} = modulus of outer (hard) jacket

a_3 = outer radius of outer jacket

$D_e = 1/\ 1/_{D1} + 1/_{D2}$ = effective modulus of the compressed surface

D_1 = modulus of sandpaper-wooden pad combine

$D_2 = E_{j1} + E_{j2}\ (\ a_3 - a_2\ /a_3)^3$ = modulus of the jackets

The value of $\emptyset(\Delta\beta_0)$ is calculated from (7.43) using (7.67) and the microbending loss per unit length γ/d is plotted in Fig. 7.4 as a function of the linear pressure f_0 for V=39 (λ =0.82 μm) and V=21 (λ=1.55 μm). A steady state as well as a uniform power distribution have been assumed. The fiber parameters used to calculate $\emptyset(\Delta\beta_0)$ are shown in Table 7.2. The spatial frequency $\Delta\beta_0$ and the shape of $\emptyset(\Delta\beta_0)$ are always chosen to be the same at different V. For given fiber parameter values, Fig. 7.4 shows that the microbending loss decreases with increasing wavelength. However, when the effect of dispersion in the fiber's Δ is considered, the power spectrum $\emptyset(\Delta\beta_0)$ will actually increase at longer wavelengths, thereby increasing the microbending loss. From Fig. 7.4 it is also seen that a uniform power distribution assumption yields higher loss values, implying that in short fiber lengths, the microbending loss would be high due to a non-equilibrium in the modal energy distribution.

A theoretical estimate of the excess transient lossses due to such mode coupling effects is verified by Olshansky's [178] measurements on the length dependent attenuation of two continuous 4 km lengths of parabolic fiber. The attenuation measured with a 2 m reference length and 0.1 launch NA were found to be on the average 1.2 dB/km higher than the steady state attenuation of 4.4 dB/km for one fiber and 5.1 dB/km for the other. The mode coupling contribution to this excess transient loss of 1.2 dB/km was reported to be =0.5 dB/km in the first kilometer [178]. In Fig. 7.5, both uniform and steady state loss curves have been drawn for NA=0.1, 0.15 and 0.2; the wavelength is fixed at 0.82 μm, hence the V numbers are 21, 29, and 39 respectively. If one assumes a realistic steady state microbending loss of =0.6 dB/km [188] for uncabled but jacketed fibers, the loss yield (corresponding to the same linear pressure) for a uniform power distribution is found to be =1.05 dB/km (for NA=0.1). Thus the predicted excess transient loss of =0.45 dB/km matches closely with the experimental observation of 0.5 dB/km, showing that this analysis is quite accurate. Furthermore, Fig. 7.5 shows that the microbending loss decreases with increasing NA, a fact that has been experimentally observed time and again [132]. A $\gamma \propto NA^{-2}$ dependence is shown in Fig. 7.5 rather than a $\gamma \propto NA^{-4.3}$ as reported in Ref. [132], because the same power spectrum $\emptyset(\ \theta\ )$ at the same spatial frequency θ has been used in all numerical evaluations indicating that as the number of modes changes, the fiber dimensions must change accordingly, keeping the value of θ constant. If the power spectrum $\emptyset(\ \theta\ )$ is allowed to change as a result of changes in θ (due to variations in NA), then our results exhibit a NA^{-4} dependence of the loss.

Table 7.2 Numerical values of parameters used to calculate the power spectrum $\emptyset(\Delta\beta_o)$ of the refractive index fluctuation.

Parameters (defined in Eq. 7.67)	Numerical Values
a_c	25 μm
a_1	62.5 μm
a_2	102.5 μm
a_3	125 μm
E_f	7000 kg/mm^2
E_{j1}	0.35 kg/mm^2
E_{j2}	33.5 kg/mm^2
σ	11 μm
D	0.63 mm
n_1	1.47214
n_2	1.4585
Δ	0.0092
$\Delta\beta_s$	5.4 mm^{-1}

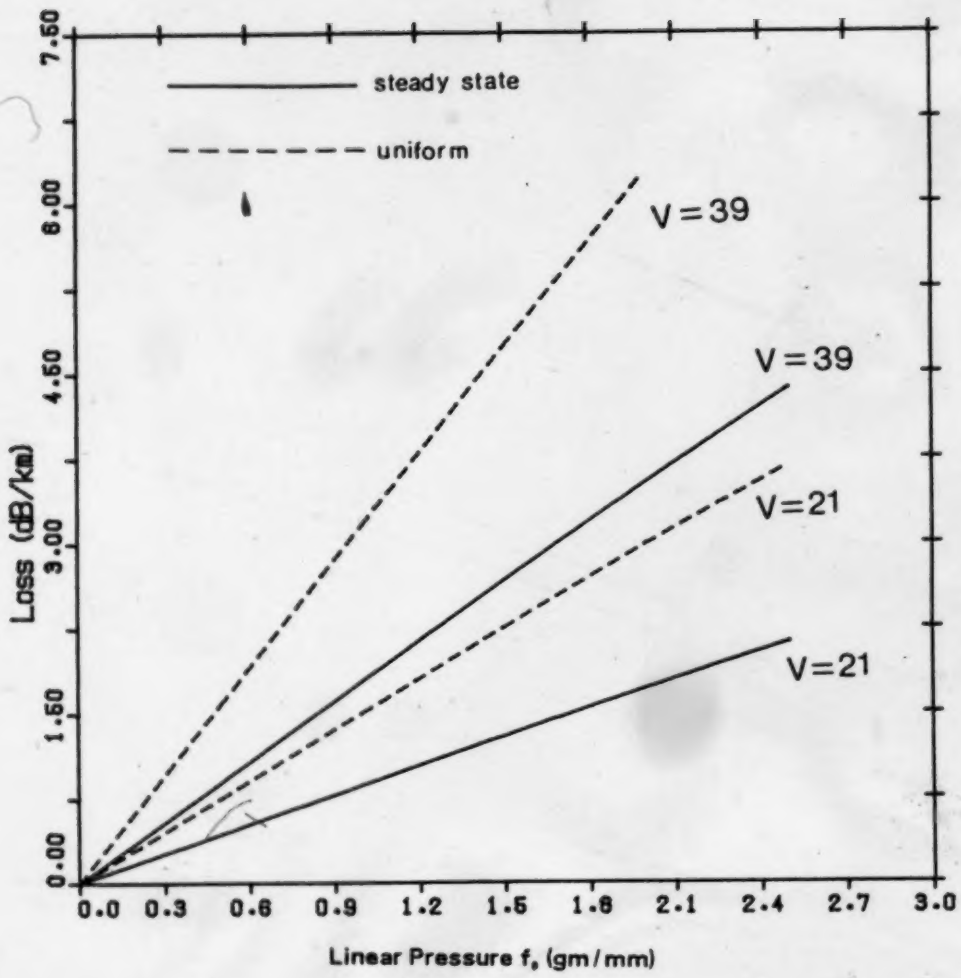

Figure 7.4 Theoretical microbending loss vs. linear pressure for parabolic-index fibers. NA=0.2, a=25 μm.

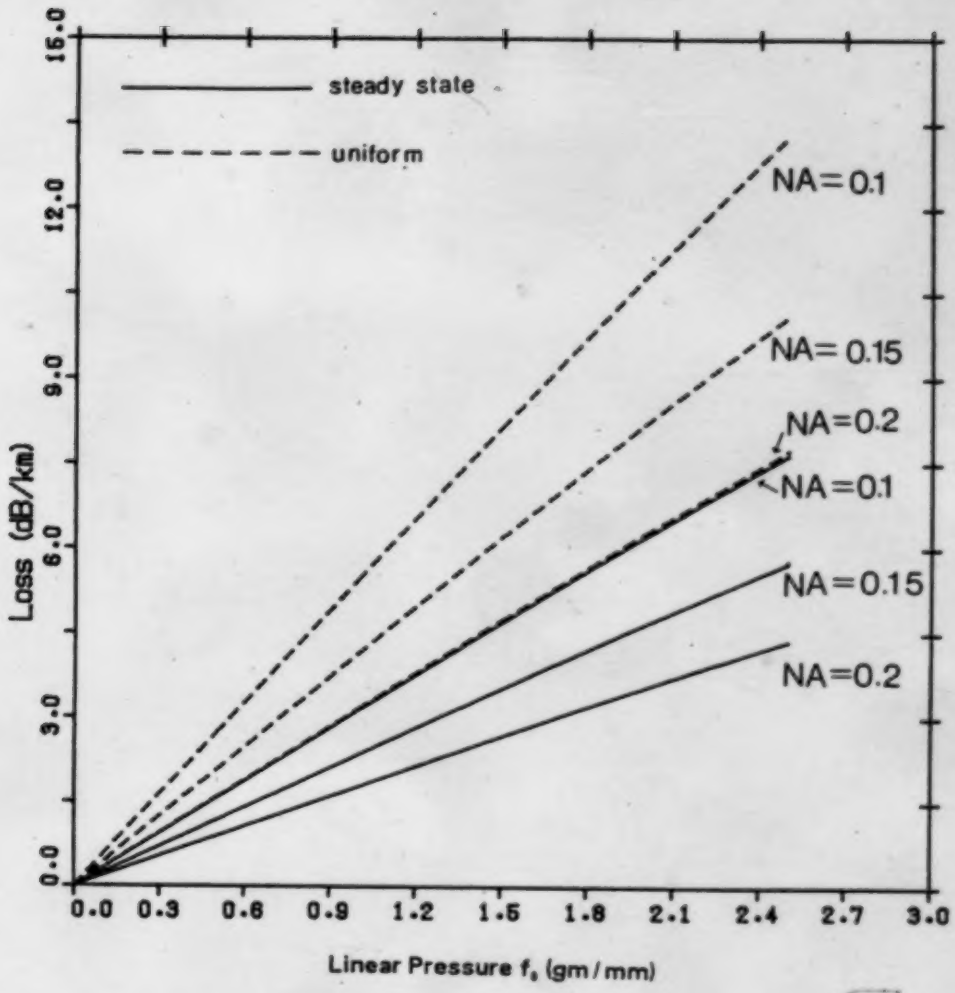

Figure 7.5 Theoretical values of the microbending loss vs. linear pressure at λ =0.82 μm for parabolic-index fibers with different NA values.

To obtain quantitative data on the microbending loss, a 985 m long CPC (Composite Protective Coating) Corning fiber was wound onto a smooth PVC drum, turn next to turn, in a single layer (see Fig. 7.6). Although efforts were made to keep the winding pitch constant, this was not possible owing to vibrations and jerking in the motor and uneven braking force on the fiber take-up drum. The winding pitch was 39 turns/cm in the first section (370 m fiber), 36 turns/cm in the middle section (345 m fiber), and dropped to 28 turns/cm in the last section (265 m fiber). The radius of the drum was 13.74 cm and it was ≈ 40 cm wide with the unilayered fiber occupying ≈ 33 cm. The total number of turns of fiber wound onto this drum was ≈ 1130. The transmitting end of the fiber was spliced onto 0.5 m pigtail of the LD transmitter. The loss due to this splice, measured by an insertion loss technique, was found to be below 0.1 dB. On the receiving side, a mode stripper was placed just before the optical power meter used to record the power loss.

For the first set of experiments, a narrow strip (33 cm × 10.4cm) of 180 grit sandpaper was placed across the width of the drum, with the rough side facing the unilayered fiber. The fiber was pressed onto the sandpaper by means of a wooden pad (curved on one side and flat on the other), weighing 180 gm and measuring 33 cm × 10.4 cm. No excess microbending loss was noticed as a result of the finite weight of this pad. The radius of curvature of the curved side was roughly equal to the radius of the drum. On top of the flat side, weights ranging between 1-8 kg were placed to stress the fiber (10.4 cm of each single turn of the fiber was under stress) so that the fiber could partially conform to the sandpaper irregularities. The sandpaper roughness was measured using a Sloan Dektak II roughness tester (stylus radius ≈ 12 μm) and the standard deviation was found to be ≈11 μm over a correlation length ≈ 0.6 mm (obtained from the material parameters H_e and D_e). Fig. 7.7 is a representative curve of the sandpaper irregularities.

Weights were loaded in 1 kg steps up to a maximum of 8 kg, in time intervals of 10 seconds for the first experiment, and in time intervals of 100 seconds for the second experiment. After reaching the 8 kg limit, weights were unloaded in the same fashion. The induced microbending loss was found to increase linearly with load. In Fig. 7.8, the loss data, normalized to dB/km is plotted as a function of the linear pressure for both load and unload cycles. It is unlikely that the modal energy distribution in the experimental fiber would attain the steady state, since it is only a kilometer long. However, the experimental data is seen to lie

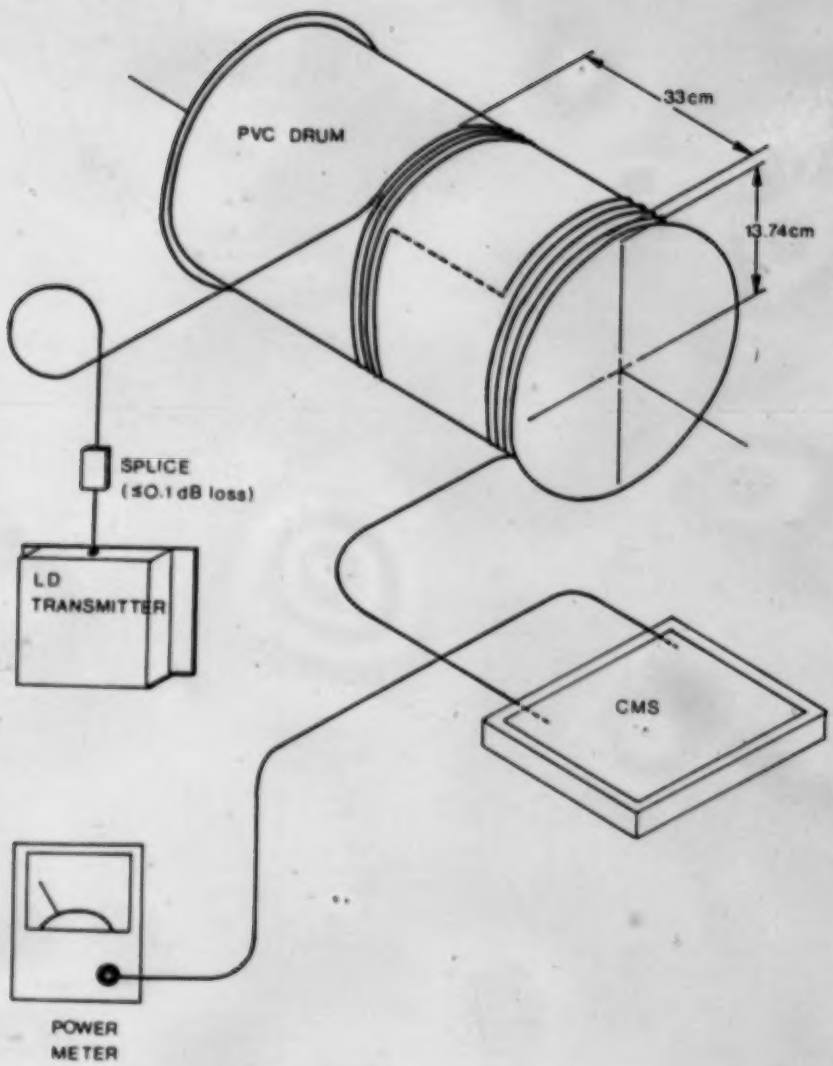

Figure 7.6 Experimental set up for microbending loss studies. CMS designates the Cladding Mode Stripper.

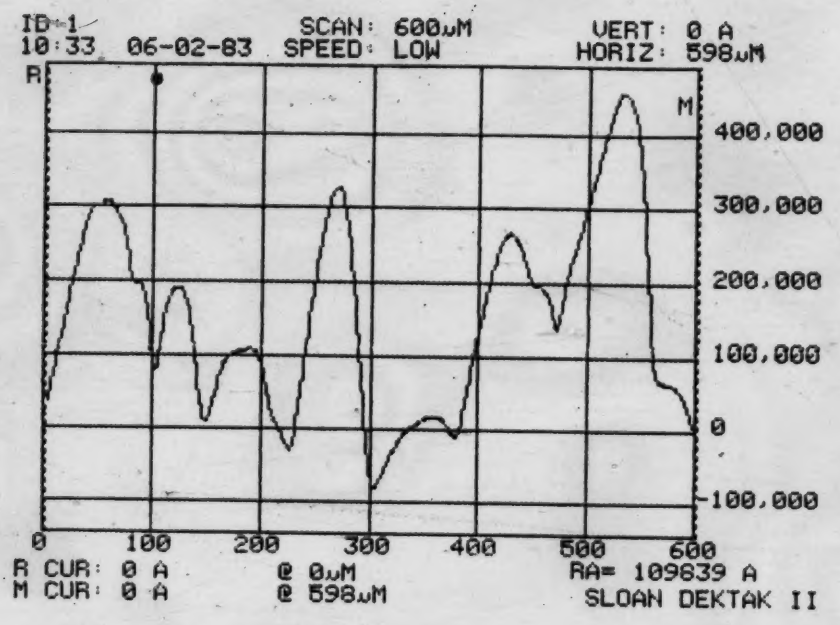

Figure 7.7 Representative sandpaper roughness function. RA denotes the standard deviation of the surface roughness.

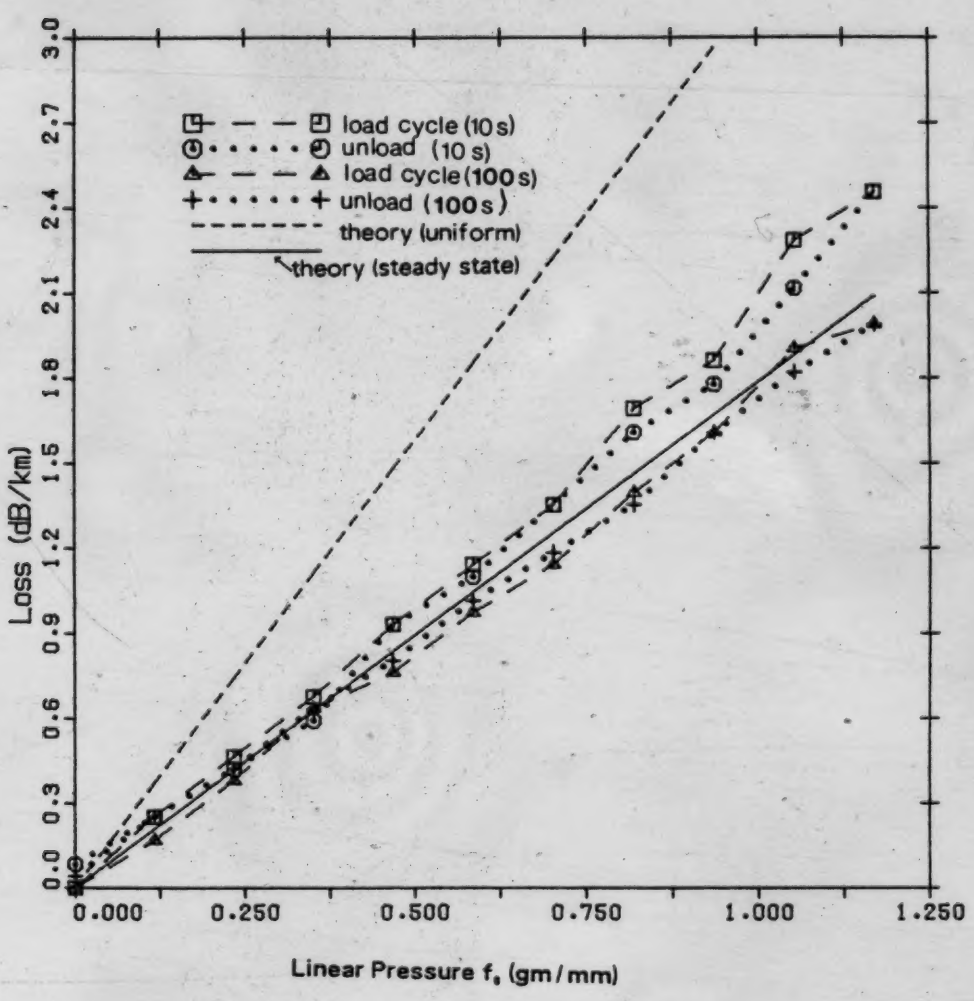

Figure 7.8 Experimental microbending loss values as a function of the linear pressure f_0 for load-unload cycles of 10 s and 100 s time intervals. Theoretical values are shown for a=25 μm, NA=0.2, and V=39.

close to the steady state curve rather than the transient loss curve. This may be because adjacent turns of the fiber are not isolated, a fact which is evident from a measured decrease in γ/d with increasing winding pitch [132]. Fig. 7.8 also shows that when the time interval between loading or unloading was 10 seconds, the measured losses are higher than those done with 100 seconds; the attenuation increase at the maximum load applied of 1.17 gm/mm of fiber length dropped from 2.5 dB/km (10 sec.) to 2.0 dB/km (100 sec.). The decrease in attenuation at longer time gap load-unload cycles can be attributed to the greater time it takes for the relaxation of the coating which relieves coating induced microbending upon the fibers. In fact, over a 24 hour stress-free period, the coating induced microbending loss decreased by 0.2 dB/km.

The next experiment concerned length dependent attenuation. For this, the same set-up of Fig. 7.6 was used. In addition, the unilayered fiber was now divided into three distinct segments (each 11 cm wide); the first, second and the third segments contained 370 m, 345 m, and 260 m of fiber respectively. The fiber lengths were unequal because of the uneven winding pitch; this was undesirable but could not be rectified due to experimental limitations. The sandpaper as well as the wooden pad were now divided into 3 separate and equal parts (11 cm ×10.4cm). Subsequently, weights ranging between 1-8 kg were placed on top of each individual segment. It is to be remembered that the second segment was at a distance of 370 m from the source and the third was 715 m away from the source. The power loss data, normalized to dB/km is shown in Fig. 7.9 along with the theoretical predictions. The measured loss data shows that segment 1 (which is closest to the source) yields the least microbending loss whereas segment 3 (which is farthest from the source) exhibits the maximum loss value. This result is contrary to what one would expect if only length dependent attenuation is taken into account. However, the high winding pitch in the first and second segments play a significant role in this experiment, they more than offset the excess transient losses that is due to a uniform power distribution, thereby reversing the loss trend. For a 38 % increase in the winding pitch, the induced loss is found to drop by atleast 3 dB/km at the maximum load applied of 2.7 gm/mm of fiber length. Hence, we can say that this experiment verifies the winding pitch dependence of the loss rather than the length dependent attenuation. However, this should not be of much concern since, earlier on, our theory was correctly verified by Olshansky's [178] data on the length dependent attenuation.

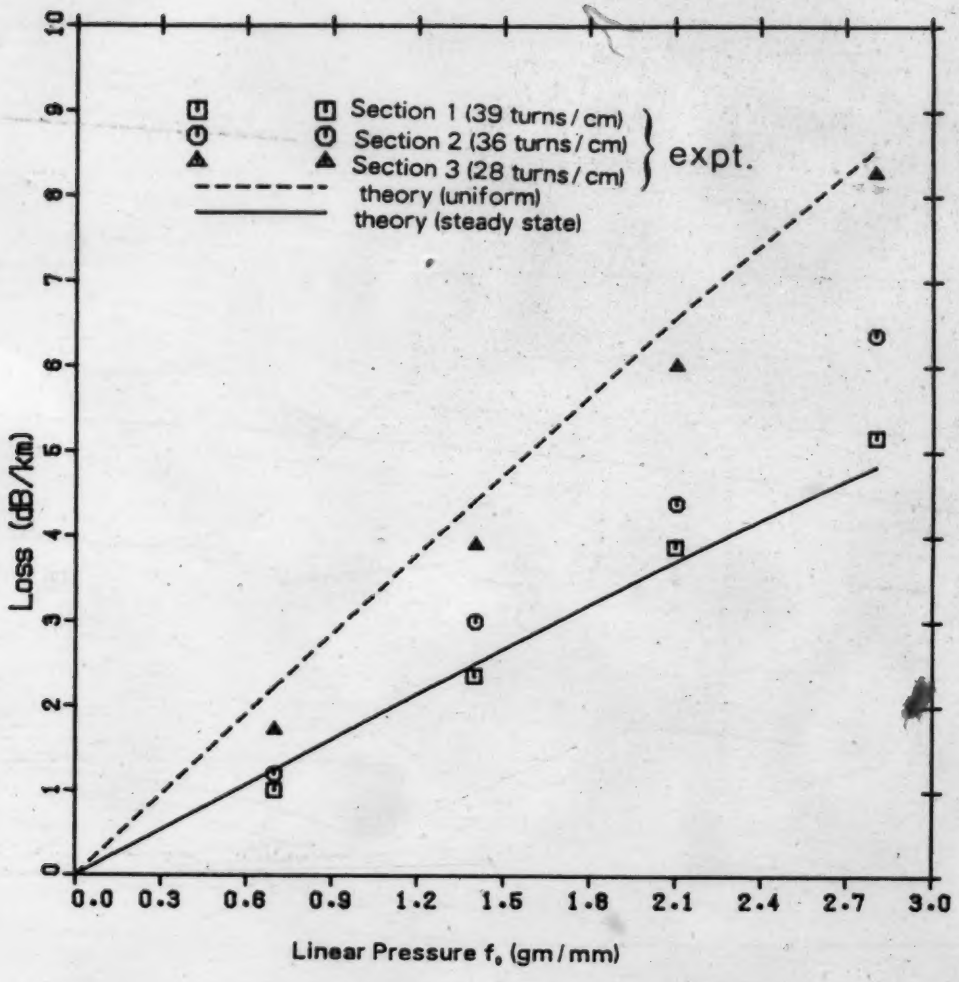

Figure 7.9 Length and winding pitch dependent attenuation measurements as a function of the linear pressure. Theoretical values for a uniform and a steady state power distribution are shown for a = 25 μm, NA = 0.2, and V = 39.

The microbending loss measurements of CPC fibers have also been carried out by Eccleston [187]; it is our intention to verify his results by (7.49). Fig. 7.10 shows the upper limit of the measured data in Ref. [187] as well as numerical results of (7.49). Good agreement is obtained between the data and the theoretical values assuming a uniform power distribution. This distribution is to be expected since the experimental fiber was only 1.625 m long.

With this we conclude the power loss aspect of microbending, having theoretically analyzed and experimentally verify this source of fiber imperfection. In the next section, results on modal noise and distortion are presented; these are caused by temporal fluctuations in the power loss.

7.6 Modal Noise and Distortion

Many authors [27],[29],[30] have proposed that mode selective loss due to microbending can give rise to modal noise. From the theoretical formalism developed in this chapter (in Sections 7.2, 7.3 and 7.4) it is found that although the mode selective loss is due to microbending, a second fiber imperfection namely, elliptic deformation, contributes to the fluctuation of this loss thus giving rise to modal noise and distortion. It is not necessary that spatial frequencies corresponding to both the deformations be present. Only one spatial frequency, either corresponding to microbending ($\Delta\beta_0$) or the elliptic deformation ($2\cdot\Delta\beta_0$), will suffice to cause the power loss. The other deformation simply helps fluctuate this loss.

These fluctuations occur when two modes with propagation constants β_{M-1} and β_{M-2} (the subscripts refer to the respective mode groups) interfere due to coherent or partially coherent excitation, and are simultaneously coupled to a third leaky mode with propagation constant β_M via microbending and the elliptic deformation respectively. In this analysis, mode groups M, M-1, and M-2 are considered because the highest order guided modes are assumed leaky and thus coupling of an adjacent mode group will lose power to this leaky wave via microbending. A rigorous solution requires that these leaky modes be replaced by a continuous spectrum of radiation modes with propagation constants $0 < |\beta_\mu| < n_2 k_0$. Considering the close agreement between our approximation and some of the previously published results in the last section, we still use the mode coupling coefficients of Appendix A4 in order to evaluate the interference coefficients.

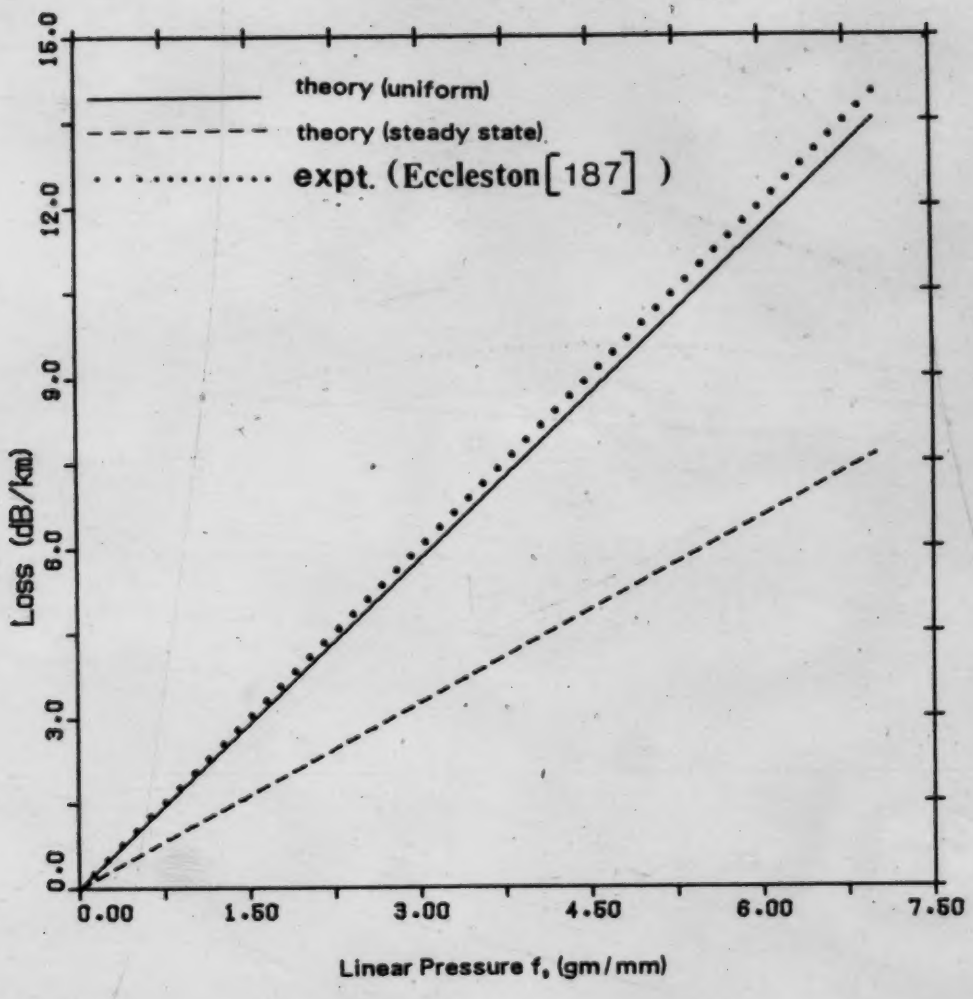

Figure 7.10 Microbending loss as a function of the linear pressure f_s for V = 39. Experimental results of Eccleston [187] are compared with theoretical predictions of Eq. (7.49).

We start by presenting the results on modal noise; the relevant computer program is listed in Appendix A5. The dc-SNR (on a power basis) is evaluated according to (7.54) and (7.55) for a coherent source as a function of the mean microbending loss. It is to be remembered that the dc-SNR is signal bandwidth-independent since spectral components of noise are assumed to be present throughout the signal bandwidth; thus worst case values are obtained for the modal noise. The length of the fiber is 1 km and in the absence of any further information we assume that there are 1000 bumps in total i.e., a bump every meter. Thus, for a total loss of 1 dB, the mean loss per bump will be 0.001 dB. In Fig. 7.11, the dc-SNR is found to drop from 50,000 for a 1 dB/km loss to 1000 for a 3 dB/km loss (V=39). Thus, the deleterious effects of increased microbending loss is clearly seen. Curves for a uniform and a steady state power distribution are drawn in the same figure; both the curves are found to merge indicating that the magnitude of modal noise is specified by a given loss and that the form of power distribution does not explicitly affect it. This is to be expected since the power P_{μ} and $P_{\times}$ (see (7.53)) for the modes μ and $\times$ of mode groups M-1 and M-2 respectively are very nearly equal. Also, for a given loss, a fiber with a higher mode volume exhibits less modal noise in agreement with Epworth's predictions [26].

It is interesting to investigate the dependence of the fiber length L on the modal noise. The results are shown in Fig. 7.12 for V=21 and for coherent illumination. As before, it has been assumed that there is one bump every meter. It is understood that as the length of the fiber increases, so does the total number of bumps as well as the total microbending loss. From Fig. 7.12 it is seen that even with modest microbending loss values (< 0.5 dB/km), the modal noise is excessive in long multimode fiber links. In our example, a loss of 0.5 dB/km would restrict the dc-SNR to 80 in a 20 km link; this SNR value is totally unacceptable for digital or analog transmission. Of course, an equivalent microbend loss of 10 dB/km in a 1 km link would yield an even worse SNR (dc-SNR=8 !), but such high losses are quite unrealistic in telecommunication systems. It is predicted that the maximum link length of digital fiber-optic systems (multimode) will no longer be limited by power loss or bandwidth, but by modal noise. This is true because such systems perform well up to a critical value of SNR and then deteriorate rapidly once that critical value is passed.

We next examine the effect of partial coherence on the dc-SNR which is evaluated according to (7.55) and (7.61). In Fig. 7.13, these results are shown as a function of

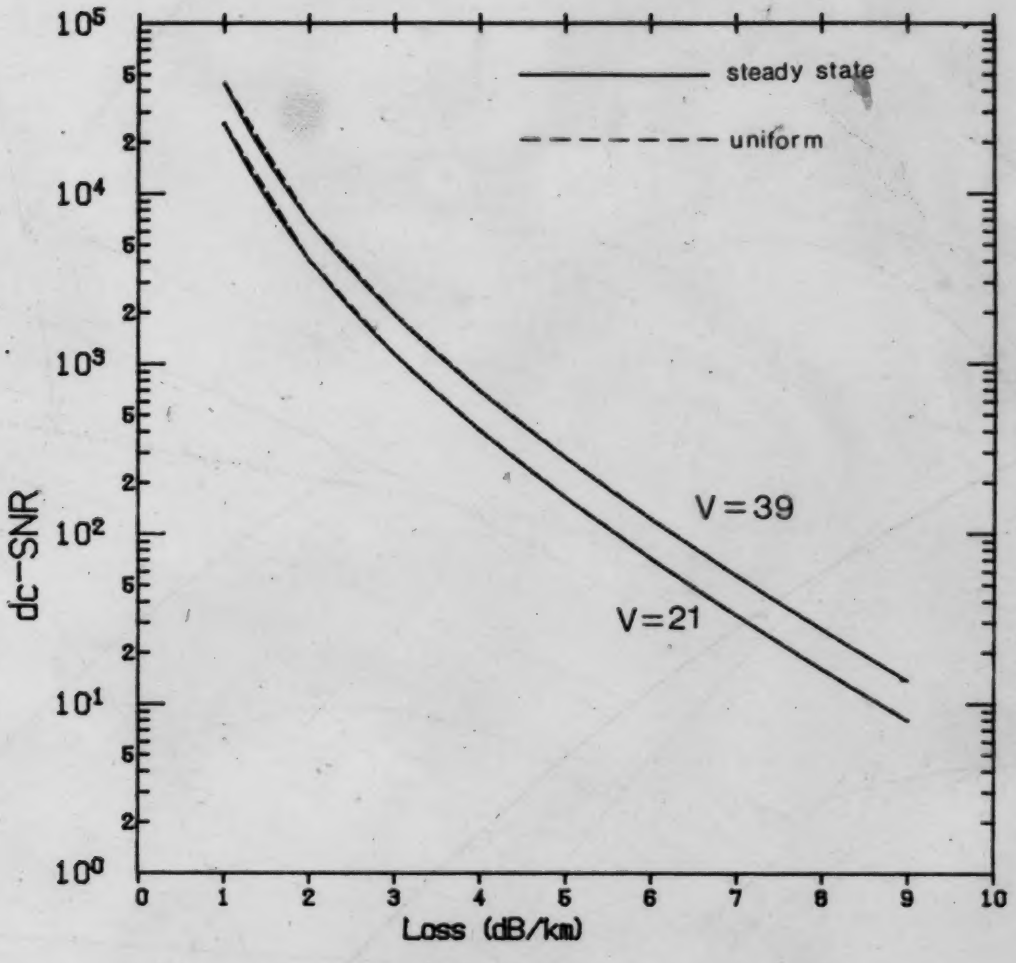

Figure 7.11 dc-SNR vs. microbending loss for coherent illumination. L=1 km, and the number of imperfections=1000.

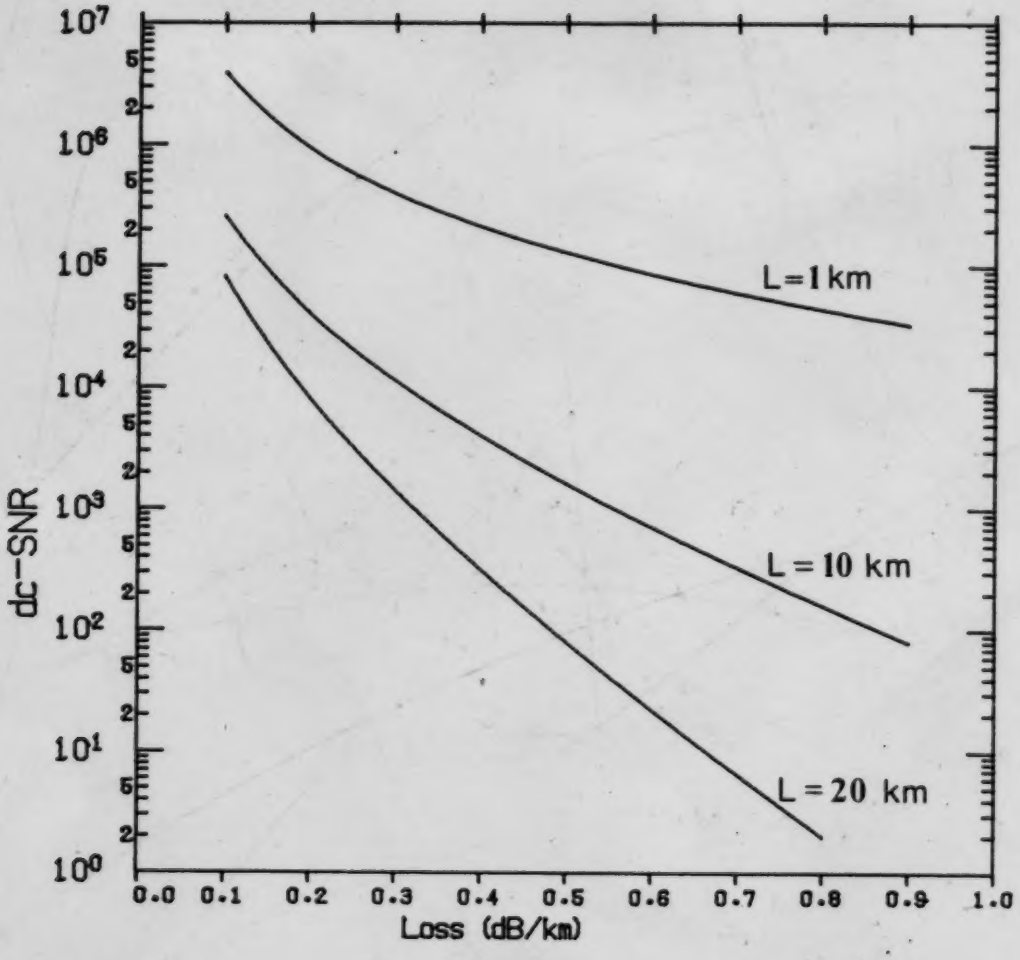

Figure 7.12 dc-SNR vs. microbending loss for different lengths of fiber (coherent source). a=25 μm, NA=0.2, V=21 and the number of imperfections= 1 per meter.

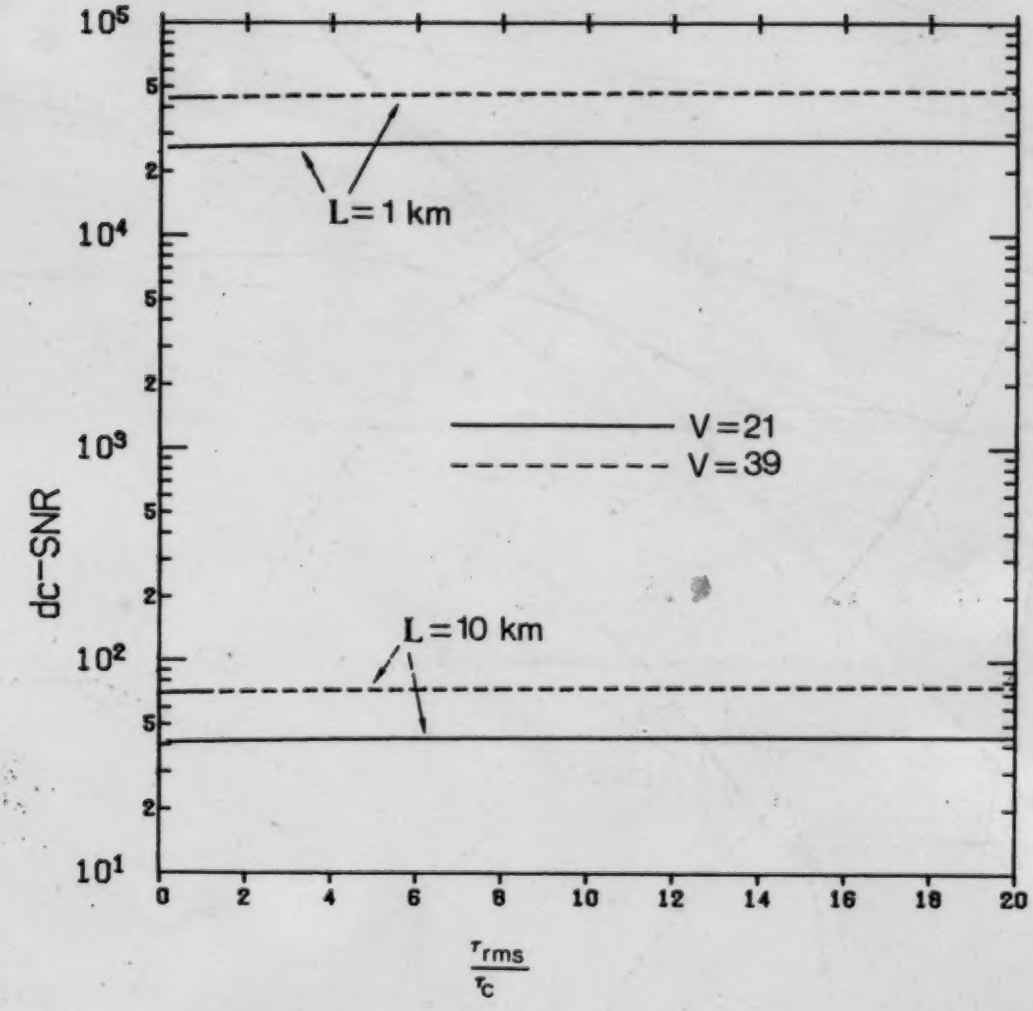

Figure 7.13 dc-SNR for partially coherent sources with coherence time τ_c. Microbending loss =1 dB/km, number of imperfections=1 per meter and τ_{rms}=1 ns/km.

τ_{rms}/τ_c for different V (V=21 and V=39), and for different L(L=1 km and L=10 km). A mean microbending loss of 1 dB/km and a bump every meter are assumed. The improvement in the dc-SNR over $0 \leq \frac{\tau_{rms}}{\tau_c} \leq 20$ (only this range was investigated) is found to be minimal. As opposed to coherent excitation ($\tau_c \to \infty$), the dc-SNR at $\tau_{rms} = 20\tau_c$ increases by a mere 7.3% and 6.8% for L=1 km and L=10 km respectively (V=21). Thus the dc-SNR/($\frac{\tau_{rms}}{\tau_c}$) slope for fiber imperfections is negligible compared to that for most geometrical misalignments at a connector. However, we have checked that as $\frac{\tau_{rms}}{\tau_c}$ increases to very high values (> 20), the dc-SNR continues to rise monotonically and eventually becomes infinite for $\tau_c = 0$ (incoherent source).

The presence of fiber imperfections will not only yield power loss and noise but can generate nonlinear distortions (called modal distortion) if the source frequency changes. In (7.57)-(7.59) and (7.63)-(7.66), this wavelength dependent transmission characteristics of fiber imperfections has been examined for coherent and partially coherent sources. We first present results for the normalized power loss fluctuations $\sqrt{\langle (\frac{d\eta}{d\omega_c})^2 \rangle} \frac{1}{\tau_{rms} \langle \eta \rangle}$ according to (7.59) for a 1 km long fiber with $\tau_{rms} = 1$ ns/km. The fluctuations tend to be higher for low V, as can be seen from Fig. 7.14. For the highest loss considered (10 dB/km), the normalized fluctuations are 0.83% for V=39 and 1.75% for V=21. For small losses (< 3 dB/km), the fluctuations show almost a linear loss dependence. For large losses (> 3 dB/km), $\langle \eta \rangle$ at the end of the waveguide drops off rapidly so that the fluctuations rise exponentially.

When the modal distortion $R_{2f/f}$ is calculated via (7.64) for partially coherent sources (loss=1 dB/km), the distortion is seen to decrease by as much as 16 dB (L=1 km with 1 bump every meter, V=21, $\tau_{rms} = 1$ ns/km, $\Omega_m = 10^9$ rad/sec.) when $\tau_{rms}/\tau_c = 20$ as compared to the coherent case (see Fig. 7.15). In longer fibers, the improvement is even better; when L=10 km, the decrease is 21 dB. However, the $R_{2f/f}$ curve for V=39 is found to decrease only half as fast as the V=21 curve over the $0 \leq \frac{\tau_{rms}}{\tau_c} \leq 20$ interval (both for L=1 km and L=10 km). It is also observed from Fig. 7.15 that with a realistic microbending loss of 1 dB/km, a 10 km long link will exhibit a relative second harmonic distortion of -40 dB ($\tau_{rms} = \tau_c$ and $\Omega_m = 10^9$ rad/sec.) which may not be acceptable in some analog applications. Commercial laser diodes will usually exhibit a higher Ω_m, indicating that the $R_{2f/f}$ just quoted is overly optimistic.

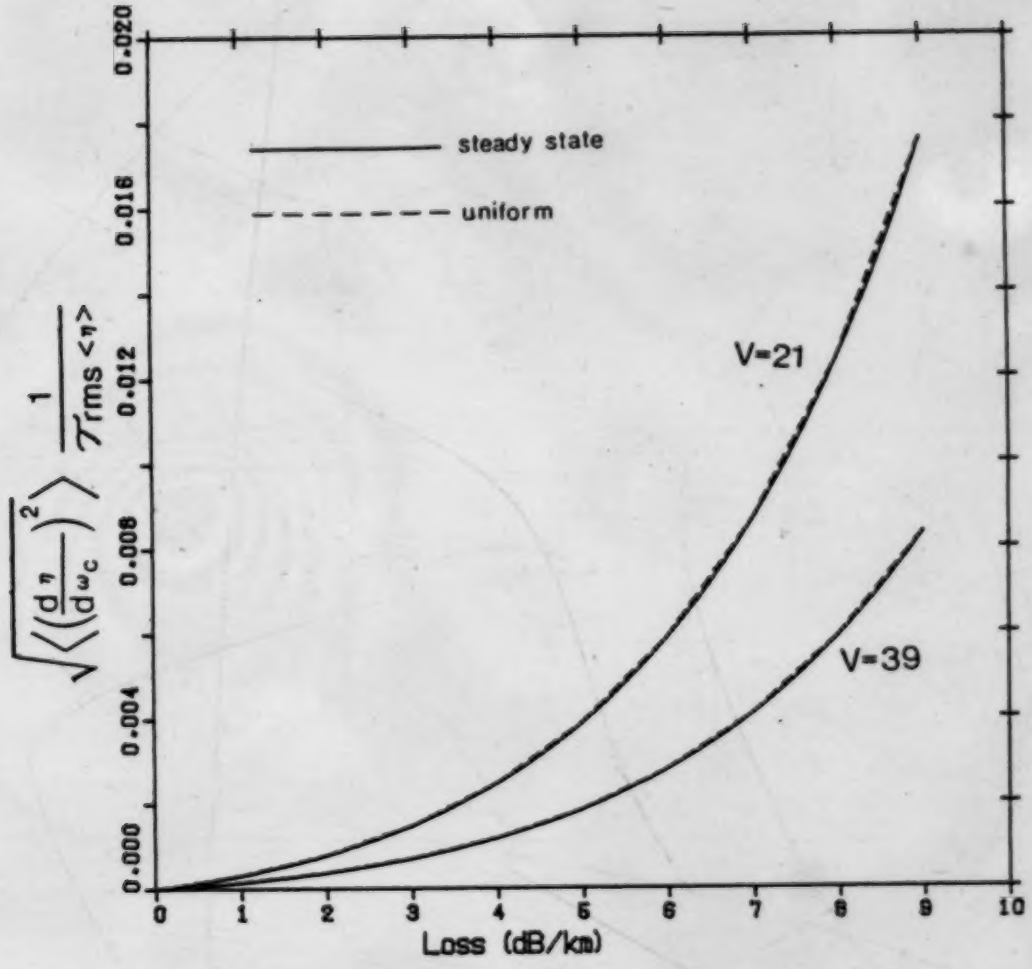

Figure 7.14 Normalized loss fluctuations as a function of the microbending loss for coherent illumination. L=1 km, number of imperfections=1000 and τ_{rms}=1 ns/km.

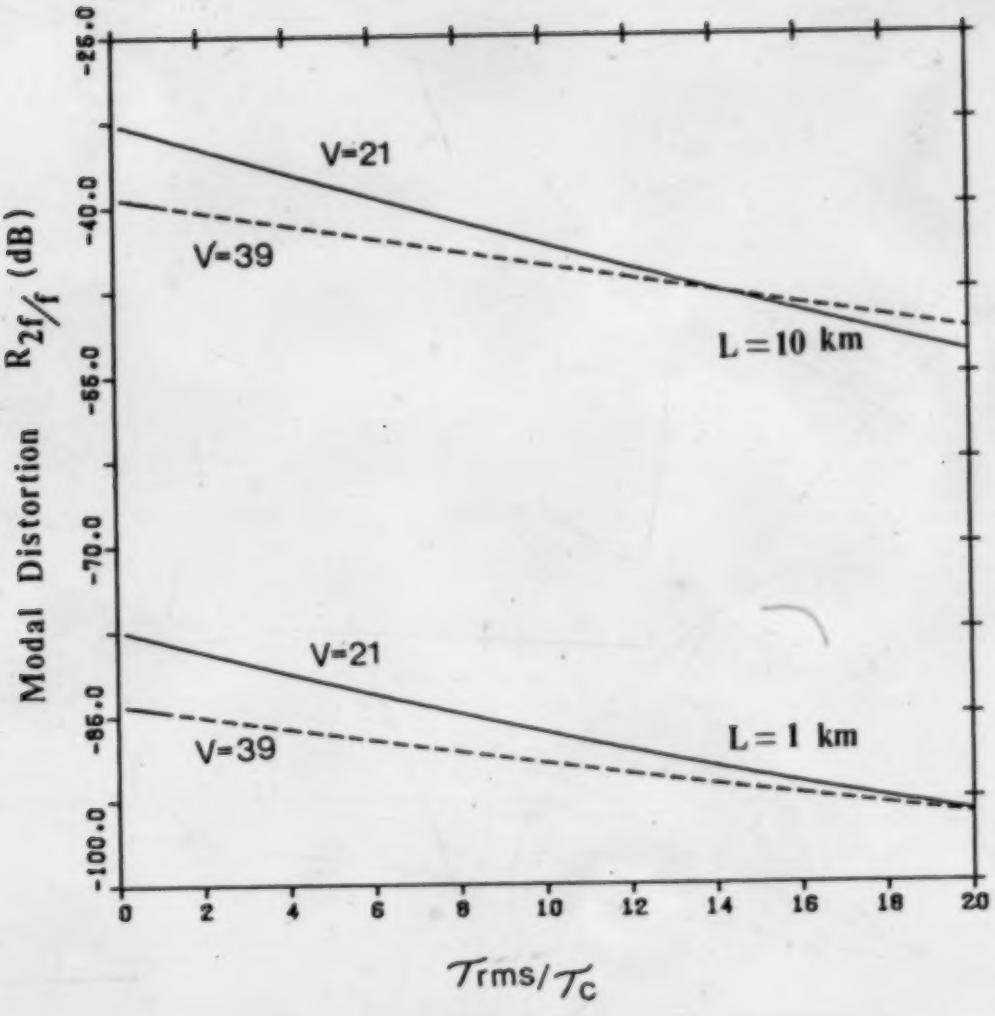

Figure 7.15 Modal distortion $R_{2f/f}$ for a partially coherent source. Microbending loss= 1 dB/km, τ_{rms}=1 ns/km, Ω_m =10⁸ rad/sec, and the number of imperfections= 1 per meter.

Stubkjaer [140] has reported some interesting measurements made on the excess nonlinear distortion introduced by long multimode graded-index fibers. The numerical values of the experimental parameters [140],[189] are listed in Table 7.3; they have been used in (7.59) to yield some representative theoretical results in Fig. 7.16. Although we do not have definite information on the possible number of bumps, (7.59) is evaluated as a function of the microbending loss for N_b=100, 1000 and 10,000. Ref. [140] reports a $R_{2f/f}$ value that fluctuated between -40 dB to -20 dB (see Fig. 2 of Ref. [140]). From Fig. 7.16 it is seen that if the number of bumps are few (say one every 10 mtrs.), then for a total microbending loss of 3 dB, the predicted $R_{2f/f}$ can be as high as -20 dB. A 3 dB microbending loss in the experimental fiber of Ref. [140] would hardly be surprising since its total loss was ≃5 dB. When a multilongitudinal mode laser diode (M_ℓ =4) was substituted for the singlemode one, the relative distortion was found to decrease by ≃5 dB (compare curve I of Fig. 3 [140] with Fig. 2 [140]). Eq. (7.59) predicts a decrease of ≃6 dB for this case. Moreover, when the modulating amplitude was reduced in Ref. [140] so that the coupled optical signal was 0.5 mW p-p instead of 1.5 mW p-p, the distortion was found to decrease further, by = 10 dB. It is well known that [177] the wavelength shift $\Delta\lambda$ (or equivalently Ω_m) is proportional to the modulation index 'm'. Thus, a three fold decrease in m will reduce Ω_m by a factor of 3. Accordingly the $R_{2f/f}$ predicted by (7.59) will decrease by 9.54 dB. The close agreement between the theoretical predictions of (7.59) and these measured results suggest that this analysis is correct.

It was desired to conduct an experiment to ascertain the relationship between microbending loss and modal distortion. For this, the set-up shown in Fig. 7.6 was used. The power meter was replaced with an APD detector and a spectrum analyzer. A RF signal source was used as the modulator. Furthermore, a steel belt (10.5 cm wide and 88 cm long) with the 180 grit sandpaper on its inside was wrapped around the fiber on the drum. Only the first 340 m of the fiber were compressed since the source had a small coherence time. The values of the parameters for this experiment are listed in Table 7.3. Theoretical curves corresponding to these values have been drawn in Fig. 7.17 along with the data. We assumed the number of bumps per unit length as 1/cm in one case and 10/cm in the other, these values could still be low considering the sandpaper grit. In any case, the theoretical values are far below the noise floor of the spectrum analyzer (≃ -47 dB) and hence a check of this theory was not made

Table 7.3 Values of the fiber and source parameters studied in Ref. [140] (Fig. 7.16) and in our experiment (Fig. 7.17).

Experimental parameters	Values from Ref.140	Values for our expt.
fiber core radius a_c	25 μm	25 μm
fiber NA	0.2	0.2
fiber τ_{rms}	0.6 ns/km	1 ns/km
fiber loss	4.5-5.00 dB/km	2.7 dB/km
source τ_c	0.367ns	0.034ns
$\Omega m/2\pi$	≈20 GH_z	≈ 2 GH_z
Modulation frequency f_m	2-400 MHz	1-55 MHz
Modulation Index	≈ 1	≈ 0.25
No. of longitudinal modes of the source 'M_ℓ'	1, 4	1

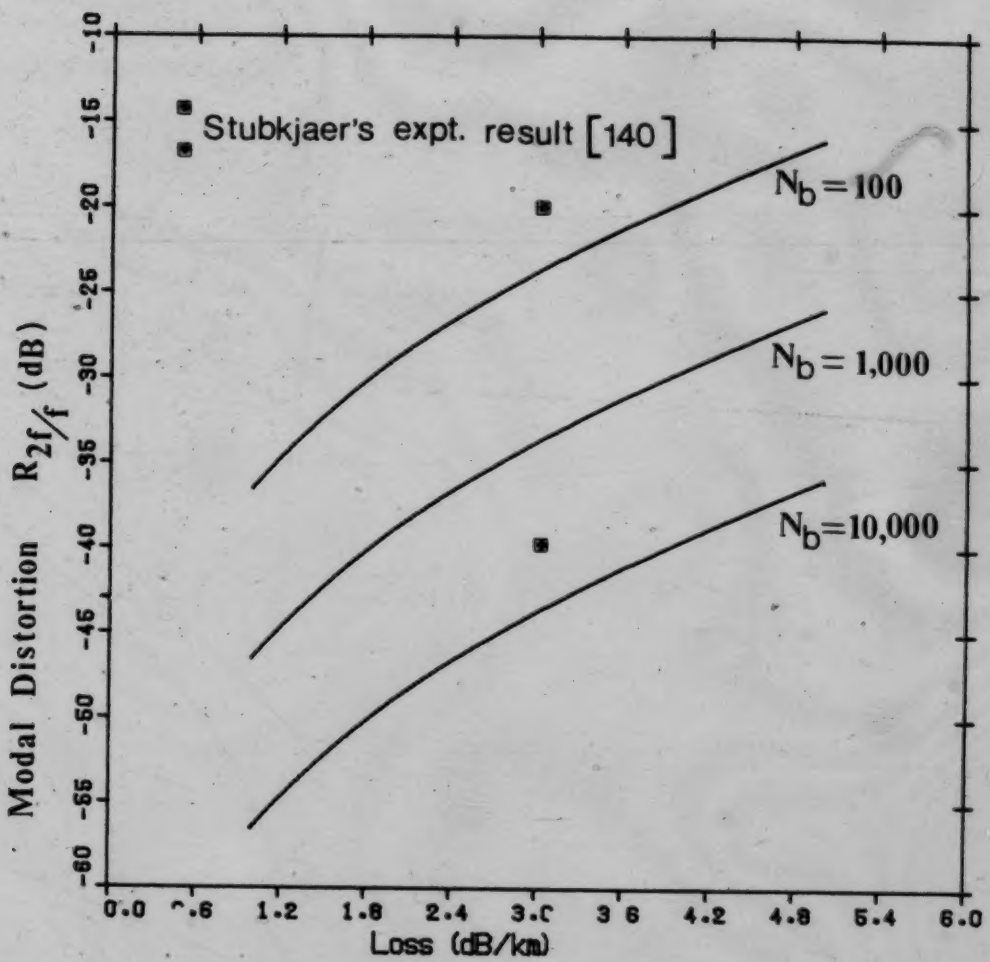

Figure 7.16 Theoretical modal distortion results as a function of microbending loss for the experimental parameters taken from Refs. [140],[189]. N_b denotes the number of fiber imperfections.

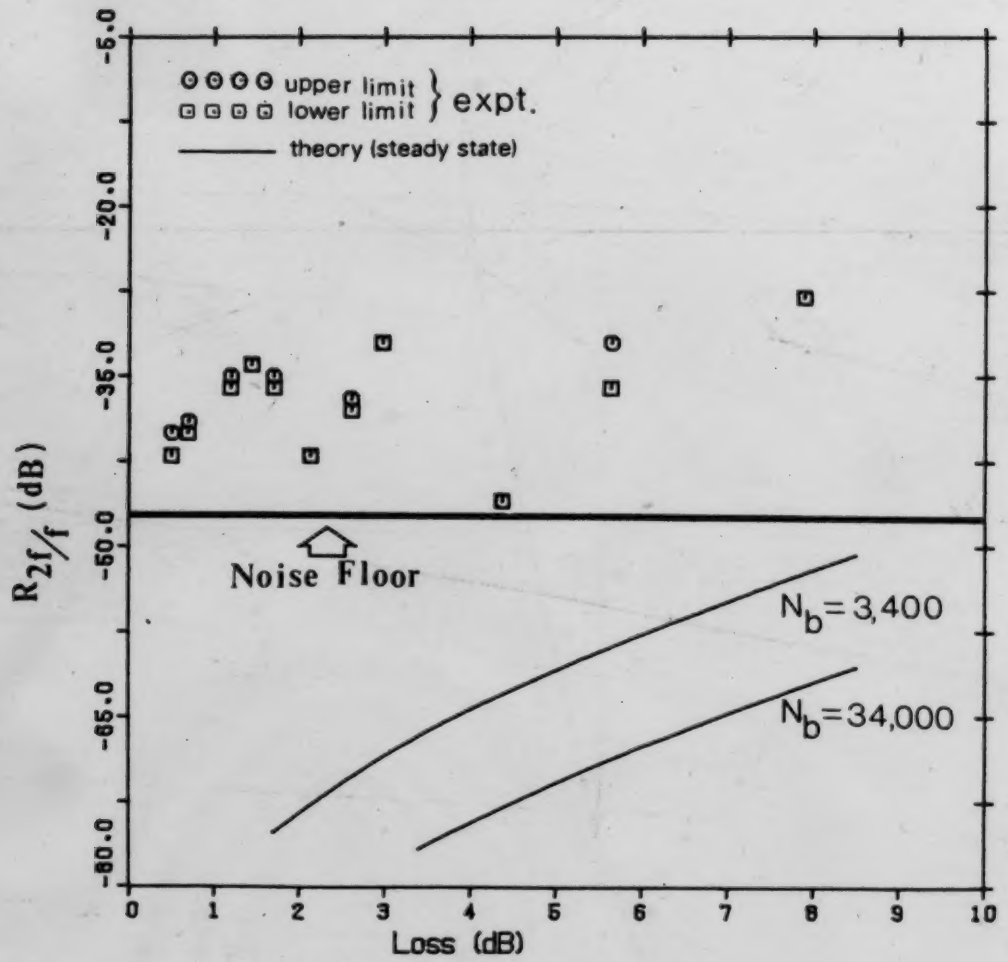

Figure 7.17 Experimental data on $R_{2f/f}$ as a function of the microbending loss. Theoretical curves have been drawn for the values of the parameters listed in Table 7.3. N_b denotes the number of fiber imperfections.

possible with our experiment. The erratic behavior of the data with changing loss (changing compressive force on the fiber) was probably caused by optical feedback which is known to disturb the source spectral characteristics and degrade the linearity [16],[23]. Since the spectral characteristics depend on both amplitude and phase of the reflected optical wave [23], it is hard to predict the resulting $R_{2f/f}$. However, if the optical feedback can be avoided by some suitable mechanism (e.g., optical isolator), one can use a source with a long coherence time ($\tau_c \simeq 1$ ns) and a large wavelength shift ($\Omega_m/2\cdot\pi = 20$ GHz) to observe modal distortion with moderate amounts of microbending. The last two conditions (i.e., long coherence time and large wavelength shift) were met in the experiment of Stubkjaer [140], whose results lend support to our theory.

7.7 Conclusions

In this chapter, a theory based on a perturbation approximation to the power diffusion between modes was developed to yield the power loss and its fluctuations caused by fiber imperfections. Good agreement has been obtained for the microbending loss between the predictions of this theory and those in Refs. [102],[106],[131],[132],[178], and [187]. New experimental results verified the theory and an accurate estimate of the excess transient losses has been made. The dependence of the loss on the wavelength, NA and fiber winding pitch were also examined. The modal noise and distortion have been quantified; it was found that the loss per fiber imperfection is a more important parameter than the overall loss. For a given loss, a small number of large amplitude bumps yield more modal noise than a large number of small bumps. An attempt was made to explain the measurements of Stubkjaer [140] using our modal distortion analysis and good agreement has been obtained. It is shown that for modest values of microbending loss (≤ 0.5 dB/km), modal noise and distortion may not be critical for short fiber links (≤ 1 km); however, the performance of longer multimode links ($L \geq 10$ km) using digital (or analog) transmission will be severely deteriorated.

CHAPTER VIII

SUMMARY AND CONCLUSIONS

In this thesis, an electromagnetic analysis has been used to study systematically, the power loss, noise and nonlinear distortions in optical communication systems due to fiber connectors and microbending. The effect of optical feedback on the source emission has been neglected in our analysis, since it concerns the physical properties of the device more than the fiber. The type of multimode fiber investigated has a parabolic-index profile whose modes are regarded, with good approximation, as TEM waves described by Hermite-Gaussian (rectangular geometry) or Laguerre-Gaussian (circular geometry) functions.

When a mode emerging from one fiber is injected into another fiber (as in a connector), a set of the modes of the second fiber is excited. The coupling to the various modes is a function of the fiber parameters and the degree of geometrical misalignment. The power transfer to the various modes can be derived from modal amplitude coupling coefficients, which are evaluated in closed form for the axial misalignment (previously derived in [34],[87],[94]), the angular (derived in Chapter 6 using [91]) and longitudinal misalignments [70]. The effect of numerical aperture (NA), core diameter and/or refractive index profile mismatch between the connecting fibers is excluded from this study. The mode coupling coefficients for fiber imperfections (e.g., microbending) are a measure of the degree to which core-boundary distortions cause an overlap of the fields of two modes. Power loss from a guided mode occurs when the mode to which it is coupled is either leaky or radiating.

For coherent or partially coherent illumination, the coupling efficiency at a connector (or the power retention efficiency at an imperfection) is very sensitive with respect to: 1)external forces, temperature changes, etc., and 2) small changes of the emission wavelength. If the transmitting fiber is, for example, subjected to random forces which change with time, the coupling efficiency and thus the power in the receiving fiber fluctuates. Since the fluctuations of external forces or temperature will be slow, the noise shows low frequency components only. High frequency noise can also occur since the coupling efficiency (or the power retention efficiency for an imperfection) is wavelength dependent — transforming any phase noise of the source to intensity noise after a fiber connector (or imperfection). The low and high frequency noise generated by this mechanism is called modal noise; however, only the low frequency (dc) noise is considered here. Furthermore, during analog modulation,

sidebands are generated. A non-uniform transmission of these sidebands at a connector (or an imperfection) yields nonlinear distortions (called modal distortions) after demodulation at the photodetector. It has been shown [34] that higher order distortions will be small in magnitude; hence, only the (dominant) relative second harmonic distortion $R_{2f/f}$ is refered to as modal distortion throughout this thesis.

We first presented results for the power loss. Subsequently, modal noise and distortion results have been presented as a function this loss. The loss due to geometrical misalignments (at a connector) as well as fiber imperfections is seen to depend strongly on the choice of the modal power distribution i.e., a uniform or a steady state one. The steady state power distribution has been derived analytically from Eve's [167] formula of the near-field intensity distribution for a multimode graded-index fiber. For a given geometrical offset, the power loss corresponding to the uniform distribution is found to be approximately 1.75 to 2 times as high as that for the steady state case for all V and NA and irrespective of the nature of the misalignment. This is because it is predominantly the higher order modes (carrying less power in the steady state) that are coupled the least. This generalization is not valid for large offsets (and particularly the axial one) where some low order modes may remain uncoupled to the receiving fiber, thus yielding almost equal loss values for both the power distributions. In any case, for a given offset (that yields power loss $\leqslant$ 2 dB with a uniform distribution assumption), connectors far from the source ($\geqslant$ mode-coupling length of the fiber) are expected to be half as lossy as those near it. The mode-coupling length, computed theoretically for certain graded-index fibers, has been found to be on the order of 1 to 4 km [190]. But in reality it is generally less than this, with a minimum of about 150 m [191].

If a long fiber is present after the connector, mode mixing at the connector would further increase the absolute connector loss value, as Cherin has predicted [82]. Hence, a very short fiber (1 m) was used as the output fiber in our experiment. The input fiber was fairly long (170 m), but not long enough to attain the steady state; thus, the measured data for all three types of geometrical misalignments were usually found to lie between the curves corresponding to the uniform and the steady state power distribution. Since different geometrical misalignments have different mode mixing effects [87], the ratio of the losses corresponding to a uniform and a steady state power distribution may not increase by the same proportion for all types of offsets.

In general, all three geometrical misalignments will be simultaneously present at a connector and superposition does not apply in such a case [87]. For power loss considerations, angular and axial offsets may be treated the same way via (6.7); the Gaussian beam divergence term for the longitudinal gap can then be incorporated into the expression (6.1) to yield the effective mode coupling coefficient. The resulting expression can then be evaluated by numerical integration for every combination of the normalized tilt (and/or axial offset) denoted by Θ_N and the normalized gap width d/a. These calculations have not been carried out in this thesis, but could be subjects of further research.

Regarding the loss predictions of individual geometrical offsets, good agreement has been obtained with our experimental measurements on the power loss. Further, our analysis is validated by a comparison of its results with those obtained from geometrical optics for a high mode volume fiber and by assuming a uniform power distribution. Using a uniform power distribution, this analysis corroborates Gloge's [63] geometrical optics result that fiber axis tilt at the splice is equivalent to an axial offset. It is also shown that this equivalence applies to the prediction of loss value only, and that the approximation gets worse as the fiber mode volume decreases.

It is well known that the absolute values of the power loss decrease by $\simeq$ 0.4 dB when index-matching is used at the connector, due to the elimination of Fresnel losses [67]. If the type of offset is a longitudinal gap, the loss is additionally reduced by 44 % (V=39, steady state) as compared to an air gap, when the normalized gap width d/a=4. The amount of loss reduction is dependent on the Gaussian beam divergence in the gap, and hence it varies with the modal power distribution, the V number and d/a.

The microbending loss (mechanical "frequencies" corresponding to this type of loss are assumed to be present only) has been calculated by a power diffusion approximation and by assuming all the highest order guided modes (in the β-space) to be leaky. For given microbending statistics, the steady state loss values approached asymptotically by long fibers are found to be approximately half (to 0.6 times) the attenuation rate in short lengths of fiber (corresponding to a uniform power distribution). This prediction is verified by Olshansky's length-dependent attenuation measurements [178].

The mode selective loss mechanisms considered so far exhibit a strong V number (i.e., mode volume) dependence; the V number can be changed by varying the fiber core diameter,

the fiber NA, and/or the emission wavelength. It has been shown in Ref. [192] that large core diameter fibers (hence, large V) exhibit lower relative power losses for fixed geometrical offsets. Our results show that, with increasing NA, the connector loss increases sharply, but the microbending loss drops. For example, when the NA is increased from 0.1 to 0.2, the air gap loss rises five fold at a connector (d/a=4 and steady state assumption), and the microbending loss reduces to half (using the same $\emptyset(\ \theta\ )$ at all NA) for all linear pressures and all modal power distributions.

For small offsets (loss $\leqslant$ 0.5 dB), the steady state connector loss is found to reduce with increasing wavelength (decreasing V). With large offsets (loss $>$ 0.5 dB), the loss is higher at longer wavelengths because of a smaller electromagnetic field spread. If a uniform power distribution prevails at the exit face of the transmitting fiber, different offsets behave differently with increasing wavelength, so no global comment about the wavelength dependence of the loss can be made (see Table 8.1). For the case of microbending, although the mode coupling strength decreases with wavelength, the power spectrum of the longitudinal perturbation (which carries power away from a guided mode) increases through dispersion in the fiber's relative index difference Δ. Thus, the microbending loss is seen to increase slightly at longer wavelengths [115],[132],[136],[188]. For realistic splice loss (0.1 dB $<$ loss $<$ 1 dB) and/or microbending loss ($\cong$ 0.5 dB/km) values, the maximum deviation of this loss is seen to be only ± 5 % over the wavelength region 0.82 μm $\leqslant\ \lambda \leqslant$ 1.55 μm. A loss deviation margin as small as this (i.e., ± 5 %), is not an important factor when weighing the pros and cons of a given wavelength.

Besides the NA and λ dependence, the microbending loss is found to decrease when the coating of the fiber has had sufficient time to relax within the jacket buffer to relieve coating induced microbending upon the fibers. Over a 24 hour stress-free period, the coating induced microbending loss decreased by 0.2 dB/km in a CPC (Composite Protective Coating) fiber. Similar behavior has also been noticed in cabled fibers. In an experiment at ITT's Electro-Optical Products division in Roanoke, Va., a multifiber cable suspended between telephone poles showed a 0.25 dB/km decrease during the nine-month recording period. This decrease was observed because residual microbending induced during insertion of the fiber into the cable, and during cable installation, is relieved as the fiber gradually moves within its buffering to a spot where it is under minimal mechanical tension [191].

Table 8.1 Power loss trend with increasing wavelength. The figures within the bracket denote the maximum deviation of the power loss, expressed as a percentage of the highest loss value at a given offset. 0.82 μm< λ <1.55 μm.

Type of Offset		Steady State	Uniform
Axial $0.04 \leq \frac{\Delta a}{a} \leq 1.0$		$\frac{\Delta a}{a} \leq 0.12$, loss decrease (37%-0.4%) $\frac{\Delta a}{a} > 0.12$, loss increase (2%-22%)	$\frac{\Delta a}{a} \leq 0.52$, loss decrease (38%-0.5%) $\frac{\Delta a}{a} > 0.52$, loss increase (1%-31%)
Tilt $0.13 \leq \theta/2\Delta \leq 0.9$		$\frac{\theta}{2\Delta} \leq 0.38$, loss decrease (2%-0.5%) $\frac{\theta}{2\Delta} > 0.38$, loss increase (1%-4%)	$0.13 \leq \frac{\theta}{2\Delta} \leq 0.9$, loss decrease (1.5%-4%)
Longitudinal	Air Gap	$\frac{d}{a} \leq 4$, loss decrease (≈ 6%) $\frac{d}{a} > 4$, loss increase (1%-5%)	$2 \leq \frac{d}{a} \leq 20$ loss increase (5.2%-0.3%)
$2 \leq \frac{d}{a} \leq 20$	Index Matched	$\frac{d}{a} \leq 8$, loss decrease (31%-4%) $\frac{d}{a} > 8$, loss increase (1%-6%)	$\frac{d}{a} \leq 4$, loss decrease (≈ 16%) $\frac{d}{a} > 4$, loss increase (1%-2.5%)

A decrease of the microbending loss over time is certainly welcome from a power budgeting point of view, but can be detrimental for systems where ultra stable timing and frequency reference signals (e.g., in NASA's Deep Space Network) are to be transmitted over optical fibers [193]. This is because, when the microbending statistics change with time, they cause refractive index fluctuations near the core-cladding boundary, resulting in phase changes. We have calculated that, for a 0.25 dB/km change of microbending loss over a period of 9 months, a 20 km single mode fiber link will exhibit a 4 ppm (parts per million) phase change for 100 seconds averaging time (an initial mean microbending loss of 0.5 dB/km is assumed). A stability of 4 ppm is not adequate for the distribution of ultra-stable frequency references with an error rate requirement of 10^{-15} for 100 seconds averaging [194]. Thus, a phase stabilization scheme against changes in microbending loss is necessary if such high accuracies are required.

Several papers [46],[49],[50] show close agreement between theoretical and measured modal noise caused by flexing, vibrating or heating the fiber which randomly perturbs the inter-mode delays (phases) and give rise to randomly changing speckle patterns downstream. This form of modal noise (dc-modal noise) may not be significant in most transmission systems as the changes are slow and only generate noise below the signal frequency band; nevertheless, a dc analysis gives important clues about the dependence of this noise on various system parameters. In a real optical fiber transmission system, fluctuations in the frequency of the laser cause much faster speckle movement and this is the cause of high frequency modal noise (also called the ac-modal noise) [195]. In Ref. [34], it has been shown that this form of modal noise is proportional to the square of the normalized fluctuations described by (3.33). Since the normalized fluctuations also determine the value of modal distortion, we expect the ac-modal noise to behave in a similar manner to modal distortion. Consequently, only results for the dc-modal noise and modal distortion have been presented.

For coherent illumination, the modal noise and distortions for a high mode volume fiber are found to be lower compared to those due to a fiber with fewer modes, because the number of speckles are proportional to the number of modes, resulting in a finer speckle pattern [27]. The larger delay between the neighboring modes (in the β-space) in a low mode volume fiber as opposed to a high V one, is of no advantage in avoiding interference, since the delay, however large it may be, will always be small compared to the source coherence time

($\tau_c \to \infty$). For partially coherent excitation however, after a certain τ_{rms}/τ_c value (the value varies with the type of misalignment), a fiber that supports fewer modes may exhibit less modal noise (as compared to a high V fiber) if the intermodal delay exceeds the source coherence time.

For realistic splice loss values ($\leq$ 2 dB) it is found that the modal noise and distortion corresponding to the uniform power distribution are higher than those for a steady state assumption. For large splice losses (> 2 dB), a steady state distribution yields an inferior signal-to-noise ratio since the lower order modes become more susceptible to the mode selective loss mechanism and consequently yield large interference coefficients. This fact has been observed for all kinds of connector misalignments. Thus, the noise and distortion intrinsically depend on the modal power distribution through the power loss, and also exhibit an extrinsic dependence which is a function of the fluctuations in the power loss. When the dc-SNR results of the e.m. theory employing a uniform power distribution are compared with those obtained from the speckle theory, it is seen that speckle theory yields a much larger (by an order of magnitude at a splice loss of 0.5 dB) fluctuation of the coupling efficiency for low splice losses ($\leq$ 1 dB), thus overestimating the magnitude of modal noise. Furthermore, for partially coherent excitation, speckle theory is unable to predict the improvemen: in the dc-SNR analytically, if the effect of speckle contrast at the endface of the upstream fiber is not taken into account [176].

Our analysis has also shown that, for a coherent source with a given loss and V number, the ac-modal noise and distortion due to longitudinal misalignments are slightly higher than those due to either axial or angular offsets. This property is most easily understood if one considers separating two fiber ends until only one speckle of the far-field pattern falls on the core of the second fiber. A small wavelength shift can cause a large change in the interference pattern such that a dark region is coincident with the fiber core, resulting in 100 % amplitude modulation. For partially coherent sources, the noise and distortion performance both improve significantly for longitudinal misalignments (dc-SNR improves by an order of magnitude when $\tau_{rms}/\tau_c = 5$, as compared to coherent illumination, gap loss=1 dB) and in fact excel those due to axial offsets and tilt. This is due to the fact that with a reduced speckle contrast the far-field pattern at a gap will have a smooth illumination so that the chances of the fiber core totally missing out individual speckles are smaller.

The modal noise for the case of microbending is evaluated by adding up the noise contribution from all fiber imperfections present in the fiber transmission line. The imperfections are due to bumps in the fiber and are assumed to be uncorrelated. The modal noise per bump increases as the square of the microbending loss due to it. Therefore, the noise due to the whole fiber increases as the square of the microbending loss per unit length. Also, the noise increases linearly with the total fiber length L. Hence, if there are a large number of small amplitude bumps (of height =15 nm) [101] so that the mean microbending loss per bump is small, then the associated noise is smaller compared with that generated by a few large amplitude bumps (of height = 1μm). Keeping the loss constant, if the number of bumps is increased by a factor of 10, then the modal noise improves by an order of magnitude and the modal distortion decreases by 10 dB. Worst case modal noise and distortion occur if a single bump generates all the mode selective loss; in this case, the bump behaves like a splice.

This study also suggests that if only microbending loss is considered, the drop in the modal noise values for partially coherent sources is not quite as great (as it was for the connector), because interference between modes of the adjacent mode groups of the highest order are considered in the power diffusion model. The validity of the power diffusion model is established by the fact that only a narrow range of mechanical 'frequencies' contribute to the microbending loss [146]. In this approximation, the dc-SNR at $\tau_{rms}/\tau_c = 20$ increases by 7.3 % and 6.8 % for fiber length L=1 km and L=10 km respectively (V=21), as compared to that for coherent illumination.

When the length dependence of microbending is investigated, it is seen that for quite low and realistic values of the microbending losses ($\leqslant$ 0.5 dB/km), the modal noise in long fiber links is found to be totally unacceptable (dc-SNR=80 in a 20 km link for a coherent source, V=21) for either digital or analog transmission. Hence, if a single longitudinal mode laser diode is used with a sufficiently high coherence time ($\tau_c \approx \tau_{rms}$), the maximum link length will no longer be limited by power loss or bandwidth, but by modal noise. This problem could be alleviated in digital systems by pulsing the laser from below threshold where it has a broad spectrum and emits in many longitudinal modes [27], the pulse duration must not be long enough for the laser to settle back into the single longitudinal mode operation.

The amount of modal distortion in analog systems is also found to rise to high values as a result of microbending loss. In the example just considered (L=20 km, loss= 0.5

dB/km, V=21), the theoretical value of the second harmonic distortion reaches $\simeq$ -40 dB when τ_{rms} =1 nS/km, τ_c =1 nS, and Ω_m =10^{6}rad/sec. The accuracy of our predictions is borne out by the experimental investigations of Stubkjaer [140], who measured a relative second harmonic distortion of -20 dB, using a 1 km long graded-index fiber (without splices). Taking the values of his experimental parameters, we have shown that such a high distortion level is possible if the microbending loss is large (= 3 dB) and the total number of imperfections small (1 bump/m.). The experimentally observed dependence of this excess distortion, on the modulation index and the number of longitudinal modes of the laser diode, have been well explained on the basis of our theory.

In conclusion, we can say that this thesis has attempted to quantify the mode selective loss, noise and nonlinear distortion due to fiber connectors/splices and microbending by deliberately exploring a wide range of source and fiber conditions. For the first time, the power loss, modal noise and distortion due to a longitudinal gap and tilt between multimode parabolic-index fibers are investigated using a steady state power distribution. Also, an electromagnetic treatment of microbending induced modal noise was undertaken for the first time. The study indicates that modal noise and distortion in multimode fiber splices can be reduced substantially by transmitting at long wavelengths (low mode volume) and by using a partially coherent laser emitting in many longitudinal modes. The optimum transmitting condition is a partially coherent source with $\tau_c \lesssim$ 100 ps (i.e., spectral width for a single lasing mode $\cong$ 0.05 nm); a bandwidth of 1 GHz-km is realizable in this case without any significant modal noise (random level fluctuations $\lesssim$ 0.2 % for 1 dB connector loss and a singlemode source). The modal noise value just quoted (i.e., 0.2 %), is an order of magnitude smaller than that reported in Ref. [7]. Furthermore, at long wavelength operation (e.g., 1.3 μm), the material dispersion is negligible ($\lesssim$ 1 ps/km for a spectral width of 0.05 nm) so that mode partition noise is small [10]. By increasing the number of longitudinal modes of emission (no extra mode partition noise is incurred as a result of this since the material dispersion is almost vanishing), modal noise penalty can be further reduced.

Our analysis has shown that the magnitude of modal noise drops off very rapidly with decreasing splice losses; thus, low-loss ($\lesssim$ 0.2 dB) fusion splices are expected to improve the noise performance by orders of magnitude (SNR improves by 3 orders of magnitude for 0.2 dB loss as compared to 1 dB loss, coherent case) over their demountable connector counterparts.

Similarly, the use of a POM (polyoxymethylene) loose-jacket fiber (multimode) that exhibits little or no microbending loss over a temperature range of -60° to 80°C [134] can alleviate the modal noise problem due to microbending in multimode systems. Furthermore, modal noise reduction will also be accomplished by any mechanism which helps the fiber attain the steady state conditions before a splice. By showing that the modal noise potential can be estimated (to an order of magnitude) from the connector loss alone and/or the microbending loss, this study has simplified the system designer's task, who often has very little knowledge about the statistics of microbending, or about the type of geometrical misalignments present in a connector.

It has been proposed [27] that a polarization maintaining single mode fiber should totally overcome the modal noise problem. This suggestion may be valid for the modal noise that is generated by connector misalignments. However, since single mode fibers are more susceptible to microbending loss than multimode ones [185], polarization mode coupling in such fibers will give rise to polarization modal noise. To our knowledge, POM loose-jacketing on singlemode fibers has not been tried so far (in order to eliminate microbending effects). More detailed study is needed in this area if an accurate characterization of the noise and the nonlinear distortion behavior of single mode fiber systems is to be made.

REFERENCES

[1] K.C.Kao, G.A.Hockham, "Dielectric-fibre surface waveguides for optical frequencies," *Proc. IEE (GB)*, Vol. 113, No. 7, pp. 1151-1158, July 1966.

[2] A.G.Chynoweth, S.E.Miller, "Evolution of optical communications," in *Optical Fiber Telecommunications*, Academic Press, New York, pp. 13, 1979.

[3] F.P.Kapron, D.B.Keck, R.D.Maurer, "Radiation losses in glass optical waveguides," *Appl. Phys. Lett.*, Vol. 17, pp. 423-425, Nov. 1970.

[4] D.A.Duke, "The fiber-optics revolution spreads," *Telecommunications*, Vol. 16, No. 13, p. 18, Dec. 1982.

[5] J.R.Kanely, "Fiber optics in telecommunications," *Telecommunications*, Vol. 16, No. 13, p. 23, Dec. 1982.

[6] J.S.Cook, O.I.Szentesi, "North American field trials and early applications in telephony," *IEEE J. Sel. Commun.*, Vol. SAC-1, No. 3, pp. 393-397, Apr. 1983.

[7] G.Mogensen, "Wide-band optical fiber local distribution systems," *J. Opt. and Quantum Electron.*, Vol. 12, pp. 353-381, 1980.

[8] S.Personick, "Photodetectors for fiber systems," in *Fundamentals of Optical Fiber Communications*, M.Barnoski Ed., Academic Press, Inc., New York, 1976.

[9] G.Arnold, K.Petermann, "Noise sources in optical fiber communication systems," *Conf. on Lasers and Electro-Optical Systems*, San Diego, Invited paper TUAA1, p. 6, Feb. 1980.

[10] Y.Okano, K.Nakagawa, T.Ito, "Laser mode partition noise evaluation for optical fiber transmission," *IEEE Trans. Comm.*, Vol. Com-28, pp. 238-243, 1980.

[11] K.Iwashita, K.Nakagawa, "Mode partition noise characteristics in high-speed modulated laser diodes," *IEEE J. Quantum Electron.*, Vol. QE-18, No. 12, pp. 2000-2004, Dec. 1982.

[12] K.Ogawa, R.S.Vodhanel, "Effects of optical injection locking on mode partition noise," *Tech. Digest of Fourth Int. Conf. Integrated Opt. and Opt. Fiber Commun.*, Tokyo, pp. 202-203, June, 1983.

[13] A.Dandridge, R.O.Miles, "Spectral characteristics of semiconductor laser diodes coupled to optical fibers," *Electron. Lett.*, Vol. 17, No. 7, pp. 273-274, April 1981.

[14] T.Kanada, K.Nawata, "Injection laser characteristics due to reflected optical power," *IEEE J. Quantum Electron.*, Vol. QE-15, pp. 559-565, July 1979.

[15] D.W.Bechtle, S.A.Siegel, "Microwave- frequency optical links," *Laser Focus*, pp. 111-115, Jan. 1983.

[16] K.Kikushima, O.Hirota, M.Shindo, V.Stoykov, Y.Suematsu, "Properties of harmonic distortion of laser diodes with reflected waves," *J. Opt. Commun.*, Vol. 3, pp. 129-132, 1982.

[17] G.Arnold, "Influence of optical feedback on the noise behaviour of injection lasers," *Proc. 7th Eur. Conf. on Optical Commun.*, Copenhagen, pp. 10.4-1 to 10.4-4, Sept. 1981.

[18] Y.C.Chen, "Noise characteristics of semiconductor laser diodes coupled to short optical fibers," *Appl. Phys. Lett.*, Vol. 37, No. 7, pp. 587-589, 1980.

[19] D.Kato, "Suppression of light feedback from an optical fiber into a diode laser," *Opt. Commun.*, Vol. 26, No. 3, pp. 335-338, 1978.

[20] T.Kanada, K.Nawata, "Coupling characteristics of a laser diode and a graded-index fiber," in *Nat. Conf. Rec. 842*, Inst. Elec. Commun. Eng. Japan, 1978.

[21] O.Hirota, Y.Suematsu, "Noise properties of injection lasers due to reflected waves," *IEEE J. Quantum Electron.*, Vol. QE-15, pp. 142-149, March 1979.

[22] L.Goldberg, A.Dandridge, R.O.Miles, T.G.Giallorenzi, J.F.Weller, "Noise characteristics in line-narrowed semiconductor lasers with optical feedback," *Electron. Lett.*, Vol. 17, No. 19, pp. 677-678, Sept. 1981.

[23] A.Dandridge, *private communication*

[24] W.Albrecht, C.Baack, G.Elze, B.Enning, G.Heydt, K.Peters, G.Walf, G.Wenke, "2.24 Gbit/s optical transmission at 0.85 μm wavelength," *Electron. Lett.*, Vol. 17, No. 18, pp. 664-666, Sept. 1981.

[25] C.Baack, G.Elze, G.Grobkopf, F.Kraus, W.Krick, L.Kuller, "Analog optical transmission of 26 t.v. channels," *Electron. Lett.*, Vol. 15, pp. 300-301, 1979.

[26] R.E.Epworth, "The phenomenon of modal noise in analogue and digital optical fiber systems," *Proc. 4th Eur. Conf. on Optical Communication*, Genoa, pp. 492-501, Sept. 1978.

[27] R.E.Epworth, "Modal noise- causes and cures," *Laser Focus*, Vol. 17, pp. 109-115, Sept. 1981.

[28] H.Olesen, E.Nicolaisen, M.Danielsen, "Quantitative experimental results on modal distortion and comparison with theory based on AM-FM conversion," *Proc. 6th Eur. Conf. Opt. Commun.*, York, pp. 84-87, Sept. 1980.

[29] C.P.Sandbank, ed., *"Optical Fiber Communication Systems,"* John Wiley & Sons, New York, pp. 264-, 1980.

[30] E.G.Rawson, J.W.Goodman, R.E.Norton, "Experimental and analytical study of modal noise in optical fibers," *Proc. 6th Eur. Conf. on Optical Communication*, York, pp. 72-75, Sept. 1980.

[31] C.Baack, G.Elze, B.Enning, G.Walf, "Modal noise and optical feedback in high-speed optical systems at 0.85 μm," *Electron. Lett.*, Vol. 16, pp. 592-593, July 1980.

[32] K.Sato, K.Asatani, "Analogue baseband TV transmission experiments using semiconductor laser diodes," *Electron. Lett.*, Vol. 15, pp. 794-795, Nov. 1979.

[33] R.E.Epworth, "The measurement of static and dynamic coherence phenomena using a michelson interferometer," *Proc. 5th Eur. Conf. on Optical Communication*, Amsterdam, Sept. 1979.

[34] K.Petermann, "Nonlinear distortions and noise in optical communication systems due to fiber connectors," *IEEE J. Quantum Electron.*, Vol. QE-16, pp. 761-770, July 1980.

[35] C.Baack, G.Elze, "Problems in optical broad-band transmission systems," *National Telecomm. Conf.*, Houston, 1980.

[36] K.Petermann, "Wavelength-dependent transmission at fiber connectors,"*Electron. Lett.*, Vol. 15, pp. 706-708, Oct. 25, 1979.

[37] K.Petermann, "Nonlinear distortions due to fiber connectors," *Proc. 6th Eur. Conf. Opt. Comm.*, York, pp. 80-83, Sept. 1980.

[38] K.Petermann, "Transmission characteristics of a single-mode fiber transmission line with polarization coupling," *Proc. 7th Eur. Conf. on Opt. Comm.*, Copenhagen, pp. 3.2-1 to 3.2-4, Sept. 1981.

[39] H.Olesen, "Dependence of modal noise on source coherence and fiber length," *Electron. Lett.*, Vol. 16, pp. 217-218, March 1980.

[40] H.Olesen, E.Nicolaisen, "Source wavelength instability and its consequence for dispersion measurements and interference noise in optical fibers, " *Proc. 7th Eur. Conf. on Opt. Comm.*, Copenhagen, pp. 4.1-1 to 4.1-4, Sept. 1981.

[41] L.Jintong, Y. Peida, "Modal noise and effect of source spectrum in multimode fiber system," *Tech. Digest of Fourth Int. Conf. Integrated Opt. and Opt. Fiber Commun.*, Tokyo, pp. 30-31, June, 1983.

[42] C.Pask, "Analysis of optical fiber connectors and modal noise generation," *Proc. Inst. Elec. Eng.*, Part H, Vol. 127, pp. 282-286, Oct. 1980.

[43] B.Culshaw, "Minimisation of modal noise in optical-fiber connectors," *Electron Lett.*, Vol. 15, pp. 529-531, July 1979.

[44] S.Heckmann, "Modal noise in single-mode fibers," *Optics Lett.*, Vol. 6, No. 4, pp. 201-203, April 1981.

[45] S.Heckmann, "Modal noise in single-mode fibers operated slightly above cutoff," *Electron. Lett.*, Vol. 17, No. 14, pp. 499-500, July 1981.

[46] B.Daino, G.De Marchis, S.Piazzolla, "Analysis and measurement of modal noise in an optical fiber," *Electron. Lett.*, Vol. 15, pp. 755-756, 1979.

[47] G.De Marchis, S.Piazzolla, B.Daino, "Modal noise in optical fibers," *Proc. 7th European Conf. Opt. Commun.*, Copenghagen, pp. 76-79, 1981.

[48] D.R.Hjelme, A.R.Mickelson, "Microbending and modal noise," *Tech. Digest of Fourth Int. Conf. Integrated Opt. and Opt. Fiber Commun.*, Tokyo, pp. 400-401, June, 1983.

[49] K.O.Hill, Y.Tremblay, B.S.Kawasaki, "Modal noise in multimode fiber links: theory and experiment," *Opt. Lett.*, Vol. 5, No. 6, pp. 270-272, June 1980.

[50] Y.Tremblay, B.S.Kawasaki, K.O.Hill, "Modal noise in optical fibers: open and closed speckle pattern regimes," *Appl. Opt.*, Vol. 20, p. 1652, 1981.

[51] T.Kanada, K.Aoyama, "Proposal of a new modal noise estimation method in optical fiber transmission systems," *Tech. Digest of Fourth Int. Conf. Integrated Opt. and Opt. Fiber Commun.*, Tokyo, pp. 32-33, June, 1983.

[52] E.G.Rawson, J.W.Goodman, R.E.Norton, "Frequency dependence of modal noise in multimode optical fibers," *J. Opt. Soc. Am.*, Vol. 70, No. 8, pp. 968-976, Aug. 1980.

[53] J.W.Goodman, E.G.Rawson, "Statistics of modal noise in fibers: a case of constrained speckle," *Opt. Lett.*, Vol. 6, pp. 324-326, July 1981.

[54] E.G.Rawson, J.W.Goodman, "Modal noise in multimode optical fibers," SPIE Proc. 355, *Fiber-Optics: Short-Haul and Long-Haul Measurements and Applications*, San Diego, August, 1982.

[55] A.Weierholt, A.Mickelson, D.Thingbo, A.Berg, "Modal noise induced signal-to-noise ratios in optical fibers," *Technical Digest, Topical Meeting Opt. Fiber Commun.*, Phoneix, p. 70, 1982.

[56] K.Sato, K.Asatani, "Superimposed pulse modulation for fiber optic analogue video transmission using semiconductor laser diodes," *Electron. Lett.*, Vol. 16, pp. 538-540, July 1980.

[57] J.Vanderwall, J.Blackburn, "Suppression of some artifacts of modal noise in fiber-optic systems," *Optics Lett.*, Vol. 4, No. 9, pp. 295-296, Sept. 1979.

[58] J.Blackburn, *private communication*

[59] G.D.Khoe, C.H.F.Velzel, R.P.Brouwer, G.Kuyt, "Practical solution for modal noise problems in optical fiber transmission systems," *Proc. 6th Eur. Conf. on Opt. Comm.*, York, pp. 88-90, Sept. 1980.

[60] J.Saijonmaa, S.J.Halme, "Reduction of modal noise by using focused beam spot excitation," *Proc. 7th Eur. Conf. on Opt. Comm.*, Copenhagen, pp. 3.5-1 to 3.5-4, Sept. 1981.

[61] M.Young, "Geometrical theory of multimode optical fiber-to-fiber connectors," *Opt. Commun.*, Vol. 7, pp. 253-255, 1973.

[62] P.Di Vita, R.Vannucci, "Geometrical theory of coupling errors in dielectric optical waveguides," *Opt. Commun.*, Vol. 14, pp. 139-143, 1975.

[63] D.Gloge, "Offset and tilt loss in optical fiber splices," *B.S.T.J.*, Vol. 55, pp. 905-916, 1976

[64] C.M.Miller, "Transmission vs transverse offset for parabolic-profile fiber splices with unequal core diameters," *B.S.T.J.*, Vol. 55, pp. 917-927, 1976.

[65] C.M.Miller, S.C.Mettler, "A loss model for parabolic-profile splices," *B.S.T.J.*, Vol. 57, pp. 3167-3180, 1978.

[66] S.C.Mettler, "A general characterization of splice loss for multimode optical fibers," *B.S.T.J.*, Vol. 58, pp. 2163-2182, 1979.

[67] F.L.Thiel, R.M.Hawk, "Optical waveguide cable connection," *Appl. Opt.*, Vol. 15, pp. 2785-2791, 1976.

[68] E.G.Neumann, W.Weidhaas, "Loss due to radial offsets in dielectric optical waveguides with arbitrary index profiles," *Archiv Elektron. and Ubertragungstech*, Vol. 30, 1976.

[69] D.Opielka, D.Rittich, "Transmission loss caused by an angular misalignment between two multimode fibers with arbitrary profile exponents," *Appl. Opt.*, Vol. 22, No. 7, pp. 991-994, Apr. 1983.

[70] H.Kogelnik, "Coupling and conversion coefficients for optical modes," *Proc. Symposium on Quasi-Optics*, Polytechnic Press, Brooklyn, 1964.

[71] D.Marcuse, "Excitation of parabolic-index fibers with incoherent sources," *B.S.T.J.*, Vol. 54, pp. 1507-1529, Nov. 1975.

[72] D.Marcuse, "Loss analysis of single-mode fiber splices," *B.S.T.J.*, Vol. 56, pp. 703-718, May-June 1977.

[73] A.Cardama, E.T.Kornhauser, "Modal analysis of coupling problems in optical fibers," *IEEE Trans. MTT*, Vol. MTT-23, pp. 162-169, 1973.

[74] J.Guttmann, O.Krumpholz, "Theoretische und experimentelle Untersuchungen zur Verkopplungzweier Glasfaser-Lichtwellenleiter," Wiss. Ber. *AEG-Telefunken* Vol. 46, pp. 8-15, 1973.

[75] W.A.Gambling, H.Matsumura, R.Ragdale, "Joint loss in single-mode fibers," *Electron. Lett.*, Vol. 14, pp. 491-493, 1978.

[76] S.I.Hosain, A.Sharma, A.K.Ghatak, "Splice-loss evaluation for single-mode graded-index fibers," *Appl. Opt.*, Vol. 21, No. 15, pp. 2716-2720, Aug. 1982.

[77] R.E.Wagner, W.J.Tomlinson, "Coupling efficiency of optics in single-mode fiber components," *Appl. Opt.*, Vol. 21, No. 15, p. 2671, Aug. 1982.

[78] J.S.Cook, W.L.Mannel, R.J.Grow, "Effects of misalignment on coupling efficiency of singlemode fiber butt joints," *Bell Sys. Tech. J.*, Vol. 52, p. 1439, 1973.

[79] Y.Murakami, I.Hatakeyama, H.Tsuchiya, "Normalized frequency dependence of splice losses in single-mode optical fibers," *Electron. Lett.*, Vol. 14, pp. 277-278, 1978.

[80] D.L.Bisbee, "Measurements of loss due to offsets and end separations of optical fibers," *Bell Sys. Tech. J.*, Vol. 50, pp. 3159-3167, Dec. 1971.

[81] H.Tokiwa, K.Mochizuki, H.Wakabayashi, "Joint characteristics between polarisation-maintaining single-mode fibers," *Electron. Lett.*, Vol. 19, pp. 485-486, June 1983.

[82] A.H.Cherin, P.J.Rich, "Measurement of loss and output numerical aperture of optical fiber splices," *Appl. Opt.*, Vol. 17, No. 4, pp. 642-645, Feb. 1978.

[83] R.B.Kummer, A.F.Judy, A.H.Cherin, "Field and laboratory transmission and OTDR splice loss measurements of multimode optical fibers," (invited) *NBS Standards Digest*, pp. 109-121.

[84] A.H.Cherin, in *"An Introduction to Optical Fibers,"* McGraw-Hill Book Co., New York, pp. 260-262, 1983.

[85] R.B.Kummer, "Precise characterization of long nonidentical-fiber splice loss effects," *Proc. 6th Eur. Conf. on Opt. Comm.*, York, pp. 302-305, Sept. 1980.

[86] R.B.Kummer, "Lightguide splice loss - effects of launch beam numerical aperture," *Bell Sys. Tech. J.*, Vol. 59, p. 44, March 1980.

[87] I.A.White, S.C.Mettler, "Modal analysis of loss and mode mixing in multimode parabolic index splices, " *Bell Sys. Tech. J.*, Vol. 62, pp. 1189-1207, May-June 1983.

[88] K.Kitayama, M.Ohashi, S.Seikai, "Mode conversion at splices in multimode graded-index fibers," *IEEE J. Quantum Electron.*, Vol. QE-16, No. 9, pp. 971-978, Sept. 1980.

[89] P.Meron, E.Marom, "Mode splitting at splices of GRIN fibers," *Appl. Opt.*, Vol. 22, No. 3, pp. 446-454, Feb. 1983.

[90] G.Coppa, P.Di Vita, U.Rossi, "Joint-loss dependence on mismatch parameters in graded-index optical fibers," *Electron. Lett.*, Vol. 19, No. 17, pp. 654-656, Aug. 1983.

[91] J.Sakai, T.Kimura, "Splice loss evaluation for optical fibers with arbitrary-index profile," *Appl. Opt.*, Vol. 17, No. 17, pp. 2848-2853, Sept. 1978.

[92] V.Rizzoli, C.G.Someda, "Mutual influence among imperfect joints in multimode-fiber link," *Electron. Lett.*, Vol. 17, No. 24, pp. 906-907, Nov. 1981.

[93] N.Kashima, "Splice loss and mode conversion in a multimode fiber," *Appl. Opt.*, Vol. 19, No. 15, pp. 2597-2601, Aug. 1980.

[94] N.Kashima, "Transmission characteristics of splices in graded-index multimode fibers," *Appl. Opt.*, Vol. 20, No. 22, pp. 3859-3866, Nov. 1981.

[95] Y.Daido, E.Miyauchi, T.Iwama, T.Otsuka, "Determination of modal power distribution in graded-index optical waveguides from near-field patterns and its application to differential mode attenuation measurement," *Appl. Opt.*, Vol. 18, No. 13, pp. 2207-2212, July 1979.

[96] H.Shigesawa, T.Matsuo, K. Takiyama,"Measurements of excitation condition and quantitative mode analysis in optical fibers," *IEEE Trans. MTT*, Vol. MTT-26, No. 12, pp. 992-997, Dec. 1978.

[97] F.Esposto, E.Vezzoni, "Connecting and splicing techniques," in *Optical Fibre Communication*, Technical Staff of CSELT Ed., McGraw-Hill Book Co., 1981.

[98] D.T.Young, "Model for relating coupled power equations to coupled amplitude equations," *Bell Sys. Tech. J.*, Vol. 42, pp. 2761-2764, 1963.

[99] R.Bergeest, H.-G.Unger, "Optische Wellen in Hohlleitern," *Arch. elekt. Ubertr.*, Vol. 23, pp. 529-538, 1969.

[100] D.Marcuse, "Derivation of coupled power equations," *Bell Sys. Tech. J.*, Vol. 51, pp. 229-237, Jan. 1972.

[101] D.Gloge, "Optical power flow in multimode fibers," *Bell Sys. Tech. J.*, Vol. 51, pp. 1767-1782, Oct. 1972.

[102] D.Marcuse, "Losses and impulse response of a parabolic index fiber with random bends," *Bell Sys. Tech. J.*, Vol. 52, pp. 1423-1437, Oct. 1973.

[103] R.Olshansky, "Mode coupling effects in graded-index optical fibers," *Appl. Optics*, Vol. 14, pp. 935-945, 1975.

[104] D.Marcuse, "Fluctuations of the power of coupled modes," *Bell Sys. Tech. J.*, Vol. 51, pp. 1793-1800, Oct. 1972.

[105] R.Olshansky, "Distortion losses in cabled optical fibers," *Appl. Optics*, Vol. 14, pp. 20-21, Jan. 1975.

[106] R.Olshansky,"Microbending losses in singlemode fibers," *Proc. 2nd Eur. Conf. Optical Fiber Transmission*, Paris, pp. 101-103, Sept. 1976.

[107] R.Olshansky, D.A.Nolan, "Mode-dependent attenuation of optical fibers: excess loss," *Appl. Optics*, Vol. 15, pp. 1045-1047, Apr. 1976.

[108] R.Olshansky, D.A.Nolan, "Mode dependent attenuation in parabolic optical fibers," *Appl. Optics*, Vol. 16, pp. 1639-1641, June 1977.

[109] W.A.Gambling, H.Matsumura, "Propagation in radially inhomogeneous singlemode fibers," *Opt. and Quantum Electron.*, Vol. 10, pp. 31-40, 1978.

[110] K.Petermann, "Loss and pulse distortion in fundamental mode transmission through randomly bent fibers," *Proc. Conf. Optical Fiber Transmission*, Williamsburg, VA, pp. TuD6 1-4, 1977.

[111] K.Petermann, "Microbending loss in monomode fibers," *Electron. Lett.*, Vol. 12, pp. 107-109, 1976.

[112] K.Petermann, H.Storm, "Microbending loss in single-mode W-fibers," *Electron. Lett.*, Vol. 12, pp. 537-538, Sept. 1976.

[113] K.Petermann, "Fundamental mode microbending loss in graded-index and W fibers," *Opt. and Quantum Electron.*, Vol. 9, pp. 167-175, 1977.

[114] K.Furuya, Y.Suematsu, "Random bend losses in single-mode optical fiber cables: power-spectrum estimation from spectral losses," *Electron. Lett.*, Vol. 14, No. 19, Sept. 1978.

[115] K.J.Blow, N.J.Doran, S.Hornung, "Power spectrum of microbends in monomode optical fibers," *Electron. Lett.*, Vol. 18, pp. 448-450, May 1982.

[116] P.Danielsen, "Simple power spectrum of microbendings in single-mode fibers," *Electron. Lett.*, Vol. 19, pp. 318-320, Apr. 1983.

[117] M.P.Varnham, D.N.Payne, R.D.Birch, E.J.Tarbox, "Bend behaviour of polarising optical fibers," *Electron. Lett.*, Vol. 19, pp. 679-680, Aug. 1983.

[118] L.Jeunhomme, J.P.Pocholle, "Experimetal determination of the radiation pattern of optical fibers," *Opt. Commun.*, Vol. 12, No. 1, pp. 89-92, Sept. 1974.

[119] L.Jeunhomme, J.P.Pocholle, "Angular dependence of the mode-coupling coefficient in a multimode optical fiber," *Electron. Lett.*, Vol. 11, No. 18, Sept. 1975.

[120] L.Jeunhomme, J.P.Pocholle, "Mode coupling in a multimode optical fiber with microbends," *Appl. Optics*, Vol. 14, pp. 2400-2405, Oct. 1975.

[121] D.Gloge, "Bending loss in multimode fibers with graded and ungraded core index," *Applied Optics*, Vol. 11, pp. 2506-2513, 1972.

[122] M.Rousseau, J.Arnaud, "Microbending loss of multimode square-law fibers: a ray theory," *Electron. Lett.*, Vol. 13, No. 9, pp. 265-267, Apr. 1977.

[123] J.D.Love, C.Pask, "Universal curves for power attenuation in ideal multimode fibers," *Electron. Lett.*, Vol. 12, No. 10, pp. 254-255, May 1976.

[124] A.W.Snyder, "Leaky-ray theory of optical waveguides of circular cross-section," *Appl. Phys.*, Vol. 4, pp. 273-298, 1974.

[125] C.Winkler, J.D.Love, A.K.Ghatak, "Power attenuation in bent parabolic-index slab and fiber waveguides," *Electron. Lett.*, Vol. 14, pp. 570-571, 1978.

[126] A.H.Cherin, E.J.Murphy, "Quasi-ray analysis of crosstalk between multimode optical fiber," *Bell Sys. Tech. J.*, Vol. 54, pp. 17-45, Jan. 1975.

[127] A.H.Cherin, E.J.Murphy, "An analysis of the effect of lossy coatings on the transmission energy in a multimode optical fiber," *Bell Sys. Tech. J.*, Vol. 54, pp. 1531-1546, Nov. 1975.

[128] J.H.Hannay, "Mode coupling in an elastically deformed optical fiber," *Electron. Lett.*, Vol. 12, pp. 173-174, 1976.

[129] Y.Katsuyama, Y.Mitsunaga, C.Tanaka, T.Waki, Y.Ishida, "Optical loss stability of a fiber cable under lateral force and optimum design of the coated fiber structure," *Appl. Optics*, Vol. 21, pp. 1337-1341, Apr. 1982.

[130] K.Tatekura, K.Itoh, T.Matsumoto, "Nylon buffering effects in multimode optical fibers," *Electron. Lett.*, Vol. 14, pp. 441-442, July 1978.

[131] D.Gloge, "Optical-fiber packaging and its influence on fiber straightness and loss," *Bell Sys. Tech. J.*, Vol. 54, pp. 245-262, 1975.

[132] W.B.Gardner, "Microbending loss in optical fibers," *Bell Sys. Tech. J.*, Vol. 54, pp. 457-465, Feb. 1975.

[133] M.J.Buckler, L.Wilson, F.P.Partus, "Optical fiber transmission properties before and after cable manufacture," *Proc. Conf. Optical Fiber Transmission*, Williamsburg, VA, paper WA1.1, 1977.

[134] F.Yamamoto, K.Nakagawa, Y.Shuto, S.Yamakawa, "Optical fiber jacketed with high-modulus low-linear-expansion-coefficient polymer," *Electron. Lett.*, Vol. 19, pp. 674-675, Aug. 1983.

[135] N.Kojima, Y.negishi, K.Iwabuchi, T.Yabuta, O.Kawata, K.Yamashita, K.Funaki, M.Inoue, "Sea trial of submarine optical fiber cable," Post deadline paper. *Proc. 6th Eur. Conf. on Opt. Comm.*, York, Sept. 1980.

[136] N.Yoshizawa, T.Yabuta, K.Noguchi, "Residual nylon-jacketed fiber shrinkage caused by cooling," *Electron. Lett.*, Vol. 19, pp. 411-412, May 1983.

[137] T.Tanifuji, M.Tokuda, "Amplitude fluctuation in laser signal transmitted through a long multimode fiber," *IEEE J. Quantum Electron.*, Vol. QE-17, No. 11, pp. 2228-2233, Nov. 1981.

[138] S.Piazzolla, G.De Marchis, B.Daino, "Signal fluctuations in an underground laid optical cable," Post deadline paper. *Proc. 6th Eur. Conf. on Opt. Comm.*, York, Sept. 1980.

[139] G.Zeidler, D.Schicketanz, "Influence of mode coupling on the noise properties of multimode-fiber systems," *Electron. Lett.*, Vol. 11, pp. 307-308, July 1975.

[140] K.Stubkjaer, "Distortion of light signals transmitted via multimode graded-index fibers," *Electron. Lett.*, Vol. 15, pp. 797-799, Nov. 1979.

[141] G.J.Meslener, "Dispersion-induced harmonic distortion in fiber systems using coherent light sources," *Technical Digest, Topical Meeting Opt. Fiber Commun.*, Phoneix, pp. 68-70, Apr. 1982.

[142] L.B.Felsen, "Rays, modes and beams in optical fiber waveguides," *J. Opt. and Quantum Electron.*, Vol. 9, pp. 189-195, 1977.

[143] D.Marcuse, *private communication*

[144] N.S.Kapany, *"Fiber Optics,"* Academic Press, New York, 1967.

[145] N.S.Kapany, J.J.Burke, *"Optical Waveguides,"* Academic Press, New York, 1972.

[146] D.Marcuse, *"Theory of Dielectric Optical Waveguides,"* Academic Press, New York, 1974.

[147] J.Arnaud, *"Beam and Fiber Optics,"* Academic Press, New York, 1976.

[148] R.L.Gallawa, *"A User's Manual for Optical Waveguide Communications,"* U.S Dept. of Commerce, 1977.

[149] H.Unger, *"Planar Optical Waveguides and Fibers,"* Oxford University Press, 1977.

[150] Howes, Morgan, Ed. *"Optical Fiber Communications,"* John Wiley & Sons, New York, 1979.

[151] A.B.Sharma, S.J.Halme, M.M.Butusov, *"Optical Fiber Systems and Their Components,"* Springer-Verlag, New York, 1981.

[152] C.K.Kao, *"Optical Fiber Systems - technology, design, and applications,"* McGraw-Hill Book Co., New York, 1982.

[153] D.Marcuse, *"Light Transmission Optics,"* Van Nostrand Reinhold, New York, 1982.

[154] S.E.Miller, E.A.J.Marcatilli, T.Li, "Research toward optical-fiber transmission systems," *Proc. IEEE*, Vol. 61, pp. 1703-1751, Dec. 1973.

[155] D.Gloge, "Propagation effects in optical fibers," *IEEE Trans. MTT*, Vol. MTT-23, No.1, pp. 106-120, January 1975.

[156] T.G.Giallorenzi, "Optical communications research and technology : fiber optics," *Proc. IEEE*, Vol. 66, pp. 744-780, July 1978.

[157] See Ref. [149], pp. 466-471.

[158] D.Gloge, "Weakly guiding fibers," *Appl. Opt.*, Vol. 10, No. 10, pp. 2252-2258, Oct. 1971.

[159] R.Olshansky, D.B.Keck, "Pulse broadening in graded-index optical fibers," *Appl. Opt.*, Vol. 15, No. 2, pp. 483-491, Feb. 1976.

[160] R.L.Gallawa, "On the definition of fiber numerical aperture," *NBS Handbook 140.*

[161] M.Nakamura, K.Aiki, N.Chinone, R.Ito, J.Umeda, "Longitudinal-mode behaviours of mode-stabilized AlGaAs injection lasers," *J. Appl. Phys.*, Vol. 49, pp. 4644-4648, Sept. 1978.

[162] B.Crosignani, B.Daino, P.Di Porto, "Interference of mode patterns in optical fibers," *Optics Comm.*, Vol. 11, No. 2, pp. 178-179, June 1974.

[163] B.Crosignani, P.Di Porto, "Speckle-pattern visibility of light transmitted through a multimode optical fiber," *J. Opt. Soc. Am.*, Vol. 66, No. 11, pp. 1312-1313, Nov. 1976.

[164] E.G.Rawson, J.W.Goodman, "Modal noise in multimode fibers: polarization effects," *Proc. CLEO*, Washington, p. 72, June 1981.

[165] K.Kobayashi, "A new method for evaluation of carrier density dependence of refractive-index in semiconductor lasers," *Digest of Technical Group on Optical Quantum Electronics of IECE of Japan*, OQE75-48, 1975.

[166] P.Melman, W.J.Carlsen, "Interferometric measurement of temporal coherence and time-varying longitudinal-mode wavelengths in GaAs diode lasers," *Proc. CLEO*, Washington, p. 72, June 1981.

[167] M.Eve, "Near field and far field power distributions in a multimode graded fiber," *J. Opt. and Quantum Electron.*, Vol. 9, pp. 459-464, 1977.

[168] S.Piazzolla, G.De Marchis, "Analytical relations between modal power distribution and near-field intensity in graded-index fibers," *Electron. Lett.*, Vol. 15, pp. 721-722, 1979.

[169] K.Petermann, G.Arnold, "Noise and distortion characteristics of semiconductor lasers in optical fiber communication systems," (invited paper) *IEEE J. Quantum Electron.*, Vol. QE-18, No. 4, pp. 543-555, Apr. 1982.

[170] I.S.Gradshteyn, I.M.Ryzhik, *"Table of Integrals Series and Products,"* Academic Press, New York, 1980.

[171] *"Operating instruction for GO-ANA transmitter,"* General Optronics Corp., New Jersey, 1981.

[172] R.E.Epworth, *private communication*

[173] H.Kuwahara, M.Goto, "Generation of harmonic distortion at fiber connectors," *Electron. Lett.*, Vol. 17, pp. 626-627, Sept. 1981.

[174] R.E.Wagner, C.R.Sandahl, "Interference effects in optical fiber connections," *Appl. Opt.*, Vol. 21, pp. 1381-1385, 1982.

[175] S. Das, P.A. Goud, C.G. Englefield, "Modal analysis of loss due to a longitudinal gap between two parabolic-index multimode fibers," in SPIE Proc. 380, *Los Alamos Conference on Optics*, Santa Fe, NM, April 11-15, 1983.

[176] S. Das, C.G. Englefield, P.A. Goud, "Modal noise and distortion due to a longitudinal gap between two multimode fibers," to be published in *Appl. Opt.*

[177] S.Kobayashi, Y.Yamamoto, T.Kimura, "Modulation frequency characteristics of directly optical frequency modulated AlGaAs semiconductor laser," *Electron. Lett.*, Vol. 17, No. 10, pp. 350-351, May 1981.

[178] R.Olshansky, M.G.Blankenship, D.B.Keck, " Length-dependent attenuation measurements in graded-index fibers, " *Proc. 2nd Eur. Conf. Optical Fiber Transmission*, Paris, pp. 111-113, Sept. 1976.

[179] D.Marcuse, H.M.Presby, "Mode coupling in an optical fiber with core distortions," *Bell Sys. Tech. J.*, Vol. 54, pp. 3-15, Jan. 1975.

[180] D.Yevick, B.Stoltz, "Effect of mode coupling on the total pulse response of perturbed optical fibers," *Appl. Opt.*, Vol. 22, No. 7, p. 1010, Apr. 1983.

[181] J.Arnaud, "Use of principal mode numbers in the theory of microbending," *Electron. Lett.*, Vol. 14, pp. 663-664, Sept. 1978.

[182] S.Kawakami, H.Tanji, "Evolution of power distribution in graded-index fibers," *Electron. Lett.*, Vol. 19, pp. 100-102, Feb. 1983.

[183] D.Marcuse, "Mode mixing with reduced losses in parabolic-index fibers," *Bell Sys. Tech. J.*, Vol. 55, pp. 777-802, July-Aug. 1976.

[184] E.G.Rawson, "Measurement of angular distribution of light scattered from a glass fiber optical waveguide," *Appl. Opt.*, Vol. 11, pp. 2477-2481, 1972.

[185] D.Marcuse, "Microbending losses of single-mode, step-index and multimode, parabolic-index fibers," *Bell Sys. Tech. J.*, Vol. 55, pp. 937-955, Sept. 1976.

[186] M.D.Rourke, "Measurement of the insertion loss of a single microbend," *Opt. Lett.*, Vol. 6, No. 9, pp. 440-442, Sept. 1981.

[187] D.J.Eccleston, "Environmental testing of uv-cured acrylate coated fibers," *Corning Application Notes*, 1982.

[188] Y.Murakami, K.Ishihara, Y.Negishi, N.Kojima, "Microbending losses of P_2O_5-doped graded-index multimode fiber," *Electron. Lett.*, Vol. 18, No. 18, pp. 774-775, Sept. 1982.

[189] K.Stubkjaer, *private communication*

[190] K.Furuya, Y.Suematsu, H.Tokiwa, "Coupling length due to random bending in multimode optical fibers," *J. Opt. and Quantum Electron.*, Vol. 10, pp. 323-330, 1978.

[191] S.L.storozum, "Mode scrambling can enhance fiber-optic system performance," *Electronics*, pp. 163-166, Feb. 1981.

[192] N.Nager, "Glass sphere lenses for better coupling," *Photonics Spectra*, pp. 52-56, Sept. 1983.

[193] G.Lutes, "Optical fiber applications in the NASA Deep Space Network," *Laser Focus & Fiberoptic Technology*, pp. 115-121, Sept. 1982.

[194] G.Lutes, *private communication*

[195] R.E.Epworth, "Modal noise in real transmission systems, the problem of measurement and predictive modelling," *Tech. Digest of Fourth Int. Conf. Integrated Opt. and Opt. Fiber Commun.*, Tokyo, pp. 28-29, June, 1983.

[196] D.Marcuse, *private communication*

APPENDIX A1

Computer Program (Axial Offset)

```
C*****************************************************************
C THIS PROGRAM CALCULATES THE LOSS, MODAL NOISE AND DISTORTION
C DUE TO AXIAL OFFSET IN FIBER CONNECTORS
C*****************************************************************
C RAD=FIBER RADIUS (MICRONS)
C ALPHA=EXPONENT OF THE REFRACTIVE INDEX PROFILE
C REF1=REFRACTIVE INDEX OF THE CORE
C REF2=REFRACTIVE INDEX OF THE CLADDING
C DELTA= RELATIVE INDEX DIFFERENCE
C LFIB=FIBER LENGTH BEFORE THE CONNECTOR(MTRS.)
C V= NORMALIZED FREQUENCY OF THE FIBER
C MG= MAXIMUM MODE GROUP NUMBER OF FIBER
C N= NUMBER OF MODES OF FIBER FOR EACH POLARIZATION
C DELA= AXIAL SEPARATION (IN MICRONS)
C W= NORMALIZED MODAL POWER WEIGHTS
C W0=FUNDAMENTAL MODE RADIUS (MICRONS)
C TCOH=COHERENCE TIME OF THE SOURCE(NS)
C FREFL=FREQUENCY FLUCTUATION OF THE SOURCE (GHZ)
C CLIGHT=VELOCITY OF LIGHT(MTRS.)
C N=10 FOR V=9, WAVLN=3.6
C N=55 FOR V=21, WAVLN=1.55
C N=105 FOR V=29, WAVLN=1.1
C N=190 FOR V=39, WAVLN=.816
C*****************************************************************
      REAL COUPL(36100),TAU12(36100),W(190)
      REAL TAU(190,190),C(190,190),F(190,190),AUTO(190,190)
      REAL LOSS,LFIB
      INTEGER V,DELA,IER
C*****************************************************************
      V=39
      N=190
C*****************************************************************
C FIBER AND SOURCE PARAMETERS
C*****************************************************************
      RAD=25.
      ALPHA=2.2
      PI=3.1415927
      REF1=1.47214
      REF2=1.4585
      CLIGHT=3.E+8
      LFIB=.17E+3
      FREFL=2.E+9
      TCOH=.35E-10
C*****************************************************************
C CALCULATION OF BEAM WIDTH, MAX. MODE GR. NO., REL. INDEX DIFF.,
C FREQ. DEVIATION IN RADIANS
C*****************************************************************
      W0=RAD*SQRT(2./FLOAT(V))
      MG=(V-1)/2
      DELTA=(REF1-REF2)/REF1
      OMEGA=2*PI*FREFL
C*************************************************************
C CALCULATION OF COEFFICIENTS RELATING TO INDEX PROFILE
C*************************************************************
      A11=(ALPHA-2.)/(ALPHA+2.)
      A12=(2.*ALPHA)/(ALPHA+2.)
      A21=((3.*ALPHA)-2.)/(ALPHA+2.)
      A22=(4.*ALPHA)/(ALPHA+2.)
      DE2=(DELTA**2)/2.
C*****************************************************************
```

```
      WRITE(5,1)
    1 FORMAT('DELA',2X,'LOSS',4X,'SNR',10X,'DTR',5X,
     1'H2(DB)')
C*****************************************************************
C CALCULATION OF THE STEADY STATE MODAL POWER WEIGHTS NORMALIZED
C TO FUNDAMENTAL MODE GROUP POWER
C*****************************************************************
      IJ=1
      DO 77 I=1,MG
      DO 77 J=1,I
      X1=FLOAT(I)*SQRT(FLOAT(I))
      X2=FLOAT(MG+1-I)/FLOAT(MG)
      X3=SQRT(X2)
      FRAC=1./(X1*X3)
      W(IJ)=FRAC
      IJ=IJ+1
 77   CONTINUE
C*****************************************************************
C CALCULATION OF THE SUM OF ALL MODAL POWER WEIGHTS 'DIV'
C*****************************************************************
      DIV=0.
      DO 12 K=1,N
C REMOVE CONTROL CARD IN NEXT LINE IF UNIFORM DISTRIBUTION
C     W(K)=1.
      IF(K.EQ.1) GO TO 76
      IF(W(K).GT.W(K-1)) W(K)=W(K-1)
 76   DIV=DIV+W(K)
 12   CONTINUE
C*****************************************************************
C AXIAL OFFSET 'DELA' DO-LOOP
C*****************************************************************
      DO 83 DELA=17,17
      DX1=FLOAT(DELA)/(W0*SQRT(2.))
      DX2=((FLOAT(DELA)/W0)**2)/2.
      DX3=(FLOAT(DELA)/W0)**2
C*****************************************************************
C MODE-MODE COUPLING COEFFICIENT DO-LOOP
C*****************************************************************
      TRMSS=0.
      JK=1
      DO 10 MG2=1,MG
      DO 10 M22=1,MG2
      M2=M22-1
      N2=(MG2-M22)
      DO 10 MG1=1,MG
      DO 10 M11=1,MG1
      M1=M11-1
      N1=(MG1-M11)
C*****************************************************************
C CALCULATION OF INTER MODE DISPERSION TAU12(JK)
C*****************************************************************
          U2=FLOAT(MG2)
          U1=FLOAT(MG1)
          UMG=FLOAT(MG)
     T2=A11*DELTA*((U2/UMG)**A12)
    1+A21*DE2*((U2/UMG)**A22)
     T1=A11*DELTA*((U1/UMG)**A12)
    1+A21*DE2*((U1/UMG)**A22)
     T21=(REF1/CLIGHT)*(T2-T1)*LFIB
     TRMSS=TRMSS+(T21**2)
```

```
121           TAU12(JK)=T21
122     C*****************************************************************
123     C COUPLING ONLY WITH SAME 'N' (OFFSET IN X-DIRECTION)
124     C*****************************************************************
125           IF(N1.NE.N2)GO TO 50
126     C*****************************************************************
127           IF(M1.GT.M2)GO TO 70
128           MMM=M2-M1
129           CALL CALFAC(M1,FACM1)
130           CALL CALFAC(M2,FACM2)
131           E1=SQRT(FACM1/FACM2)
132           E2=SQRT(2.**MMM)
133           E3=EXP(-DX2)
134           E4=DX1**MMM
135           CALL ALAG(M1,MMM,DX3,E5)
136           RESL=E1*E2*E3*E4*E5
137           GO TO 52
138      70   MMM=M1-M2
139           CALL CALFAC(M2,FACM2)
140           CALL CALFAC(M1,FACM1)
141           E1=SQRT(FACM2/FACM1)
142           E2=SQRT(2.**MMM)
143           E3=EXP(-DX2)
144           E4=DX1**MMM
145           CALL ALAG(M2,MMM,DX3,E5)
146           RESL=(E1*E2*E3*E4*E5)*((-1.)**(M2-M1))
147           GO TO 52
148      50   RESL=0.
149      52   COUPL(JK)=RESL
150           JK=JK+1
151      10   CONTINUE
152     C*****************************************************************
153     C CONVERT THE COUPLING VECTOR COUPL(I) TO A COUPLING MATRIX C(I,J)
154     C*****************************************************************
155           KL=1
156           DO 655 III=1,N
157           DO 655 KKK=1,N
158           C(KKK,III)=COUPL(KL)
159      655  KL=KL+1
160     C*********************************************************
161     C FIND THE INTERFERENCE MATRIX F(I,J)
162     C*********************************************************
163           CALL VMULFP(C,C,N,N,N,N,N,F,N,IER)
164     C*********************************************************
165     C FIND THE ROOT MEAN SQUARE INTERMODAL DELAY 'TRMS'
166     C*********************************************************
167           TRMS=SQRT(TRMSS)/FLOAT(N)
168     C*********************************************************
169     C IF CALCULATIONS DESIRED FOR PARTIAL COHERENT SOURCES
170     C REMOVE CONTROL CARDS, TRMS/TCOH=0.2 TO 20, 15 VALUES
171     C USE ONLY ONE VALUE FOR DELA (E.G., 10 MICRONS)
172     C*********************************************************
173     C       DO 83 IH=1,15
174     C       IF(IH.LE.5) TCOH=TRMS/(0.2*IH)
175     C       IF(IH.GT.5) TCOH=TRMS/(2.*(IH-5))
176     C       FD=TRMS/TCOH
177     C*****************************************************************
178     C CONVERT THE DISPERSION VECTOR TAU12(I) TO A DISP. MATRIX TAU(I,J)
179     C CREATE THE SOURCE AUTO-CORRELATION MATRIX AUTO(I,J)
180     C*****************************************************************
```

```
      KL=1
      DO 88 I=1,N
      DO 88 J=1,N
      TAU(J,I)=ABS(TAU12(KL))
      AUTO(J,I)=EXP(-TAU(J,I)/(TCOH))
C*****************************************************************
C IF CALCULATIONS DESIRED FOR VERY COHERENT SOURCES; AUTO(J,I)=1.
C REMOVE CONTROL CARD IN THE NEXT LINE
C*****************************************************************
      AUTO(J,I)=1.
      KL=KL+1
 88   CONTINUE
C*************************************************
C FIND THE COUPLING EFFICIENCY 'EFF'
C*************************************************
      SUM=0.
      DO 49 I=1,N
      SUM=SUM+W(I)*F(I,I)
 49   CONTINUE
      EFF=SUM/DIV
C*****************************************************************
C FIND THE STANDARD DEVIATION OF THE COUPLING EFFICIENCY 'SD'
C FIND THE DERIVATIVE OF THE COUPLING EFFICIENCY W.R.T
C THE CENTER FREQUENCY 'DC'. 'DTR' IS THE NORMALIZED VALUE
C OF 'DC' W.R.T TRMS AND EFF.
C*****************************************************************
      DS=0.
      VAR=0.
      DO 54 J=1,N
      DO 54 K=1,N
      IF(K.NE.J) VAR=VAR+(F(J,K)**2)*W(J)*W(K)*AUTO(J,K)
      Y=ABS(F(J,K))*TAU(J,K)
      IF(Y.LT.1.E-35) GO TO 103
      GO TO 104
 103  Y=0.
 104  DS=DS+(Y**2)*AUTO(J,K)*W(J)*W(K)
 54   CONTINUE
      SD=SQRT(VAR)/DIV
      DC=SQRT(DS)/DIV
      DTR=DC/(TRMS*EFF)
C*************************************************
C CALCULATE SNR USING RESULTS FROM SPECKLE THEORY
C*************************************************
      SPCKL=(FLOAT(V)*SQRT(EFF/(1.-EFF))/2.)**2
C*************************************************
C CALCULATE THE LOSS, SEC. HARMONIC DIST., SNR
C*************************************************
      LOSS=10.*ALOG10(EFF)
      SNR=(EFF/SD)**2
      HAR=(DC*OMEGA)/((2.*EFF)+(4.*DC*OMEGA))
      HAR2=20.*ALOG10(HAR)
      WRITE(5,7)DELA,LOSS,SNR,DTR,HAR2,FD
 7    FORMAT(I3,2X,F6.3,2X,E10.3,2X,E10.4,2X,E10.4,2X,F6.2)
 83   CONTINUE
      STOP
      END
C*****************************************************************
C SUBROUTINE TO FIND THE FACTORIALS
C*****************************************************************
      SUBROUTINE CALFAC(NN,FACTNN)
```

```
241           FACTNN=1.
242           IF(NN.LE.1) GO TO 3
243           DO 2 II=2,NN
244         2 FACTNN=FACTNN*FLOAT(II)
245         3 RETURN
246           END
247     C*************************************************************
248     C SUBROUTINE TO FIND THE GENERALIZED LAGUERRE VALUES
249     C*************************************************************
250           SUBROUTINE ALAG(N,LPHA,X,ALX)
251           M=N+1
252           ALX=0.
253           DO 101 IJ=1,M
254           IA=IJ-1
255           IL=N+LPHA
256           IK=N-IA
257           IM=LPHA+IA
258           CALL CALFAC(IA,FACTIA)
259           CALL CALFAC(IL,FACTIL)
260           CALL CALFAC(IK,FACTIK)
261           CALL CALFAC(IM,FACTIM)
262           UGURRE=((-1)**IA)*(FACTIL/(FACTIK*FACTIM*
263          1FACTIA))*(X**IA)
264           ALX=ALX+UGURRE
265       101 CONTINUE
266           RETURN
267           END
```

APPENDIX A2

Computer Program (Longitudinal Offset)

```
C*****************************************************************
C THIS PROGRAM CALCULATES THE MODAL AMPLITUDE COUPLING
C COEFFICIENTS FOR THE CASE OF SPACING BETWEEN FIBERS ENDS.
C TO CALCULATE THE LOSS, MODAL NOISE AND DISTORTION, SUBSTITUTE
C LINES 19 TO 148 OF THIS PROGRAM FOR LINES 44 TO 151
C OF THE PROGRAM LISTED IN APPENDIX A1. ALSO INCORPORATE THE
C SUBROUTINE (148-170) AT THE END.
C*****************************************************************
C NSP= NORMALIZED SPACING
C K0= FREE-SPACE WAVE NUMBER
C REFM=REFRACTIVE INDEX OF THE MATCHING MEDIUM
C KM=WAVE NUMBER IN THE MATCHING MEDIUM
C W= NORMALIZED MODAL POWER WEIGHTS
C W0=FUNDAMENTAL MODE RADIUS (MICRONS)
C D= SPACING DISTANCE
C WD= BEAM WIDTH AT A SPACING DISTANCE 'D'
C REFM=1. FOR AIR GAP
C REFM=REF1 FOR INDEX-MATCHED CASE
C*****************************************************************
C CALCULATION OF BEAM WIDTH, MAX. MODE GR. NO., REL. INDEX DIFF.,
C FREE SPACE WAVE NO., WAVE NO. OF MATCHING MEDIUM, FREQ. DEVIATIOI
C IN RADIANS.
C*****************************************************************
      REFM=1.
      W0=RAD*SQRT(2./FLOAT(V))
      MG=(V-1)/2
      DELTA=(REF1-REF2)/REF1
      K0=2.*PI/WAVLN
      KM=K0*REFM
      OMEGA=2*PI*FREFL
C*************************************************************
C CALCULATION OF COEFFICIENTS RELATING TO INDEX PROFILE
C*************************************************************
      A11=(ALPHA-2.)/(ALPHA+2.)
      A12=(2.*ALPHA)/(ALPHA+2.)
      A21=((3.*ALPHA)-2.)/(ALPHA+2.)
      A22=(4.*ALPHA)/(ALPHA+2.)
      DE2=(DELTA**2)/2.
C*****************************************************************
      WRITE(5,1)
    1 FORMAT('GAP',2X,'LOSS(DB)',4X,'SNR',10X,'HILL',5X,
     1'DTR',2X,'TRMS(NS)')
C*****************************************************************
C CALCULATION OF THE STEADY STATE MODAL POWER WEIGHTS NORMALIZED
C TO FUNDAMENTAL MODE GROUP POWER
C*****************************************************************
      IJ=1
      DO 77 I=1,MG
      I1=I-1
      I2=I1/2+1
      DO 77 J=1,I2
      X1=FLOAT(I)*SQRT(FLOAT(I))
      X2=FLOAT(MG+1-I)/FLOAT(MG)
      X3=SQRT(X2)
      FRAC=1./(X1*X3)
      W(IJ)=FRAC
      IJ=IJ+1
   77 CONTINUE
C*****************************************************************
```

```
C CALCULATION OF THE SUM OF ALL MODAL POWER WEIGHTS 'DIV'
C*****************************************************************
      DIV=0.
      DO 12 K=1,N
C REMOVE CONTROL CARD IN NEXT LINE IF UNIFORM DISTRIBUTION
      W(K)=1.
      IF(K.EQ.1) GO TO 76
      IF(W(K).GT.W(K-1)) W(K)=W(K-1)
 76   DIV=DIV+W(K)
 12   CONTINUE
C*****************************************************************
C NORMALIZED SPACING 'NSP' DO-LOOP
C*****************************************************************
      DO 83 NSP=1,20
      IF(NSP.LE.6) D=RAD*NSP
      IF(NSP.GT.6) D=FLOAT(NSP-5)*4.*RAD
      W1=((2.*D)/((W0**2)*KM))**2
      WD=W0*SQRT(1.+W1)
      ALPH=2./(W0**2)
      BETA=2./(WD**2)
      GAMA=(ALPH+BETA)/2.
C*****************************************************************
C MODE-MODE COUPLING COEFFICIENT DO-LOOP
C*****************************************************************
      TRMSS=0.
      JK=1
 35   DO 10 MG2=1,MG
      IMG2=MG2-1
      IMQ2=IMG2/2+1
      DO 10 Q22=1,IMQ2
      Q2=Q22-1
      L2=(IMG2-2*Q2)
      DO 10 MG1=1,MG
      IMG1=MG1-1
      IMQ1=IMG1/2+1
      DO 10 Q11=1,IMQ1
      Q1=Q11-1
      L1=(IMG1-2*Q1)
C*****************************************************************
C CALCULATION OF INTER MODE DISPERSION TAU12(JK)
C*****************************************************************
           U2=FLOAT(IMG2)
           U1=FLOAT(IMG1)
           UMG=FLOAT(MG)
     T2=A11*DELTA*((U2/UMG)**A12)
    1+A21*DE2*((U2/UMG)**A22)
     T1=A11*DELTA*((U1/UMG)**A12)
    1+A21*DE2*((U1/UMG)**A22)
     T21=(REF1/CLIGHT)*(T2-T1)*LFIB
     TRMSS=TRMSS+(T21**2)
     TAU12(JK)=T21
C*****************************************************************
C COUPLING ONLY BETWEEN MODES WITH SAME AZIMUTHAL NO. 'L'
C*****************************************************************
      IF(L1.NE.L2) GO TO 50
C*****************************************************************
      F11=WD*W0*GAMA
      F1=(2./F11)**(L1+1)
C*********************************
      I1=Q1+Q2+L1
```

```
      I2=L1+Q1
      I3=L2+Q2
      CALL CALFAC(I1,FACTI1)
      CALL CALFAC(I2,FACTI2)
      CALL CALFAC(I3,FACTI3)
      CALL CALFAC(Q1,FACTQ1)
      CALL CALFAC(Q2,FACTQ2)
      F22=SQRT(FACTI2*FACTI3*FACTQ1*FACTQ2)
      F2=FACTI1/F22
C*****************************************
      F3=(1.-(ALPH/GAMA))**Q2
      F4=(1.-(BETA/GAMA))**Q1
C*****************************************
      J1=-Q2
      J2=-Q1
      J3=-Q1-Q2-L1
      Z1=GAMA*(GAMA-ALPH-BETA)
      Z2=(GAMA-ALPH)*(GAMA-BETA)
      Z=Z1/Z2
      CALL HYP(J1,J2,J3,Z,HYPZ)
C*****************************************
      GO TO 51
 50   RESL=0.
      GO TO 52
 51   RESL=F1*F2*F3*F4*HYPZ
 52   CONTINUE
      COUPL(JK)=RESL
      JK=JK+1
 10   CONTINUE
C*********************************************************************
C SUBROUTINE TO FIND HYPERGEOMETRIC SERIES VALUES
C*********************************************************************
      SUBROUTINE HYP(I,J,K,Z,HYPZ)
      REAL F(15)
      IF (I.EQ.0) GO TO 43
      IF (J.EQ.0) GO TO 43
      IAB=IABS(I)
      JAB=IABS(J)
      IJ=MIN0(IAB,JAB)
      IJ1=IJ+1
      F(1)=FLOAT(I)*FLOAT(J)*Z/FLOAT(K)
      HYPZ=1.+F(1)
      DO 45 MM=2,IJ1
      M=MM-1
      F(MM)=F(M)*FLOAT(I+M)*FLOAT(J+M)*Z/((FLOAT(MM)*FLOAT(K+M)))
 45   HYPZ=HYPZ+F(MM)
      GO TO 64
 43   HYPZ=1.
 64   CONTINUE
      RETURN
      END
```

APPENDIX A3

Computer Program (Tilt Offset)

```
C*************************************************************
C THIS PROGRAM CALCULATES THE MODAL AMPLITUDE COUPLING
C COEFFICIENTS FOR THE CASE OF TILT.
C TO CALCULATE THE MODAL NOISE AND DISTORTION, SUBSTITUTE
C LINES 11 TO 124 OF THIS PROGRAM FOR LINES 89 TO 151
C OF THE PROGRAM LISTED IN APPENDIX A1.
C*************************************************************
      COMPLEX COUPL(10000),C(100,100),SUM,F(100,100),YT
      REAL TAU12(10000),W(100),FF(100,100)
      REAL TAU(100,100),AUTO(100,100)
C*************************************************************
C NORMALIZED ANGULAR OFFSET 'GAM' DO LOOP
C ANGULAR OFFSET 'PHI' IS IN DEGREES
C*************************************************************
      DO 83 IPHI=3,3
      PHI=FLOAT(IPHI)
      GAM=(PHI*PI/180.)/SQRT(2.*DELTA)
      EV=FLOAT(V)
      DELT=(GAM**2)*EV/4.
C*************************************************************
C MODE-MODE COUPLING COEFFICIENT DO-LOOP
C*************************************************************
      JK=1
      TRMSS=0.
 35   DO 10 MG2=1,MG
      IMG2=MG2-1
      IMQ2=IMG2/2+1
      DO 10 Q22=1,IMQ2
      Q2=Q22-1
      L2=(IMG2-2*Q2)
      DO 10 MG1=1,MG
      IMG1=MG1-1
      IMQ1=IMG1/2+1
      DO 10 Q11=1,IMQ1
      Q1=Q11-1
      L1=(IMG1-2*Q1)
C*************************************************************
C CALCULATION OF INTER MODE DISPERSION TAU12(JK)
C*************************************************************
          U2=FLOAT(IMG2)
          U1=FLOAT(IMG1)
          UMG=FLOAT(MG)
     T2=A11*DELTA*((U2/UMG)**A12)
    1+A21*DE2*((U2/UMG)**A22)
     T1=A11*DELTA*((U1/UMG)**A12)
    1+A21*DE2*((U1/UMG)**A22)
     T21=(REF1/CLIGHT)*(T2-T1)*LFIB
     TRMSS=TRMSS+(T21**2)
     TAU12(JK)=T21
C*************************************************************
      IX=IABS(L1-L2)
      IY=L1+L2
      IZ=Q1+Q2
      IV=Q1-Q2
      L1V=L1+IV
      L2V=L2-IV
      IXV=L1-L2-Q2+Q1
      IIXV=L2-L1-Q1+Q2
      IVM=-IV
```

```
C*****************************************************************
C CALCULATION OF THE MODE COUPLING COEFFICIENTS COUPL(JK)
C*****************************************************************
      IF(L1.EQ.0)EL1=1.
      IF(L1.NE.0)EL1=2.
      IF(L2.EQ.0)EL2=1.
      IF(L2.NE.0)EL2=2.
      F02=SQRT(EL1*EL2)
      CALL CALFAC(Q1,FACQ1)
      CALL CALFAC(Q2,FACQ2)
      Q1L1=Q1+L1
      Q2L2=Q2+L2
      CALL CALFAC(Q1L1,FQ1L1)
      CALL CALFAC(Q2L2,FQ2L2)
      F03=SQRT((FACQ1*FACQ2)/(FQ1L1*FQ2L2))
      F1=F02*F03
      F2=(-1)**IZ
      F3=EXP(-DELT)
      F4=EV**(FLOAT(IY)/2.)
      F5=2.**(-IY-1)
      F6=GAM**IY
      IF(L1V.GE.0) CALL ALAG(Q2,L1V,DELT,F7)
      IF(L1V.LT.0) CALL AALAG(Q2,L1V,DELT,F7)
      IF(L2V.GE.0) CALL ALAG(Q1,L2V,DELT,F8)
      IF(L2V.LT.0) CALL AALAG(Q1,L2V,DELT,F8)
      IF(L1.GE.L2)GO TO 544
      IF(L1.LT.L2)GO TO 545
  544 F10=FQ2L2/FACQ2
      IF(IXV.GE.0) CALL ALAG(Q2L2,IXV,DELT,F14)
      IF(IXV.LT.0) CALL AALAG(Q2L2,IXV,DELT,F14)
      IF(IVM.GE.0) CALL ALAG(Q1,IVM,DELT,F15)
      IF(IVM.LT.0) CALL AALAG(Q1,IVM,DELT,F15)
      GO TO 567
  545 F10=FQ1L1/FACQ1
      IF(IIXV.GE.0) CALL ALAG(Q1L1,IIXV,DELT,F14)
      IF(IIXV.LT.0) CALL AALAG(Q1L1,IIXV,DELT,F14)
      IF(IV.GE.0) CALL ALAG(Q2,IV,DELT,F15)
      IF(IV.LT.0) CALL AALAG(Q2,IV,DELT,F15)
  567 F11=EV**(FLOAT(IX)/2.)
      F12=2.**(-IX-1)
      F13=GAM**IX
      F16=F1*F2*F3
      F17=F4*F5*F6*F7*F8
      F18=F10*F11*F12*F13*F14*F15
C*****************************************************************
C CHECK IF THE DIFFERENCE BETWEEN THE AZIMUTHAL NUMBERS
C L1 AND L2 IS AN EVEN OR AN ODD NUMBER TO YIELD REAL
C OR IMAGINARY AMPLITUDE COUPLING COEFFICIENTS RESPECTIVELY
C*****************************************************************
      IF(FLOAT(IY/2).NE.FLOAT(IY)/2.)GO TO 357
C*****************************************************************
      IZX1=(-1)**(IY/2)
      IZX2=(-1)**(IX/2)
      RESL2=F16*((F17*IZX1)+(F18*IZX2))
      YT=CMPLX(RESL2,0.)
      GO TO 43
  357 IAS1=(-1)**((IY-1)/2)
      IAS2=(-1)**((IX-1)/2)
      RESL2=F16*((F17*IAS1)+(F18*IAS2))
      YT=CMPLX(0.,RESL2)
```

```
120        43   CONTINUE
121        86   FORMAT(I2,2X,I2,2X,2E10.3)
122             COUPL(JK)=YT
123             JK=JK+1
124        10   CONTINUE
```

APPENDIX A4

Mode Coupling Coefficients for Fiber Imperfections

The aim of this appendix is to evaluate the coupling coefficients $K_{\mu\nu}$ (see eq. (7.38)) between guided modes and guided and radiation modes of weakly guiding optical fibers for slight core boundary imperfections. Since we already assumed the highest order guided mode to be leaky, it is sufficient to calculate the coupling between guided modes only. The fiber core boundary is determined by the function in (7.32). Mode coupling is provided by implanting a refractive-index perturbation in to the fiber core [179]. The perturbed refractive-index distribution n^2 can be expanded into a power series [179],[185],[196]

$$n_p^2 = f(z) \left(\frac{r}{a}\right)^n \cos(n\phi) \qquad |r| \leq a \qquad (A4.1)$$

The dependence of (7.38) on cos nø imposes the selection rule (7.39). The r dependence indicated in (7.74) is quite arbitrary [185]. It is necessary that (A4.1) vanishes at r=0 in order to have a well defined value of the function at this point. The n th power dependence is not only the simplest function that vanishes at r=0 but also one for which the coupling coefficients can be evaluated [185]. Substituting the normalized mode field expressions for the guided modes into (7.38) leads to the following coupling coefficient of the $LP_{\ell p}$ -mode

to the $LP_{\ell+1,p}$ -mode

$$K_{\ell p,\ (\ell+1)p} = \frac{k}{4n_1}\left[\frac{\varepsilon_\ell\ (p+\ell)}{V}\right]^{\frac{1}{2}} \qquad (A4.2)$$

to the $LP_{\ell-1,p+1}$ -mode

$$K_{\ell p,\ (\ell-1)(p+1)} = \frac{k}{4n_1}\left[\frac{\varepsilon_{\ell-1}\, p}{V}\right]^{\frac{1}{2}} \qquad (A4.3)$$

to the $LP_{\ell-1,p}$ -mode

$$K_{\ell p\ \ (\ell-1)p} = \frac{k}{4n_1}\left[\frac{\varepsilon_{\ell-1}\ (p+\ell-1)}{V}\right]^{\frac{1}{2}} \qquad (A4.4)$$

to the $LP_{\ell+1,p-1}$ -mode

$$K_{\ell p\ \ (\ell+1)(p-1)} = \frac{k}{4n_1}\left[\frac{\varepsilon_\ell\,(p-1)}{V}\right]^{\frac{1}{2}} \qquad (A4.5)$$

to the $LP_{\ell+2,p}$ -mode

$$K_{\ell p,\ (\ell+2)\ p} = \frac{k}{4n_1}\left[\frac{\varepsilon_\ell\ (p+\ell)\ (p+\ell+1)}{V^2}\right]^{\frac{1}{2}} \qquad (A4.6)$$

to the $LP_{\ell-2,p}$ -mode

$$K_{\ell p,\ (\ell-2)\ p} = \frac{k}{4n_1}\left[\frac{\varepsilon_{\ell-2}\ (p+\ell-2)\ (p+\ell-1)}{V^2}\right]^{\frac{1}{2}} \qquad (A4.7)$$

with ε_n defined by

$$\varepsilon_n = \begin{cases} 1 & \text{for } n \neq 0 \\ 2 & \text{for } n = 0 \end{cases}$$

The coupling coefficients in (A4.2), (A4.3), (A4.4) and (A4.5) are due to microbending with $\Delta m = \pm 1$, whereas (A4.6) and (A4.7) are due to the elliptic deformation with $\Delta m = \pm 2$. The coefficients in (A4.2) and (A4.3) couple modes with compound mode number m to modes with m+1, and (A4.4) and (A4.5) for modes with m to modes with m-1. Simillarly, (A4.6) denotes coupling between modes with m to modes with m+2, and (A4.7) for m with m-2.

APPENDIX A5

Computer Program (Fiber Imperfections)

```
C*********************************************************************
C THIS PROGRAM CALCULATES THE LOSS, MODAL NOISE AND DISTORTION
C DUE TO MICROBENDING.
C*********************************************************************
C AC=FIBER CORE RADIUS (MM)
C A1=FIBER CLADDING RADIUS (MM)
C A2=RADIUS OF INNER JACKET (MM)
C A3=RADIUS OF OUTER JACKET (MM)
C E1=YOUNG'S MODULUS OF SILICA (KG/(MM**2))
C E2=YOUNG'S MODULUS OF INNER JACKET (KG/(MM**2))
C E3=YOUNG'S MODULUS OF OUTER JACKET (KG/(MM**2))
C ROUGH=STANDARD DEVIATION OF SANDPAPER SURFACE ROUGHNESS (IN MM)
C CL=CORRELATION LENGTH OF THE RANDOM BENDS (MM)
C HC=COMBINED STIFFNESS OF FIBER AND JACKETS (KG-MM**2)
C DC=COMBINED ELASTIC MODULUS OF THE COMPRESSED SURFACE I.E.,
C THE JACKET, THE SAND PAPER, THE WOODEN SECTION (OR THE STEEL BELT
C (KG/(MM**2))
C LP=LINEAR PRESSURE (KG/MM)
C ALPHA=EXPONENT OF THE REFRACTIVE INDEX PROFILE
C REF1=REFRACTIVE INDEX OF THE CORE
C REF2=REFRACTIVE INDEX OF THE CLADDING
C DELTA= RELATIVE INDEX DIFFERENCE
C WAVLN=WAVELENGTH OF THE SOURCE (MICRONS)
C DBETA=PHASE LAG BETWEEN TWO NEIGHBOURING MODES(PER MM)
C V= CHARACTERISTIC MODAL PARAMETER, 'V' NUMBER OF FIBER
C NA= NUMERICAL APERTURE OF THE FIBER
C MG= MAXIMUM MODE GROUP NUMBER OF FIBER
C N= NUMBER OF MODES OF FIBER, SINGLE POLARIZATION AND ORIENTATION
C K0= FREE SPACE WAVE NUMBER
C W= NORMALIZED MODAL POWER WEIGHTS
C W0=FUNDAMENTAL MODE RADIUS (MM)
C TCOH=COHERENCE TIME OF THE SOURCE (NS)
C FREFL=FREQUENCY FLUCTUATION OF THE SOURCE (GHZ)
C LFIB=LENGTH OF FIBER UNDER MICROBENDING (M)
C LSEC=LENGTH OF FIBER SECTION (SPECKLE PATTERN PERIODICITY)(M)
C CLIGHT=VELOCITY OF LIGHT (M./SEC)
C N=6 FOR V=9, WAVLN=3.6
C N=30 FOR V=21, WAVLN=1.55
C N=56 FOR V=29, WAVLN=1.1
C N=100 FOR V=39,WAVLN=.816
C*********************************************************************
      REAL TAU(100,100),C1(100,100),C(100,100),F(100,100),W(100)
      REAL LOSS,LFIB,K0,LP,NA
      INTEGER Q11,Q1,Q22,Q2,V,IER,P1,P2
C*********************************************************************
      V=39
      N=100
      WAVLN=.816E-3
C*********************************************************************
C FIBER, JACKET, SAND PAPER AND SOURCE PARAMETERS
C*********************************************************************
      EV=FLOAT(V)
      PI=3.1415927
      CLIGHT=3.E+8
      AC=25.E-3
      A1=62.5E-3
      A2=102.5E-3
      A3=125.E-3
      E1=7000.
      E2=0.3515
```

```
      E3=33.5
      ROUGH=50.E-3
      CL=0.6E+00
      ALPHA=2.2
      REF1=1.47214
      REF2=1.4585
      NA=0.2
      LFIB=1.05E+3
      BUMP=LFIB*1000./CL
      FREFL=113.E+9/(2.*PI)
      TCOH=.37E-9
C*********************************************************************
C CALCULATION OF BEAM WIDTH, MAX. MODE GR. NO., REL. INDEX DIFF.,
C FREE SPACE WAVE NO., PHASE LAG 'DBETA', FREQ. DEVIATION
C IN RADIANS.
C*********************************************************************
      W0=AC*SQRT(2./EV)
      MG=(V-1)/2
      DELTA=(REF1-REF2)/REF1
      K0=2.*PI/WAVLN
      DBETA=SQRT(2.*DELTA)/AC
      CO=K0/(4.*REF1)
      OMEGA=2*PI*FREFL
C*********************************************************
C CALCULATION OF COEFFICIENTS RELATING TO INDEX PROFILE
C*********************************************************
      A11=(ALPHA-2.)/(ALPHA+2.)
      A12=(2.*ALPHA)/(ALPHA+2.)
      A21=((3.*ALPHA)-2.)/(ALPHA+2.)
      A22=(4.*ALPHA)/(ALPHA+2.)
      DE2=(DELTA**2)/2.
C*********************************************************************
C CALCULATION OF THE STEADY STATE MODAL POWER WEIGHTS NORMALIZED
C TO FUNDAMENTAL MODE GROUP POWER
C*********************************************************************
      IJ=1
      DO 77 I=1,MG
      I1=I-1
      I2=I1/2+1
      DO 77 J=1,I2
      X1=FLOAT(I)*SQRT(FLOAT(I))
      X2=FLOAT(MG+1-I)/FLOAT(MG)
      X3=SQRT(X2)
      FRAC=1./(X1*X3)
      W(IJ)=FRAC
      IJ=IJ+1
 77   CONTINUE
C*************************************************************
C CALCULATION OF THE SUM OF ALL MODAL POWER WEIGHTS 'DIV'
C*************************************************************
      DIV=0.
      DO 12 K=1,N
C REMOVE CONTROL CARD IN NEXT LINE IF UNIFORM DISTRIBUTION
      W(K)=1.
      IF(K.EQ.1) GO TO 76
      IF(W(K).GT.W(K-1)) W(K)=W(K-1)
 76   DIV=DIV+W(K)
 12   CONTINUE
C*********************************************************************
C COMPUTATION OF THE FACTORS NEEDED TO EVALUATE THE POWER SPECTRUM
```

```
C OF THE FIBER'S LATERAL DISPLACEMENT
C*****************************************************************
      HC=(PI/4.)*((E1*(A1**4))+E2*
     1(A2**4-A1**4)+E3*(A3**4-A2**4))
      DC=E2+E3*(((A3-A2)/A3)**3)
      G1=1.698*(ROUGH**2)/((CL**5)*(DBETA**6))
      G2=(64./225.)*(HC**2)*SQRT(HC)*
     1DC*SQRT(DC)*(ROUGH**4)/(CL**10)
      G3=(1.+((DBETA**4)*HC/DC))**2
C*****************************************************************
C MODE-MODE COUPLING COEFFICIENT DO-LOOP
C*****************************************************************
      TRMSS=0.
      JK=0
 35   DO 10 MG2=1,MG
      IMG2=MG2-1
      IMQ2=IMG2/2+1
      DO 10 Q22=1,IMQ2
      Q2=Q22-1
      L2=(IMG2-2*Q2)
      JK=JK+1
      LK=0
      DO 10 MG1=1,MG
      IMG1=MG1-1
      IMQ1=IMG1/2+1
      DO 10 Q11=1,IMQ1
      Q1=Q11-1
      L1=(IMG1-2*Q1)
      LK=LK+1
C*****************************************************************
C CALCULATION OF INTER MODE DISPERSION TAU12(JK)
C*****************************************************************
          U2=FLOAT(IMG2)
          U1=FLOAT(IMG1)
          UMG=FLOAT(MG)
      T2=A11*DELTA*((U2/UMG)**A12)
     1+A21*DE2*((U2/UMG)**A22)
      T1=A11*DELTA*((U1/UMG)**A12)
     1+A21*DE2*((U1/UMG)**A22)
      T21=(REF1/CLIGHT)*(T2-T1)*LFIB
      TRMSS=TRMSS+(T21**2)
      TAU(JK,LK)=ABS(T21)
      IF((MG2.LT.MG-2).AND.(MG1.LT.MG-2)) TAU(JK,LK)=0.
C*****************************************************************
      C1(JK,LK)=0.
      P1=Q1+1
      P2=Q2+1
      FX=0.
      IF((MG1.EQ.MG).AND.(MG2.GE.MG-2)) GO TO 351
      GO TO 100
 351  IF((L2.LE.1).AND.(L1.LE.2))GO TO 36
      GO TO 100
  36  IF((P1.EQ.P2).AND.(L2-L1.EQ.1))GO TO 45
      IF((P1.EQ.P2).AND.(L1.NE.0).AND.(L1-L2.EQ.1))GO TO 65
      IF((P2-P1.EQ.1).AND.(L1.NE.0).AND.(L1-L2.EQ.1))GO TO 55
      IF((P1-P2.EQ.1).AND.(L2-L1.EQ.1))GO TO 75
      IF((P1.EQ.P2).AND.(L2-L1.EQ.2)) GO TO 85
      IF((L1.GT.1).AND.(P1.EQ.P2).AND.(L1-L2.EQ.2)) GO TO 105
      GO TO 100
  45  IF(L1.EQ.0) FX=2.*FLOAT(P1+L1)/EV
```

```
      IF(L1.NE.0) FX=FLOAT(P1+L1)/EV
      GO TO 100
   55 IF(L2.EQ.0) FX=2.*FLOAT(P1)/EV
      IF(L2.NE.0) FX=FLOAT(P1)/EV
      GO TO 100
   65 IF(L2.EQ.0) FX=2.*FLOAT(P1+L2)/EV
      IF(L2.NE.0) FX=FLOAT(P1+L2)/EV
      GO TO 100
   75 IF(L1.EQ.0) FX=2.*FLOAT(P2)/EV
      IF(L1.NE.0) FX=FLOAT(P2)/EV
      GO TO 100
   85 IF(L1.EQ.0) FX=2.*FLOAT(P1+L1)*FLOAT(P1+L1+1)/(EV**2)
      IF(L1.NE.0) FX=FLOAT(P1+L1)*FLOAT(P1+L1+1)/(EV**2)
      GO TO 100
  105 IF(L2.EQ.0) FX=2.*FLOAT(P1+L2)*FLOAT(P1+L2+1)/(EV**2)
      IF(L2.NE.0) FX=FLOAT(P1+L2)*FLOAT(P1+L2+1)/(EV**2)
  100 C(JK,LK)=CO*SQRT(FX)
      IF((MG1.EQ.MG).AND.(MG2.EQ.MG-1)) C1(JK,LK)=C(JK,LK)
   10 CONTINUE
C*************************************************************
C FIND THE ROOT MEAN SQUARE INTERMODAL DELAY 'TRMS'
C*************************************************************
      TRMS=SQRT(TRMSS)/FLOAT(N)
C*************************************************************************
C FIND THE SUM OF ALL POWER COUPLING COEFFICIENTS FOR MICROBENDING
C*************************************************************************
      EFF=0.
      DO 765 I=1,N
      DO 765 J=1,N
  765 EFF=EFF+(C1(I,J)**2)*W(I)
      EFF1=EFF/DIV
C*****************************************************
C FIND THE INTERFERENCE MATRIX F(I,J)
C*****************************************************
      DO 95 I=1,N
      DO 95 K=1,N
      C(K,I)=C(I,K)
      SUM=0.
      DO 94 J=1,N
   94 SUM=SUM+C(I,J)*C(J,K)
      F(I,K)=SUM
   95 CONTINUE
C*************************************************************************
C IF CALCULATIONS DESIRED FOR PARTIAL COHERENT SOURCES
C REMOVE CONTROL CARDS, TRMS/TCOH=0.2 TO 20, 15 VALUES
C*************************************************************************
C     DO 83 IH=5,15
C     IF(IH.LE.5) TCOH=TRMS/(0.2*IH)
C     IF(IH.GT.5) TCOH=TRMS/(2.*(IH-5))
C     FD=TRMS/TCOH
C*************************************************************************
C CALCULATION OF THE POWER SPECTRUM EXPONENT OF THE CORE-CLADDING
C DEFORMATION 'PS'(MM), 'XLOSS' IS THE POWER LOSS IN 'DB/KM', IT HA
C BEEN DIVIDED BY 2 SINCE THE FIBER IS STRESSED IN ONE PLANE ONLY
C 'VP' IS THE LINEAR PRESSURE IN GM/MM, 'LP' IS THE LINEAR
C PRESSURE IN KG/MM , 'XXX' IS THE POWER SPECTRA CONVERSION FACTOR,
C FROM THE DOMAIN OF REFRACTIVE INDEX FLUCTUATIONS (MM) TO THE
C DOMAIN OF FIBER'S LATERAL DISPLACEMENT (MM**3)
C*************************************************************************
      XXX=16.*(REF1**4)*(DELTA**2)/(AC**2)
```

```
C      DO 83 ILP=5,25,5
       DO 83 ILOSS=1,5
       GLOSS=0.23*1.E-6*ILOSS
       PS=GLOSS/EFF1
       ALOSS=ILOSS*LFIB/1000.
C      VP=ILP/10.
C      LP=VP*1.E-3
C      PS=G1*XXX/(G3*SQRT(SQRT(1.+(G2/(LP**4)))))
C      XLOSS=EFF1*PS*1.E+6/0.23
C      ALOSS=XLOSS*LFIB/1000.
C*****************************************************************
C FIND THE STANDARD DEVIATION OF THE COUPLING EFFICIENCY 'SD'
C FIND THE DERIVATIVE OF THE COUPLING EFFICIENCY 'DC' W.R.T
C THE CENTER FREQUENCY, FIND THE NORMALIZED FLUCTUATIONS 'DTR'
C*****************************************************************
       Q=CL*DBETA/2.
       SQ=1.+(Q**2)
       PSD=PS/DBETA
       DS=0.
       VAR=0.
       DO 54 J=1,N
       DO 54 K=1,N
C*******************************************************
C VARIANCE FOR COHERENT SOURCE
C*******************************************************
C      VAR=VAR+(F(J,K)**2)*BUMP*W(J)*W(K)
C*******************************************************
C NORMALIZED FLUCTUATIONS FOR COHERENT SOURCE
C*******************************************************
C      FSDD=(BUMP**3)*(TAU(J,K)**2)*W(J)*W(K)*(F(J,K)**2)/3.
C*******************************************************
C VARIANCE FOR PARTIALLY COHERENT SOURCE
C*******************************************************
C      IF(TAU(J,K).EQ.0.) GO TO 534
C      ALPH=TAU(J,K)/TCOH
C      ALPH1=1./ALPH
C      AL2=1.-EXP(-ALPH)
C      VAR=VAR+(ALPH1*AL2*(F(J,K)**2)*BUMP*W(J)*W(K))
C      GO TO 523
C534   VAR=VAR+(BUMP*(F(J,K)**2)*W(J)*W(K))
C523   CONTINUE
C*******************************************************
C NORMALIZED FLUCTUATIONS FOR PARTIAL COHERENCE
C*******************************************************
       IF(TAU(J,K).EQ.0.) GO TO 79
C      ALPH=(2.*ALOSS*0.23/BUMP)-(TAU(J,K)/(TCOH*BUMP))
       ALPH=-TAU(J,K)/(TCOH*BUMP)
       IF(ALPH.EQ.0.) GO TO 364
       Z11=2./(ALPH**3)
       Z12=(BUMP**2)/ALPH
       Z13=2.*BUMP/(ALPH**2)
       Z14=EXP(BUMP*ALPH)
       ZWQ=-Z11+(Z14*(Z12-Z13+Z11))
C      ZWQ=-Z11
       GO TO 365
  364  ZWQ=(BUMP**3)/3.
  365  FSDD=ZWQ*(TAU(J,K)**2)*(F(J,K)**2)*W(J)*W(K)
       GO TO 49
   79  FSDD=0.
C*******************************************************
```

```
 49   DS=DS+FSDD
 54   CONTINUE
C*****************************************************
C CALCULATION OF THE VARIANCE AND THE DC-SNR
C*****************************************************
C      VARI=VAR*SQ*(PSD**2)/(DIV**2)
      ZEFF=EXP(-(ALOSS*0.23))
C      SNR=(ZEFF**2)/VARI
C*****************************************************
C CALCULATION OF THE NORMALIZED FLUCTUATION AND
C THE SECOND HARMONIC DISTORTION
C*****************************************************
      DC=SQRT(DS)*PSD*SQRT(SQ)/(BUMP*DIV)
C      DTR=DC/(TRMS*ZEFF)
      HAR2=20.*ALOG10(DC*OMEGA/(2.*ZEFF))
C*****************************************************
      WRITE(5,7)ALOSS,HAR2,TRMS
 83   CONTINUE
 7    FORMAT(F6.2,2X,F6.2,2X,E13.6)
      STOP
      END
```